FERROMAGNETISM IN HIGHLY PERFECT METALLIC PLATELETS

A Thesis

submitted for the

DEGREE OF DOCTOR OF PHILOSOPHY

IN THE UNIVERSITY OF LONDON

by

MERVYN EVAN JONES

Department of Electrical Engineering,

City and Guilds College,

Imperial College,

LONDON S.W.7.

1970

ABSTRACT

This thesis is a study of the magnetic properties of small but highly perfect ferromagnetic platelets, as found from observations of their domain structures. The thickness range of these platelets, 0.1-10.0 μm., overlapped that of thin magnetic films, whose properties have already been extensively studied. Thus, a knowledge of the structure and behaviour of domains and domain walls in thin films is an essential background to this work. The various terms which contribute to the total magnetic free energy of a body are reviewed in Chapter 1, together with the experimental and theoretical work studying domain walls in thin films. The variety of techniques available for the observation of magnetic domains are reviewed in Chapter 2, outlining their limitations and suitability for different specimens.

The platelets themselves were produced by the hydrogen reduction of bromides of the elements concerned in a vapour transport reaction. As a ready supply of crystals was necessary for the observations described in Chapters 5 and 6, considerable attention was paid to the nature of these processes. These investigations are described in Chapter 3 together with a discussion of the platelet and related whisker growth habitats and a possible explanation of their development.

The platelets grew with (100) faces and low index crystallographically limited edges, usually as triangles or rectangles. The majority of investigations were made on nickel platelets where the domain patterns were complicated by the fact that no easy axis existed in the platelet plane. The formation of these domains and their

behaviour during the application of in-plane magnetic fields are discussed in Chapter 5. In thicker platelets, planar magnetisation configurations no longer had the minimum energy and more complicated stripe domain patterns were formed. The structure and behaviour of these and their relation to stripe domains in thin films are discussed in Chapter 6.

The small dimensions of these platelets caused their domain behaviour to be strongly affected by the magnetostatic energy. This energy, however, cannot be expressed analytically and requires a numerical treatment. The problems of correlating observed domain behaviour with a theoretical approach are discussed in Chapter 7.

"But if any see fit not to agree with the opinions here expressed and not to accept certain of my paradoxes; still let them note the great multitude of experiments and discoveries."

"And let whosoever would make the same experiments, handle the bodies carefully, skilfully and deftly, not heedlessly and bunglingly; when an experiment fails, let him not in his ignorance condemn our discoveries, for there is naught in this book that has not been investigated and again and again done and repeated under our eyes."

William Gilbert

De Magnete 1600

ACKNOWLEDGEMENTS

The work described in this thesis was carried out in the Materials Laboratories of the Electrical Engineering Department, Imperial College, under the direction of Professor J.C. Anderson. It formed part of a Ministry of Technology contract awarded to Dr. K.D. Leaver, who supervised this project. The help and encouragement given by both Professor Anderson and Dr. Leaver throughout this work are acknowledged with grateful thanks.

The platelets were grown in the Crystal Growth laboratory under the direction of Dr. E.A.D. White. I am most grateful for his experienced advice and also to Dr. J.H.E. Jeffes, Reader in Extraction Metallurgy, for useful discussions on the application of thermodynamics to Chemical Transport.

I would like to thank Mr. A.I. Webb of the Electronics Division, Harwell for an invaluable supply of colloid and for useful discussions on the technique of colloid preparation.

My thanks go to Dr. T.H. O'Dell for many stimulating discussions and for critically reading the manuscript of this thesis.

I thank Dr. V.E. Cosslett for access to the High Voltage Electron Microscope at the Cavendish Laboratory, Cambridge and Dr. R.P. Ferrier for assistance in its use.

I am grateful to my contemporaries in the laboratory and the Senior Technician, Mr. E.G. Hall, for their assistance with numerous enquiries.

The help given by the Analytical Service Laboratories in the

analysis of the platelets, and the Computer Unit for access to IBM 7094 and CDC 6600 computers is acknowledged.

This thesis was typed by Miss J. Cobb and the diagrams drawn by Mr. R. Puddy and Mrs. M. Rathbone. Their care and attention to detail has been greatly appreciated.

Finally, I would like to thank the Science Research Council and the Ministry of Technology for my personal maintenance grants.

CONTENTS

INDEX TO FIGURE NUMBERS

GLOSSARY OF SYMBOLS

a	Domain Wall Width
a	Lattice Spacing
a	Thermodynamic Activity (Chapter 3)
A	Exchange Constant
B	Frequency Factor (Chapter 3)
C	Elastic Moduli
d	Stripe Domain Spacing
E	Total Magnetic Energy of a Body
E_{ex}	Exchange Energy
E_H	Field Energy
E_K	Anisotropy Energy
E_ω	Wall Energy
H	Total Local Magnetic Field
H'	Demagnetising Field
H_o	Applied Magnetic Field
J	Exchange Integral
k	Molecular Gas Constant (Chapter 3)
K	Reaction Equilibrium Constant (Chapter 3)
$K_1 K_2 K_u$	Anisotropy Coefficients
m	Mass of Atom (Chapter 3)
M	Gram Atomic Weight (Chapter 3)
M	Magnetisation
M_s	Saturation Magnetisation
n	Surface Normal
n	No. of Atoms/Spins per unit volume
N	Nucleation Rate (Chapter 3)

p	Vapour Pressure (Chapter 3)
r	Distance Vector
R	Molar Gas Constant (Chapter 3)
s	Spin Momentum per Atom
S	Surface Area
t	Film or Crystal Thickness
T	Absolute Temperature
x,y,z	Position Co-ordinates
$\alpha_1,\alpha_2,\alpha_3$	Direction Cosines
α	Supersaturation (Chapter 3)
γ	Wall Energy Density
ΔC_p	Constant Pressure Specific Heat (Chapter 3)
ΔG	Free Energy Change of a Reaction (Chapter 3)
ΔH	Enthalpy Change of a Reaction (Chapter 3)
ΔS	Entropy Change of a Reaction (Chapter 3)
λ	Magnetostriction Coefficients
λ_s	Distance (Chapter 3)
μ	Permeability
μ_o	Permeability of Free Space
ρ	Density
σ	Stress
σ	Surface Free Energy (Chapter 3)
τ	Volume
ϕ	Magnetostatic Potential
ϕ,θ	Angles

PREFACE

During the late 1950's and the 1960's the magnetic properties of thin polycrystalline ferromagnetic films were extensively investigated because of their potentiality for computer applications. Digital storage, fast switching achieved by coherent magnetisation rotation, and possible ease of fabrication made them initially very attractive.

Switching, however, did not always occur by coherent rotation and the possible reversal by domain wall motion introduced difficulties in the utilisation of these devices. Even the structure of the domain walls was found to show a complicated dependence on film thickness, making film parameters even more difficult to classify.

The majority of these films were prepared by the condensation of a vapourised metal beam on a glass substrate. A refinement of this process produced single crystal films by expitaxial deposition. Although this was of no commercial advantage, these films had crystalline anisotropies which gave rise to 90° as well as 180° walls. However, they suffered from strains and imperfections which a non-epitaxial method of preparing these crystals would avoid.

Such a technique for the growth of free-standing platelets was found by the vapour phase reduction of ferromagnetic bromides. This produced small facetted platelets with thicknesses in the range 0.1 - 10.0 μm, i.e. overlapping with the thin film thickness range. Much of the information gained from investigations on thin films therefore forms a background to a study of platelet properties.

Observations of magnetic domains, and the growth of these

platelets were first reported by De Blois (1965), and continued an earlier line of research into the properties of ferromagnetic whiskers. The thinner platelets showed regular and simple structures, as seen by the magnetic colloid collections but in thicker platelets these became very much more complex and stripe structures appeared.

This thesis describes further observations made on platelet domain structures, both as they are initially formed after growth, and as they behave in applied fields. The colloid technique used for these investigations suffers from the disadvantage that the surface collection can give a misleading interpretation of the underlying magnetic structure. This restricts the number of cases where direct comparisons can be made between observed domain configurations and theoretical calculations of such structures.

Some comparisons are made but further possible ones are prevented, largely through the inability to cope with the magnetostatic energy, which controls the magnetic behaviour of specimens the size of these platelets. An incomplete attempt to surmount this difficulty by an entirely numerical approach is included.

Although stripe domains have been observed in thin films, the sub-division of domains that occurs in the thicker platelets is more varied and interesting. The origin of the 'out of plane anisotropy' is crystalline and can therefore be assumed as known, unlike the thin film case. Yet despite this, many of the observations are not entirely explained because the Bitter colloid technique gives no clear indication of the internal magnetic structure.

The conditions necessary for the production of thin strain-free platelets suitable for these investigations are fairly stringent. It has therefore also been necessary to study the problems involved in obtaining one and two dimensional growth habits of ferromagnetic materials, by the process of vapour phase chemical transport reactions.

CHAPTER 1

THE THEORY OF DOMAINS IN FERROMAGNETS

INTRODUCTION

At the turn of the century it was common knowledge that the overall magnetisation of a suitably prepared ferromagnetic specimen could be changed from zero to a large saturation value by the application of a small field. This fact, however, was inconsistent with the Langevin theory of a paramagnetic gas, where thermal agitation prevents the large ordering influence of a small applied magnetic field.

Weiss (1907) modified the theory by postulating the existence of a large internal molecular field proportional to the magnetisation. This led to the prediction that all ferromagnets below their Curie temperature would be magnetised, even in zero field. Weiss overcame this difficulty by further postulating that, although saturated in small regions, overall demagnetisation was accomplished by the random orientation of these regions. The effect of an applied magnetic field was then to align these regions, or domains, to give a total saturation. The internal molecular field has subsequently been justified quantum mechanically by the exchange force, and domain theory understood in terms of magnetic field energies.

Indirect experimental evidence for the existence of domains first came in 1919 with the observation by Barkhausen that the application of a continuously varying field on a magnetic specimen produced discontinuous changes in magnetisation. Although at the time this effect was wrongly attributed to the rotation of magneti-

sation in whole domains, it is now known to correspond to irreversible movements of domain boundaries.

During the 1930's workers accepted the existence of domains as a basis for magnetisation curve explanations, but in this state the theory could only produce limited quantitative results. A theory of the transition layer separating adjacent domains was first proposed by Bloch (1932) who supposed the local spontaneous magnetisation to go through zero at the mid plane of the wall. On this basis he made the first calculation of the thickness and free energy of the transition layer, now known as the 'Bloch Wall'.

This work was superceded by the model of Landau and Liftshitz (1935) in which magnetisation of constant magnitude was assumed to rotate about an axis normal to the wall. Their calculation gave expressions for the direction of magnetisation at any point inside the wall, its thickness and its surface energy density. The paper is an important watershed, being one of the first calculations in micromagnetics.

In domains and domain wall calculations a model is postulated and its energy calculated, perhaps allowing one parameter to vary. Micromagnetic calculations however are performed by minimising the total free energy of a system with respect for the imposed constraints. It is a more basic and rigorous approach, treated fully by Brown (1962a and 1963), but is often insoluble without approximations. Observed domain structures should arise as a natural solution to micromagnetic problems correctly formulated. However, the theory has not yet reached the stage where it can be generally applied so domain calculations still play a very importart role in explanations of magnetic behaviour.

1.1 THE MAGNETIC FREE ENERGY

A necessary prerequisite to the understanding of domain configurations in magnetic materials is a knowledge of the various

factors contributing to the total magnetic free energy of a body.

1.1.1 Exchange Energy

In ferromagnets the magnetic moments of neighbouring electrons are coupled via an exchange interaction which tends to align them. This interaction operates between the uncompensated spins of partly filled 3d electron shells and appears as an extra term of electrostatic origin, not present in a classical treatment of the interaction between neighbouring atoms. This extra term is denoted by the expression for the potential energy of neighbouring spins of $-J\ \underline{S}_i \cdot \underline{S}_j$. S_i is the spin angular momentum of atom i measured in units of $\hbar$, and J is the exchange integral which is positive for ferromagnetic alignment. By considering only nearest neighbour interactions we may write the exchange energy E_{ex} as

$$E_{ex} = -\int 2\ J\ S^2 \sum_{i>j} \cos \phi_{ij}\ d\tau$$

where S is the total spin momentum per atom, ϕ_{ij} the angle between spin momentum vectors of atoms i and j, and $d\tau$ is an element of volume. If ϕ_{ij} is assumed small the exchange energy between each pair of spins is:-

$$\Delta E_{ex_{ij}} = J\ S^2\ \phi^2$$

The full expression for a cubic lattice as first proposed by Landau and Liftshitz (1935) is:-

$$E_{ex} = A \int \left[(\nabla \alpha_1)^2 + (\nabla \alpha_2)^2 + (\nabla \alpha_3)^2 \right] d\tau \qquad (1.1)$$

where α_1, α_2, α_3 are the direction cosines of the magnetisation vector and A, the exchange constant = $n\ J\ S^2/a$ for a lattice constant of a.

n = 1 for a s.c. lattice

= 2 for a b.c.c. lattice

= 4 for a f.c.c. lattice

The exchange constant cannot be measured directly but may be estimated from the Curie temperature where thermal energy is approximately equal to exchange energy; from a direct relationship with the constant in the Bloch law for the temperature dependence of the saturation magnetisation at low temperatures; or from spin wave resonance experiments. Although not discussed further the limitations (on calculations involving spin transitions such as domain walls) of an imprecise value for the exchange constant of materials is important.

This term then is a measure of the tendency of the spins, or magnetisation, in a ferromagnetic body to self align, and opposes variations in the magnetisation direction throughout the body. To give an estimate of the magnitude Kittel and Galt (1956) quote A for iron as 2.0×10^{-6} erg/cm.

1.1.2 Anisotropy Energy

Exchange energy was seen to arise from mutual spin interactions as an angular function of neighbouring spins. The complete spin system could adopt any angle with respect to the crystal structure without affecting the exchange energy. There is, however, an interaction between the electron spins and the crystal lattice which removes this degeneracy to make certain directions preferred. This results from the combined effects of spin-orbit interaction and partial quenching of the orbital angular momentum by inhomogeneous crystalline electric fields. Thus the free energy becomes a function of the orientation of the spontaneous magnetisation.

The effects of this anisotropy show up very markedly in the magnetisation curves of specimens which can be saturated with the expenditure of considerably less energy in some directions than in others. This gives rise to the terminology of easy and hard directions of magnetisation. There is a tendency for the anisotropy energy to be high for crystals with a lattice of magnetic ions of low symmetry, and low for crystals with high symmetry.

Phenomenologically this anisotropy may be expressed as a power series of the direction cosines of the magnetisation vector with respect to the crystal axes, the expression having the same symmetry as the crystal lattice to which it applies.

For cubic crystals

$$E_K = \int \left[K_1(\alpha_1^2\alpha_2^2 + \alpha_2^2\alpha_3^2 + \alpha_3^2\alpha_1^2) + K_2\alpha_1^2\alpha_2^2\alpha_3^2 + \ldots \right] d\tau \qquad (1.2a)$$

In this form with K_1 positive the cube edges are easy directions and the body diagonals hard directions, as in iron, with K_1 negative the directions are reversed, as in nickel.

For uniaxial crystals the magnetocrystalline anisotropy is more conveniently expressed in polar co-ordinates, even though the hexagonal nature of the basal plane symmetry of say cobalt is lost. This gives

$$E_K = \int \left[K_{u_1} \sin^2\theta + K_{u_2} \sin^4\theta + \ldots \right] d\tau \qquad (1.2b)$$

Anisotropy can also arise from other sources. Uniaxial anisotropy may be induced in some bulk ferromagnets by heat treating or cold rolling in a magnetic field, leading to materials of great technological importance. Polycrystalline films show several types of anisotropy, the most important being the M induced uniaxial anisotropy. The origins of this anisotropy are interesting and complex and the reader is referred to the reviews of Prutton (1964) and Cohen (1969) for a study of the various contributing mechanisms.

General reviews on magnetic anisotropy have been given by Chikazumi (1964) and Kanamori (1963). Anisotropy constants can be determined from magnetisation curves, Stoner (1950), by ferromagnetic resonance and by torque magnetometry; the last being the most accurate method. The most recent results obtained by torque magnetometry have been given by Franse and De Vries (1968) and Aubert (1968) for nickel and Franse (1969) for iron.

Values at 300°K

	K_1	K_2	
Fe	45	0	x 10^3 J/m^3
Ni	-5.7	-2.3	

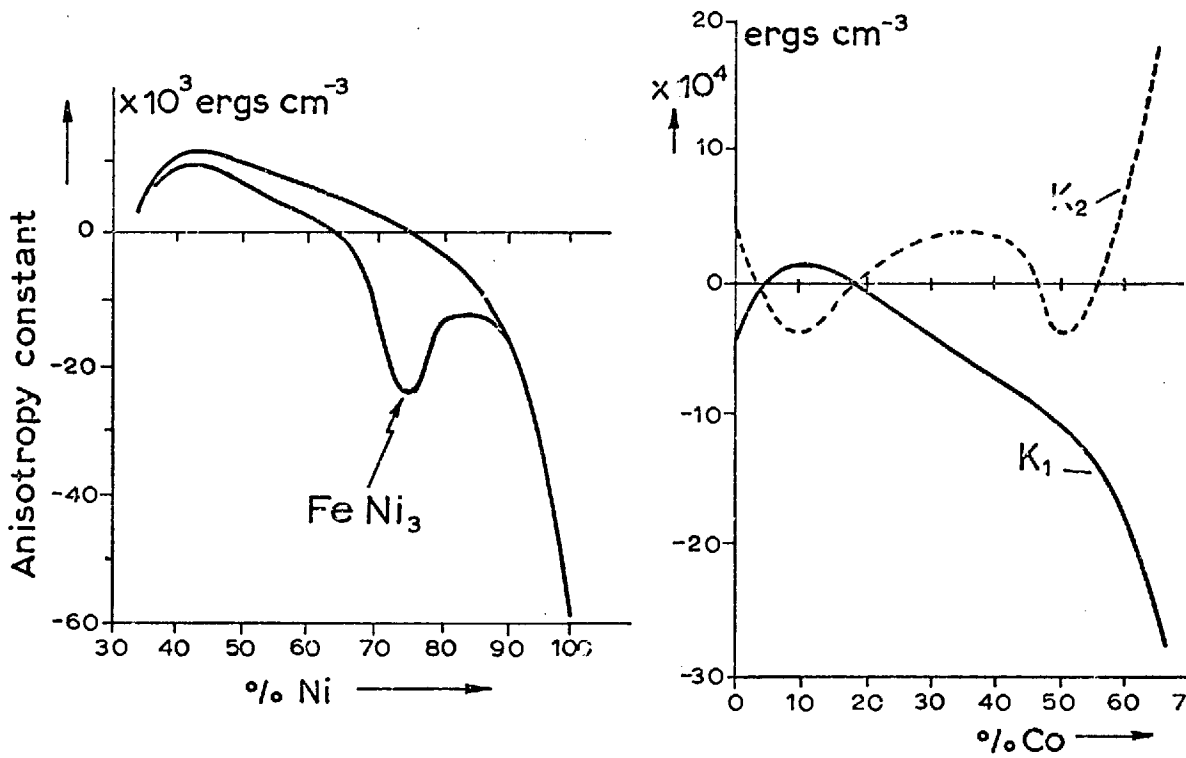

Fig. 1.1 Magnetocrystalline anisotropy in the Ni/Fe and Ni/Co systems. (At room temperature)

The specification of temperature is important because anisotropy constants are strongly temperature dependent, varying as the tenth or

higher powers of the saturation magnetisation. In alloy systems the anisotropy constants are functions of the alloy composition. This variation can be of great interest especially in low valued regions where the anisotropy is changing sign, as in, say, permalloy. FIG (1.1) shows the anisotropy values of the Ni/Co and Ni/Fe systems referred to later.

1.1.3 Magnetoelastic Energy

Like exchange energy anisotropy energy is dependent on the lattice spacing of the crystal, hence any change in spacing gives rise to a further contribution to the free energy. The magnetoelastic energy arises from the interaction between the magnetisation and the mechanical strain of the lattice, being defined zero for an unstrained lattice. Magnetostriction, the relationship between strain and magnetisation has been the subject of reviews by Lee (1955), Birss (1959) and Callen (1968). The preferred directions of domain magnetisation are thus controlled not only by the magnetocrystalline anisotropy but also by the strained regions within the material which effectively alter the directions of the anisotropy energy minima.

Kittel (1949) shows that under conditions of constant stress the lattice deforms and there is an increase in the anisotropy energy

$$\Delta E_{K_\lambda} = \int \left[\Delta K_1 (\alpha_1^2\alpha_2^2 + \alpha_2^2\alpha_3^2 + \alpha_3^2\alpha_1^2) \right] d\tau \qquad (1.3)$$

where $$\Delta K_1 = \frac{9}{4}\left[(C_{11} - C_{12})\lambda_{100}^2 - 2\, C_{44}\lambda_{111}^2 \right]$$

C_{11}, C_{12} and C_{44} are the elastic moduli

λ_{100} and λ_{111} are the magnetostriction constants.

For iron $\frac{\Delta K}{K} \sim 10^{-3}$ and for nickel $\sim 10^{-1}$

If for simplicity we assume isotropic magnetostriction λ_s, constant stress at an angle θ to the magnetisation, the expression for magnetoelastic energy reduces to

$$\Delta E_{K_\lambda} = \frac{3}{2} \lambda_s \sigma \sin^2\theta$$

However because of the approximations involved, this expression should be used with caution.

1.1.4 Magnetostatic Energy

By virtue of its own magnetic state any magnetic body possesses a potential energy arising from the interaction of its magnetisation with ambient magnetic fields. It is necessary to distinguish between applied fields $\underline{H}_o$ and fields from the magnetic material itself $\underline{H}'$, the total local field being given by

$$\underline{H} = \underline{H}_o + \underline{H}'$$

$\underline{H}_o$ is assumed to be unaffected by the body itself and in this work can be taken as uniform throughout. The energy from the applied field is

$$E_{H_o} = -\mu_o \int \underline{H}_o \cdot \underline{M} \, d\tau \qquad (1.4)$$

M is the magnetisation per unit volume. $\underline{H}'$ is the field arising from the magnetic body itself and in this type of work is most readily explained as arising from free pole effects. H' can be derived from the scalar magnetic potential ϕ: $H' = -$ grad ϕ.

In any element d the dipole moment is $\underline{M}$ d and the magnetostatic potential can, by analogy with the electrostatic potential, be written as:-

$$\phi = \frac{1}{4\pi} \int \underline{M} \cdot \text{grad} \left(\frac{1}{r}\right) d\tau$$

where differentiation is with respect to the co-ordinates of the volume element d

Using the vector identity

$$\text{div} \left(\frac{\underline{M}}{r} \right) = \frac{1}{r} \text{div } \underline{M} + \underline{M} \cdot \text{grad} \left(\frac{1}{r}\right)$$

we have

$$\phi = \frac{1}{4\pi}\int \text{div}\left(\frac{\underline{M}}{r}\right) d\tau - \frac{1}{4\pi}\int \frac{1}{r} \text{ div } \underline{M}\, d\tau$$

which, by using Gauss's divergence theorem, becomes

$$\phi = \frac{1}{4\pi}\int_S \frac{\underline{M} \cdot \underline{ds}}{r} - \frac{1}{4\pi}\int_V \frac{\text{div } \underline{M}}{r} d\tau \qquad (1.5)$$

showing that the potential can be attributed to an apparent surface distribution of magnetic charge $\underline{M} \cdot \underline{ds}$, and a volume distribution of density - div $\underline{M}$. This equation is of great importance in that it allows $\underline{H}'$ to be derived from given charge distributions, and will be referred to later. It is usually necessary to assume uniform magnetisation with div $\underline{M}$ = 0, but this is only true for ellipsoids where the demagnetising field is proportional to M, $H' = NM$, N being the demagnetising factor. Values for N along major semi-axes of various shaped ellipsoids are well tabulated, Osborn (1945) and Stoner (1945). For specimens which cannot be approximated to ellipsoids the application of equation (1.5) and numerical methods are dictated. But for every volume of material for which $\underline{H}'$ can be determined, the self energy will be

$$E_{H'} = -\frac{1}{2}\mu_o \int \underline{H}' \cdot \underline{M}\, d\tau \qquad (1.6)$$

Unlike H_o, H' will usually lie in a direction such that $\underline{H} \cdot \underline{M}$ is negative.

This then gives a total magnetostatic energy of

$$E_H = -\mu_o \int (\underline{H}_o + \frac{1}{2}\underline{H}') \cdot \underline{M}\, d\tau \qquad (1.7)$$

1.1.5 Domain Wall Energy

Energy arises at the boundary between domains from the magnetisation rotating out of an easy direction, showing a rapid variation with position etc. If complete micromagnetic calculations could be attempted this term would not be necessary, however it is in

fact more convenient with these sudden transitions to consider the energy of the domain wall as a separate entity. Various models have been proposed for the form that walls take in bulk materials or thin films, for varying physical properties. These will be discussed in the following sections of this chapter.

It suffices here to attribute an energy density to the wall area γ such that:-

$$E_\omega = \int \gamma \, ds \qquad (1.8)$$

where ds in an element of wall area.

1.1.6 The Total Free Energy

The magnetic energy of a sample may now be expressed as :-

$$E = E_{ex} + E_K + \Delta E_{K_\lambda} + E_H + E_\omega \qquad (1.9)$$

One or more of these terms may dominate according to the nature of the specimen, its shape, composition or physical state but the domain structure will adjust to produce a minimum in the free energy. Thus a specimen with a large anisotropy may adopt an equilibrium domain configuration with a high magnetostatic energy which would not have formed in a specimen of lower anisotropy. The minimisation of the total energy of a body computed from the above expressions should theoretically predict observed domain configurations. However because of its complexity this is seldom possible, although qualitative thinking based on these principles can be most rewarding.

1.2 DOMAIN WALLS IN BULK MATERIALS

Estimates of the energy and thickness of a Bloch wall were made by Lifshitz (1944) and Néel (1944), also by Kittel (1949a) using a simpler model. Kittel summed the exchange and anisotropy energies and found a minimum in the total energy as a function of wall width. From this he deduced a wall energy density and width given as:-

$$\gamma = 2\sqrt{AK}$$
$$a = \sqrt{\frac{A}{K}} \log \tan \theta \qquad (1.10)$$

where θ is the angle between the spin direction and the magnetisation in one of the bounding domains.

A typical value for the energy density γ is 1 erg/cm^2 with a width a of 1000 Å.

This solution only provides for a transition through 90° but by including the effects of magnetostriction it becomes possible to consider the 180° wall as being composed of two successive 90° walls. The solution is acceptable within its accuracy, which is limited by the importance which can be attached to the value of the exchange constant A. The effect of magnetostriction on the value of the wall energy is small but it does affect the spin orientation and hence the width. Also, if the magnetocrystalline anisotropy is low and the stress large magnetostriction effects contribute significantly to the wall parameters.

Earlier calculations were extended by Lilley (1950) to include walls in crystals, with uniaxial anisotropy and positive or negative cubic magnetocrystalline anisotropy, to give energies and widths of the domain boundaries in important directions. In addition the effect of the magnetoelastic anisotropy was also considered.

In bulk materials the nature of the wall types is basically very simple but the domain structures alter with the magnetic parameters of materials, showing great variety. Complications are introduced by the presence of inclusions, imperfections or strain within crystals, but the nature of the structures is still determined by the energy considerations outlined in the previous section. The multitude of reported observations on a wide variety of materials have been reviewed by Craik and Tebble (1965).

1.3 DOMAINS IN THIN FILMS

With the possibility of single domain particle behaviour, reversal by coherent rotation, and the report by Blois (1955) of an induced uniaxial anisotropy, thin magnetic films appeared to have good potential for digital storage. The realisation of this potential has not been easy and has raised many fundamental problems in magnetism. Many of the problems that have been encountered have centered around the behaviour of the domain walls which exist in films, their structure and their effect on hysteresis behaviour. These domain structures are a function of film thickness, physical structure and past magnetic history, and thus display considerable variety in properties. Polycrystalline films with uniaxial anisotropy have been subject to the greatest research effort and an understanding of the domains and walls in these films is a prerequisite to the study of domains, first in single crystal films and then in platelet crystals.

Reviews of all aspects of magnetic thin films have been given by Prutton (1964) and Cohen (1969). In addition two bibliographies have appeared listing the thousands of articles on the subject, Chang and Feth (1964) and Chang and Lin (1967).

1.3.1 The Bloch Wall

In bulk materials we saw that the transition in $\underline{M}$ inside the wall is accomplished by a rotation of $\underline{M}$ about the wall normal. No volume pole distribution is created, the ends of the wall are so far removed that the influence of the surface poles can be neglected and the normal component of $\underline{M}$ is continuous across the wall. The wall shape is then determined by a balance between exchange and anisotropy energies.

In a thin film the energy contribution of the magnetostatic field from surface poles can no longer be neglected and must be included in the energy sum to be minimised. However, in order to

estimate the stray field energy the magnetisation distribution in the wall must first be known, yet this itself is influenced by the stray field. One method of avoiding this situation is to postulate a magnetisation distribution inside the wall and to base calculations on this distribution. Although distributions have been proposed by several workers the first and simplest due to Néel (1955) is still the most widely used, in a modified form due to Middelhoek (1961).

A 180° wall parallel to the easy axis of a uniaxial film is considered, ϕ is defined as the angle between the magnetisation and the film normal in the plane of the wall, and x the co-ordinate normal to the wall. The rotation is shown in FIG (1.2a).

$$\begin{aligned} \phi &= -\frac{\pi}{2} && \text{when} && x \leqslant -\frac{a}{2} \\ &= \pi\frac{x}{a} && && -\frac{a}{2} < x < \frac{a}{2} \\ &= \frac{\pi}{2} && && x \geqslant \frac{a}{2} \end{aligned} \qquad (1.11)$$

Straightforward account is taken of the exchange and anisotropy energies, and the stray field energy is calculated by approximating the wall to a cylinder with elliptical cross section, seen in FIG (1.2c).

This gives an expression for the energy per unit area of a Bloch wall as

$$\gamma_B = A\left(\frac{\pi}{a}\right)^2 a + \frac{1}{2} a K_u + \frac{\pi a^2}{a + t} M_s^2 \qquad (1.12)$$

K_u is the uniaxial anisotropy, t the film thickness.

γ_B can be minimised with respect to a and the resulting value reinserted to obtain the actual value of γ_B. The equations do not give a simple analytical expression, except when t $\ll$ a and t $\gg$ a, and have to be evaluated numerically.

For t$\gg$a, i.e. bulk material, the results give :-

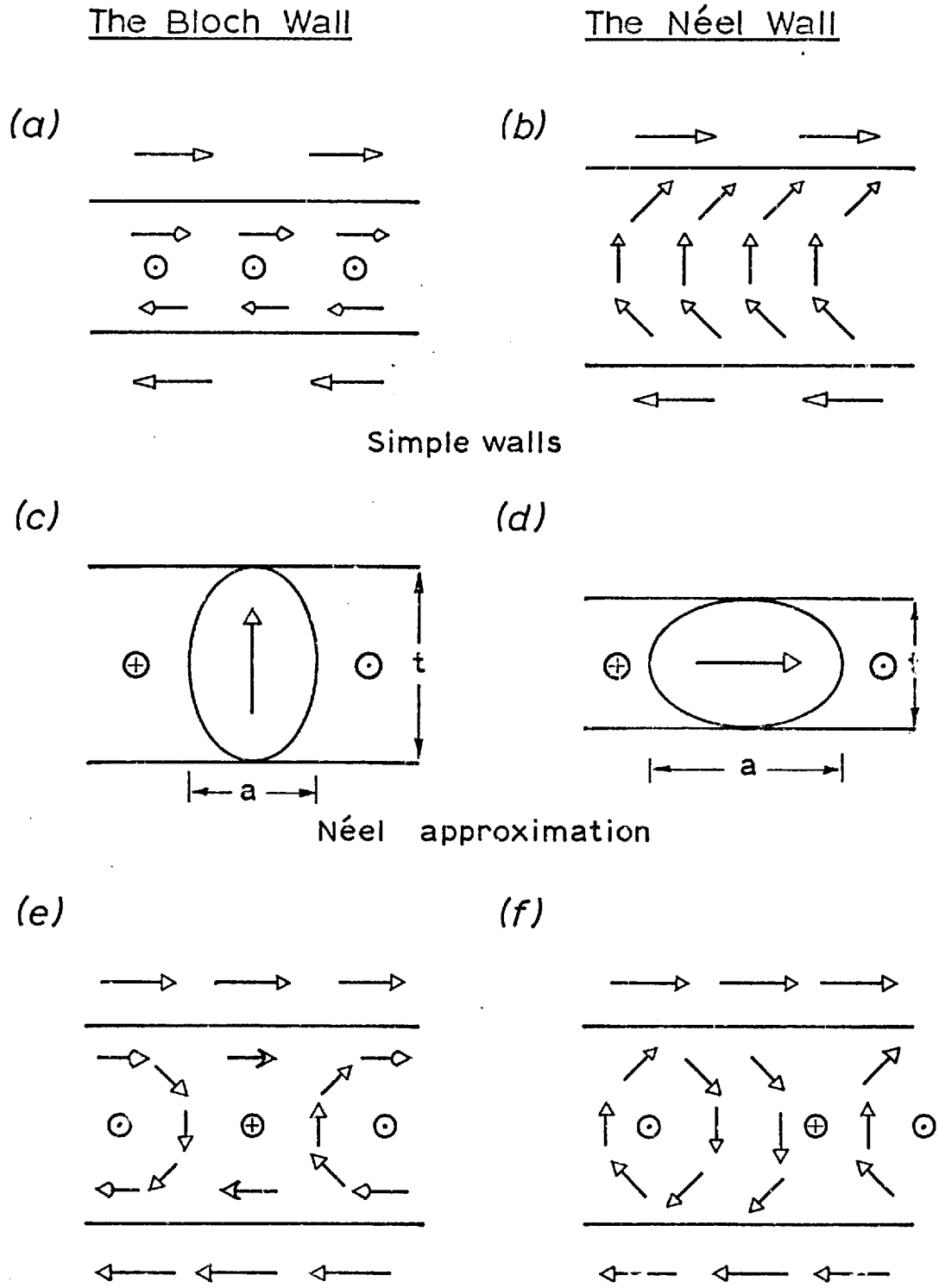

Fig. 1·2 Simple wall models

$$\gamma_B = \pi\sqrt{2}\sqrt{AK_u}$$
$$a_B = \pi\sqrt{2}\sqrt{\frac{A}{K_u}} \qquad (1.13)$$

These may be compared with the exact solutions for a Bloch wall determined from the tangent to the theoretical spin orientation at the middle of a bulk wall

$$\gamma_o = 4\sqrt{AK}$$
$$a_o = \pi\sqrt{\frac{A}{K}} \qquad (1.14)$$

The variation of wall energy and width with film thickness is found by successive numerical evaluation and illustrated graphically in FIG (1.3). It is found that the Bloch wall energy can be one or two orders of magnitude higher in very thin films than the value in bulk material.

1.3.2 The Néel Wall

Néel (1955) showed that below a certain film thickness, with increasing magnetostatic energy, the Bloch wall becomes energetically unfavourable compared with a distribution where $\underline{M}$ rotates in the plane of the film. No surface poles are produced but a volume pole distribution is formed within the film at the edges of the wall, and the normal component of $\underline{M}$ is no longer continuous.

As before $\qquad \phi = \pi\frac{x}{a} \qquad -\frac{a}{2} < x < \frac{a}{2}$

but now ϕ is the angle between the magnetisation and a direction normal to the wall in the plane of the film. The rotation is seen in FIG (1.2b). Again the wall is approximated by an elliptic cylinder, but this time it lies in the plane of the film, FIG (1.2d), so that the energy density is

$$\gamma_N = A\left(\frac{\pi}{a}\right)^2 a + \frac{1}{2}\,a\,K_u + \frac{\pi\,a\,t}{(a+t)}\,M_s^2 \qquad (1.15)$$

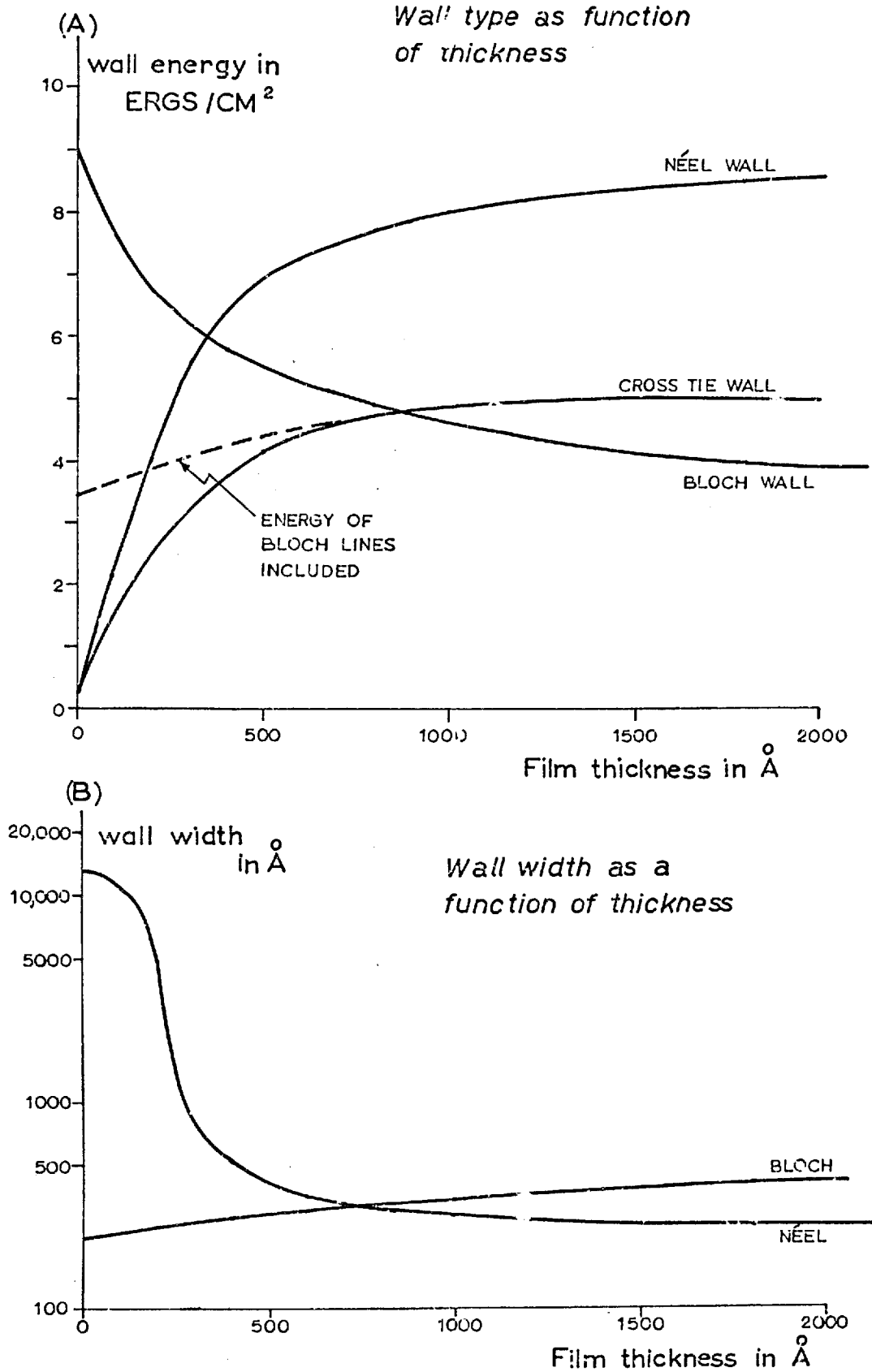

Fig.(1.3) Wall energy and width in uniaxial films (after Middelhoek)

As in the case of the Bloch wall the expression can be minimised but does not lead to a simple analytical expression and the results have to be numerically evaluated. For very thin films, $t \ll a$, we can approximate to get

$$\gamma_N = \pi \sqrt{2} \sqrt{AK}$$
$$a_N = \pi \sqrt{2} \sqrt{\frac{A}{K}} \qquad (1.16)$$

The similarity of the result with (1.13) is to be expected from stray field energy considerations. The variation of wall energy and width with film thickness are again illustrated graphically in FIG (1.3). It will be noticed that in the thickness range where the Néel wall becomes energetically favourable the width has increased by an order of magnitude.

The structure and behaviour under fields of Néel walls has been observed with Lorentz microscopy, (see section 2.3.3), by Feldtkeller and Liesk (1962). Lorentz microscopy measurements by Fuchs (1961) on permalloy films have shown that the uniform rotation model used by Middelhoek is less applicable to Néel walls than to Bloch. He found that the magnetisation changed very rapidly near the centre of the wall, passing through 80° in only 400 Å, the remaining 100° rotation occurring over a much larger distance to give a total width near 6000 Å. Further discussion of this will appear later.

1.3.3 Orientation Dependence of Wall Energy

So far we have only considered domain walls between anti-parallel domains, and in the absence of external fields these are the only stable structures in uniaxial films. The application of hard axis fields however removes this restriction and the change in wall energy with angle must be considered. A more general type of wall is taken as bisecting the magnetisation in two domains making angles θ_o and $-\theta_o$ with the centre of the wall. Again we use equation (1.11) to define ϕ.

For a Bloch wall the anisotropy contribution is much less than the exchange or magnetostatic energies and can be neglected. The magnetisation can be considered as turning on a cone shaped shell, thus making the total angle through which it turns $\pi\cos\theta_o$. So we can write the exchange energy

$$E_{ex} = A\left(\frac{\partial\theta}{\partial x}\right)^2 = A\left(\frac{\pi\cos\theta_o}{a}\right)^2$$

The component of $\underline{M}$ normal to the film plane is $M\sin\theta_o$ and this gives a stray field energy of $(\pi\ a\ t/(a + t))\ M^2\ \sin^2\theta_o$.

By summing these two terms and minimising with respect to the wall width Middelhoek expressed the energy as a function of the 180° wall energy.

$$\gamma_{B\theta_o} = \gamma_{B\pi}\cos^2\theta_o \qquad (1.17)$$

But as θ_o approaches $\frac{\pi}{2}$ the equation begins to lose its validity.

The angular variation of Néel wall energy can also be found by a similar method although in this case the magnetostatic energy alone is the dominating factor. Repeating the calculations Middelhoek derived the variation with respect to the 180° walls as

$$\gamma_{N\theta_o} = \gamma_{N\pi}(1 - \sin\theta_o)^2 \qquad (1.18)$$

These variations of Bloch and Néel wall energy densities are displayed graphically as a function of the angle θ_o in FIG (1.4), and the stabilities at given film thicknesses and angles shown in FIG (1.5).

1.3.4 Néel and Bloch Lines

The energy of walls can be lowered in certain circumstances by the inclusion of Néel lines in Bloch walls or Bloch lines in Néel walls.

In a sub-divided Bloch wall regions where the magnetisation rotates in a left handed sense are separated from regions with a right handed rotation by a transition region. The centre of this transition

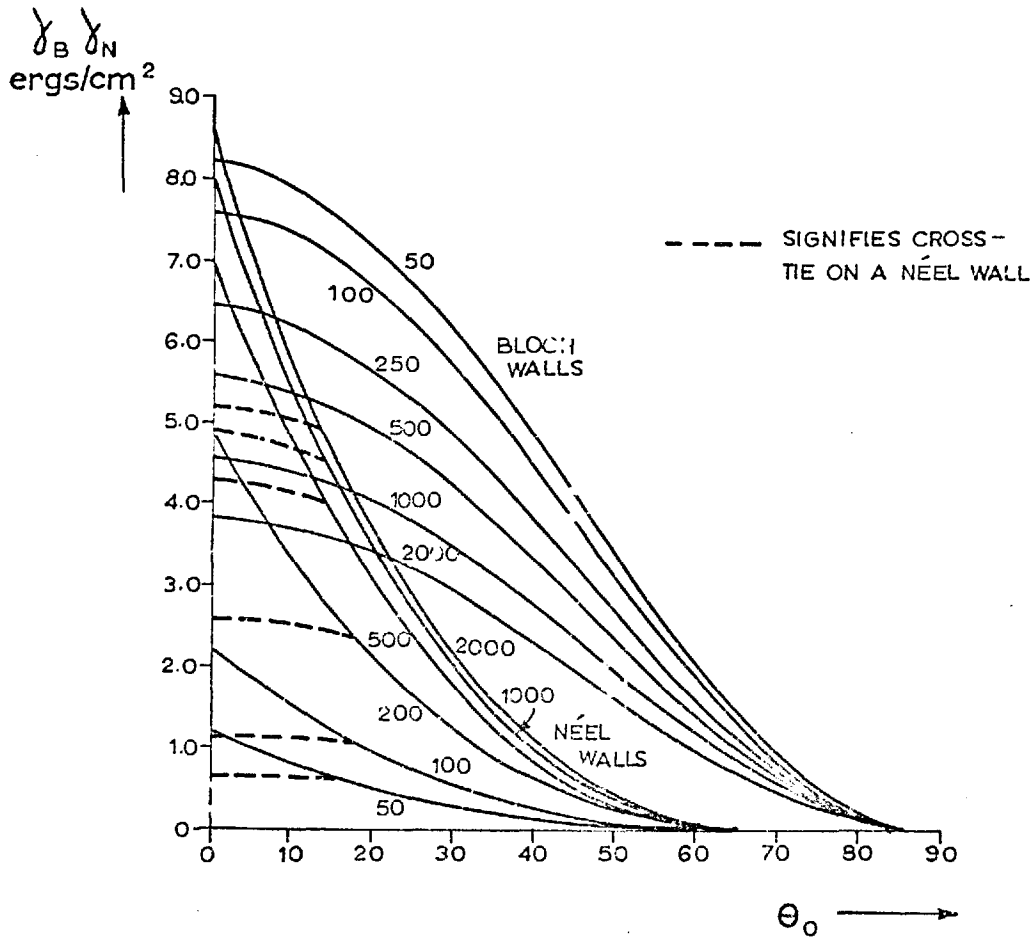

Fig.(1.4) Wall energy as function of angle

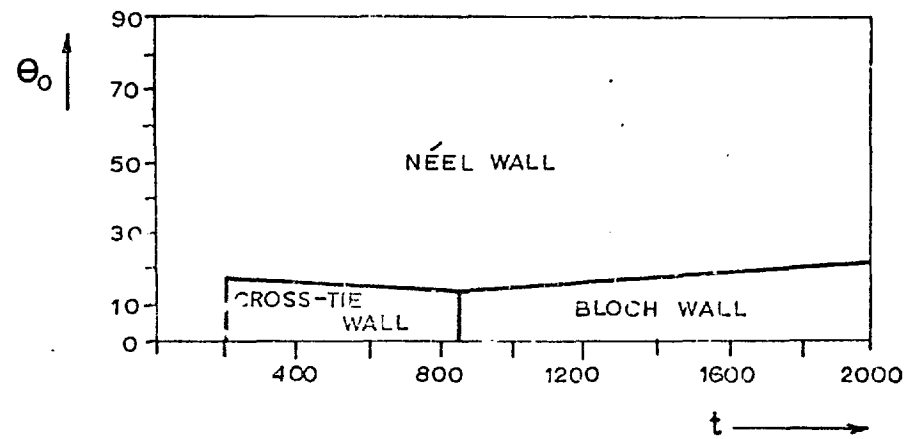

Fig.(1.5.) Stability of wall type as function of thickness and magnetisation angle

region is effectively Néel in form as seen in FIG (1.2e). Sub-divided Bloch walls were first reported from observations on Perminvar by Williams and Goertz (1952), and on iron whiskers by De Blois and Graham (1958). Harrington (1958) from his work on silicon iron considered simultaneous spin transitions along two axes. He predicted the presence of alternating polarities from his general equations for the magnetisation directions and assumed the changes which occurred along the wall length to be gradual.

Shtrikman and Treves (1960a & b) treated De Blois and Graham's results by considering the wall as being a sub-domain structure itself and showed how their observed displacement of different sections of a wall could be explained by relative movements of the sections near the surface, to lower the magnetostatic energy. A more elaborate model was produced by Bhide and Shenoy (1963), using gradual spin transitions, which gave better agreement with the observed spacing of sub-divisions. The energy density, however, is high, which accounts for the infrequent appearance of this type of structure, but is also a limitation of the model. Finally, Janak (1966) extended the Shtrikman and Treves approach and showed that the energy gain of Bloch wall subdivision would only be favourable if the anisotropy of the material involved was sufficiently low.

Bloch lines in Néel walls play a very important part in the structure of Cross-Tie walls as we shall see in the next section, and have been studied by Feldtkeller (1961) and Feldtkeller and Thomas (1965). Parts of a Néel wall in which the magnetisation rotates clockwise and anti-clockwise are separated by a transition region in which the magnetisation points vertically out of the film plane. This gives it a Bloch character with attending surface charging, see FIG (1.2f). Feldtkeller and Fuchs (1964) have shown how a mixed wall can be formed by the enlargement of the Bloch or Néel lines into small sections of wall, as seen in FIG (1.6), and Feldtkeller (1965) has paid attention to the energies of these point singularities.

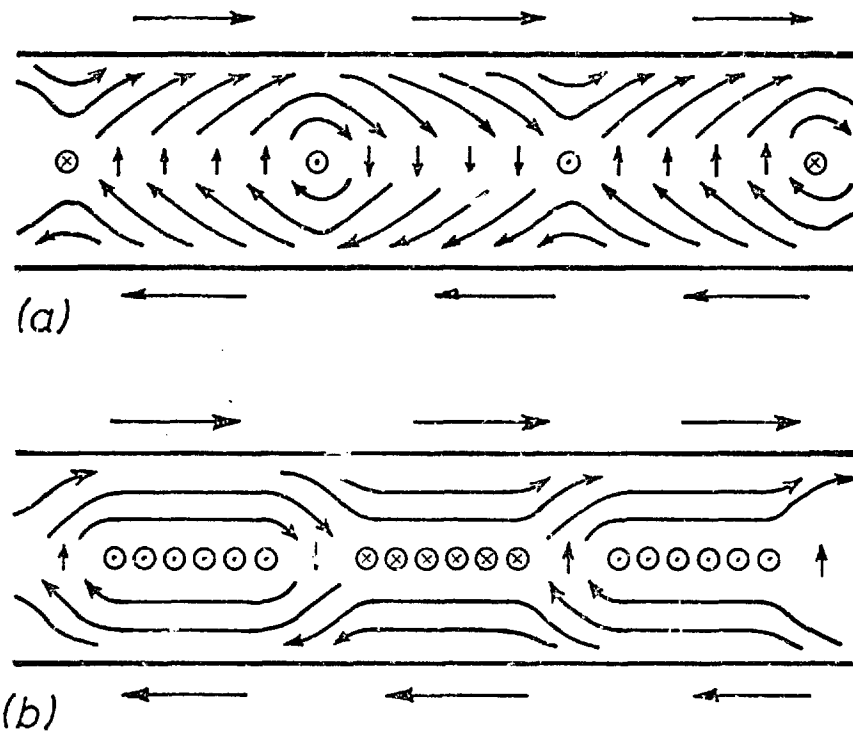

Fig. 1·6 (a) Bloch segments in Néel wall
(b) Néel segments in Bloch wall

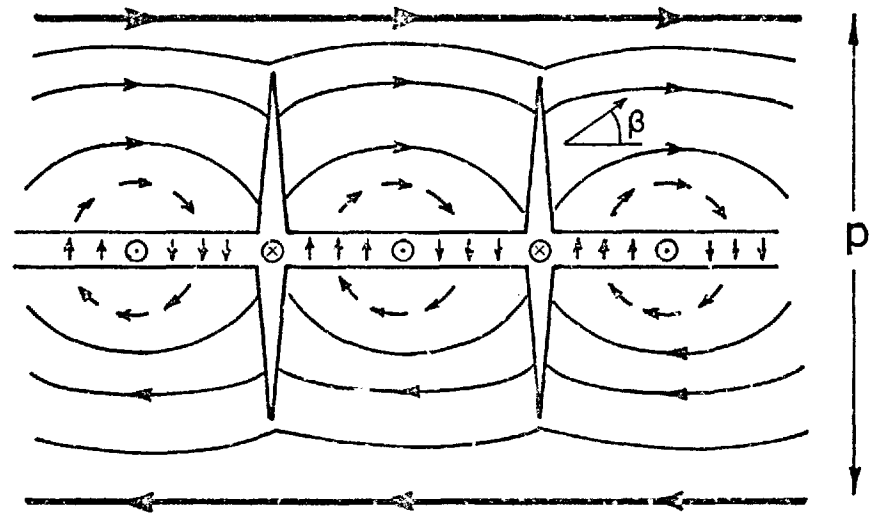

Fig. 1·7 The cross tie wall

It is possible for Bloch lines to behave independently of the walls and interaction between lines and walls can lead to the formation of 360° walls. The Barkhausen jumps which lines make under alternating fields contribute to the phenomenon of creep, Kayser (1967) and Torok et al (1969), a hazard of thin film storage. This type of wall hysteresis has been observed by Lorentz microscopy (Cohen, 1965).

1.3.5 The Cross Tie Structure

We have shown that with decreasing film thickness the Bloch wall is replaced by a lower energy Néel wall structure, with FIG (1.3) showing a definite thickness for the transition to occur. By equating Bloch and Néel wall energies Middelhoek derived an approximate expression for this transition thickness as

$$t_{trans} = \frac{2.5\sqrt{A}}{M_s} \qquad (1.19)$$

The actual change over however is not sudden and an intermediate structure, known as a Cross-tie wall, was first observed by Huber et al (1958) on permalloy films and later by Fuller and Rubinstein (1959) and Rubinstein and Spain (1960). High resolution Bitter patterns were obtained by Moon (1959) and the structure confirmed with Lorentz microscopy by Fuchs (1962).

A Néel wall broken into segments by Bloch lines, to provide greater flux closure, forms the basis of a Cross-tie wall, but this simultaneously gives localised fields at alternate Bloch lines in opposition to the magnetisation direction. Closure is thus made between every second segment with the rapid change in magnetisation at alternate segments leading to the Cross-tie colloid collection, see FIG (1.7).

Due to the complexity of the cross-tie structure exact evaluation of the energy is impossible but by making suitable approximations Middelhoek derived an expression for the energy of the wall as:-

$$\gamma_{CT} = 0.6\,\gamma_{N\pi} \qquad (1.20)$$

and length of cross-ties p as

$$p = 1.6\left[\frac{\gamma_{N\pi} - t\,M_s^2}{K_u}\right] \qquad (1.21)$$

The length of the cross-ties reach a maximum when t$\sim$400 Å. Up to this thickness $\gamma_N \propto t$ thus making p proportional to t, but at greater thicknesses γ_N increases more slowly and p consequently decreases.

We see from FIG (1.3) that at t = 900 Å a transition from Bloch to Cross-tie walls is expected but no transition from Cross-tie to Néel as the Cross-tie energy is always more favourable. No allowance has been made, however, for the energy of the Bloch lines which separate the positive and negative Néel wall segments. The energies of Bloch lines, like the walls, increase with decreasing film thickness and if this energy is now included in the total Cross-tie energy the Neel wall appears as a more favourable configuration below 200 Å.

Under the influence of hard axis fields the angle through which the magnetisation turns increases in one type of section but decreases in the other. This would have the effect of keeping the wall energy constant were it not for the Bloch lines which are not fixed but move so as to decrease the total energy. The angular variation can thus be expressed in similar terms to the Bloch wall as

$$\gamma_{CT\theta_o} = \gamma_{CT\pi}\cos^2\theta_o \qquad (1.22)$$

Prutton (1960) devised a model using the equations of Harrington (1958) but these gave a Néel structure to the centre of the Cross-tie, which from subsequent Lorentz microscopy was found not acceptable. More recently Mohiuddin (1966) has extended Cross-tie calculations to thin foils but again had difficulty in accounting for the Bloch line energy.

Finally, mention must be made of the work of Gomi and Odani (1960) who examined the effect of scratches parallel to the easy axis of films in the Cross-tie thickness range. These films showed interesting flux closure patterns across the scratches to give chain and displaced Cross-tie wall structures.

1.3.6 Intermediate Walls

The gradual transition between wall types as a film thickness varies has been observed experimentally by Methfessel et al (1960). For values of $t > 1000$ Å the lowest energy state is the Bloch wall with sections of opposite polarity separated by Néel lines. The energy gain from Néel lines is not large because most of the flux closure occurs outside the film. As t decreases below 900 Å Néel walls begin to have comparable energies and Cross-tie structures form around the small Néel sections. With further decrease true Cross-tie walls are formed which eventually become pure Néel walls as the energy of the Bloch lines rise.

When a hard axis field is applied the magnetisation vectors on either side of a wall turn away from a 180° angle and both Cross-tie and Bloch walls transform into Néel walls, see FIGS (1.4 and 1.5). Under a.c. fields a hysteresis occurs in this effect Middelhoek (1962) which causes deviations from the expected hard axis loop. It also extends the range over which various wall types are expected, Middelhoek (1963).

More recently the film thicknesses at which various wall structures are expected were thought to be less well defined, and the type of structure more diffuse. Torok et al (1965) have shown by Lorentz microscopy that the Néel to Bloch transition is gradual with Néel and Bloch components superposed to give a hybrid of the two, an intermediate structure. They also conclude that there exists a critical angle θ_c for films of any given thickness such that walls with $\theta_o \geqslant \theta_c$ are of pure Neel type and walls with $\theta_c > \theta_o > 0$ are of an

intermediate type. This angle θ_c increases with increasing thickness. Finally, only when $\theta_o = 0$ do the walls become pure Bloch, and then they are unstable and degenerate into intermediate walls, with the Néel component changing direction by 180° periodically along the wall to give a Cross-tie like structure.

From low angle diffraction patterns (see p.51) Ricker (1968 and 1969) has suggested a spin distribution for 180° walls in films of intermediate thickness. The wall consists of an extended outside or tail region of Néel type in which the magnetisation vector rotates within the plane of the film, until a transition angle ϕ_o is reached. In the small kernel of the wall the magnetisation turns out of the film plane on a cone shaped shell, i.e. like a Bloch wall under the influence of a hard direction field. This field component is generated by the rotated magnetisation in the Néel type region. As the film thickness increases ϕ_o decreases, reaching zero as t approaches 1000 Å.

A different and interesting approach was adopted by Wang (1968) who approximated the spin configuration in a transition layer by a generalised functional form of spiral. Equilibrium wall widths and energies were obtained by minimisation of the total energy. For each case the cone angle provided an additional parameter with external conditions causing the spins to follow a different cone angle. From the results a phase plot was given for a 180° Néel wall of wall width against film thickness for different helices.

1.3.7 Domains in Single Crystal Films

By deposition on heated single crystal substrates it has proved possible to obtain single crystal films by epitaxial growth. Cleaned or polished crystals of NaCl, LiF or MgO have enabled films of Fe, Ni or Co to be grown by Gondo and Funatogawa (1962) and Sato and his co-workers (1962, 1963, 1964). More recently improved epitaxy has been obtained by Blackburn and Ferrier (1968) using PbTe coated substrates.

(100) films of iron show biaxial anisotropy with the third magnetocrystalline axis suppressed by shape anisotropy. Domain structures form with both 180° and 90° walls to give checkerboard type patterns which decrease in size with decreasing film thickness because nucleation of domains becomes more sensitive to imperfections.

Cross-ties are found to form on 180° walls but not on 90° walls. One reason is that on 90° walls this would entail the introduction of 270° segments which would only increase the energy of the wall. Blackburn and Ferrier (1968) showed that in iron films the energy of the 90° Neel wall is substantially lower than the 180° wall and thus unlike the polycrystalline case there is less tendency to form Cross-tie sections. However, they assumed the 90° wall to be completely Néel which need not be the case and the energy difference is probably not as great as they predicted.

F.C.C. cobalt films have also been deposited in the (100) orientation and show similar patterns to the iron films, but rotated through 45° indicating the negative anisotropy coefficient of cobalt in this phase.

Domains on nickel films have been much more difficult to observe. This probably due to the higher magnetostriction and consequent sensitivity to the strain, inherent from lattice mismatching. The presence of negative biaxial anisotropy modifies the Middelhoek equations for domain wall energy. Equations (1.12 and (1.15) now become, from Appendix (A)

$$\gamma_{B\pi} = A\left(\frac{\pi}{a}\right)^2 a + \frac{7}{32} K_1 a + \frac{\pi a^2}{a + t} M_s^2 \qquad (1.23)$$

$$\gamma_{N\pi} = A\left(\frac{\pi}{a}\right)^2 a + \frac{1}{8} K_1 a + \frac{\pi a t}{(a + t)} M_s^2 \qquad (1.24)$$

The variation of wall width and thickness as a function of film thickness is shown for nickel in FIG (1.8).

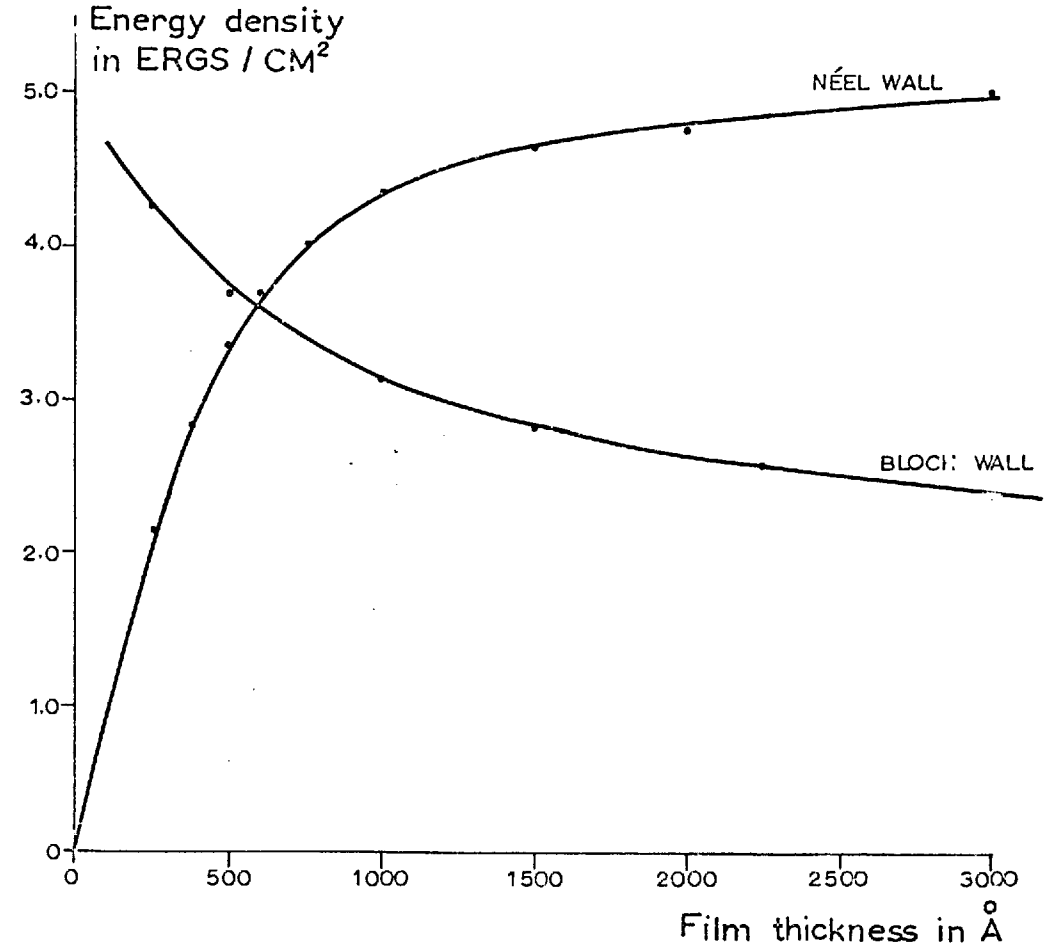

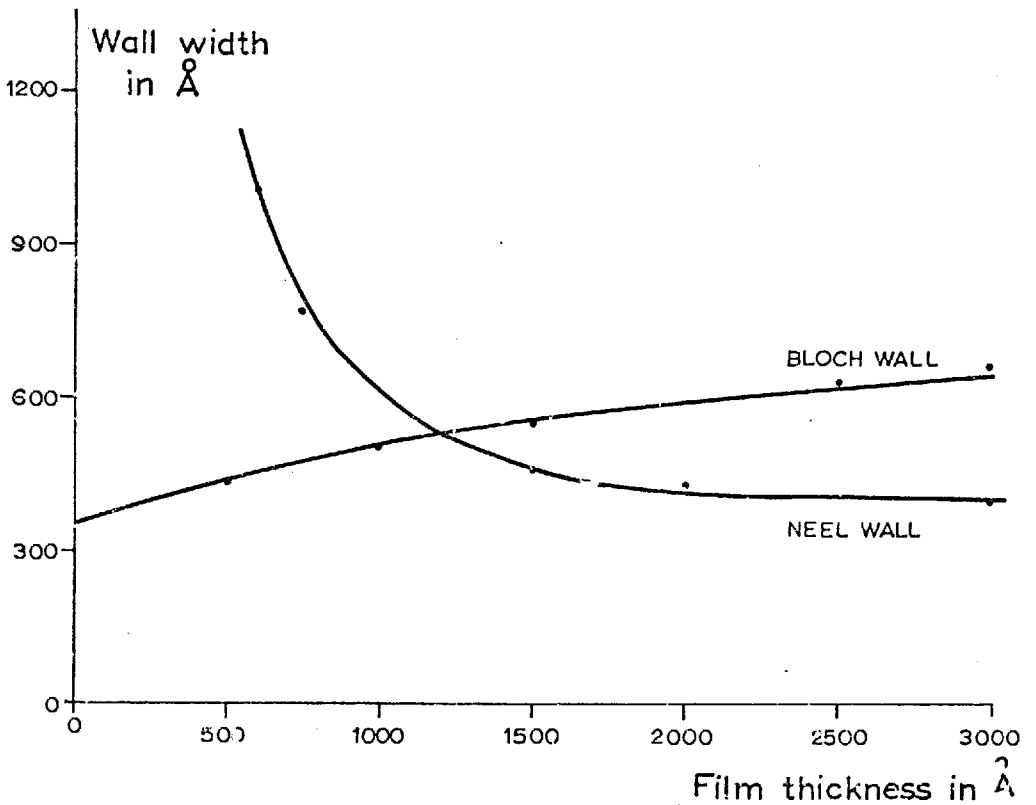

Fig. (1.8.) Wall energies for negatively biaxial anisotropy

Kaczer (1957) has made calculations for Bloch walls using a more rigorous derivation of the stray field energy and obtaining expressions for the energy density of 180° and 90° walls. He finds, in agreement with Middelhoek,

$$\frac{\gamma_\pi}{\gamma_{\pi/2}} = 2$$

1.3.8 Domain Substructures

It was tacitly assumed at the beginning of this chapter that the magnetisation within a domain was uniform. However, from their investigations by Lorentz microscopy, Fuller and Hale (1960) found that on a microscopic scale the domain magnetisation was non-uniform. Defocussed electron micrographs showed patterns of intensity variation which were interpreted as local in-plane angular variations of the magnetisation called RIPPLE.

Two possible configurations which would give rise to the observed striations on micrographs are called longitudinal and transverse modes

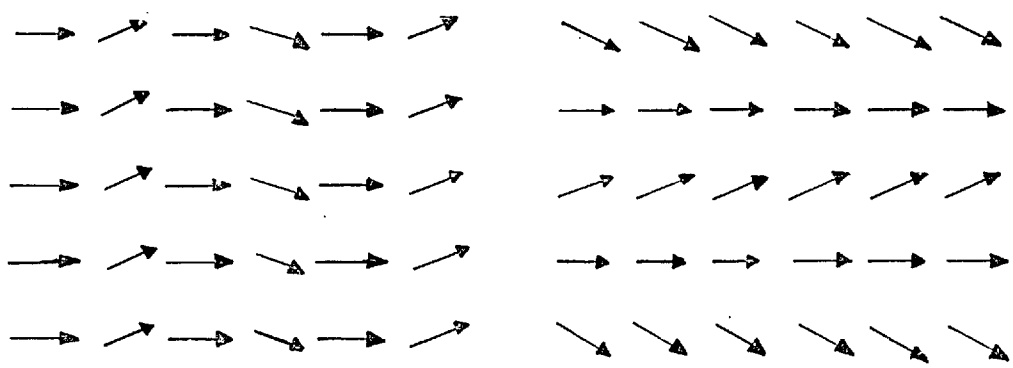

The exchange energy density for the two modes is similar but the longitudinal mode has a lower magnetostatic energy and is thus more favourable. Ripple is thought to arise from the variations in the local anisotropy and is thus intimately connected with the structural and magnetic variations encountered in thin films. This

makes the theoretical treatment of ripple complicated from the nature of the models used. The current state of ripple theories has been recently reviewed by Leaver (1968) and Hoffmann (1968). The effect of ripple variation is greatly reduced through the diminished local anisotropy variations of single crystal films, Spain and Pulchalska (1964).

Ripple is usually small enough to have only secondary effects on the hysteresis properties. However, films produced under slightly non-standard conditions show strange properties, e.g. inverted films, with wall coercivity larger than rotational coercivity, can show Néel walls forming normal to the easy axis.

Films with negative magnetostriction can give mottled Bitter patterns above a critical thickness arising from an out of plane easy axis. This disappears when the film is removed from its substrate, showing how film stresses affect the easy axis. These films also show rotatable initial susceptibility (R.I.S.). R.I.S. films demonstrate similar hysteresis loops in all directions and from studies by Cohen (1962) appear to fall into two types.

The importance of R.I.S. films lies in the tendency of thicker samples to demonstrate stripe domain patterns. These stripe domains form structures rather like ripple structures but in a direction normal to the film plane. These will be discussed in greater detail when we come to study the domain patterns obtained from thicker platelets, Chapter 6.

1.4 DOMAINS IN WHISKERS

A precursor to the studies on platelets, described in this thesis, were the investigations made in the late 1950's on the properties of whiskers. Reduction of ferrous chloride by a very dilute stream of hydrogen (see Chapter 3) gave whiskers with smooth strain free surfaces in simple crystallographing orientations, ideal

for domain investigation.

Domains in <100> Fe whiskers were first studied by Coleman and Scott (1957, 1958) who noted the simple structures with complete flux closure. They studied the wall movement with Bitter colloid under longitudinal and transverse fields up to 200 oe where domains could no longer be seen.

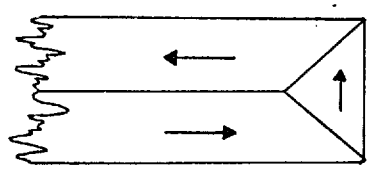

SIMPLE
END CLOSURE

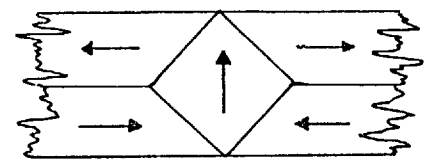

CLOSURE AFTER
TRANSVERSE FIELD

Fowler et al (1960, 1961) using Kerr effect studied the end closure structures which were found to persist up to at least 5 k.oe., thus reducing the large demagnetising fields which would otherwise form at the corners. Shtrikman and Treves (1960c) used these results to provide an explanation for Brown's paradox

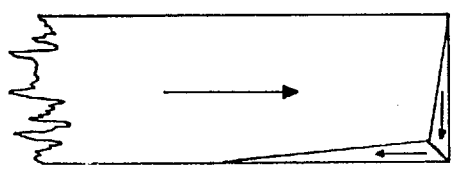

HIGH
FIELD
CLOSURE

De Blois and Graham (1958) studied the effect of stress on whiskers of this same orientation. Axial compression introduced an easy axis normal to the stress and the direction of magnetisation of the domains was seen to change until all that remained was a Bloch line along the centre of the whisker, as shown overleaf. When a whisker was bent opposite faces came under tension and compression and a serrated domain wall appeared along the neutral axis, flux closure being made internally.

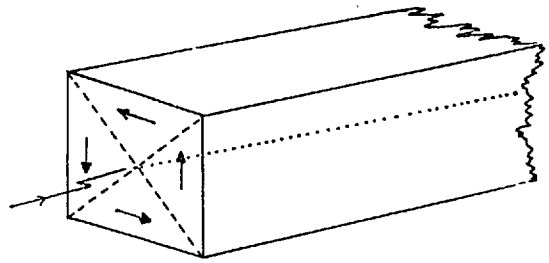

EFFECT OF
COMPRESSIVE
STRESS

<111> axis whiskers with (110) faces have also been studied by Coleman and Scott. These whiskers have a hexagonal cross section but cubic end faces which show interesting closure patterns

HEXAGONAL
CROSS
SECTION

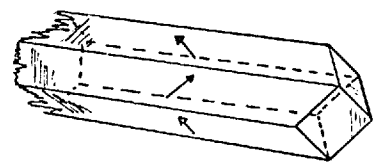

CUBIC
END
FACES

These patterns have been explained by Kaczer and Gemperle (1959a) by postulating the existence of one or two domain walls which do not appear on the surface of the material. Later (1959b) this work was extended to the more complicated case of cobalt whiskers.

1.5 DEVELOPMENTS IN DOMAIN WALL THEORY

Several theoretical objections can be made to Middelhoek's treatment of Bloch and Néel walls which subsequent workers have attempted to circumvent. As we have seen Middelhoek assumed $\underline{M}$ to rotate linearly across the wall and estimated the magnetostatic energy E_H' from an ellipsoidal cylinder. The resulting total energy was minimised with respect to the wall width parameter. It is apparent that E_H' is not calculated from the same magnetisation distribution as the other terms and the final result could be too high or low.

Furthermore, no indication of the wall structure is given because it is an a priori assumption of the model. Thus intermediate structures cannot emerge as minimum energy configurations at any stage.

The primary difficulty in any wall calculation lies in estimating the stray field energy. Dietze and Thomas (1961) used a parametric form for the M distribution, $\cos \phi = a^2/(a^2 + x^2)$ which allowed a precise analytic expression to be included for the stray field, thus overcoming the first objection to Middelhoek's work. The total energy was summed and minimised with respect to the wall width giving the energy as a function of thickness. Feldtkeller (1963) by using two parameters was able to obtain lower values for the wall energy, thus illustrating a drawback of the method. Although a functional form can be chosen so that all energies can be calculated analytically there is no assurance that the true distribution is even a close approximation to the class of functions being considered.

Brown and La Bonte (1965) circumvented this difficulty by replacing the continuous by a discreet distribution for which the static energy can be exactly calculated. The wall is divided into cells in which M is constant but may have varying orientation, and the conditions for minimising the total energy found by variational methods. The resulting equation is then used to find the equilibrium structure. The method shows that the magnetostatic field due to the main reversal is such that at the outer edges of the Bloch wall M is reverse rotated to give a component normal to the plane opposite to that in the centre. It is hence possible for external field lines to begin and terminate on the same side of the film thus lowering the magnetostatic energy. For Bloch walls the energy versus thickness curve is parallel to Middelhoek's but at lower energy values.

With the number of cells used it was found that the solution of the Néel wall calculation did not converge but certain factors emerged. The Néel distribution was found to be very dependent on the wall width to film thickness ratio which, if sufficiently large,

showed the Néel wall to be more favourable than the Bloch wall. The transition was predicted at 700 Å which is closer to observations than Middelhoek's 350 Å. In addition the long Néel tail was predicted in agreement with Lorentz observations.

Aharoni (1966a) replaced Brown's expression for the magnetostatic energy by a plausible approximation, later justified. Using this he was able to obtain an energy for the Bloch wall in good agreement with Brown and La Bonte's result. The calculation was extended to the Néel wall giving values at the most a few percent below previous estimates, but predicting a functional form for the tail distribution as tanh(x/a).

Later Aharoni (1966b) extended the calculation to embrace the cross-tie type structure. He calculated E_{ex} and E_K analytically and obtained an overestimate of E_H' by using a volume charge distribution applicable for infinite film thickness and a surface distribution for zero film thickness. These assumptions gave an upper bound of 10 ergs/cm^2, and estimates for the Bloch line radius and Cross-tie separation as 100 Å and 1000 Å.

However, in 1967 Aharoni showed that although an exact solution to Brown's equations was impossible, inspection revealed that they could not have a solution with one component of $\underline{M}$ being zero unless E_H' vanished. Minimisation in one dimension always gives a solution with one component of $\underline{M}$ identically zero and thus can only approximate energy minima when E_H' is small, i.e. zero thickness films for Néel walls and infinite thickness films for Bloch walls. This implies that previous models have been approximations and to obtain smaller energy values solutions should be sought which decrease E_H' at the expense of E_{ex} and E_K.

Aharoni assumed a functional form for $\underline{M}$ with three parameters. The energy could be minimised with respect to these, and values chosen for two of them to enable the energy to be calculated analytically

before minimisation was performed. A lower energy was obtained than from the Brown-La Bonte calculations, the lower limit for one dimensional models. However, the wall energy reaches a minimum then tends to infinity for increasing thickness, unlike earlier calculations, indicating that these are more likely to apply at greater thicknesses.

In 1968 Aharoni showed how self consistency checks could be made on wall models by deriving two expressions for the energy of a domain wall. For a minimum energy configuration the ratio of the two energies, the self consistency, should be unity. Consideration of previous results shows Bloch wall models to approach a self consistency of unity with, ironically enough, the Middelhoek model serving well as a working result. The Néel walls, however, all show high self consistencies with only the Aharoni model approaching unity for zero and infinite film thicknesses.

La Bonte (1969) executed a complete calculation with the magnetisation allowed to vary in two dimensions, thus overcoming the objections of Aharoni (1967) to 1D models. The structure of the 2D Bloch wall was generated from an iterative micromagnetic energy minimisation equation and the result, found to differ markedly from the 1D calculations, is seen in FIG (1.9).

The magnetisation varies through the thickness of the film as well as in the plane normal to the wall. Essentially the rotation is Bloch-like in the centre of the film with a transition to Néel-like rotation in the outer regions, causing a considerable reduction of the free pole densities on the film surfaces. The centre of the wall consists of a magnetisation vortex but is asymmetric with respect to the x co-ordinate as seen in FIG (1.9). As the film thickness is increased the vortex becomes relatively more compact but the overall width is considerably greater than its 1D counterpart and essentially a linear function of thickness, in qualitative agreement with the results of Suzuki et al (1968).

The model not only indicates a significantly different wall

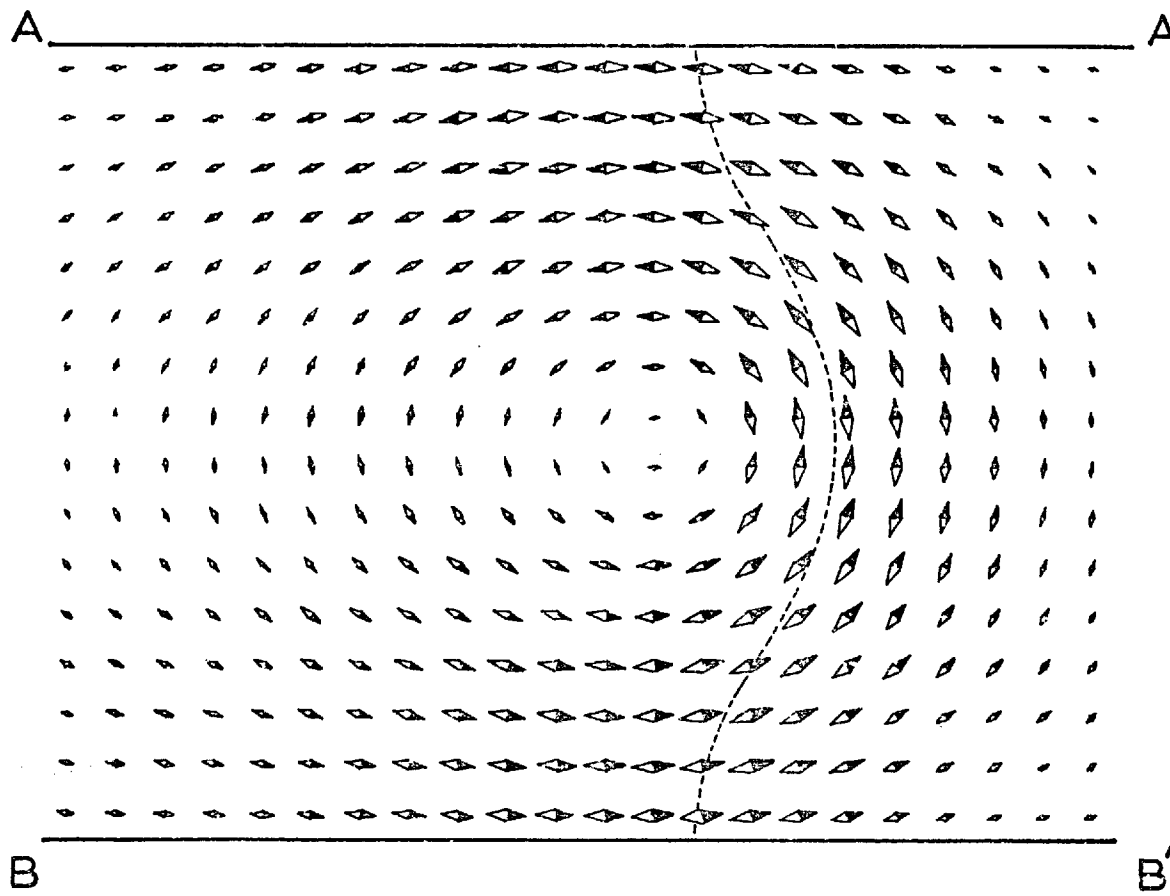

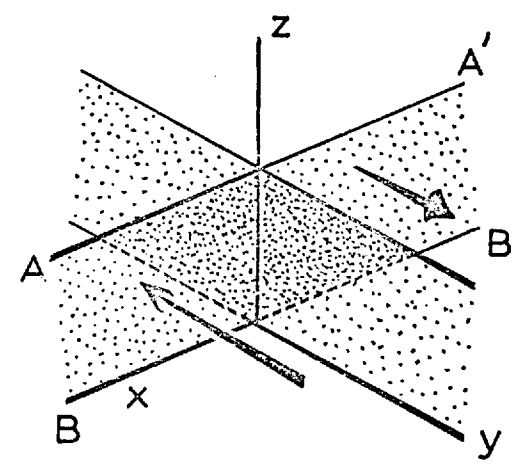

Fig. 1.9 The La Bonte wall model

Vector plot of hard direction magnetisation distribution across the plane shown. The dashed line denotes wall centre defined by $\alpha_2 = 0$ (or $\alpha_1 + \alpha_3 = 1$), the direction cosines of magnetisation.

structure but also predicts a lower energy density where the exchange contribution is high and the anisotropy and magnetostatic contribution low. Finally, the self consistency is shown to be within 1% of unity, a marked improvement on previous models.

The wall energies predicted by various models are seen in FIG (1.10).

The results of La Bonte's calculation provide an interesting comparison with those of Hubert (1969) who performed wall calculations using stray-field-free micromagnetic configurations as a starting parameter. The resulting spin configuration for a Bloch wall is similar to La Bonte's. The Néel wall has a more complicated structure and a higher energy than the Bloch wall but this rapidly decreases in an applied field. Hubert suggests that the stray-field-free Néel wall may form the kernel of an actual Néel wall whilst the tail, of necessity, produces a stray field.

Olson (1967) using the Brown-La Bonte type calculation had shown that the stray field above a calculated Bloch wall is an order of magnitude below the measured field above a Néel wall at 10,000 Å above the wall centre. This he had assumed to arise from the opposite rotation of the wall edges on the Brown-Le Bonte model but which we can understand to result from the more complex structure of the 2D La Bonte model. Thus with this result we do not expect the 180° walls to show up strongly with magnetic colloid.

Olson et al (1967) also applied this same technique to the intermediate wall structure, postulated by the group in 1965, and showed that the Bloch component fell off very much more quickly than the Néel component above the film surface and thus as the dominant wall component changes so also does the visibility.

Interest then now lies in the extension of 2D calculations to Néel walls to see whether a better self consistency can be achieved, and the nature and contribution of its stray field.

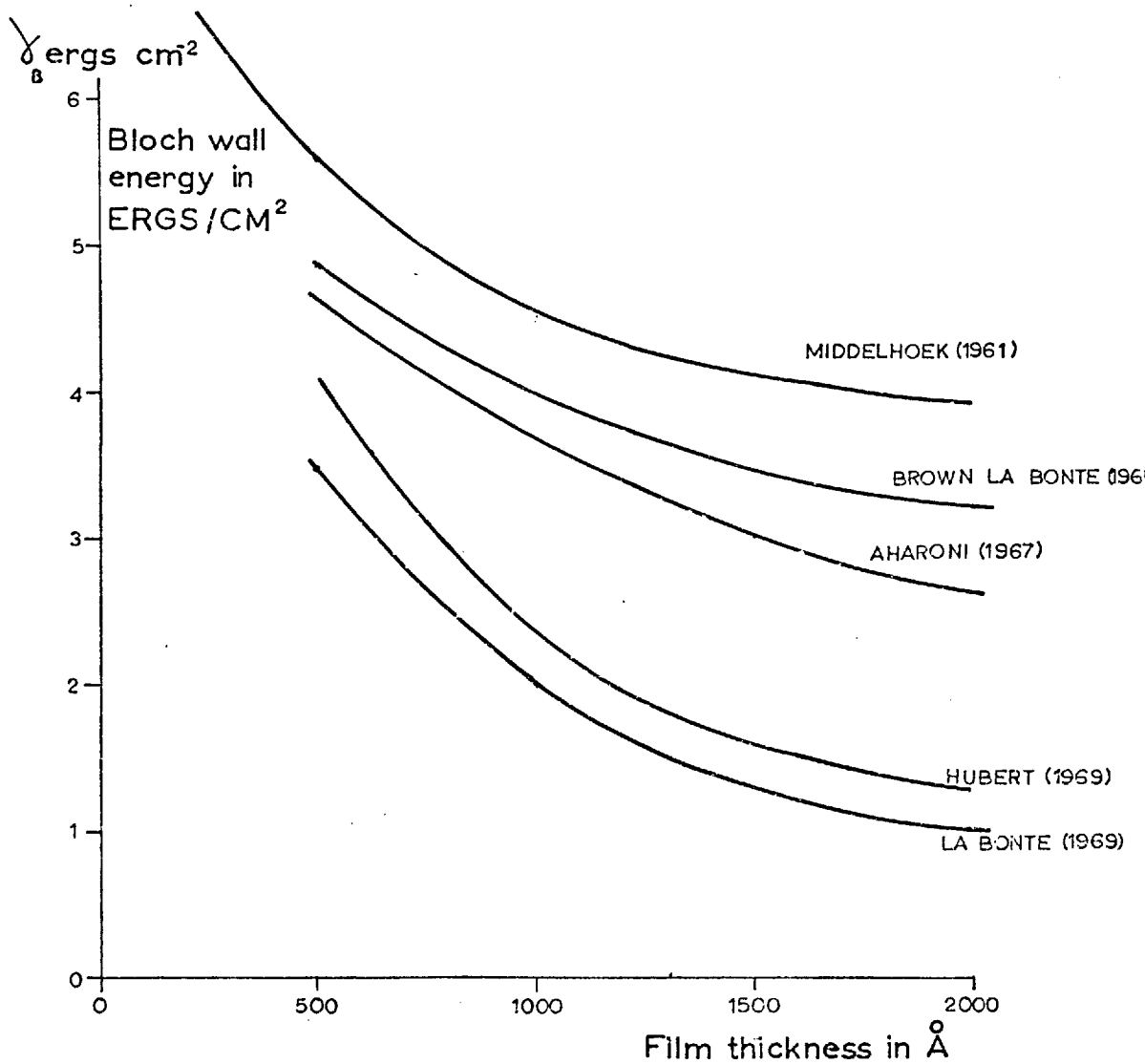

Fig. (1.10.) Wall energies of theoretical Bloch wall models

CHAPTER 2

TECHNIQUES OF DOMAIN OBSERVATION

INTRODUCTION

The various techniques for domain observation are reviewed, outlining their chronological development. Finally a comparison is drawn between the different methods. The work in this thesis used the Bitter colloid method and transmission microscopy, for reasons discussed in Chapter 4, which reports the experimental details.

2.1 THE BITTER COLLOID TECHNIQUE

As first suggested by Bitter (1931) and von Hámos and Thiessen (1931) independently, the Bitter technique was to observe magnetic discontinuities on the surface of magnetic specimens by sprinkling a fine powder of magnetic particles over the surface. Patterns were formed through the attraction of these particles by stray magnetic fields. Although impossible to interpret, the results gave the first direct evidence of the existence of domains. In 1932 Bitter replaced the powder by a suspension of γ ferric oxide in alcohol or ethyl acetate, thus giving the particles more time to settle. The patterns he observed were not truly representative of the specimens because the particle size of his suspension was too large to respond to the small fields, and his specimen surfaces were not sufficiently smooth and strain free.

McKeeham and Elmore (1934) made the first truly colloidal suspension with Fe_2O_3 and observed the type of pattern now associated with surface strain. In a series of papers Elmore developed the

technique further using Fe_3O_4 : recognising the misleading effect of a strained surface (1937), giving a recipe for colloid preparation (1938a), studying the behaviour of magnetite and siderac colloids (1938b) and interpreting their behaviour using the Boltzman distribution law (1940).

To obtain domain patterns a drop of colloid is placed on the specimen surface to be examined and formed into a thin layer by placing a cover slip on top. The pattern that forms can be observed under a microscope and is seen to best advantage under dark field conditions.

A modification to the Elmore recipe was given by Baker et al which with a low chlorine ion concentration gave less surface damage, cf. Bozorth (1951, p.533). At the same time Williams et al (1949) developed the technique for electropolishing surfaces. Together these techniques gave the very important results on unstrained iron surfaces. The staining of specimen surfaces which had previously occurred was overcome by Craik and Griffiths (1957) using a stabilising solution of Celacol. In addition, Craik (1956), Craik and Griffiths (1958) and Garrood (1962) first coated the specimen surface with a layer of collodion. This enabled a colloid pattern that had been allowed to dry, to be removed from the specimen surface and examined by electron microscopy.

An analysis of the formation of Bitter patterns has been given by Kittel (1949a & b). He has shown that the density distribution of colloid particles is determined by a balance between the local field from the domain wall and the Brownian motion of the particles. For pattern formation to occur $\mu\Delta H > 3kT$, where μ is the magnetic moment of the colloid particles and ΔH is the local field variation. The interaction between particles is neglected, and the inequality cannot be realised by multi-domain particles, which play no part in the process.

Bergmann (1956) separated the field which influences the single domain particles into two parts, the dispersion field above the magnetic surface and the self field of the colloid particles. Using the Kittel criteria he was able to show that particles above a certain critical size would form self-closing aggregates and play no part in the formation of patterns. Similarly by estimating the stray field at a distance above a 180^{o} Bloch wall he was able to deduce a lower limit for pattern formation. These two limits are close to one another and indicate that only particles with diameters near to 10^{-6} cms. contribute to pattern formation. This value is less than the critical radius for single domain behaviour, Kittel (1949a, p.573), justifying the rejection of multi-domain particles. The size range was confirmed by electron microscope observations on sols both of iron and magnetite.

Garrood (1962) noticing the change after storage of some colloids paid attention to the ageing of aggregates. He found that the sensitivity of colloids could be improved by initially precipitating the magnetite in a magnetic field. The particles thus have a greater tendency to form chains rather than closed loops and the chains then aggregate into cylinders giving a larger net moment. In addition he found that boiling, whilst still alkaline, has the effect of artificially ageing the solution thus accelerating the process of aggregation.

With the action of these colloids being so dependent on aggregate size it is essential to have good stability. This can be achieved with most lyophobic sols if the pH is sufficiently far from the iso-electric point. Magnetite sols however are only stable in acid solutions, the limit of stability being at pH5.2 with the iso-electric point at pH6.5. Garrood investigated the improvement in stability attained by the addition of a lyophylic sol, such as Celacol. He found it necessary to achieve charge stability in the dispersing medium before dispersion could take place, then on reduction of the

acidity the stability became entirely due to the protecting sol.

Garrood's paper gives two recipes for colloid production. The work reported in this thesis used a colloid made by following a modified version of his recipe for the coarse colloid. The walls in the specimens investigated are mostly Bloch type or else have a large Bloch component, thus producing lower stray fields. This dictates the choice of a coarse colloid. However despite Garrood's assertion that the resolution with the coarse colloid is lower, it was found that the resolution of this work was as high as any reported using this technique. Details are given in Appendix (B).

The visibility of Bitter patterns is dependent upon the nature of the stray fields above the walls which vary with the wall type viz. Methfessel et al (1960). This becomes very important when the nature of the walls themselves is being considered, (see p.152).

Much useful information can be obtained quickly and simply from the Bitter technique and this explains its widespread use. However it remains essentially static in its mode of operation and cannot be applied to materials with low anisotropy where the walls become wide and the field intensity insufficient to gather colloid particles. The suspended particles must remain mobile hence the temperature range over which observations can be made is restricted although observations have been made down to -90°C with methyl-cyclohexane as dispersant, Bates and Spivey (1964) and up to 380°C with paraffin oil, Andra (1956a).

A further disadvantage has been noted by Kranz et al (1964). By correlating magneto-optic and colloid patterns they found that Bitter patterns need not lie directly above domain walls because it is the overall stray field distribution which affects the colloid particles.

Finally with many samples there is the possibility of an acidic oxidising attack on the surfaces under investigation. This decreases

the time for observation and necessitates fresh preparation of the surface after investigation.

2.2 MAGNETO-OPTICAL TECHNIQUES

Since Kerr's first observation in 1876 that plane polarised light on reflection off an energised electromagnet became elliptically polarised magneto-optics has played a very important role in the investigation of magnetic properties, both static and dynamic. This is demonstrated by a recent survey, Palik (1967), in which almost 200 references are quoted covering work done in all four possible modes of operation. Explanations for the effects have been advanced, amongst others, by Voigt (1908) and Robinson (1964) using classical electromagnetism and Argyres (1955) using quantum mechanics and will not be discussed here. Recent investigations on thin films have been reported by Lambeck (1968).

2.2.1 The Faraday Effect

On Transmission through a ferromagnetic specimen the plane of polarisation of a plane polarised electromagnetic wave is rotated by any component of magnetisation in the direction of propagation. The extent of this rotation is governed by the saturation magnetisation of the specimen and its thickness, but is typically 100°/mm. The fact that it is a transmission technique places limitations on the thickness of material which can be used. Within these limits there is a further restriction that the magnetocrystalline anisotropy should be sufficiently large for the magnetisation to remain normal to the specimen surface, despite the large demagnetising energy invoked in so doing. The use with metals is very restricted because they are opaque above 2000 Å and have high saturation magnetisations, thus minimising any components normal to the plane. Fowler and Fryer (1956) have used this technique with permalloy films, obtaining a magnetisation component in the beam direction by tilting the film.

The observational apparatus is straightforward: light source, polarizer, specimen at objective focus, microscope and analyser, with camera or photomultiplier attached. If the analyser is set for the acceptance of light transmitted by domains with one direction of magnetisation, other domains will show up in darker contrast.

The Faraday effect has given useful results on garnets, Dillon (1960) and on ferrites, Kooy and Enz (1960). Dillon's first study of domains in ferrimagnetic garnets (1958 a & b) is also of interest being the first time that a magnetic material was found to be transparent in the bulk. The technique has subsequently been extended at the Bell Laboratories by Bobeck et al (1969) and Perneski (1969) to observe the action of domains in orthoferrites and apply them to act as domain wall devices.

Recent reviews of Faraday rotation have been given by Dillon (1968) and Bongers (1969). The extension of the Faraday effect into the infra-red is most useful for materials with windows in this region. Applications at these wavelengths to devices have been discussed by Cooper et al (1969).

2.2.2 The Kerr Effect

Generally reflection from a metallic surface causes plane polarised light to become elliptically polarised. If the plane of polarisation is parallel or perpendicular to the plane of incidence then from symmetry considerations the reflected beam remains plane polarised. If the surface is magnetic, the symmetry is destroyed, the reflected light is again elliptically polarised and the component perpendicular to the incident light called the Kerr component. This effective rotation of the beam is much smaller than the Faraday effect. The effect can be observed in three different forms corresponding to the relative direction of magnetisation with respect to the incident beam.

The POLAR effect is the interaction of a component of magnetisation normal to the specimen surface with the reflection process. It is the only effect which is non zero at normal incidence. For the LONGITUDINAL effect the magnetisation component must lie both in the plane of incidence and in the plane of the reflecting surface. Finally the TRANSVERSE effect which is not a rotation of the polarization but a change in surface reflectivity for light polarised in the plane of incidence. Here the surface magnetisation must lie normal to the plane of incidence.

(a) Polar Mode

The polar effect was the first magneto-optic effect to be used for the investigation of magnetic domains, but like the Faraday effect is restricted to materials with non zero normal components of magnetisation. The technique has been described by Williams et al. (1951) reporting their work on the basal cobalt plane, and has been used by Andra (1956b) and Mayer (1960) to study manganese bismuthide.

(b) Longitudinal Mode

The longitudinal effect has proved the most useful of the Kerr techniques, first observations being made by Fowler and Fryer (1952) using a photomultiplier detector. The technique has certain inherent disadvantages which during the subsequent fifteen years have been slowly understood and in as much as it is possible, counteracted.

The basis for subsequent designs was given by Prutton (1959). A collimated beam of monochromatic radiation was polarised and focused on the specimen's reflecting surface. The reflected beam passed through an objective, quarter wave plate to reduce ellipticity, analyser, and was focused at a photographic emulsion. The rotation is small and the optical image suffers from low brightness and lack of contrast. In addition light scattered from imperfections of rough surfaces is not extinguished by the crossed polarisers; this

however can be overcome by an elaborate double exposure technique, Fowler and Fryer (1954a & b).

In the 1959 paper Prutton reported an effective Kerr rotation of one degree. He obtained this by using an anti reflection dielectric coating and quarter wave plate, following the work of Kranz (1956) and Kranz and Dreschel (1958). The effect of the dielectric coating was studied by Lissberger (1961 & 1964) whose theory involving multiple-beam reflections between the dielectric surfaces gave good agreement with his dispersion curves. The action of the blooming is now well understood.

Treves (1961) considered the factors limiting the technique paying particular attention to the ellipticity from metallic reflections, and measured both this and the Kerr rotation as functions of the angle of incidence. Apparatus was built incorporating these results, Fowler et al (1960, 1961) differing from Prutton's in using a low angle of incidence and a microscope instead of a telescope for observation. This was the apparatus used for whisker observations (cf. p.30).

Greater resolution was obtained by Green and Prutton (1962) using a single lens as condenser and objective. Together with Carter (1963) they considered the factors affecting domain visibility, measuring them as functions of angle of incidence and condenser numerical aperture. These improvements were incorporated in a "high" resolution microscope suitable for Faraday or Kerr modes of working. The details of this can be found in Carey and Isaac (1966, p.73).

Difficulties encountered, maintaining contrast and at the same time keeping a reasonable field of view in focus were overcome by selecting different orientations of the objective lens, Feldtkeller and Stein (1967).

The increased visibility shown by Green et al (1963) to result from the use of a low numerical aperture condenser, and the desirability

of monochromatic illumination has made lasers ideal light sources. For visual observation the coherence of a laser beam is undesirable but can be suitably avoided, Dey et al (1969). Currently workers are able to observe domain wall motion at speeds limited by the sub-nano second rise time of the photodetector across areas limited by optical diffraction, Genovese and Chang (1968). It is also possible to compare the static and dynamic flux reversal processes by photographically recording the domain movements with exposures of 10 n.secs., Kryder and Humphrey (1969).

(c) Transverse Mode

The transverse effect has received less attention than the longitudinal effect, but uses a similar experimental arrangement. No advantage is gained by blooming the specimen. It was used to photograph domains by Dove (1963) who improved the contrast by further reflection from a surface of the same material as that under investigation. The effect was also used by Green and Thomas (1966) in constructing a simple hysteresis loop plotter.

2.2.3 Use of Wave Optics

The application of wave optics to magneto-optical techniques extends the scope of the methods, as it does for Lorentz microscopy cf. pp.50 & 51.

Boersch and Lambeck (1964) showed how the analyser could be set for phase contrast and demonstrated Fresnel fringes through the magnetic structure acting as a phase changing object. Lambeck (1964) showed that magnetic domains could act as a grating to give Fraunhofer diffraction, and by placing a diaphragm in the focal plane of the microscope obtained dark field pictures of the domain boundaries.

Lambeck (1965) applied the phase contrast and dark field settings to the study of hysteresis loops. In this was he was able simultaneously to observe the total magnetisation change from domain wall motion, using the conventional bright field; the position of

the domain walls, from dark field; and any rotation of the magnetisation, from the quadrature signal obtained in the phase contrast setting.

These ideas, applicable to the Faraday or Kerr effects and with no inherent frequency restrictions, should gain increasing importance.

2.3 ELECTRON BEAM TECHNIQUES

The interaction of electron beams with the magnetic fields above or inside specimens, via the Lorentz force provides the basis of a variety of methods for domain observation. Currently transmission microscopy is the most widely used but the application of scanning microscopy gives exciting possibilities.

2.3.1 Reflection Microscopy

An electron beam incident on a magnetic specimen at grazing incidence is scattered by the leakage fields above it an a complex series of curves can be recorded on a photographic plate placed in the reflected beam. Blackman and Grunbaum (1957) first applied this technique to cobalt crystals. A fine electron beam is required, $\sim$6μm wide, which after distortion by the fields above the surface produces cycloid type patterns on the photographic plate. The correlation of this shadow pattern with actual domain structures is difficult and the specimen is liable to damage and contamination but the technique can be applied to materials with very low intrinsic magnetisations.

2.3.2 Mirror Microscopy

Mirror microscopy is an alternative technique using a normally incident electron beam on a sample maintained at a slight negative potential with respect to the cathode of the system. The surface thus acts as an electron optical mirror with any irregularity

altering the local electric field hence affecting the density distribution of the returning beam. The first design was given by Mayer (1955) using a co-linear incident and reflected beam, but this was later modified to separate the two. Using this technique Mayer observed domains on barium ferrite (1957) and on silicon iron (1959). Barnett and Nixon (1967) replaced the electrostatic focusing by magnetic lenses, giving illustrations of the results.

As with reflection microscopy the complexity of the image forming process makes the interpretation of micrographs difficult. However it is possible to observe properties which cannot be studied by other methods, with a resolution of about 100 Å.

2.3.3 Transmission Microscopy

The use of transmission microscopy to observe domains was first reported by Hale et al (1959) and in more detail by Fuller and Hale (1960a & b) after investigations on nickel/iron films. They described the two modes in which the microscope can be operated, Fresnel and Foucault, and observed for the first time the effect of local variations in the direction of magnetisation within domains, called magnetisation ripple. From this important work the technique known as Lorentz Electron microscopy has grown. It has recently been well reviewed by Grundy and Tebble (1968).

The magnification of the technique is high and the resolution of conventional electron microscopy 10-50 Å. Thus it is easy to correlate magnetic and physical structures. Set against this there is a thickness upper limit of about 2000 Å for 100kV electrons, confining observations to thin films and thinned bulk specimens, with their large demagnetising fields normal to the plane.

The Lorentz force on an electron passing through a magnetic thin film is sufficient to deflect the beam by 10^{-4} radians. With an objective aperture of 10^{-2} radians such scattering leads to no appreciable variation in intensity across the specimen at focus. If,

however, the focus is changed to a position above or below the specimen a lateral displacement of the domain images is observed. This displacement depends on the magnetisation direction of the domains and leads to an overlap or divergence of the images thus indicating the position of domain walls as light or dark lines. An alternative to this method is to use the microscope with the objective lens off and image with the intermediate and projector lens, but the magnification and resolution is lower. Operation of the microscope in this mode is called Fresnel microscopy and is seen in FIGS.(6.8a & 8.1c).

The diffraction pattern from an area containing say a 180° domain wall will display a splitting of each diffraction spot by about 5% of the separation of the low order spots. Moving the objective aperture to cut out one of the subspots has the effect of introducing magnetic contrast into the focussed image. The intensity of the darkened domains is not zero because of inelastic scattering and aberrations. The relative orientation of the domain magnetisations can be found from the splitting of the diffraction spots, or if this is known the thickness of the specimen can be determined, Warrington et al (1962). Operation in this mode is called Foucault microscopy, by analogy with the optical equivalent and is seen in FIGS.(8.1a, b & d).

Normally a specimen is supported above the objective lens and near to its focal plane. Here the magnetic field of the lens can be very high, often sufficient to eliminate any domain structure and saturate the specimen. It is therefore necessary to displace the holder and increase the focal length of the lens. The magnetic field is still present, although much weaker, and normal to the specimen plane. Specimen stages have been built which allow magnetic fields to be applied in the specimen plane, with compensation for beam deflection, enabling direct observation of wall motion to be made.

Developing from the many studies on thin films and foils

Lorentz microscopy is the one method of domain observation from which it should be possible to measure wall widths. Indeed, using the defocussing mode Fuller and Hale (1960a) compared the intensity distribution across a wall image with a theoretical distribution. Wall thicknesses have been measured in this manner by Fuchs (1962) and Suzuki et al (1968).

Wall widths were also measured by Wade (1962) in Ni, Fe and permalloy, using large defocussing distances so that geometrical optics could be employed, and measuring both diverging and converging wall images. But, with certain limitations on the method the results were not accurate. Warrington (1964) studied the effect of resolution upon domain wall images considering the effects of beam convergence and coherence. He suggested that the arbitrary fitting of the intensity profile across the domain boundary can be improved by measuring the intensity at the centre, for a range of defocussing distances of which it is a function.

In a similar manner the Foucault displaced aperture technique has been used to obtain wall widths by Grundy (1965) on the basal plane of magneto-plumbite, by Jakubovics (1966) on a near basal plane of cobalt and by Rogers (1965). Rogers defocussed in addition to displacing the aperture thus changing the step in intensity at a wall into a slope, allowing correlation with theoretical curves for iron, nickel and permalloy.

The mechanism of contrast formation in both modes of operation of the microscope had generally been interpreted in terms of geometrical optics. However it had been noted by Boersch et al (1961, 1962) that the magnetic structure of the film presented a phase rather than an amplitude object to the beam and hence contrast interpretation should be made by wave optics. The electron deviation produced by a wall corresponds to the action of a Fresnel biprism with variations in effective refractive index corresponding to thickness variations.

This work was neglected until Wohlleben (1966, 1967) showed that the geometrical approach was an approximation for the wave treatment which is invalid for high resolution work. He showed that the variation in momentum at two neighbouring points on deflection was such that the uncertainty principle dictated the application of wave optics.

The application of wave optics also suggests the further possibility of using Zernike phase microscopy or interference microscopy, but the same resolution limit applies to each mode. Cohen (1967) reviewing the wave optical aspects concluded that the defocussed mode seemed the most promising for practical application, using Fresnel diffraction for domain wall problems, and Fraunhofer diffraction with low angle diffraction techniques, cf. Ferrier (1967), for ripple investigation.

2.3.4 Scanning Electron Microscopy

The Scanning Electron Microscope has become a useful research tool for the study of surface topographies and electrostatic potentials in specimens. Its mode of operation and range of applications were reviewed in 1965 by Oatley et al. However, conclusive evidence for the existence of magnetic contrast was not reported by this method until 1967 by Banbury and Nixon.

An electron beam is focussed on the specimen in the chamber and secondary electrons are produced, which are then collected by an anode near the specimen. The incident electron beam is scanned across the specimen and the varying collected intensity displayed on a cathode ray tube whose scan is synchronised with the incident beam scan. In this way a visual image of the object is established on the screen with pseudo dimensionality.

If the specimen is magnetic, electrons in the neighbourhood of the specimen will be deviated by localised Lorentz forces from magnetic fields above the specimen surface. Banbury and Nixon

collected the secondary electrons emitted within a narrow energy bandwidth using a directional analyser, so that small deflections in the electron trajectories caused appreciable changes in collector efficienty. In addition an accentuation of the deflection due to specimen fields was realised by inserting screens at specimen potential before the collector and normal to the surface under examination. These restricted the lateral spread of the attracting field of the detector so that magnetically deflected electrons found themselves in a reduced detector field, thus decreasing their probability of collection.

Joy and Jakubovics (1968) made a more detailed investigation into the origins of magnetic contrast. They deduced that contrast is caused by the Lorentz force acting on the secondary electrons with energies of 100eV. Observations on the basal plane of cobalt showed a reversal of contrast when the specimen was rotated 180° about the beam axis, and a collector efficiency dependent on energy and initial direction of travel of the secondary electrons. In 1969 they reported further studies on domains in cobalt observing internal structures not apparent on the surface.

Although very new, the technique shows great promise, but in a complementary role to transmission microscopy. The specimen surfaces do not require the careful preparation of other techniques as they need not be microscopically smooth. Against this, the resolution is currently no better than by the Bitter technique, 1μm, however it should be possible to reduce this. As with X-ray Topography, to be discussed next, it is also possible to obtain indications of internal domain structures. not intersecting the surface.

2.4 X-RAY TOPOGRAPHY

The use of X-ray diffraction topography for the observation of ferromagnetic domains is an extension of the technique which

enables different lattice defects in single crystals to be made visible, Bonse et al (1967). A well collimated X-ray beam is allowed to fall on a crystal and a variation in the diffracted intensity, due to elastic strains in the neighbourhood of defects, is recorded on fine grained emulsion photographic plates. A resolving power of 1-2μm can be obtained with a special goniometer and fine focus X-ray tube.

Several of the methods have been used to observe domains, the most popular being the transmission arrangement of Lang (1959). In this a thin crystal is mounted at the Bragg angle for a set of lattice planes making a large angle with the crystal slice. The directly transmitted beam is blocked by an opaque screen, but the diffracted beam is allowed to fall on a film placed behind the screen. To obtain a picture of the complete crystal, the crystal and emulsion are kept fixed at the same orientation whilst being traversed backwards and forwards across the beam.

There is in general a change in magnetostrictive deformation between domains and in accomodating this mismatch the lattice is put into a state of strain at the domain wall. The strain gives rise to diffraction contrast effects making the walls visible. Domains were first seen, in silicon iron, by Polcarova and Lang (1962) and by Roessler et al (1965). In 1967 Basterfield and Prescott observed domains in terbium iron garnet $Tb_3Fe_5O_{12}$.

Only certain types of wall give rise to significant diffraction contrast. Lang and Polcarova (1965) have shown that no contrast appears at 180° walls because no lattice mismatch is produced and the strain within the wall itself is insufficient to give any readily observed contrast effects. Conditions for diffraction contrast from domain walls in silicon iron were studied by Polcarova and Kaczer (1967) using reflection topography. They showed that 90° walls are visible if $(\underline{m}_1 - \underline{m}_2).\ \underline{g} \neq 0$ where $\underline{m}_1$ and $\underline{m}_2$ are the magnetisation directions in neighbouring domains and $\underline{g}$ is the diffraction vector.

In 1968 Polcarova and Lang showed that the basic properties of the contrast can be derived theoretically from a model treating a 90° wall as a coherent twinning boundary, and Schlenker et al (1968) gave a detailed treatment using the dynamical theory of diffraction.

The power of this technique was recently demonstrated by Polcarova (1969) when studying (110) plates of silicon iron. She found fine domain substructures inside a specimen which had previously shown a conventional surface pattern under examination by Bitter colloid.

This is the strength of the technique; the facility to study the internal magnetic structure in bulk specimens and the correlation of this structure with the crystal perfection. Against this have to be balanced several severe disadvantages. The observational apparatus is very critical in allignment and hence difficult to set up, the resolution can be good but is not high and exposure times of many hours preclude the possibility of any type of dynamic work. Finally the specimens must have a high perfection to present defect and imperfection contrast from completely masking all magnetic effects.

2.5 PROBE TECHNIQUES

The stray fields which domains or domain walls create above the surface of a magnetic specimen enable a plot of surface domain structure to be made from local field variations. This however is difficult, firstly because the stray fields fall off very rapidly with increasing distance above a specimen surface, and secondly because the probe size is limited by the small dimensions over which field changes occur. The success of the method therefore depends upon having a uniform surface and a sensitive probe.

Two probe techniques, the Hall probe and the vibrating permalloy probe have been described by Carey and Isaac (1966 p.108 et seq.) together with instrumental details and typical results. Limitations

imposed by the probe and surface however reduce what might have been an interesting technique to a difficult way of obtaining results which could more accurately be observed by other methods. Unless a reliable and microminiature probe can be engineered this technique will remain as only academically interesting.

2.6 COMPARISON OF TECHNIQUES

All the techniques mentioned above have their strength and weaknesses and the choice of a given technique for an investigation may finally not be very wide.

The Bitter Technique has had the widest application because of its low cost and ease of operation, however its basic simplicity can be misleading. The production of colloids to study specimens with low stray fields for example can be very unpredictable, and the distribution of the colloid collection can lead to the wrong interpretation of the underlying patterns.

The two other methods in most common use today are the Kerr effect and Lorentz microscopy. Lorentz microscopy suffers from the thickness limitation but with the increasing use of high accelerating voltages this should be less of a problem. The apparatus is, however, not cheap or convenient. The Kerr effect has in recent years become more widespread in application and been used with increasing accuracy.

The following table enables comparisons to be made between the available techniques to assess their relative suitabilities for a given investigation.

TABLE (2.1) COMPARISON OF TECHNIQUES

METHOD	CAUSE	EFFECT OBSERVED	SPEED	RESOLUTION	MAX. MAGNIFICATION	COMMENTS
BITTER COLLOID	stray fields	domain walls (domains if extra fields are applied)	quasi-static	1 μm	1,500	Simple in use, wide in application, not suitable for low anisotropy or wide temperature ranges.
WITH COLLODION			static	500 Å	10,000	
MAGNETO-OPTICS						
FARADAY EFFECT	magnetisation	domains and walls	fast	1 μ	1,000	Only suitable for limited range of materials but very good within that.
KERR EFFECT	magnetisation		fast	1 μ	500	Apparatus critical for accuracy, powerful technique especially for dynamic work.
ELECTRON BEAM						
REFLECTION	stray fields	domains	fast	100 Å	1,000	Complex experimental arrangement for results which are difficult to interpret.
MIRROR			fast			
TRANSMISSION	magnetisation	domains and walls	fast	10-50 Å	20,000	Restricted to thin specimens but very powerful method for investigating these.
SCANNING	stray fields	domains	static	1 μm	1,000	No specimen preparation required can detect sub-surface structures, difficult to apply fields.
X-RAY TOPOGRAPHY	elastic lattice strains	lattice deformation caused by magnetisation	static	2 μm		Difficult to set up, crystal has to have high perfection, can detect internal structures.
PROBE	stray fields	local magnetic field above specimen	static	-	-	Elaborate apparatus, extremely difficult to correlate results.

CHAPTER 3

GROWTH OF FERROMAGNETIC PLATELETS

INTRODUCTION

Although this thesis is primarily concerned with the study of the magnetic properties of thin platelets, the method of their production is of considerable intrinsic interest. The theory relating to this particular growth form and the nature of the experimental technique used to grow platelets are discussed in this chapter.

Morphological considerations relate the essentially two dimensional platelet growth forms to the one dimensional whisker growth and so earlier work on vapour grown whiskers is examined. Proposed mechanisms for the growth of these whiskers are discussed prior to considering the observations on platelet formation.

3.1 THE GROWTH OF WHISKERS

The study of whiskers has been motivated by the discovery of their unusual physical properties. Many of these, such as high strength, perfect surfaces, freedom from dislocations etc., result from the perfection of the lattice. At the same time others, such as the magnetic fields required for saturation or nucleation, result from their unusual shape as well. General reviews of the existing knowledge of the nature of whisker growth have been given by Nabarro and Jackson (1958) and Coleman (1964). Whiskers can be grown, from the melt, from solution, and from the vapour : but attention is confined here to the last of these processes.

Growth from the vapour phase can occur by two general methods,

the easily reversible condensation of a supersaturated vapour, or in a more complex system as the product of a chemical reaction. In the condensation process vapour atoms or molecules impinging on a substrate surface are adsorbed, releasing part of their latent heat of condensation in the process. They can then migrate across the crystal face until, on encountering a growth site, they either release their remaining latent heat and become incorporated into the crystal lattice, or else re-evaporate.

In the chemical process the vapour atoms or molecules are chemically different from those in the growing crystal and the molecules adsorbed on the surface are either thermally decomposed or chemically reduced to release the atoms of the growing crystal. This method of growth, an example of heterogeneous catalysis, is very complex and the atomistic details almost completely unknown.

Although large crystals can be grown by vapour condensation this has not been exploited for metals because in most condensation processes many crystals are nucleated and the crystals remain small from lack of control of the transport. However, growth from vapourised metal compounds has several advantages, high transport rates are possible at temperatures well below the crystal's melting point and the purity of the crystals can be exceptionally high. The crystals formed are grown under near-equilibrium conditions and are free from constraint, having a minimum of stress and possessing flat, well defined faces. The technique is limited to metals with volatile and easily reduced compounds, and for the transition metals the halide compounds are suitable.

Vapour phase growth has been reviewed by Cabrera and Coleman, and the vapour growth of metals by Brenner, both in Gilman (1963). Before considering the mechanism of halide reduction it is useful to review some of the results from direct condensation experiments.

3.1.1 Growth from the Vapour

Crystals grown from their own vapour are small and are generally formed by sealing the required metal into a tube which is either evacuated or filled with an inert gas. A temperature gradient is established with the metal effusing from the highest temperature region to condense on the colder walls. Because of their high vapour pressures Zn, Cd and Mg have been the most frequently studied. It has been found that the presence of a foreign gas has a significant effect on the aspect ratios of the crystals, probably through lowering the surface nucleation rate by reducing the supersaturation near the crystal interfaces.

Anisotropic growth in metal crystals was first studied by Volmer and Estermann (1921) who, when transporting mercury observed thin platelets to nucleate on a glass surface and grow 10,000 times faster in width than thickness. They concluded that an intermediate condensation stage exists in which the atoms are in a mobile adsorbed state, and postulated that Hg atoms impinging on the surface are unable to form new layers and migrate to the platelet edge where they are incorporated into the lattice.

This work on Hg was repeated by Sears (1953, 1955a and 1956) who found that the growth habit could be altered to give whiskers by controlling the temperature of the condensing vapour. The transition between platelets and whiskers was found to be a smoothly varying function of the vapour temperature. By measuring the bending of the whiskers under Brownian motion Sears was able to estimate their radius as $\simeq 0.01\mu m$. He measured their growth rate as 1.5×10^{-4} cm/sec, but calculated it as 3×10^{-8} cm/sec using an equation derived from gas kinetics.

$$\dot{i} = \frac{p}{\rho}\left(\frac{m}{2\pi kT}\right)^{\frac{1}{2}} \qquad (3.1)$$

p is vapour pressure above whisker ρ is density of whisker

m is mass of condensing atom k is molecular gas constant
T is absolute temperature

Thus the actual growth rate is 5,000 times that calculated, and if the assumption of constant whisker radius during growth had not been made the discrepancy would have been even larger. The calculation assumes that only atoms striking the advancing end contribute to axial growth. The result implies, however, that those striking elsewhere must also contribute.

If the nucleation of a new layer on the surface of a low index plane is considered the nucleation rate $\dot{N}$ in nuclei/cm^2/sec for surface nucleation is given by : $\dot{N} = B \exp(-\Delta f/kT)$ where Δf is the free energy of formation of a critical sized surface nucleus and B is the frequency factor (usually taken as 10^{20} sec^{-1}).

$$\Delta f = \frac{\pi a \sigma^2 M}{RT \ln \alpha}$$

where σ is the surface free energy of the solid
M, the gram atomic weight of a condensing atom
R, the molar gas constant
a, the atomic spacing

Combining these two equations the rate of 2D nucleation can be related to the supersaturation of the vapour by

$$\ln \alpha = \frac{\pi a \sigma^2 M}{kRT^2 \ln\left(\frac{B}{\dot{N}}\right)} \qquad (3.2)$$

If it is assumed that growth proceeds by the successive nucleation of fresh layers, a value for the nucleation rate $\dot{N}$ of 2×10^{15} nuclei/cm^2/sec is required. This from equation (3.2) would require a supersaturation α of 10^{24}, whereas the measured value lies between 10^2 and 10^3.

Homogeneous 2D nucleation cannot therefore account for the

observed growth rate and a face containing a permanent growth step must be exposed, i.e. the whisker must contain an axial screw dislocation, Frank (1949). The importance of spirals had been implicitly recognised far earlier in observations on preferential growth sites such as kinks and growth steps, Stranski (1928). The screw dislocation provides a method of continuously avoiding the formation of 'complete' planes, Buckley (1951). Since 2D nucleation cannot occur on the side faces, atoms impinging on the side are adsorbed and can migrate to the advancing end. If all adatoms within a distance λ_x of the advancing end can contribute, equation (3.1) becomes for a whisker of radius r :-

$$1 = \frac{2\lambda_x}{r} \frac{p}{\rho}\left(\frac{m}{2\pi kT}\right)^{\frac{1}{2}} \qquad (3.3)$$

λ_x is the distance travelled during a finite adsorbed lifetime of $_s$ before re-evaporation (Burton et al (1951)).

The axial screw dislocation could arise either from the original nucleus, or could have been introduced later. Beyersdorf's electron microscope investigations of glass surfaces (1952) showed that within the vitreous body, small crystalline regions were scattered which presented screw dislocation spirals. These sites could provide preferential nucleation positions which would allow propagation of the dislocation into the metal crystal.

Similar arguments to those stated above apply to the growth of platelets, but lateral growth was assumed by Sears to involve a set of crossed screw dislocations. A crystal bearing such a set of dislocations is actually a bicrystal with a small angle twist boundary, and must grow laterally in all directions, for however much the crystal grows the edges always present screw dislocation ends. The nuclei leading to whisker or platelet formation are assumed to differ only in the crystallographic direction of the screw axis. For the mercury crystals investigated a whisker nucleus was believed to form with a

(100) face parallel to the glass substrate and a platelet nucleus with a (110) face parallel. Both habits have comparable growth velocities and the nucleation event was thought to favour either one or the other with small variations in deposition conditions.

In 1955(b) Sears extended the work by growing whiskers of Zn, Cd, Ag and CdS. The results confirmed earlier observations that a critical condition for the growth of whiskers appears to be that the supersaturation ratio must be maintained below a value characteristic of the material, which is taken as being the value for surface nucleation.

From observations on the interactions of Zn whiskers Sears and Coleman (1956) claimed evidence for screw dislocation and tip growth of whiskers. After growth runs they observed two whiskers in contact and at the point of contact a platelet. They assumed that when whiskers crossed the grain boundary so formed was a twist boundary defined by a set of crossed screw dislocations. This was taken as evidence for a platelet growth mechanism, with the absence of whisker thickening implying the absence of local screw dislocations. Furthermore, the fact that on touching another whisker growth did not proceed in such a manner as to make the whisker bow, was taken as evidence for tip as opposed to basal whisker growth.

Coleman, with Sears (1957) and with Cabrera (1957), studied the growth of Zn and Cd whiskers in atmospheres of He and H, and found the crystals grew to a greater length and in more profusion than those grown in vacuum. The abnormal growth observed was accounted for by the limitations imposed by the diffusion of condensing vapour through the gas phase. Exact calculations could not be made but an upper limit was placed on the idealised growth rate by the dimensions of the vessel in which the reaction was occurring.

Growth under more controlled conditions was achieved by Price (1960) in his study of Cd whiskers grown in an atmosphere of argon. He found the number and form of the crystals to vary greatly with

(100) face parallel to the glass substrate and a platelet nucleus with a (110) face parallel. Both habits have comparable growth velocities and the nucleation event was thought to favour either one or the other with small variations in deposition conditions.

In 1955(b) Sears extended the work by growing whiskers of Zn, Cd, Ag and CdS. The results confirmed earlier observations that a critical condition for the growth of whiskers appears to be that the supersaturation ratio must be maintained below a value characteristic of the material, which is taken as being the value for surface nucleation.

From observations on the interactions of Zn whiskers Sears and Coleman (1956) claimed evidence for screw dislocation and tip growth of whiskers. After growth runs they observed two whiskers in contact and at the point of contact a platelet. They assumed that when whiskers crossed the grain boundary so formed was a twist boundary defined by a set of crossed screw dislocations. This was taken as evidence for a platelet growth mechanism, with the absence of whisker thickening implying the absence of local screw dislocations. Furthermore, the fact that on touching another whisker growth did not proceed in such a manner as to make the whisker bow, was taken as evidence for tip as opposed to basal whisker growth.

Coleman, with Sears (1957) and with Cabrera (1957), studied the growth of Zn and Cd whiskers in atmospheres of He and H, and found the crystals grew to a greater length and in more profusion than those grown in vacuum. The abnormal growth observed was accounted for by the limitations imposed by the diffusion of condensing vapour through the gas phase. Exact calculations could not be made but an upper limit was placed on the idealised growth rate by the dimensions of the vessel in which the reaction was occurring.

Growth under more controlled conditions was achieved by Price (1960) in his study of Cd whiskers grown in an atmosphere of argon. He found the number and form of the crystals to vary greatly with

supersaturation. At low values the predominant habits were whiskers and thin platelets, but at higher growth rates these became gradually more equant. Price advanced an alternative mechanism for whisker growth by the addition of atoms at the whisker tip. He assumed a pure axial screw dislocation might suddenly become a pure edge dislocation and run out to a lateral surface. If the temperature was sufficiently high it might then be possible to maintain an equilibrium concentration of vacancies around it. At the surface there would be an under-saturation in vacancies, corresponding with a supersaturation in adsorbed surface atoms. A concentration gradient would thus be established in which vacancies would diffuse to the surface from the edge dislocation and thus cause it to climb. Every rotation of the edge dislocation around the axis would incorporate a new plane of atoms so that the whisker would be continually lengthened.

3.1.2 Growth by Chemical Transport

Interest in the production of metal crystals by reduction of their halide vapours has increased in recent years because relatively large whiskers can be obtained with simple equipment.

A technique which has been employed by several workers was first developed by Brenner (1956), who was able to observe the growth of the ferromagnetic metals, copper and silver formed by the hydrogen reduction of their halides. As this method has been used as the basis for the production of ferromagnetic platelets it is discussed in detail below.

Brenner constructed a furnace which enabled him to make direct observations during the growth process. He paid particular attention to the growth of copper whiskers from the reduction of CuI according to the reaction

$$2(CuI) + (H_2) \longrightarrow 2(HI) + 2(Cu)$$

$$(Cu) \longrightarrow \langle Cu \rangle \text{ whisker}$$

N.B. () indicates gas phase and ⟨ ⟩ solid.

It is instructive to record some of his observations. He found the hydrogen flow rate, if above a certain threshold value, to have little effect on whisker growth. The whiskers were observed to grow from the tip and not the base, but their orientation was not constant, the majority having ⟨110⟩ and ⟨111⟩ axes and a few with ⟨100⟩ axes. Some of the whiskers developed into blades, the broad side always corresponding to (110) planes. The measured growth rates varied between 4 and 23 μm/sec.

Brenner assumed the reduction of CuI to occur in the vapour phase and the mean free path of the adsorbed atoms to be 1 mm. He estimated the supersaturation near the whisker surface to be 10^4. Calculating the supersaturation as the ratio of the partial pressures of CuI to Cu at the growth temperature (950°K) he found the value of $2.\times 10^{10}$ to be 10^6 larger than necessary to explain the observed growth rate. Thus with these well developed platelets, bounded by smooth planes and apparently growing at high supersaturations, he was forced to conclude either that the growth mechanism was different from that postulated by Sears, or that 2D nucleation was more difficult than was estimated from an equation such as (3.2). One possibility he considered was that the surface of the whiskers might be covered by adsorbed gases, such as HI, thus lowering the non-coherent 2D nucleation frequency leaving the whisker sides free from overgrowths. This is termed the homogeneous mechanism of growth.

Coleman and Sears (1957) proposed in the case of copper whiskers that CuI acted as the carrier in the vapour phase and the whiskers grew by condensation of the vapour on the whisker face with preferential reduction of the adsorbed CuI molecules occurring at the tip:

$$2\ \langle \mathrm{CuI} \rangle + (\mathrm{H_2}) \longrightarrow 2(\mathrm{HI}) + 2\ \langle \mathrm{Cu} \rangle$$

Perfect columnar surfaces were ineffective in catalysing the reduction, thus contact between these surfaces and the supersaturated vapour did

not occur with this transport mechanism since the copper was not formed in the vapour phase. This is termed heterogeneous reduction.

If this mechanism is correct the axial growth rate should be proportional to the rate of arrival of CuI molecules at the tip. This hypothesis presumes that the reduction of CuI in the vapour phase is negligible, and the tip has different properties from the sides of the whisker. A permanent growth step provides such a differentiating catalytic activity. Further evidence for this is the increased deposition observed on crystalline surfaces compared with polished silica glass.

Morelock and Sears (1959) showed that the vapour from which copper whiskers grow was not highly saturated with copper. Therefore homogeneous reduction could not have been effective, and the carrier through the vapour was CuI. The heterogeneous mechanism is appropriate for small temperature gradients as rapid condensation of CuI will not occur. It is believed to be the general mechanism by which metal halides, having appreciable vapour pressures at the reduction temperature, can yield metallic whiskers by hydrogen reduction.

This mechanism is understood further in terms of Brenner and Sears' paper considering growth in systems where transport is limited by material or heat diffusion, in effect dendritic growth from the vapour phase. Any real surface, they realised, contained screw dislocations and could act as a deposition sink at low supersaturations. The vapour concentration in the neighbourhood of the advancing face decreases and the concentration gradient normal to the growing face becomes less steep. When the supersaturation is very small and only sufficient to cause growth by the Frank mechanism, closely spaced screw dislocations yield a smoothly advancing surface, but an isolated one forms a growth cone. As the summit of the cone rises it no longer depends on unidimensional diffusion for growth and begins to approach a spherical diffusion configuration, thus growing more rapidly and

finally attaining a constant rate. This mechanism appears to support Brenner's observations where transport is limited by gaseous diffusion. The supersaturation at the growth steps is very low but there is a steep concentration gradient.

3.2 CRYSTAL GROWTH BY HALIDE REDUCTION

The Brenner technique for the growth of low vapour pressure metals has been used by Frait et al (1966), Gemperle (1966) and De Blois (1965, 1966) in their studies on ferromagnetic platelets. Kotrbova and Hauptman (1965) have studied the transport of iron as ferrous chloride, to give iron platelets, and Cech (1959, 1960) has made the only detailed study of the nickel halide reduction reactions.

Gorsuch (1959a) had previously shown that the presence of iron oxide was necessary to grow whiskers of cube oriented iron. Studying the nucleation of Ni whiskers on NiO Cech (1959) measured the orientation of the whiskers with respect to the oxide and found a large degree of ordering. He was thus able to rule out any hypothesis of nucleation on accidental dirt particles. Similarly he was able to eliminate vapour deposition as a possibility and suggested that nucleation was achieved by hydrogen reduction of the nickel oxide. However, this mechanism could only apply when a metal halide and oxide were both present in an atmosphere capable of reducing these compounds to metal.

In 1960 Cech extended the investigations and examined the reaction mechanisms. A boat containing $NiBr_2$, with NiO as an impurity, and with water of crystallization, was rapidly heated to a temperature where the bromide was volatile. During the heating process steam evolved which blanketed the bromide thereby holding it in an oxidising atmosphere, hence:-

$$(NiBr_2) + (H_2O) \longrightarrow \langle NiO \rangle + 2(HBr) \qquad (3.4,1)$$

As heating continued the charge was gradually dehydrated and the

atmosphere became reducing, with the system then containing $NiBr_2$, NiO, H_2 and H_2O.

Under these conditions the reaction

$$\langle NiO \rangle + (H_2) \longrightarrow \langle Ni \rangle + (H_2O) \qquad (3.4,2)$$

occurred and small particles of reduced nickel were found in the surface of the NiO substrates. As soon as Ni particles of a supercritical size had been formed hydrogen began to react with the $NiBr_2$.

$$\langle NiBr_2 \rangle + (H_2) \longrightarrow \langle Ni \rangle + 2(HBr) \qquad (3.4,3)$$

Nickel formed in this way deposited epitaxially on the metal particles formed in the surface of the oxide.

These reactions suggest that hydrogen reduced the bromide at a faster rate than the oxide if there was a suitable metal surface available for growth.

Cech also suggested that the oxide may be reconverted to bromide thus

$$\langle NiO \rangle + 2(HBr) \longrightarrow (NiBr_2) + (H_2O) \qquad (3.4,4)$$

with the HBr in reaction (4) being produced in (3). It is therefore possible for the oxide at the base of the whisker to be incorporated into the whisker via the bromide. Thus Cech postulated a halide cycle with Ni being transported from the oxide to the metal via the halide with the chemical force being supplied by the oxidation of hydrogen to steam:

$$\begin{array}{ccc} NiO + 2HBr & \longrightarrow & NiBr_2 + H_2O \\ & \nwarrow \quad \swarrow & \\ H_2 + NiBr_2 & \longrightarrow & 2HBr + Ni \end{array} \qquad (3.5)$$

It had been suggested by Price et al (1958) and Sears (1958) that crystal growth could be poisoned by the adsorption of impurities. If

the crystal was growing above a critical rate there would be no hindrances to growth, but below this rate impurities could cover the growth sites and completely inhibit further growth. Whisker growth was suggested to occur if all faces except one grew at less than this critical rate and Price suggested that statistical fluctuations could provide the initial non-uniformity.

However, Cech showed that the H_2/H_2O ratio at the base of a growing crystal would be decreased relative to the top, because of the presence of the oxide causing an auxilliary reaction (3.4,4) to occur. Thus a smaller proportion of the hydrogen diffusing into the system would be available for growth on the side surfaces of a nucleus compared with the top. For the mechanism to operate one preferred growth face must on average be at a greater distance from the substrate than the others, and those faces favourably oriented should be found as whiskers with axes nearly perpendicular to the oxide substrate. A histogram of experimentally measured whisker orientations on oxide substrates appeared to confirm this.

3.3 THERMODYNAMIC CONSIDERATIONS IN HALIDE TRANSPORT

Transport reactions, in which a metal is transported from one part of a system to another as a gas phase of limited stability, have been the subject of close thermodynamic scrutiny because of their importance in industrial refining processes. The scattered early work on these processes has been collected and reviewed by Schäfer (1964), and the necessary thermodynamic background can be gathered from Swalin (1962).

For convenience Schäfer divided the transport process into three separate steps: the heterogeneous reaction on the starting solid, the motion in the gas phase and a reverse heterogeneous reaction depositing the solid. The quantity of material transported could then be found from considerations of the gas motion and the partial pressure difference ΔP between the initial and final solid substance. Considering

various diffusion controlled reactions Schäfer concluded that the variations in gas motion were small but the value of ΔP was significant in evaluating transport properties. If the partial pressure difference was significant then transport generally occurred. By artificially splitting the equilibrium forward and reverse reactions, the difference between the equilibrium pressures could be obtained from basic thermodynamic values, ΔH° the enthalpy of the reaction and ΔS° the entropy.

Schäfer considered the simplest type of reaction

$$\langle X \rangle + y(Y) \longrightarrow (XY_y) \qquad (3.6)$$

under conditions of $\sum P = 1$ atm. and formulated a set of ten rules for transport involving heterogeneous equilibria. Although these are not listed here in detail it is instructive to consider some of the conclusions reached.

Schäfer noted that reactions which supported transport had an equilibrium position which was not extreme and with no solids present on one side of the equilibrium. The sign of ΔH° determined the transport direction, and for any value of ΔS° there existed a value of ΔH° which gave maximum transport, the transport increasing with increasing ΔS°. But for large ΔS° transport was only possible if ΔH° and ΔS° had the same sign. As an alternative the change in log K, the equilibrium constant of the reaction, effected by temperature variations can influence transport considerably.

With these results in mind Schäfer considered the transport of the ferromagnetic elements according to the dihalide reaction equilibrium.

$$\langle \text{Metal} \rangle + 2(\text{halide}) \longrightarrow (\text{Me } X_2)$$

Observations confirm Schäfer's rules. $FeCl_2$, $FeBr_2$ and $NiCl_2$ will not support transport because of their large ΔH° values - extreme equilibria. Conversely NiI_2 with low ΔH° decomposes too rapidly to

allow substantial transport. The transport maximum lies in the region of log K=0 with $NiBr_2$, FeI_2 and CoI_2 being acceptable compounds, in order of increasing ease of decomposition.

Schäfer's rules are not always easy to apply and Alcock and Jeffes (1967) and Jeffes (1968) have developed a method enabling the most efficient conditions for vapour transport to be determined on the basis of only a few of these rules. They considered the information that could be obtained by treatments based on the Ellingham diagram (1944). This is a plot of the standard free energy changes of reactions, ΔG°, shown as a function of temperature. It is a useful method of assessing reactions for values of ΔH° and ΔS° likely to give efficient transport.

Consider again the reaction (3.6) for the transport of a solid X, with the forward and reverse reactions occurring in two separate zones. It is assumed that the gases are in equilibrium with the solid in both zones.

The equilibrium constant for the reaction, from Swalin, is

$$K = \frac{P_{XY_y}}{(P_Y)^y} \frac{1}{a_X}$$

To produce transport it is necessary to lower the equilibrium activity of X below unity at the point of removal and raise it above at the point of deposition. This can be achieved by changing K (by a temperature variation) or the ratio $P_{XY_y}/(P_Y)^y$ (by altering the total pressure within the system), the former being the most convenient.

The most suitable ranges of operating conditions may be determined from the Ellingham diagram using the fact that

$$\Delta G^\circ = - RT \ln K = \Delta H^\circ - T\Delta S^\circ \qquad (3.7)$$

Differentiating

$$\frac{d \ln K}{d\left(\frac{1}{T}\right)} = - \frac{\Delta H^\circ}{R}$$

Thus, the greater the value of ΔH° the greater the variation in K for a given temperature difference, with a fundamental requirement that $\Delta H^{\circ} \neq 0$ making K insensitive to temperature variations.

Jeffes has shown that large changes in K are very inefficient on thermodynamic grounds. For reactions with a multiplicity of one, (the ratio of the number of moles of reacting gas to the number of moles of gas produced), 40% of the theoretical maximum transport occurs by varying K over one decade, with only a further 10% being added by considering an additional five orders. Thus it is necessary for reactions with large ΔH° values also to have large ΔS° values to bring ΔG° close to zero at a convenient temperature. Since large values of ΔS° are produced by changes in the total number of moles of gas through reaction it follows that the most efficient reaction is that accompanied by a large volume change, an exothermic reaction involving a diminution in volume and an endothermic an increase.

Hence we see that for efficient transport the enthalpy change of the reaction must be reasonably large but the entropy change such that K has a suitable value at a convenient temperature. If we are also to consider the co-transport of other species, to form compounds, additional constraints are imposed. The partial pressure of the transporting vapours must be approximately in the stoichiometric ratio of the final compound, and the chemical potentials of the constituents at the points of vapourisation and deposition of the compound must have suitable values.

3.3.1 Application to Whisker and Platelet Growth

It was shown in section (3.1) that 1D and 2D growth morphologies are favoured by maintaining a low supersaturation level, below that for 2D nucleation. In transport reactions the amount of transported material is closely related to the supersaturation, and for the particular growth form required this transport must be kept at a low level. Thus, unlike most metallurgical applications, thermodynamic considerations are used to control rather than to maximise transport

rates. This would imply the use of reactions with low ΔH° values, having small temperature dependencies, and thus allowing relatively large temperature differences to be used. If ΔH° is too small however, reactions will occur without transport, cf. $NiI_2 \longrightarrow Ni + I_2$.

It is advantageous for a reaction to proceed at the lowest possible temperature to keep the vapour pressure, which depends exponentially on temperature, at a low level. It will also be shown later that the gas flow is important in controlling the arrival and removal of gaseous compounds. Halides have already been shown to be useful transporting agents, being volatile and easily reduced, and were used in these investigations.

Strictly speaking the ΔG of a reaction at temperature T can be written as:-

$$\Delta G_T = \left[\Delta H_{298} + \int_{298}^{T} \Delta C_p \, dT\right] - T \left[\Delta S_{298} - \int_{298}^{T} \frac{\Delta C_p}{T} \, dT\right]$$

But it is acceptably accurate for this work to neglect the finite heat capacity changes, but not the heats and entropies of phase changes, which are important. When these are included the above expression reduces to $\Delta G^{\circ} = \Delta H^{\circ} - T\Delta S^{\circ}$.

If we consider the hydrogen reduction of the halides, the heats of reaction are -30, -24 and -26 k cals/mole for the chloride, bromide and iodide of nickel respectively. Attention has been focussed on the bromide reactions, which potentially show the lowest transport. Hydrogen, diluted in argon or nitrogen was passed through water and over bromide heated to ~ 700°C. The probably reaction sequence was:-

dehydration:

$$\langle NiBr_2 - 3H_2O \rangle \xrightarrow{\text{at } 200^{\circ}C} \langle NiBr_2 \rangle + 3(H_2O) \qquad (1)$$

sublimation:

$$\langle NiBr_2 \rangle \longrightarrow (NiBr_2) \qquad (2)$$

hydrolysis:

$$(NiBr_2) + (H_2O) \longrightarrow \langle NiO \rangle + 2(HBr) \qquad (3)$$

reduction:

$$\langle NiO \rangle + (H_2) \longrightarrow \langle Ni \rangle + (H_2O) \qquad (4)$$

$$(NiBr_2) + (H_2) \longrightarrow \langle Ni \rangle + 2(HBr) \qquad (5)$$

(3.8)

Reaction (1) is of no importance in itself except that it helps to provide a suitable atmosphere for the hydrolysis reaction (3) to occur. The effect of reaction (2) is to lower the magnitude of the ΔH_{298} of $NiBr_2$, by vapourising it, and to increase its entropy, both facts being important in the subsequent reactions. The state functions of these reactions were calculated at 298°K, accounting for sublimation changes at this temperature from values given by Kubaschewski et al (1967) or estimated from related values, these are shown in TABLE (3.1).

TABLE (3.1)

REACTION number	ΔH°_{298} kcals/mole	ΔS°_{298} cals/mole/deg	ΔG°_{1000} kcals/mole	K
3	- 24.2	- 13.8	- 10.4	1.7×10^2
4	- 0.3	+ 11.9	- 12.2	3.8×10^2
5	- 24.5	- 1.9	- 22.6	7.4×10^4

From these values the Ellingham diagram of the reactions can be drawn, (FIG. 3.1a). The fact that these calculations were made for ΔH at 298°K may decrease the accuracy but in no way invalidates the subsequent remarks. It is immediately apparent that reaction (4) with its low ΔH° value will occur without transport but that transport is possible with reactions (3) and (5), which have similar ΔH° values and multiplicities of unity. The difference between these two reactions lies in the lower entropy value of hydrogen than of water.

The results of the experimental section (3.4) are anticipated

here to record that a typical condition for the successful growth of nickel was to have a flow of 50 ccs/min of argon carrying 0.7-0.8 ccs/min of H_2 bubbled through water and passed through the furnace at 700°C. The total pressure in the system was atmospheric (760 mm.Hg) and was considered to have a saturated water vapour pressure at room temperature, i.e. 20 mm.Hg. At this temperature the partial pressure of ($NiBr_2$) is 0.0123 mm.Hg and of Ni 10^{-11} mm.Hg. It can be seen by checking the reaction $2Ni + O_2 \longrightarrow 2NiO$ on a plot of oxygen potentials in the oxide systems (Swalin), that the P_{H_2}/P_{H_2O} ratio is sufficient to inhibit the oxidation of any nickel if greater than 1%, and P_{O_2} must be kept below 10^{-16}.

Using the values of ΔG° at the operating temperature the equilibrium constant K can be calculated from $\Delta G^\circ = -RT \ln K$, and the results are shown in TABLE (3.1). The equilibrium constant for reaction (3) is

$$K_3 = \frac{(P_{HBr})^2 \; a_{NiO}}{(P_{H_2O})(P_{NiBr_2})}$$

By assuming the activity of NiO to be unity the equilibrium partial pressure of HBr produced was calculated to be 5 mm.Hg. Similarly from reaction (5)

$$K_5 = \frac{(P_{HBr})^2 \; a_{Ni}}{(P_{H_2})(P_{NiBr_2})}$$

and by assuming unit activity for Ni the equilibrium partial pressure of HBr produced in this reaction was estimated to be 105 mm.Hg.

In fact, these reactions do not occur under equilibrium conditions and the activities of the solids will not be unity. However, from comparison of the values of the equilibrium pressures in the two reduction reactions it is clear that reaction (5) leads to a far higher equilibrium pressure, and thus would be more sensitive to any back pressure applied down the growth tube.

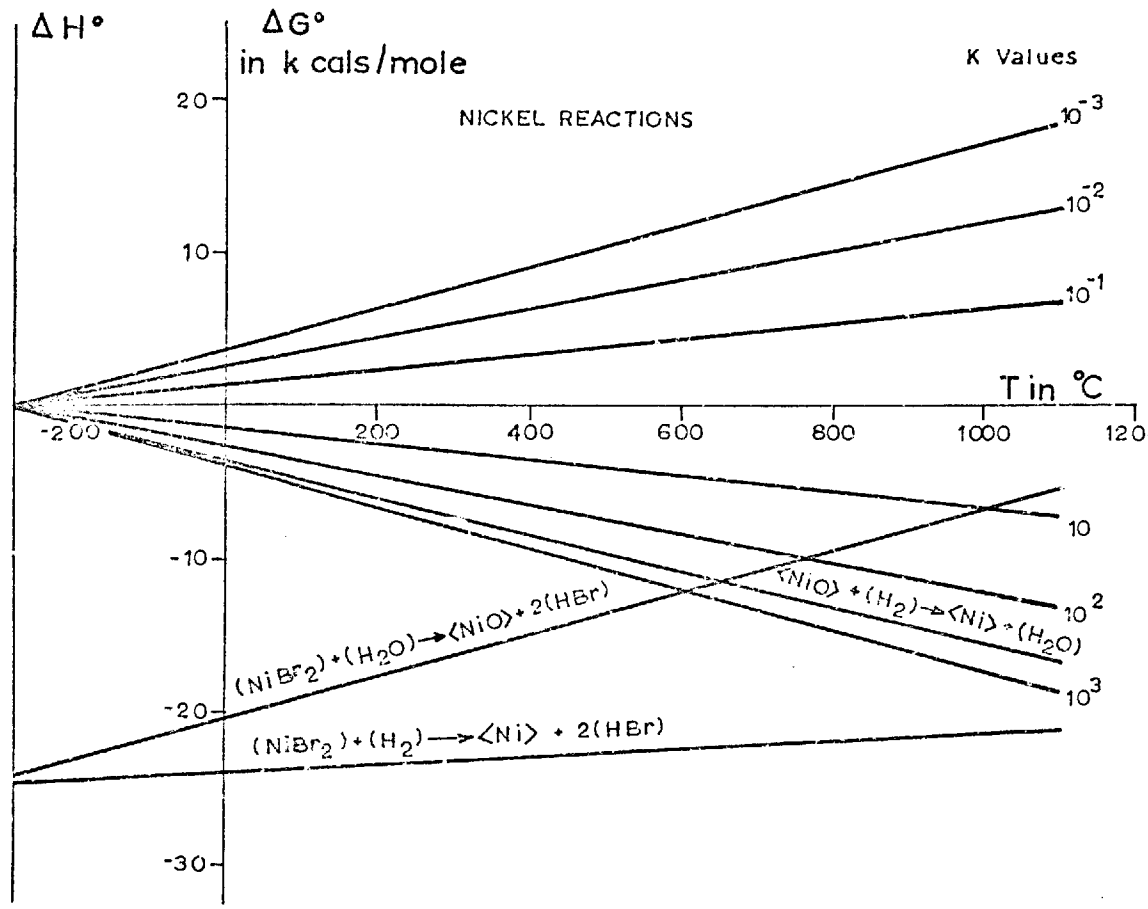

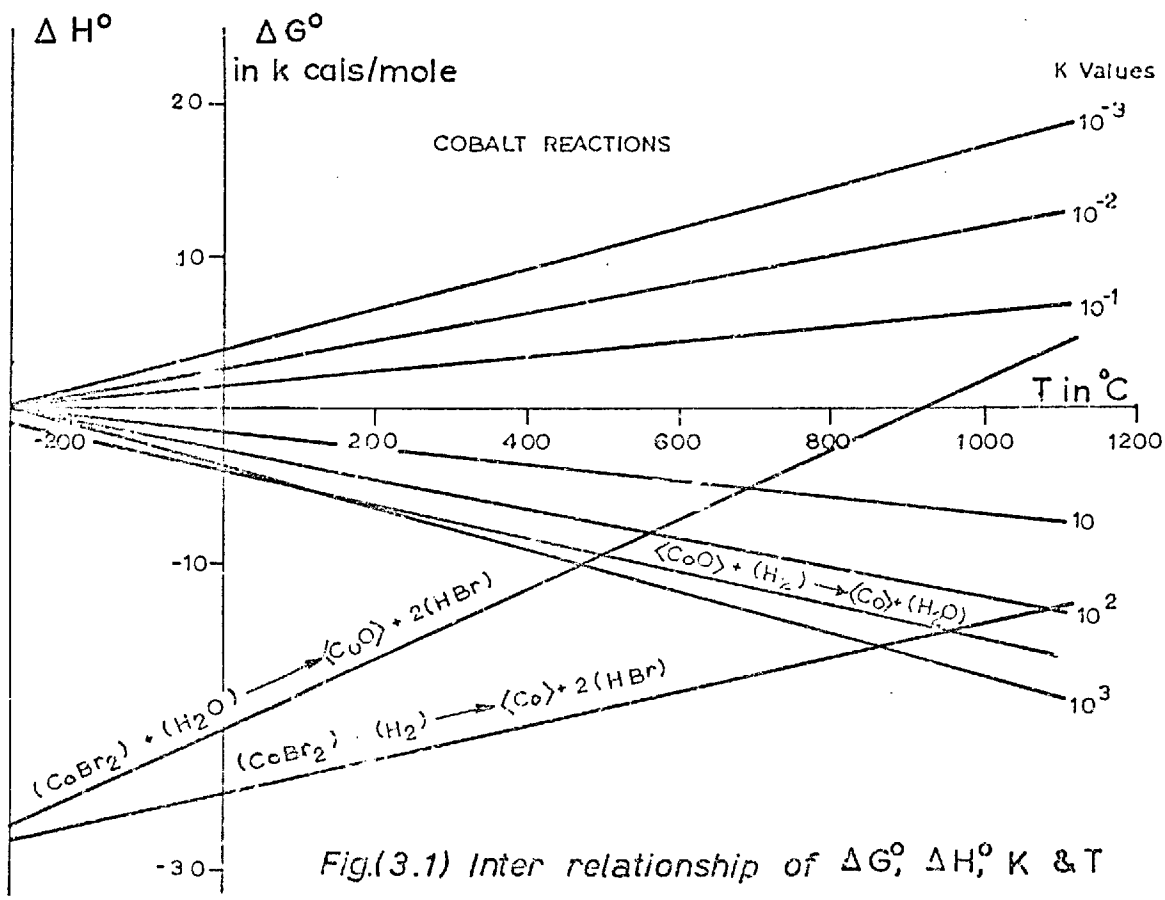

Fig.(3.1) Inter relationship of ΔG°, ΔH°, K & T

Observations on the amount of liquid condensed at the end of the tube and its acidity at the end of a run have indicated that not enough HBr has been produced to have accounted for a partial pressure of 110 mm. during the whole duration of the growth period, (say 8 hrs.). This implies that the reaction processes are determined not by equilibrium conditions but by the arrival at the $NiBr_2$ growth sites of H_2 and H_2O in the vapour stream. Thus control of gas flow is important.

3.3.2 On Alloy Growth by Co-transport

The magnetic properties of both Ni/Co and Ni/Fe alloy systems are of interest because of the variations that occur in anisotropy and magnetostriction constants with composition.

(a) The Ni/Co System

If the cobalt system is considered first the reaction equations equivalent to (3.8) are:-

dehydration:

$$\langle Co\,Br_2 - 6H_2O\rangle \xrightarrow{\text{by } 130^\circ C} \langle Co\,Br_2\rangle + 6(H_2O) \qquad (1)$$

sublimation:

$$\langle Co\,Br_2\rangle \longrightarrow (Co\,Br_2) \qquad (2)$$

hydrolysis:

$$(Co\,Br_2) + (H_2O) \longrightarrow \langle Co\,O\rangle + 2(HBr) \qquad (3)$$

reduction:

$$\langle Co\,O\rangle + (H_2) \longrightarrow \langle Co\rangle + (H_2O) \qquad (4)$$

$$(Co\,Br_2) + (H_2) \longrightarrow \langle Co\rangle + 2(HBr) \qquad (5)$$

(3.9)

and as before the state functions for these reactions can be calculated and are shown in TABLE (3.2).

TABLE (3.2)

REACTION number	ΔH^{o}_{298} kcals/mole	ΔS^{o}_{298} cals/mole/deg	ΔG^{o}_{1000} kcals/mole	K
3	- 27.2	- 23.1	- 4.1	7.7
4	- 0.7	- 11.0	- 11.7	3.5×10^{2}
5	- 28.1	- 11.1	- 17.0	2.3×10^{3}

From these values the Ellingham diagram FIG.(3.1b) is drawn, which is seen to resemble FIG.(3.1a) and comparisons may be made between the two systems. The ΔH^{o} values are comparable but the ΔS^{o} values of reactions (3) and (5) are much larger, thus reducing the ΔG^{o} values and hence the equilibrium constants K of these reactions, for the same operating temperature as the nickel reactions.

The lower magnitude of these ΔG^{o} values for the Co reactions indicate a more efficient transport than for Ni. From this the growth of platelets rich in Co would be expected when starting with an equal ratio of bromides. This is, in fact, not the case and will be discussed further in section (3.4.2).

(b) The Ni/Fe System

The growth of iron platelets has not been attempted by the author. Platelets and whiskers both of iron and of cobalt have been grown by Kotrbova and Hauptman (1965), but by using a sealed system and diffusion controlled processes. The thermodynamic work of Schäfer is more applicable to this type of reaction and quantitative predictions have been found to hold well.

Open tube reductions of iron chlorides and bromides were extensively investigated by Gorsuch (1959) for the production of iron whiskers. His results showed that the presence of the oxide, either as an impurity or deliberately introduced, was necessary for the growth of these whiskers, and may also affect the orientation of the whiskers. Fe_2O_3 appears to be very effective in increasing the whisker yield

from $FeBr_2$.

It would be possible to write chemical equations for the hydrolysis and reduction of $FeBr_2$ via haematite Fe_2O_3 or magnetite Fe_3O_4. However, there is no evidence to support any reaction sequence and iron platelets have yet to be produced by this method.

De Blois (1968) reports the growth of permalloy platelets with iron concentrations up to 26% by introducing a very low flow of oxygen. The gas flow ratios of argon to hydrogen to oxygen are 1000 : 10 : 1. At these low supersaturations iron was introduced into the nickel platelets but iron platelets themselves were not grown. No attempt has been made to determine the thermodynamic relationships for the process.

3.3.3 Limitations of Application

By rearranging equation (3.2) the critical supersaturation ratio below which whisker growth can occur is:

$$\alpha_c = \exp\left[\pi a \sigma^2 M/\rho R\, k\, T^2 \ln\left(\frac{B}{N}\right)\right] \qquad (3.10)$$

And from equation 3.7:

$$\Delta G^\circ = -RT \ln K = \Delta H^\circ - T\Delta S^\circ$$

The first derivative of the free energy of deposition with respect to T is given by:

$$\left(\frac{\partial\, \Delta G^\circ}{\partial T}\right)_p = -\Delta S^\circ$$

Thus to a first approximation it can be argued that:

$$\Delta G^\circ = -\Delta S^\circ\, \Delta T$$

where ΔT is the temperature difference between the source and growth regions.

It has already been shown that $\Delta G^\circ \sim 0$ for efficient transport,

thus $\Delta S^{o} \sim \Delta H^{o}/T$, hence

$$\ln K = \frac{\Delta H^{o}\ \Delta T}{RT^{2}} \qquad (3.11)$$

In a simple system of a condensing vapour, K in (3.11) becomes synonymous with the supersaturation of the vapour. Thus Morelock and Sears (1961) were able to relate ΔH^{o} to ΔT and determine the maximum value of ΔT, ΔT_{c}, compatible with 1D growth conditions.

In the case of growth by halide reduction the equilibrium constant does not bear a simple relationship with the supersaturation of a depositing vapour, as seen on page 60, and equations (3.10) and (3.11) cannot be directly related.

Of the possible reactions leading to a given solid phase, that with the smallest enthalpy will have the largest ΔT_{c}. Referring to FIG.(3.1), however, it is seen that there is little difference in the reaction enthalpies, and at the operating temperature the assumption that $\Delta G^{o} \sim 0$ is questionable.

Observations on the growth of platelets, reported later in this chapter, indicate that although thermodynamic analysis is useful it is limited. There are insufficient data available to enable reaction kinetics to give meaningful results.

3.4 GROWTH OF FERROMAGNETIC PLATELETS

3.4.1 Experimental Procedures

Investigations on aspects of crystal growth by halide reduction and the production of platelets were made in the furnace arrangement seen in FIG.(3.2).

The furnace itself consisted of an impervious Mullite tube 60 cms. long with 6.5 cms. o.d. (Morgan Refractories) would with 100 turns of Kanthal A1 resistance wire (1.6 Ω/ft.) with a centred

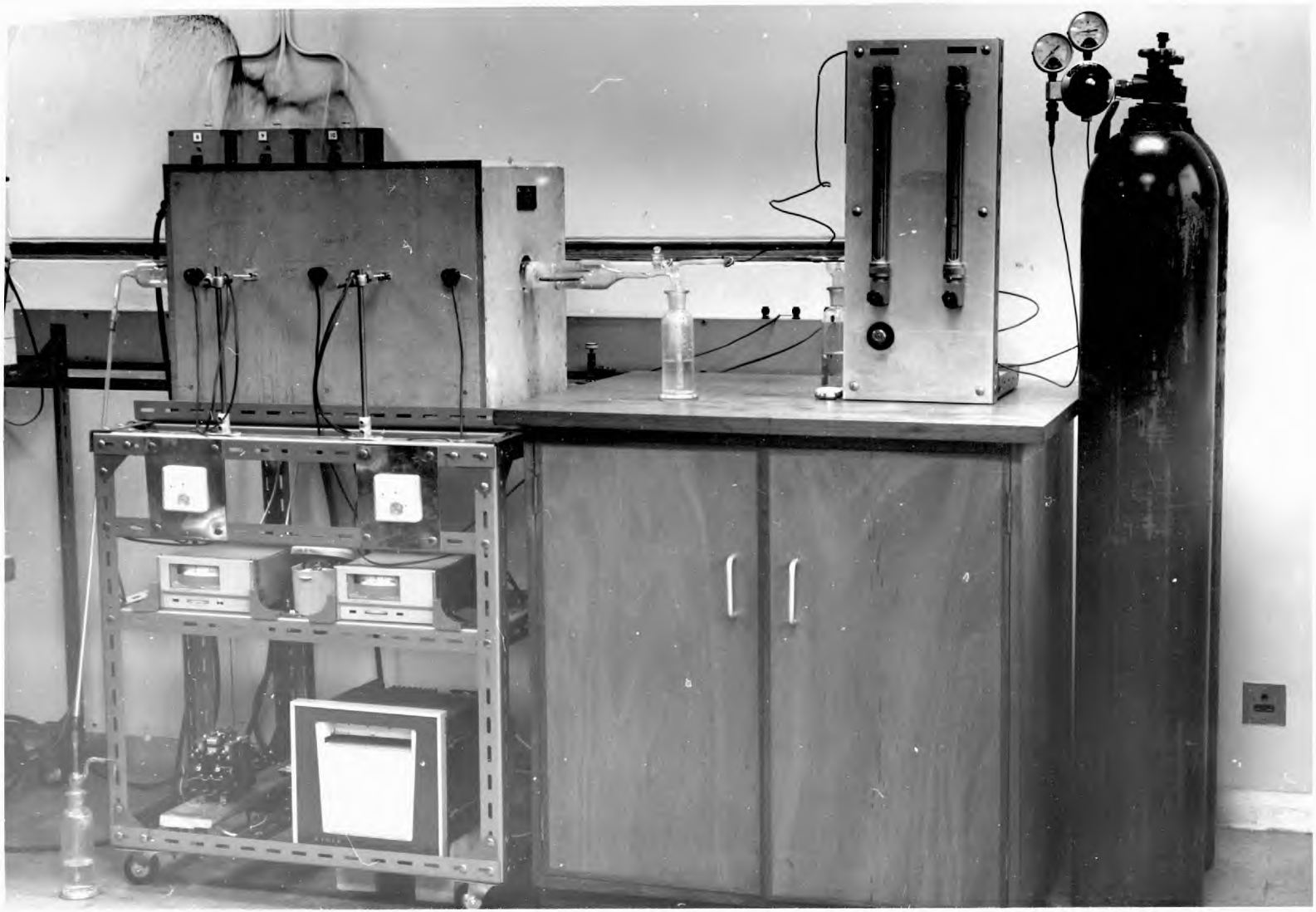

Fig. (3.2) Apparatus for vapour growth of platelets

earth tapping. The wire was held by $\frac{1}{2}$" thickness of alumina Tri-mor heat set cement (Morgan Refractories) applied in two coats. The tube and windings were supported on fire bricks in a $\frac{1}{2}$" thick Sindanyo case filled with Micafil.

The current in each half of the furnace was independently controlled by two P.I.D./S.C.R. stepless three-term controllers (Eurotherm). Temperature sensing was by two Pt/Pt 13% Rh thermocouples resting in indentations in the winding cement 26 cms. apart. These same thermocouples served to record the temperatures of either half on a chart recorder. The controllers were activated by a Venner time switch operating a contactor to the main power supply.

The split winding allowed adjustment of the controllers so that the temperature profile could be altered at will; typical forms are given, FIG.(3.3). These were found by traversing the length of the inner tube with a Cr/Al thermocouple for specific settings of the controllers.

Gas flows of high purity hydrogen and argon or nitrogen were monitored by flow meters and an additional silicone fluid bubbler was used for the hydrogen. The two flows were then mixed and bubbled through about 6 cms. of water before passing through a vitreosil silica tube, 5 cms. o.d. (Jencons) in the furnace. The exiting gases were again bubbled through water (to dissolve the HBr formed) before being expelled from the system. Thus the system was held slightly above atmospheric pressure.

A typical growth run was made with a chain of three glazed porcelain boats, 5 x 3 x 1 cm. (Royal Worcester), placed in pairs at known locations inside the growth tube. To grow Ni platelets approximately 10 g. of $NiBr_2.3H_2O$ (B.D.H. Reagents, Lab. grade) were placed in uniform layer across the bottom of each boat. The fit between the boats was not perfect and it was possible for gases to diffuse between the gaps.

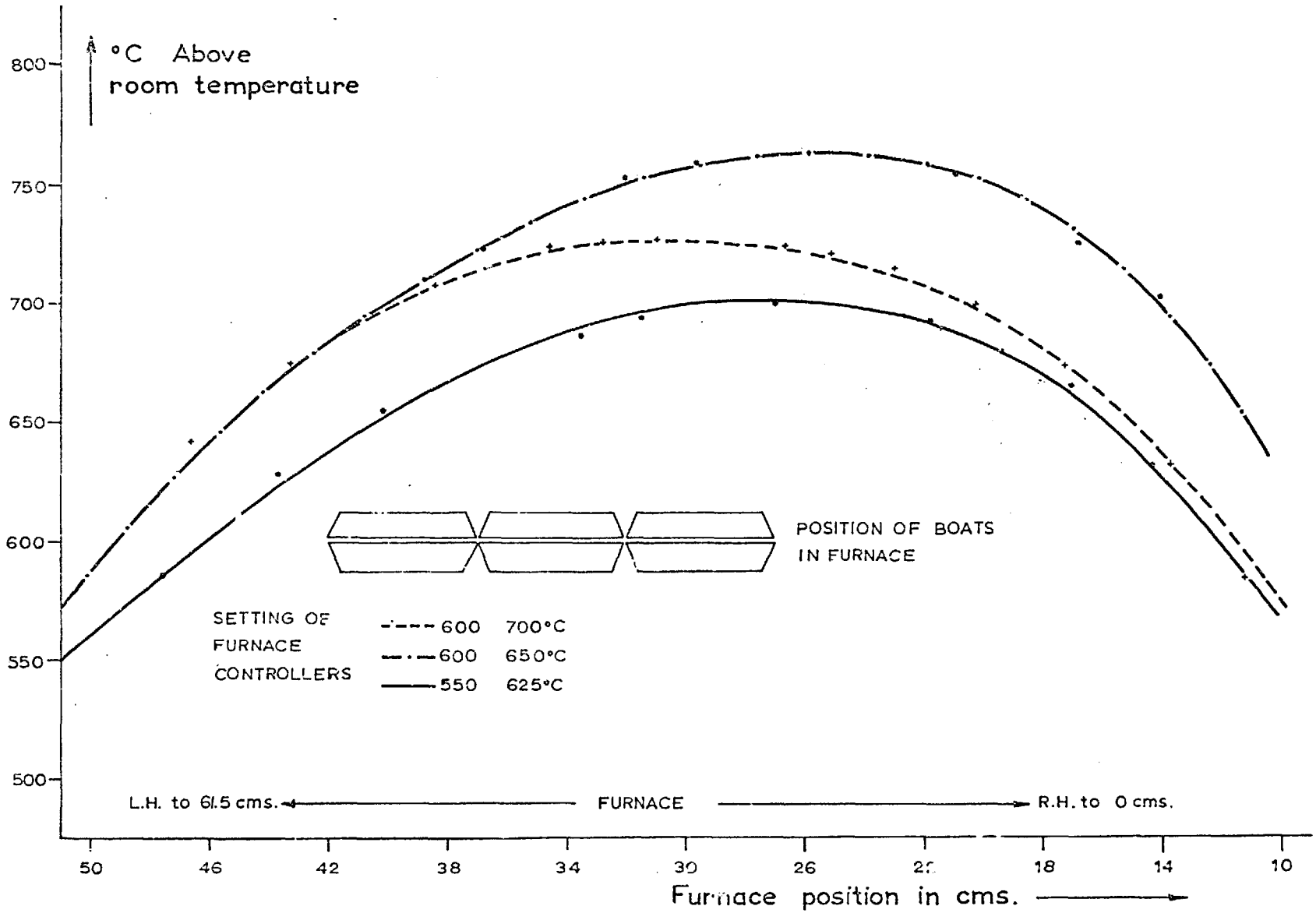

Fig.(3.3.) Temperature profiles of furnace

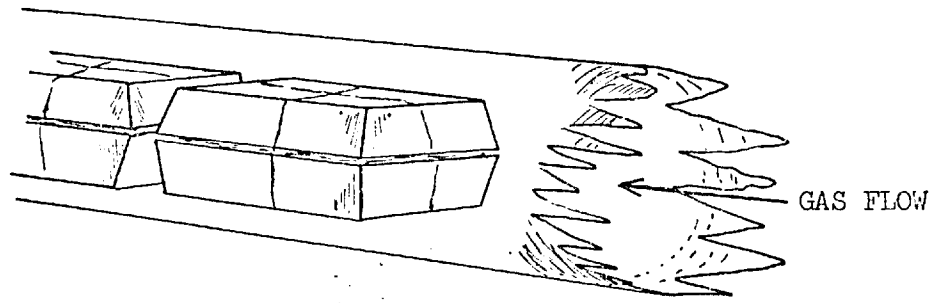

Gases were allowed to flow through the silica tube in the required ratio for 2 hours to ensure that the correct atmosphere existed inside the tube. During this period adjustments could be made to critically control the hydrogen flow. The furnace was switched on and reached the chosen operating temperature within $\frac{1}{2}$ hour and was controlled at this setting for 8 hours. To terminate the run the furnace was allowed to cool with the gas flow remaining unaltered. The insulation was very effective in reducing the cooling rate, and 4 hours were usually allowed to elapse before the boats were removed. An improvement to the method might have been to increase the hydrogen flow rate on cooling to remove any surplus bromide deposited on the crystal surfaces, but usually this was not troublesome.

The boats were placed with the front of the first boat at the peak of the temperature profile and successive boats at lower temperatures as seen in FIG.(3.3). As soon as the furnace heated up water began to condense at the end of the tube, being at first colourless but developing a strong brown/purple colouration which intensified as the run continued and the water dissolved more HBr gas. At the end of a run it was possible to pour off about 5 ml. of HBr solution. Throughout the duration of the run a certain amount of $NiBr_2$ was transported to the cold end of the tube and condensed as a fibrous brown/green mass across the entire tube section.

Ideally to obtain the largest and most perfect specimens, platelets

should be grown with minimal flow rates of the gases. This is difficult to achieve because the free passage of reactants and products to and from the growth site is also needed, and a certain flow is necessary. The complexity of the reactions and the number of interdependent parameters inhibit quantitative interpretation of the results, however certain observations can be made as a result of many growth runs.

The critical parameters are the temperature and the flow rates. For Ni the temperature must lie within certain limits; if too low, insufficient transport of the $NiBr_2$ occurs, and if too high reduction becomes too rapid with equant growth resulting. Satisfactory conditions were found with a temperature maximum inside the tube of 700°C and a temperature gradient which increased on either side of the peak plateau to reach a maximum of 6°/cm. after about 10 cms., see FIG.(3.3). If the hydrogen flow is too low then, as shown in the previous section, excessive oxidation will occur, whereas a high hydrogen flow will encourage reduction and equant growth. A satisfactory lower limit for the diameter of tube was found with a hydrogen flow of not less than 0.7 ml./min. mixed in ar argon or nitrogen flow of 30-50 ml./min., the nature of the carrier gas being unimportant.

One interesting example of the effect of low hydrogen flow was the growth of NiO platelets, which formed during a run in which the hydrogen flow tube became blocked. These were typically 200 μm long with regular sides. They were transparent and green in colour. Some showed extinction patterns under crossed polaroids which were attributed to local strains within the platelets. This was not investigated further.

3.4.2 Observations on Growth

The extent of reduction in the boats at the end of a run was found to vary according to their position in the furnace. The first boat placed at the highest temperature and facing the incoming gases

showed the greatest amount of reduction and loss of material, with $NiBr_2$ being transported outside the "clamshell" formed by the boats. The reduction and transport decreased at the lower temperatures in successive boats so that even at the end of a run a large amount of $NiBr_2$ in the third boat remained unchanged. It was also possible for the surface layer of $NiBr_2$ to become reduced thus acting as a barrier to the sublimation of further quantities of $NiBr_2$ and maintaining a low supersaturation of $NiBr_2$ vapour.

Platelets and whiskers produced in the manner described grew on the inside of the top boat of the clamshell and on the sides of the lower boat, either individually or in clumps, FIGS.(3.4a & b). Platelets also grew from condensed bulk crystals as seen in FIG.(3.4c).

Occasionally platelets were found growing in profusion on the outside surfaces of both upper and lower boats. Although these platelets were often comparatively large they were usually unsatisfactory, being apparently more susceptible to acid attack and having poor surfaces. Small gaps between the upper and lower boats must play an important role in establishing diffusion conditions, but this is not understood. Thermocouple measurements, made without the boats present, indicated no radial temperature variation in the tube. However, during growth the presence of the clamshell must have introduced a diffusion or temperature barrier sufficient to displace the conditions from equilibrium for growth to occur.

De Blois (1968) reports the use of shallower boats, with a longer lower boat supporting two separate upper boats, as an aid to the growth of larger platelets. This probably promotes a freer interchange of vapours within the clamshells while at the same time still acting as a barrier to incoming gases.

In experiments using boats with lapped edges the rate of reaction predictably was found to be lower and the growth slightly more perfect, but in such a complex system experiments of this type were difficult to

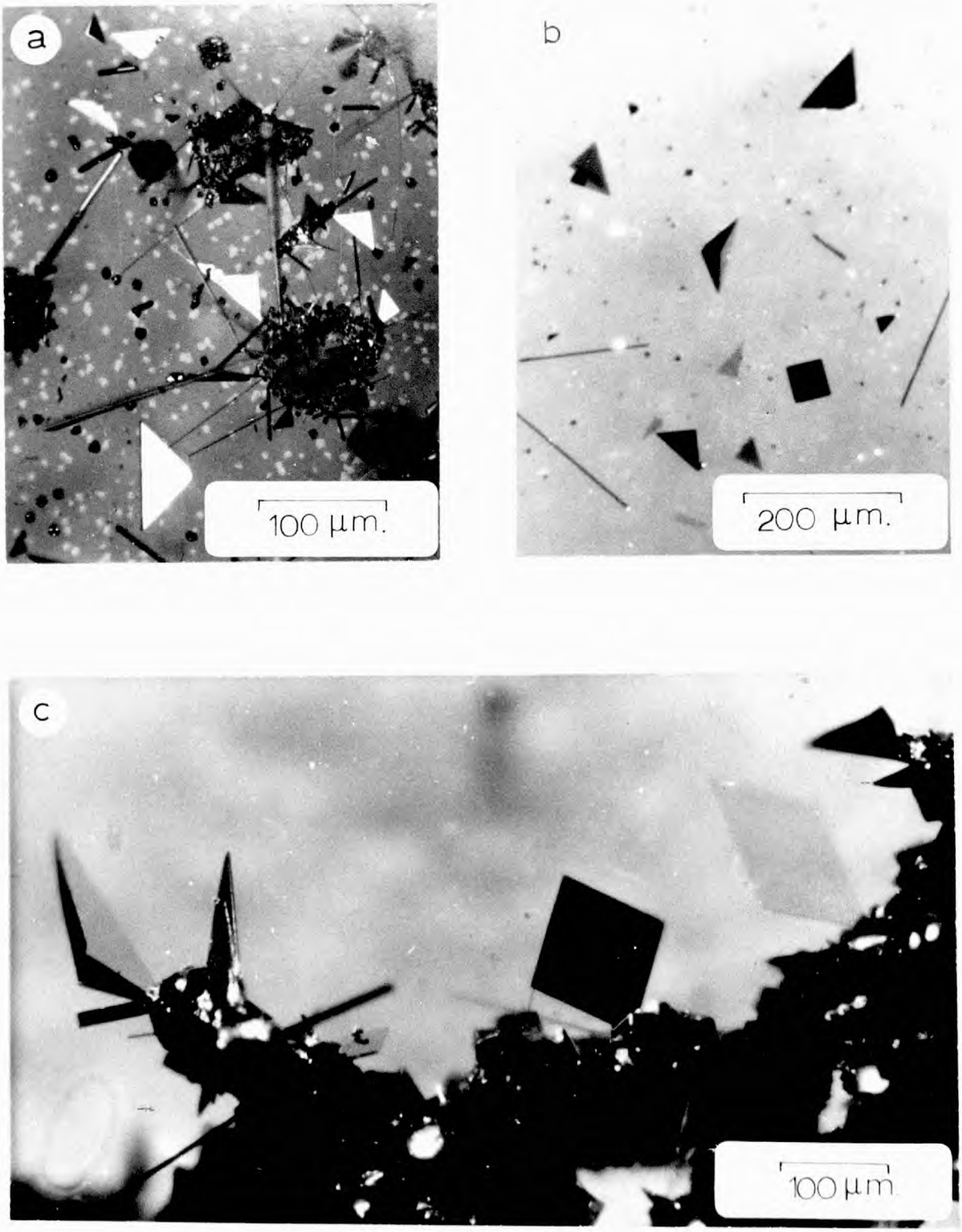

Fig. (3.4) Crystal growth formations on ceramic surfaces

interpret due to the difficulty in measuring temperatures and concentrations and identifying the gases species in situ. However, at the end of a growth run vapours were occasionally seen to have condensed on the end of the tube in such a way as to indicate that a definite convective flow pattern had been followed during the run.

Between runs the growth tube was cleaned in cold HNO_3 and the boats in hot HNO_3 for 24 hours. Repeated heating and cleaning was found to destroy the glaze on the boats and produce a slight adverse effect on the nucleation conditions. Conditions appeared to slightly favour 1D growth in newer boats, but this was not considered to be an important factor.

The effect of the substrate was further investigated by the insertion of crystals of alumina and quartz inside the roof of the clamshell. Results of these experiments were inconclusive indicating, if anything, that the surface upon which 1 and 2D growth forms, plays only a secondary role. The nature of these morphologies will be further discussed in the following section.

Crystals of alloyed Ni/Co were also grown by reduction of a mixed bromide charge. This charge was obtained by recrystallising a mixed solution of Ni and Co bromides of known concentrations. The residue was ground and spread over the bottom of the boats. This procedure was considered to give a uniform starting charge.

The starting ratio normally used was Ni : Co = 50 : 50 and the results of many runs made with various gas flows and temperatures indicated that the conditions for the growth of alloys were not identical to those for pure Ni. More suitable conditions with the 50 : 50 charge used the same inert gas flow of 50 ml./min., but with the hydrogen flow reduced to less than 0.3 ml./min., and the maximum temperature raised to 730°C. With a higher hydrogen flow, comparable with that used for Ni growth, excessive transport and equant growth occured. However, even with the lower flow the amount of material

transported to the end of the tube appeared to be higher with the alloy composition. This gave the fibrous mass a pink colour from the $CoBr_2$ content, and confirmed thermodynamic calculations of greater transport (see FIG.(3.1)). One further difference noted was the decreased number of rectangular and square platelets obtained with the mixture compared with the pure Ni.

Some runs were also made starting with higher Co contents and the required conditions were found to differ further from those for Ni although insufficient data are available to enable further conclusions to be drawn.

Electron Microprobe analysis, see section (4.2), of the alloy platelets produced showed that the final Ni : Co ratio of a platelet differed markedly from that of the starting bromide. Samples were taken from positions along the boats filled with a 50 : 50 starting charge The recorded compositions of the platelets analysed showed the Ni content to vary between 80 and 87% and to have no systematic variation or correlation with other parameters, such as the temperature of the growth site.

This variation of final platelet composition from the ratio of starting bromides was further confirmed by taking Debye-Scherrer powder photographs of the residual oxides in boats at the end of a run. From lattice parameter measurements it was found that an oxide with spacing 4.205 Å, equivalent to 85% Ni, was formed from a 50 : 50 bromide mixture and an oxide with spacing 4.235 Å, equivalent to 45% Ni, was formed from a 25 : 75 Ni : Co starting mixture.

This change between the starting material and the final platelet composition can be explained by comparing the equilibrium constants at 1000°K for $NiBr_2$ reduction, 7.4×10^4, and for $CoBr_2$ reduction, 2.3×10^3. By assuming unit activity for the metal we find the ratio of the equilibrium partial pressures of Co and Ni in these reactions is 5.5. Thus we see that whilst being compatible with equilibrium conditions

there is a greater tendency for $CoBr_2$ to remain in the vapour phase and be finally carried out of the reaction zone than to deposit through chemical reduction leading to crystal growth. This also explains the observed increase in condensed $CoBr_2$ at the end of a growth run, mentioned earlier.

During co-transport examples have been found of compositional variations across a platelet, but generally this variation was not considered to be a problem although every platelet of interest was analysed.

3.5 THE PROBLEM OF GROWTH MORPHOLOGY

3.5.1 The Growth of Whiskers

It was seen in section 3.1.1 that to explain whisker growth at low supersaturations Sears had assumed an axial screw dislocation, previously proposed by Frank. Eshelby (1953 & 1958) showed theoretically that such a dislocation parallel to the axis of the whisker produced a lattice twist approximately proportional to the Burgers vector and the inverse square of the radius. Hirth and Frank (1958) considered the stability of such a dislocation and suggested that it could slip out of the whisker, which while not affecting the strength of the whisker could lead to a cessation of growth.

Against this conclusion Eshelby's 1958 calculations showed that the whisker centre is an equilibrium position and only when the dislocation is displaced by 0.54 of the radius will it slip out of the whisker. Hirth and Frank also showed that when the supersaturation of the vapour falls, the screw step which rotates about the tip of the dislocation exerts a net force on the dislocation, such that the whisker tip becomes a favourable site for the dislocation to slip out of the whisker. This, they have suggested could lead to the possibility of kinking.

The twist in the whisker lattice should in principle be measurable

from the tilt of the equitorial Laue spots formed using a micro focus x-ray tube, the twist being proportional to the tangent of the tilt angle. Attempts have been made on many materials to detect this twist. Webb et al (1957) failed to observe this in many whiskers, including nickel, but detected it in sapphire whiskers. They suggested that there may be an equal number of opposing Burgess vectors in each whisker or else that the screw dislocation is forced out through the lateral surface of the whiskers.

Gorsuch (1959b) in his studies on Fe whiskers also failed to find evidence for a screw dislocation. Although twist boundaries were observed there was no evidence of discontinuous lateral growth, indicating that a screw dislocation is not the controlling growth mechanism. However, the presence of tilt and twist boundaries is consistent with the postulate that impurities build up in front of an advancing growth interface and are precipitated out at periodic intervals.

An alternative to the screw dislocation model was proposed by Wagner and Ellis (1964). Their "vapour-liquid-solid" mechanism emerged from observations that Si whiskers did not contain an axial dislocation but were seen to have a globule of material at the tip. Impurities were found to be essential for whisker growth. The role of the impurity is thought to be in the formation of a liquid droplet of low freezing temperature. This becomes a preferred site for the deposition of vapour, which causes the liquid to become supersaturated with material, which precipitates onto the growing whisker. Later authors have thought this V.L.S. mechanism to account for the growth of several different types of whisker.

Observations on the growth of Cu whiskers have been made by Brenner (1956), Allan and Webb (1959) and Hauptmann and Svoboda (1965). The results of these workers have shown that growth can occur both from the base and the tip of whiskers. Base growth can occur by direct addition of Cu from a supersaturated liquid halide to a growth step at

the bottom, and tip growth by vapour phase deposition onto a screw dislocation or by liquid film migration with a V.L.S. mechanism operating. In fact possible growth boules indicating a V.L.S. mechanism are claimed to have been seen by several workers.

It is quite possible for two mechanisms to operate simultaneously and a recent study by Regis and Calviac (1969) has shown that separate mechanisms with different growth rates can change in their relative significance during different stages of the reduction process.

Finally, it is interesting to mention the work of Bacigalupi (1963) who attempted to grow iron whiskers in a magnetic field of 4.5 K.gauss and found the "stalagmites" that grew from the boat were polycrystalline, with an average crystallite size of 10^{-3} cms. He attributed this aligned polycrystalline growth to an additional crystallization energy which he thought to arise from the interaction of unsatisfied spin structures of the iron atoms.

Despite its simplicity the screw dislocation thus need not be the only mechanism for whisker growth, and indeed its existence can often be questioned.

3.5.2 The Growth of Platelets

The possible growth mechanisms for platelets are more complicated than those for whiskers, and the theory has been less developed. Sears and Coleman (1956) have suggested that platelets can grow by the action of a set of crossed screw dislocations, and Sears (1956) has proposed a mechanism for the vapour deposition of mercury platelets by a single screw dislocation with the preferential nucleation of (001) planes occurring on active sites. Hirth and Frank (1958) predicted theoretically that a dislocation in a metal whisker, having edge components with respect to the whisker axis, would slip out of the whisker more easily than a pure screw dislocation, and by this slip would initiate growth perpendicular to the whisker axis.

Chikawa and Nakayama (1964) made a detailed structural study of

the growth of CdS crystals and concluded that whiskers grew in the initial stages of every crystal. When the whiskers contained two parallel dislocations along the axis platelets were formed by the thickness increase of the whiskers in a direction perpendicular to the axis. They showed theoretically that two parallel axial dislocations are much more stable than any single axial dislocation. The two dislocations were thought to have different Burgess vectors, one being an edge type, and one mixed. The edge dislocation was thought to be responsible for axial growth but both could slip easily out of the crystal to leave dislocation half loops on the side surfaces. The ends of these dislocation half loops acted as new sites for crystal growth in directions perpendicular to the axis, thus forming a platelet.

From observations on the growth of ZnS and ZnSe platelets Fitzgerald et al (1967) failed to find evidence for dislocation half loops and suggested instead that whiskers first grew by an axial dislocation mechanism which then broadened into platelets by the 2D nucleation of atomic planes on the surface of the whisker. With this mechanism they were able to satisfactorily explain the formation and distribution of stacking faults in relation to the crystal habit.

An alternative possible growth mechanism is by a re-entrant edge twin plane, proposed by Faust and Johns (1965). This occurs under certain restricted conditions: the growth must be crystallographically limited, i.e. facetted, and must be possible at a lower supersaturation than that necessary for 2D nucleation; the growth direction must lie in the twin planes and be parallel to at least one of the facetting planes. For F.C.C. structures the only possible facetting planes which satisfy these conditions are the {111} planes with the twin boundaries lying in these same planes.

Under these conditions it is possible for a platelet to grow out, but a twin plane would be expected through the centre of the platelet, to provide a self perpetuating step. Twinning can play an important

role in crystal growth and can often be observed macroscopically by the presence of 'butterfly' twins, the angle between the wings being related to the twinning plane. An example of frequent growth in this morphology is $BaTiO_3$, but even here the reason for the precise form of the twin is not clear, White (1955).

3.5.3 The Growth of Ferromagnetic Platelets

The habit of the ferromagnetic platelets which have been grown is particularly difficult to explain. FIG.(3.5) shows a selection of typical platelet shapes produced by vapour transport and placed on a filter paper. These platelets all have (100) faces bounded by [100] or [110] edges. The first two groups, (a) and (b) show the more conventional rectangles and triangles. The rectangles show no outstanding features except for the not infrequent loss of a corner from the edge attached to the substrate, as shown by the separated specimen in (a). The triangles were less often complete and could be found with curved growth edges or as perfect trapezoids. The centre crystal of (b) also shows growth along a higher index edge, [130], in addition to a fine whisker-like extension at either end of the [110] edge. Whereas rectangles were most frequently found growing vertically from the boat the triangles and related forms were found growing with a corner attached, or sometimes just lying on the surface of the boat, as seen in FIG.(3.4).

FIG.(3.5c) shows a 'kite' shape always found growing with the extended tip (arrowed in photograph) attached to the substrate, and it is interesting to note that the outward edges are facetted but curved edges fall away to the substrate base. Finally, FIG.(3.5d) shows some of the more peculiar growth forms which were typically found, but which currently defy explanation.

Strong evidence was found to connect whisker and triangular platelet growth habits, but for the size of specimen involved optical microscopy was rather limited. Useful results were obtained by

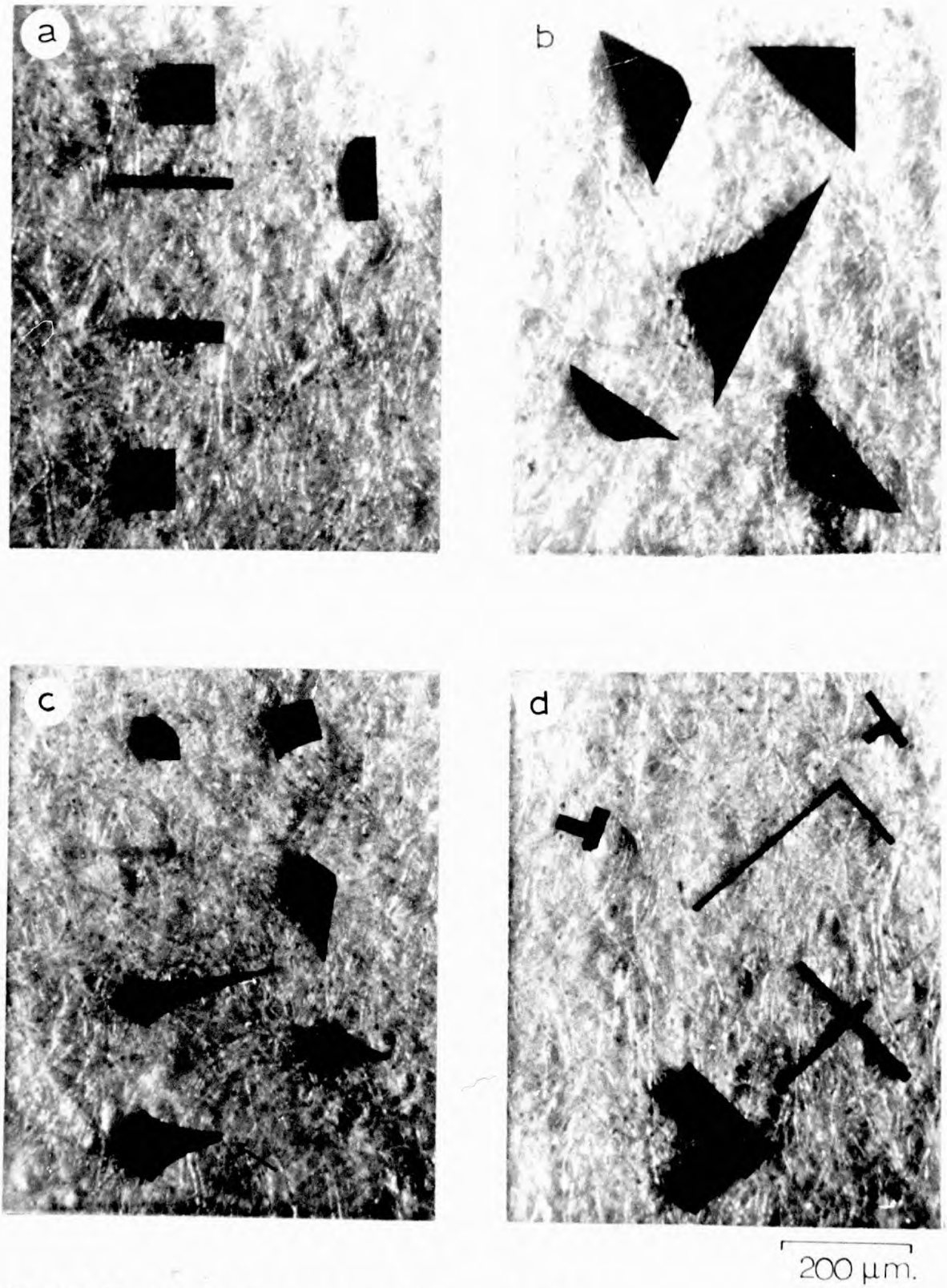

Fig. (3.5) Varieties of growth morphologies

electron microscopy using a J.E.M.7 microscope operated at 100 kV. Diffraction patterns from thinner platelets showed a simple cubic lattice pattern and from thicker specimens sharp Kikuchi lines, indicating the perfection of the lattice.

FIG.(3.6a) shows a micrograph of the 45° tip of a right triangle platelet with a very pronounced thickening along the [110] hypotenuse of the platelet, which extended slightly beyond the end. This extension is even more pronounced in (b) where a second minute platelet is seen to have formed completely isolated from the main one. The thickening is thought to be a whisker which exists down the whole length of the hypotenuse. This is confirmed in (c) which shows an area in the centre of that edge. Other observations have shown that the whisker can extend beyond the platelet onto the substrate, which suggests that the whisker may be formed in the initial stages of growth, with the platelet developing later.

A micrograph (d) taken with a scanning electron microscope (SEM) shows the existence of this whisker edge in more detail. The black patch can be ignored as this was due to charging of the platelet by the incident electron beam.

Typical scanning microscope observations made on whiskers with a Stereoscan (SEM) are seen in FIG.(3.7). In (a) the tip of a <100> axis whisker is seen, showing the sharpness of the edges and smoothness of the visible faces. The slight displacement near the top of the whisker can be ignored, being instrumental in origin. The specimen was sprayed with a conducting Aerosol spray before insertion in the SEM and this is thought to account for the mottled surface appearance.

Another <100> axis whisker is seen in (b) with a terminating set of (111) planes clearly visible. Again the vertical discontinuity is instrumental, but the peculiar tip above the (111) planes is real. A region lower down the whisker, whose tip was seen in (a), is shown in (c). The edge between the two (100) faces is now seen to have flattened

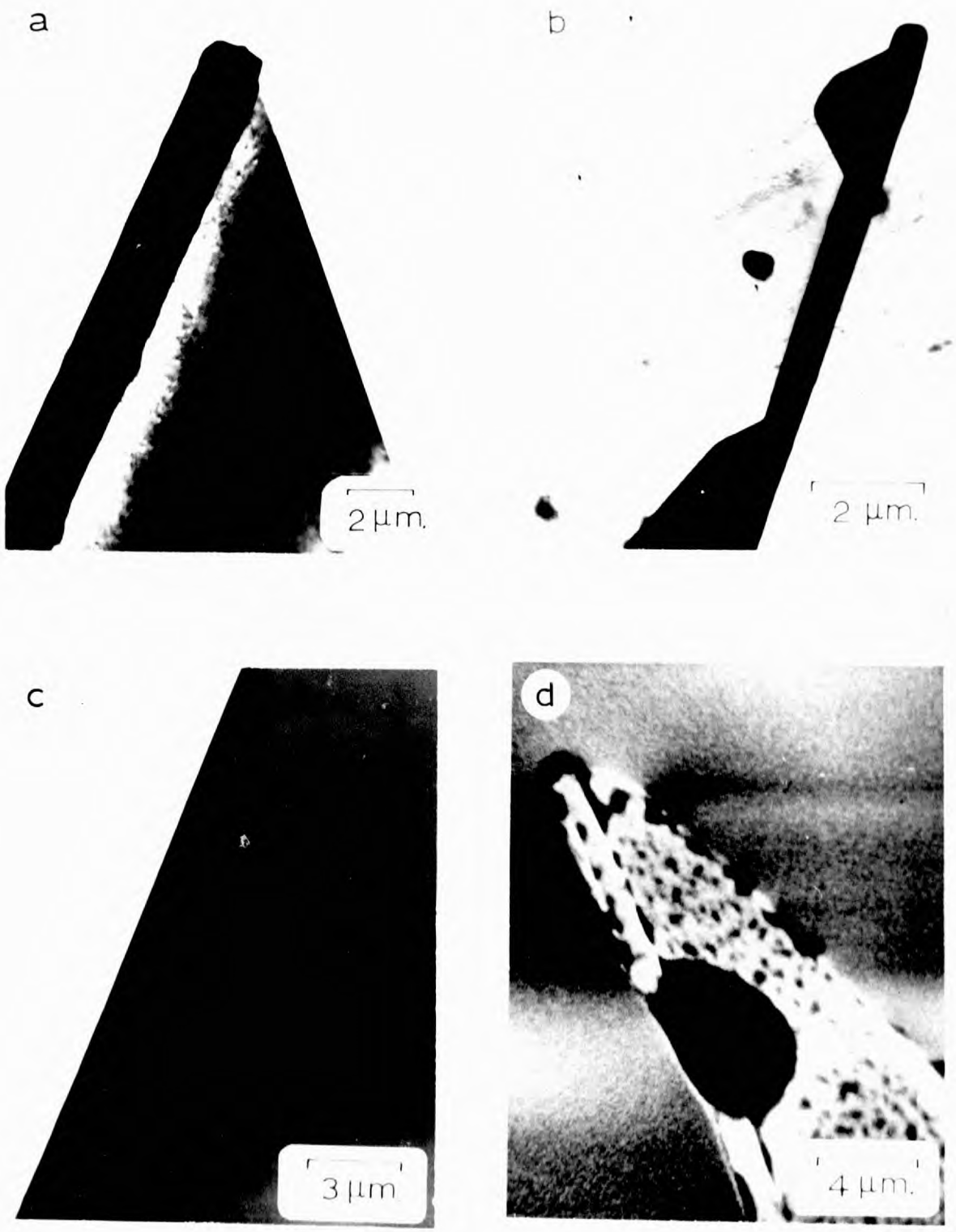

Fig. (3.6) Electron micrographs of platelets

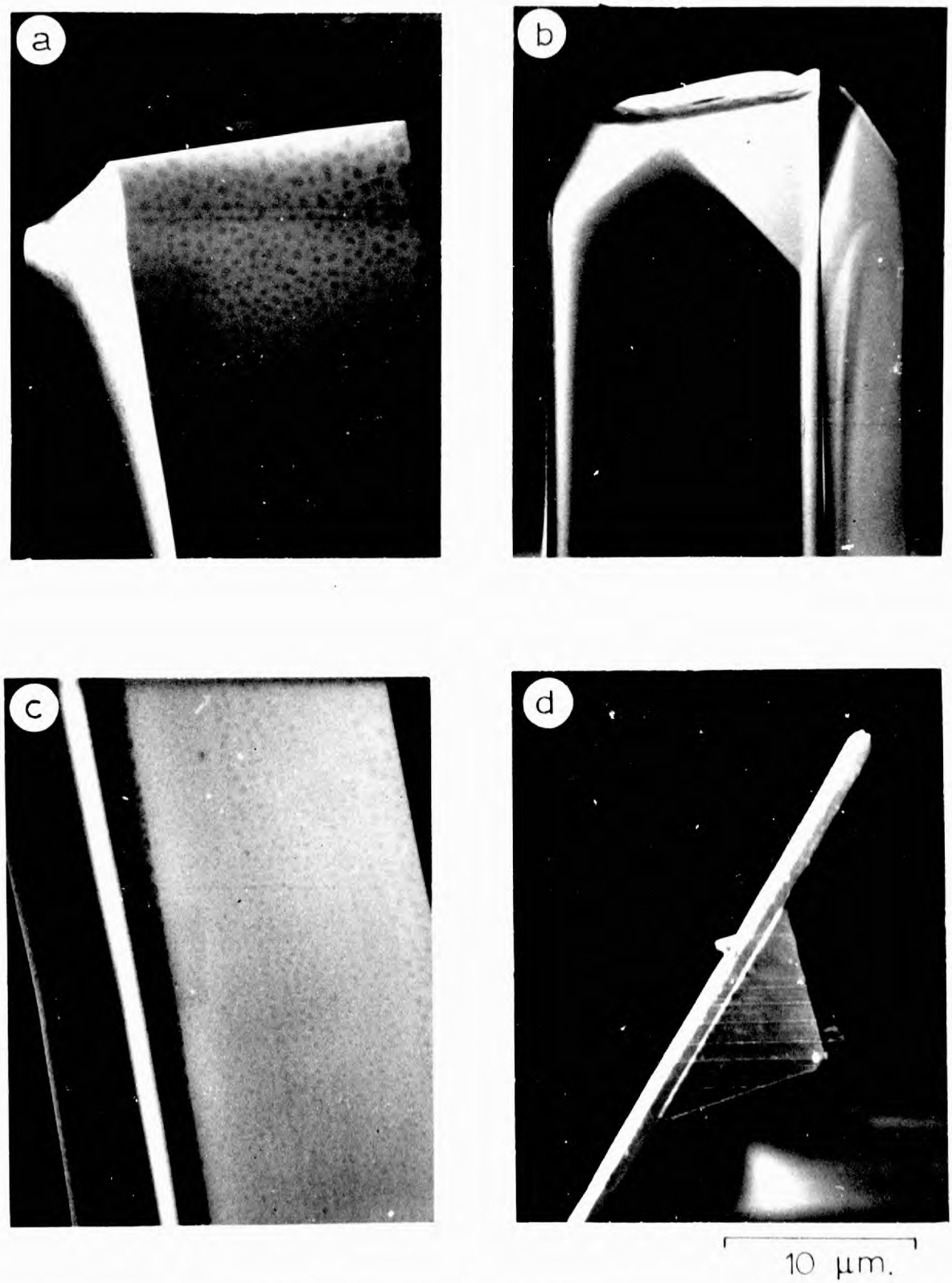

Fig. (3.7) Scanning Electron Micrographs of whiskers

to show (110) features. This is thought to be a possible place from which a platelet could grow out. Finally, (d) shows a small platelet growing out from a <110> axis whisker, with the relationship between them clearly shown, with growth possibly starting from a (110) face.

An attempt was made to get further information on the relationship between platelet and whisker growth by using single crystal x-ray diffraction. The results of these investigations are seer in FIG.(3.8) with the layer lines from <100> and <110> axis whiskers seen in (a) and (b) respectively. These investigations have shown identical patterns from several samples of each type of whisker, but the <110> axis whisker appeared to be the more frequent habit. The layer lines from a (100) plane platelet rotated about the <110> axis is seen in (c). These results have shown no indication of a screw axis in the whiskers or of twinning in the platelet.

It is unfortunate that observations have not been made during the growth of platelets to try to understand further the link between whiskers and platelets. Although not impossible, such an experiment would be difficult to perform because a reasonable magnification would be required and the range of conditions over which platelets grow is narrow. In addition many of the vapours present would make visibility a severe problem.

However, FIG.(3.9) shows a series of optical micrographs taken at the end of a run from the surface of only two boats. If arranged in the sequence shown they indicate the possible mode of development of a completed platelet. The beginnings of growth are seen in (a) - (c) and its continued development in (d) - (f). Two completed platelets are seen connected in (g) but oriented at 90° to each other. This is again seen with the end platelet in (h), and finally the top platelet in (i) is an example of a butterfly twin. This last picture suggests that the whisker forms the spine of a butterfly twin in a similar way to the spine observed in $BaTiO_3$, with a twin plane lying

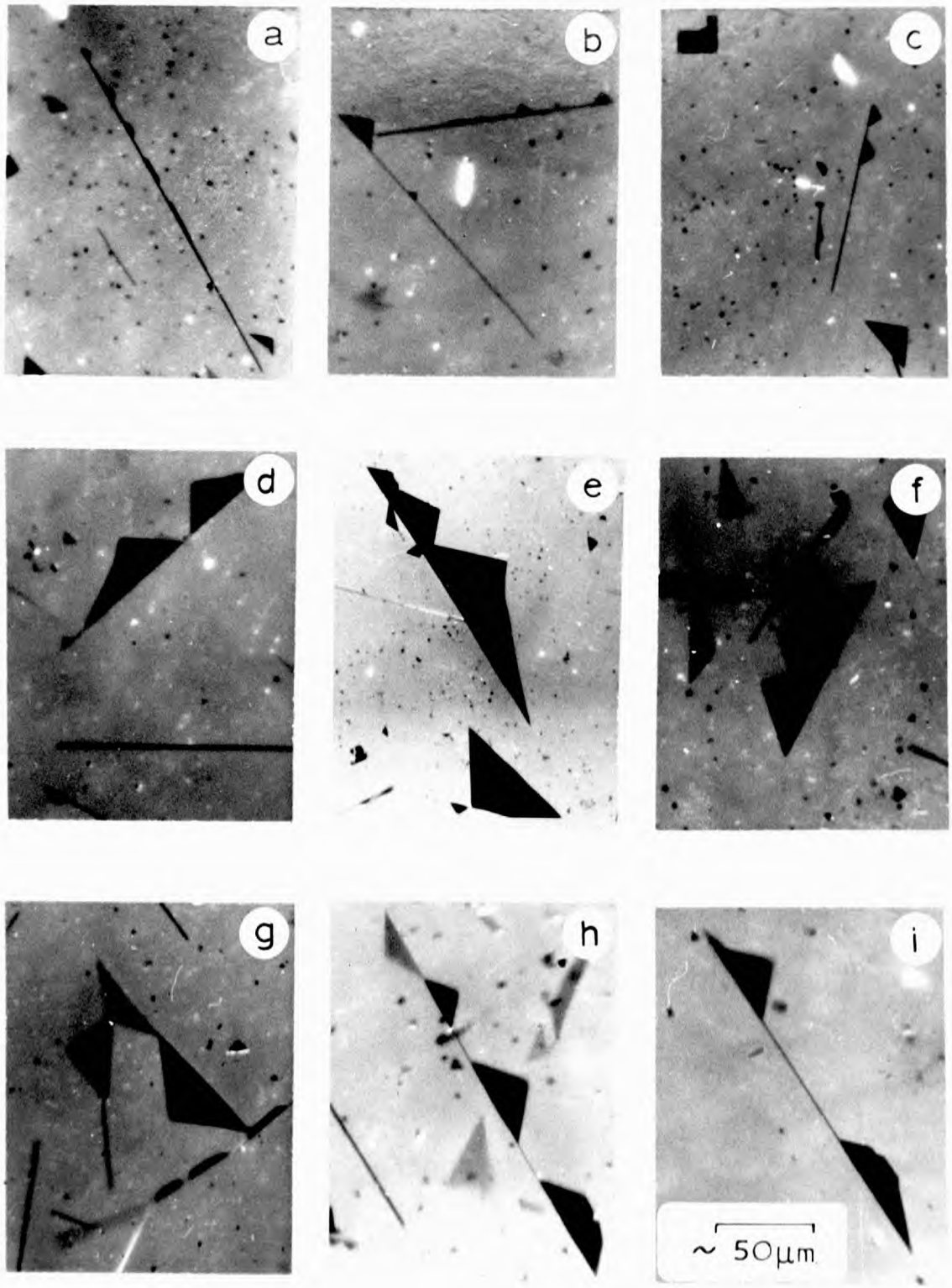

Fig. (3.8) Possible growth sequence for triangular platelets

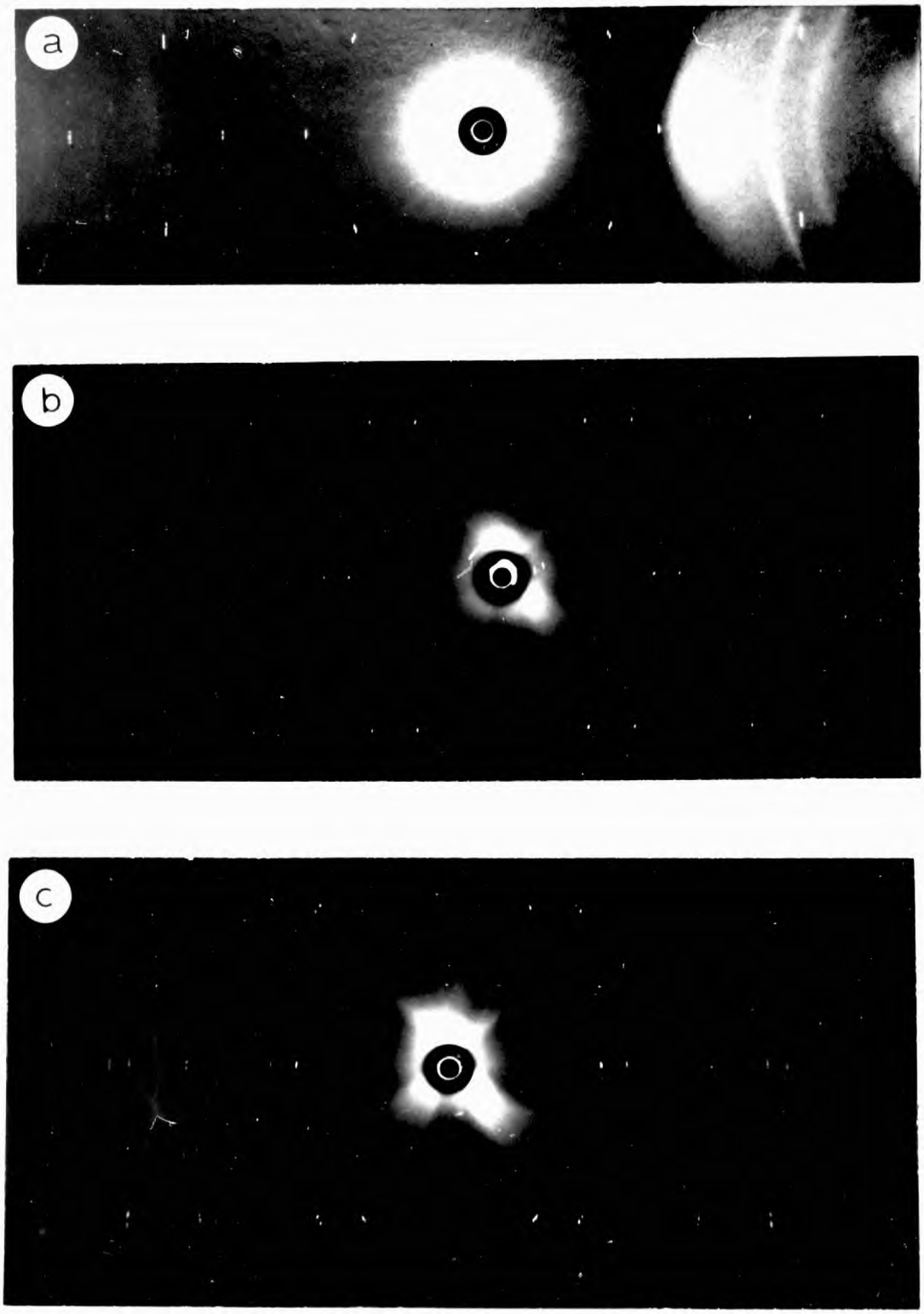

Fig. (3.9) Rotation X-Ray Photographs

along the joint with either wing. With a (111) plane exposed rough interface growth occurs from the whisker until the crystal is bounded by (100) faces and a right triangular platelet formed with completed planes, Buckley (1951).

Because of the small size of the crystals the spine of the twin, unlike $BaTiO_3$, is not easy to observe. However, the angle between the wings of the butterflies of Ni has been measured to within a degree or two as being 40°. This is very similar to the angle of $38^\circ 49'$ recorded for $BaTiO_3$ indicating a strong connection between the two growths.

The formation of a twin rather than a platelet is probably governed by whether one or two twin planes are formed on a whisker/spine, and whether growth proceeds at both twin planes simultaneously.

No evidence has been found to correlate whiskers with the rectangular platelets. It is possible that they grow from a $\langle 100 \rangle$ whisker formed along the surface of the boat, the width of the whisker defining the final width to which the platelet grows.

Finally, FIG.(3.10) shows one of the platelets (arrowed) seen in FIG.(3.5c) secured by one of the rectangular edges and observed in the SEM. The surface circles (distorted by perspective into ellipses) can be ignored as they arise from the aerosol spray. Two interesting features are visible. The point of attachment to the substrate is clearly shown with layering visible, possibly arising from an emergent screw dislocation lying along the diagonal of the platelet. The end of the bottom edge shows a 'V' angle possibly formed by (111) planes, indicating the possibility of growth by twin planes running through the thickness of the platelet.

Platelets have also been seen with growth steps visible across the plane faces. These have been of little interest magnetically but indicate the further possibility of layer growth thickening after lateral growth has terminated. Two of these steps are just visible

Fig. (3.10) Scanning Electron Micrograph of Kite Shaped Platelet stood on edge. (This platelet is the one arrowed in Fig. (3.5.c))

in FIG.(3.10) towards the far side of the platelet.

Summarising; the screw dislocation, though never confirmed, remains the only satisfactory mechanism for the growth of ferromagnetic whiskers. The evidence suggests a strong connection between platelet and whisker growth, but the exact mechanism is unknown. No evidence has supported mechanisms proposed for platelet growth of other materials. It would also appear that more than one mechanism must be operative.

CHAPTER 4

EXPERIMENTAL METHODS

This chapter briefly reports experimental techniques used during the course of this work stressing in particular non-standard features relevant to the investigations.

4.1 THE USE OF ELECTRON PROBE MICRO ANALYSIS

4.1.1 Determination of Composition

The problems of knowing the composition of binary alloy platelets produced by co-transport, and the thickness of all platelets, were simultaneously solved by the use of electron-probe micro-analysis (EPMA), a method first used by Castaing and Descamps (1955).

X-ray fluorescence is a well established technique for analysing the average composition of specimens to within 0.1%, by using the X-ray spectra excited by fluorescence. Such a method is too gross to be directly suitable for the samples used in these investigations. EPMA however extends the range of X-ray spectrochemical analysis to embrace local regions of the order of a micron and quantities less than a microgram. It accomplishes this by using a fine focus beam of electrons rather than X-rays to excite the characteristic spectra.

Two advantages of EPMA are firstly that the flux contained in a beam of electrons focussed to a micron spot is sufficient to excite strong X-ray spectra, whereas a masked beam of primary X-rays would be far too weak. Secondly that the penetration of the electron beam as well as the diameter is of the order of a micron so that the total

volume excited is approximately one cubic micron. Curved analyser crystals, similar to those for X-ray fluorescence, placed above the specimen, enable the wavelength and intensity of the characteristic X-rays to be measured. A subsidiary optical system enables the specimen to be accurately positioned under the beam.

Although the minimum detectable concentration of 30 ppm. is larger than that with X-ray fluorescence, (1 ppm.), through background interference from electron excitation, the minimum detectable quantity is 10^{-14} gm. in one cubic micron. This is very much smaller than the comparable amount by fluorescence of 10^{-8} gm. in a larger volume.

The electron beam deflection mechanisms are similar to those used in the Scanning Electron Microscope (SEM), (cf. section 2.3.4), and enable the beam to sweep out a square raster on the specimen surface. The changing X-ray intensity can be used to modulate the intensity on a C.R.O. display thus enabling compositional pictures to be made of the specimen. The electron current collected by the specimen (beam current minus back scattered electrons) can also be used to give a restricted SEM micrograph. However quantitative results are not obtained quite so easily because the collected or back scattered current varies slowly with composition, there being a relationship between the back scattered coefficient and the atomic number of each element.

Samples were prepared for insertion in the microscope column by supporting each platelet in position on a glass cover slip with Durofix*. The specimens were coated with an evaporated layer of carbon $\sim$ 200 Å thick, which provided an earthed path for the specimen current and thus prevented the platelet from charging.

Two side analyser spectrometers enable simultaneous detection to be made of two elements, counting say Ni intensity in the L.II.

---

* Durofix is the trade name of an amyl acetate soluble glue.

analyser and Co intensity in the R.H. A series of known bulk standards are also placed inside the column enabling the emission to be standardised each time against the bulk, and a ratio of the emission counts in a given time, I_{sample}/I_{∞}, obtained which is independent of instrumental variations. This ratio is also used as the basis for platelet thickness determination. A specimen left under the beam for any length of time is liable to damage, thus counts were made while the beam was moved across the sample at 20 μm/min.

4.1.2 Measurement of Platelet Thickness

The determination of platelet thickness would have been an impossible undertaking without the use of EPMA. Three possible direct methods for thickness measurement of thin films can be considered for possible extension to platelets, multiple beam interferometry of a sharp step edge, amplified stylus pickup across a similar edge (Talysurf), or microbalance weighing of a deposit of known area and density. The first two techniques rely on absolute contact between the film or specimen and the substrate. Interferometry was attempted but rejected as a method because the contact could not be guaranteed. The third method also had to be rejected because the mass of a typical platelet 10^{-8} gms., was too small for useful work.

We have seen however that in EPMA the depth of penetration of the electron beam is ~ 1 μm., and for a given material the intensity of the back scattered X-rays will be a function of specimen thickness. Attempts have been made to measure thickness absolutely in terms of the parameters of a given instrument, see for example Hutchins (1966), but there are limitations in this method.

Instead a series of Ni films from ~ 50 Å to ~ 6000 Å were vacuum deposited at $\sim 10^{-5}$ torr onto thin glass substrates of known area. The thickness of these films was determined by assuming the bulk density for Ni and noting the increase in weight through

deposition, obtained with a microbalance.

A ratio of the counts from each of these specimens to the count from a pure bulk sample of Ni was obtained. Further counts were made from the glass alone and from the glass plus a typical amount of Durofix used in securing the platelets. These proved negligible by comparison and the effect of the platelet support in any thickness count could be neglected. The beam was scanned during the count and from these counts a plot made of $R = I_{sample}/I_{\infty}$ as a function of film thickness. These plots and a linear approximation are shown in FIG (4.1).

Least square fits were made to obtain a linear relationship of the form $T = A_o + A_1R$, where T is the film thickness in Ångstrom units with $A_o = 26.0$ and $A_1 = 6623.1$. A similar fit was made to a parabolic curve of the form $T = B_o + B_1R + B_2R^2$ with $B_o = 113.7$, $B_1 = 5657.4$ and $B_2 = 1290.1$. The linear relationship appeared to be the more satisfactory, especially for thinner specimens, because of the smaller value of A_o than B_o. There is however no intrinsic reason why either should be considered as more accurate for any physical reasons.

Beyond values of $R > 0.7$ the above relationship no longer holds as there is a slow approach to the saturation value of unity. This places the upper limit for measurable thickness at ~ 6000 Å.

The thickness of a binary alloy can be obtained from direct ratios. The total count is composed of $\left[(I/I_{\infty})_{Ni} + (I/I_{\infty})_{Co} \right]$ and if the percentage of Ni in the material is say x the total thickness will be given by the thickness as from FIG (4.1) for the $(I/I_{\infty})_{Ni}$ value multiplied by the factor 100/x. The microprobe system is thus seen to be capable of coping with the composition and thickness of binary alloys.

4.1.3 Variations Within Platelets

Several results of general interest arise from these

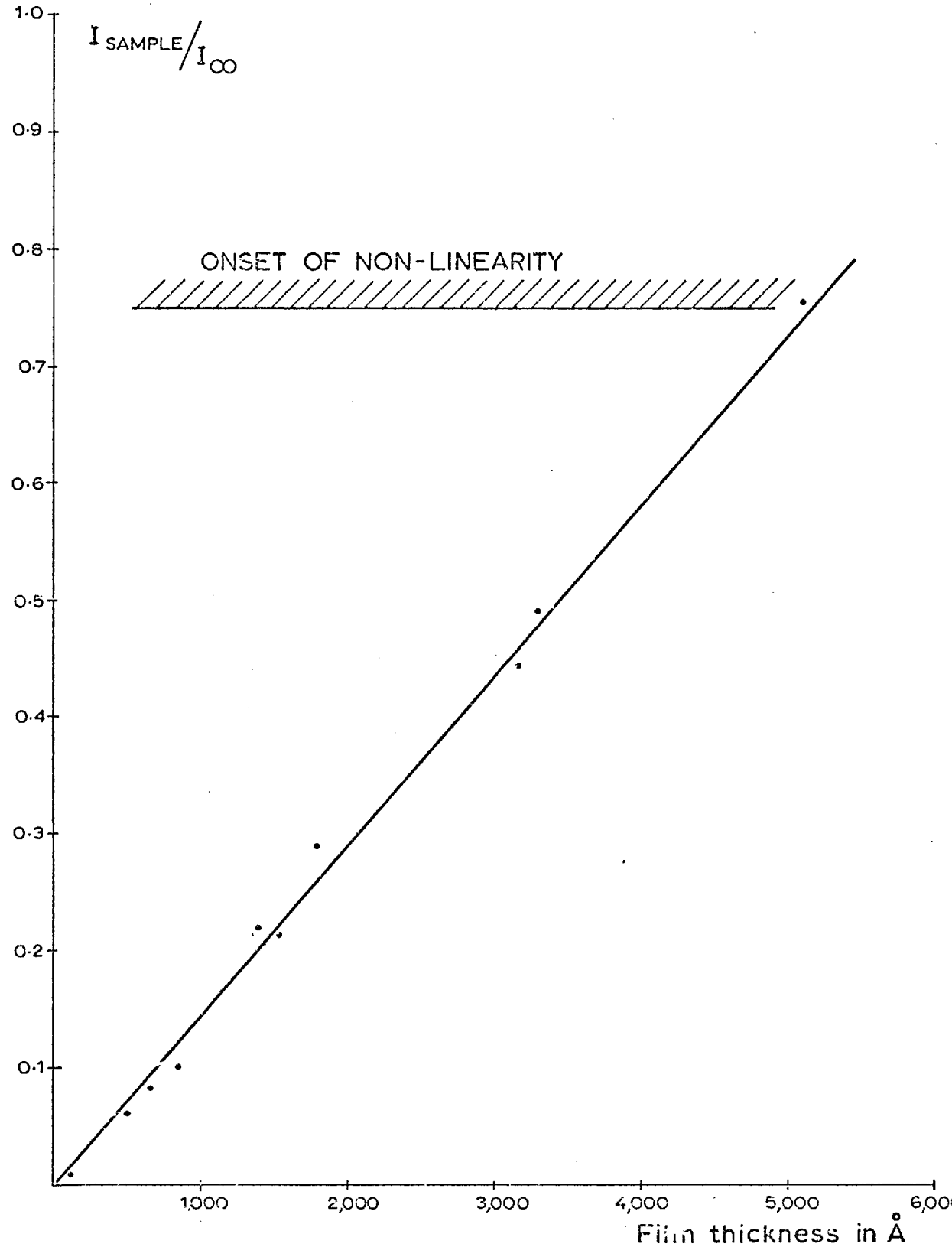

Fig. 4.1 Thickness calibration of electron microprobe

investigations. Ni crystals were found to contain less than 0.1% of ferromagnetic impurities, either Fe or Co. Ni/Co alloys grown from a 50/50 starting mixture of bromides were found to vary in composition both from run to run and within the same growth run and to contain between 80 and 88% Ni, thus decreasing the Co concentration from the starting bromide.

An additional feature which proved useful enabled plots of the Ni and Co concentrations, together with the specimen current, to be made simultaneously during the course of a traverse of the beam across a platelet. A knowledge of the specimen current at any point gave a constant monitor of the total thickness of the specimen, thus from these scans compositional and thickness variations could be located on the specimen.

The thickness was frequently found to be uniform but on occasions a thinning was observed in the centre. Compositional variations were also detected at constant thickness with, for example, several triangular platelets, and showed an enriched cobalt content towards the apex. However variations of this nature were not investigated per se.

4.2 OBSERVATION OF MAGNETIC DOMAINS IN PLATELETS

4.2.1 Choice of Techniques

In Chapter 2 the various available techniques which have been used for the observation of magnetic domains were reviewed. Many of these techniques were seen to be complicated, especially for the type of work being considered here, but three are worthy of attention; Bitter colloid, Longitudinal Kerr Effect, and Lorentz Electron Microscopy.

The Bitter technique is basically simple and has good resolution although unreproducible when used under stringent conditions, such as the observation of Bloch walls in platelets. It also suffers from

being quasi-static and having a limited life-time on the specimen before flocculation occurs.

The Kerr Effect would seem attractive as both static and dynamic experiments could be performed in the same apparatus. Unfortunately a large magnification is needed for most platelet work and for reflection this would involve using a condenser with high numerical aperture, thus lowering the resolution. This problem might be overcome by using a laser, as a source of high intensity, and destroying the coherence of the beam to remove the diffraction rings from dust particles. However this has not been attempted at the high magnification, which would be required for the work.

Lorentz Electron Microscopy could provide useful information on specific domain problems such as the nature of the nucleation processes or the actual orientation of the magnetication vector. However the main limitation is the low acceptable specimen thickness of ~ 1000 Å with 100kV electrons. This thickness can be extended by the use of a larger accelerating potential and some experiments were carried out with 500 and 750kV accelerating potentials. The problems of high voltage microscopy have been discussed by Dupouy and Perrier (1962) and Cosslett, who described the 750kV Cambridge microscope (1968), which was used during the course of these investigations.

The potentialities of this technique are large but difficulties may be experienced in suitably mounting specimens to ensure that the crystal and hence the domain pattern is that of an unstrained specimen. This problem is similarly encountered in colloid work, but is more easily overcome.

4.2.2 Preparation of Specimens

The majority of domain studies in this thesis used the Bitter colloid technique made according to the process described in Appendix B. The platelets by their very nature have highly reflecting surfaces and required no prior preparation. For observations under

the microscope the platelets were secured to a glass substrate by the finest smear of grease, just enough to stop the platelet rotating into the field direction when a hard axis field was applied. The colloid was confined to the region of the platelets by a narrow ring of grease, and covered by a thin micro-cover square of glass to give a flat viewing surface, and to stop evaporation. In this way observations could sometimes be made on the same specimen for 24 hours.

For investigations inside the electron microscope the platelets were mounted on 3.05 mm. diameter copper grids. Two alternative techniques were used. Either the platelet was placed on a 200 mesh grid and then covered with a 200 Å film of carbon, or alternatively a carbon film was placed across a 50 mesh grid and the platelet put in the centre of one of the squares, before being covered with a second carbon film. This latter method has the advantage of giving an unimpeded access to the crystal, but without solid support the crystal is liable to bend and strain. The former method is thus generally preferable.

4.2.3 Magnetic Fields in the Optical Microscope

Magnetic fields up to 150 oe. could be applied in the plane of specimens under observation in the optical microscope from a pair of external Helmholtz coils. From several early observations it became apparent that after a field had been applied and removed the domain pattern exhibited by a platelet was typical not of a zero field configuration, but one in low field. This field was found to arise from parts of the microscope near the specimen stage such as lens mountings, which could not easily be replaced, although this might be one possible answer.

A more satisfactory solution was found by placing a Hall probe, connected to an R.F.L. 3265 'Gauss Meter', in the exact location of a platelet under observation. The field was measured as a function of the coil current and found not to be linear, but a function of the

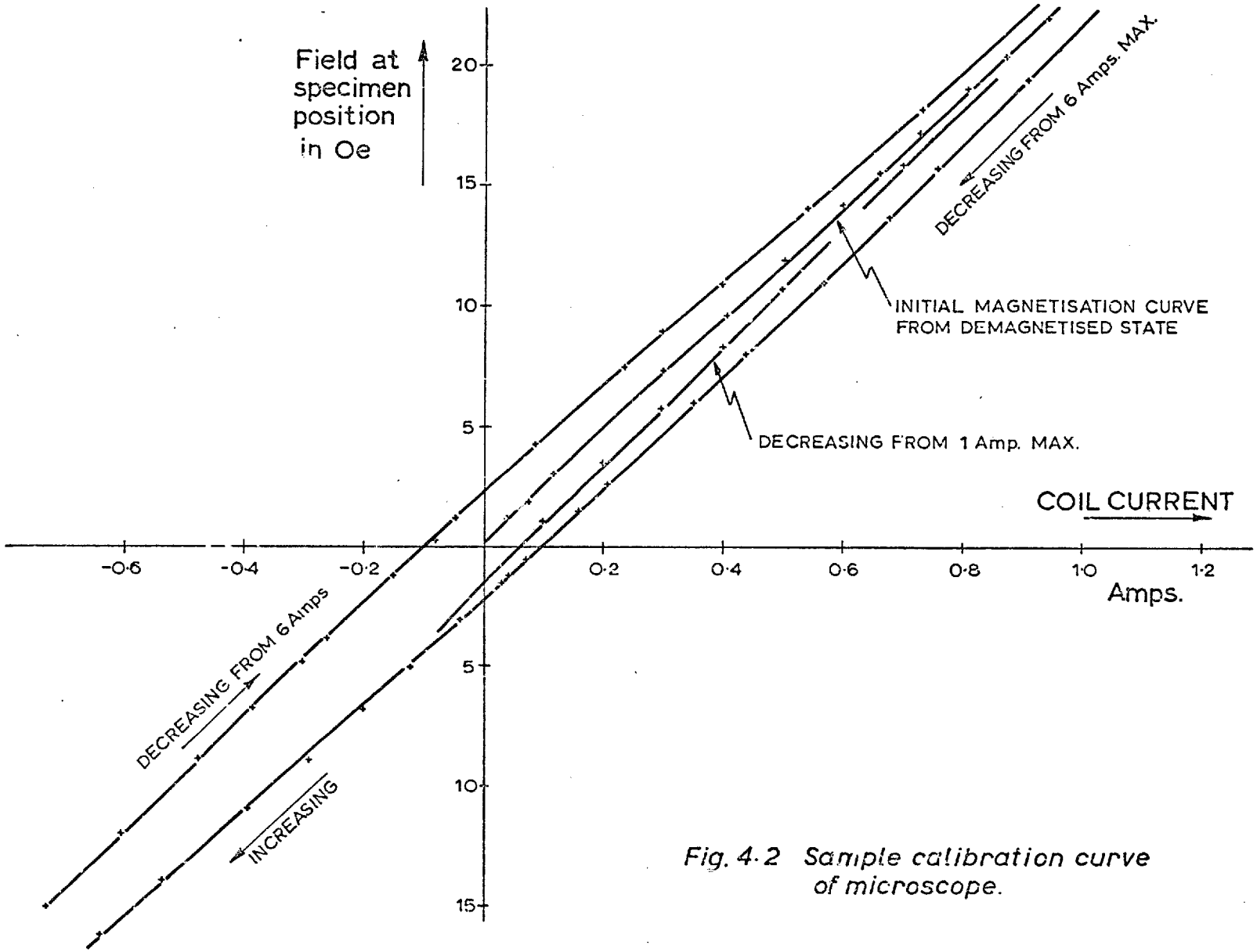

Fig. 4·2 Sample calibration curve of microscope.

recent history. Arrangements were also made to pass alternating current and this facilitated the demagnetisation of the microscope.

The field under the objective was zero after demagnetisation and increased with current up to the maximum of 150 oe. with 6 amps. On decreasing from this value a zero in the measured field was reached with a coil current of 100 ma. still flowing, but when the current fell to zero the existing field was already 2 oe. and oppositely directed. Several calibration curves were therefore made, the one for 6 amps being seen in FIG (4.2). The value of coil current giving zero field was found to vary with the maximum value from which the current was being reduced, hence a calibration curve was always used to obtain the correct field value.

Measurements were also made on the transverse and vertical fields. The transverse field was negligible at all times and the vertical field, although not linear, could be approximated as a 1 oe/amp relationship. Thus, provided that the microscope was demagnetised before commencing any experiment, the horizontal field could be known and the vertical field neglected.

CHAPTER 5

DOMAINS IN THIN PLATELETS

INTRODUCTION

Ferromagnetic platelets produced by the technique described in Chapter 3 are usually strain free and have atomically smooth surfaces. The platelets grow to completion as rectangles with (001) faces bounded by ⟨100⟩ edges, or right triangles again with (001) faces bounded by a [110] and two ⟨100⟩ edges. Their thicknesses range from 0.1 to 10μm. In addition to these observations on (001) faces, De Blois has reported a few observations made on platelets with (111) faces.

The near perfection of these platelets has been established by x-ray and electron beam techniques, section 3.5.3, and magnetically by the thin width of the F.M.R. line, observed in Ni by Rodbell as 114 oe at 9 k.Mc./sec. (1964, 1965) and in Fe by Frait et al (1966). This perfection makes these specimens ideal for various ferromagnetic domain studies. The imperfections in most crystals restrain the motion of domain walls, giving rise to non-equilibrium configurations with hysteresis, remanence and coercivity. However, in these platelets the degree of perfection is such as to give domain configurations that are in stable or metastable equilibrium, with the domain walls moving reversibly, without hysteresis, as long as the configuration of the structure is not broken. A change in field of <0.01 oe produces a detectable motion of the domain walls in the centre of the specimen. In addition, the low indices of the surfaces and edges of the platelets lead to structures that are often classically simple.

The domain structure of a platelet in zero field is independent of the direction of previously applied fields provided these have not altered the initial configuration of the structure. However, unlike a thin film, the small diameter to thickness ratio of a platelet causes the demagnetising fields at the edges to largely determine the equilibrium domain configurations. These domain properties have been studied in iron platelets by Gemperle (1966 and 1969) and by De Blois (1965, 1966, 1967 and 1968) on nickel and a variety of its alloys, including permalloy.

Platelets of compositions having a negative magnetocrystalline anisotropy have easy axes <111> pointing out of a (001) plane at an angle of 35.3°. This leads to domain structures in these platelets which are critically dependent on thickness. Below about 4000 Å the magnetisation lies in the plane of the specimen because the surface demagnetising field dominates the crystal anisotropy. At this thickness, however, complicated stripe domain configurations begin to form with fine scale oscillations of the magnetisation occuring about the plane of the platelet. This effect is absent in platelets with positive anisotropies.

The properties of thin platelets where the domain magnetisation is considered uniform, and homogeneous throughout the thickness, are considered in this Chapter; and the more complicated properties of the thicker platelets considered in Chapter 6.

5.1 DOMAIN STRUCTURES IN PLATELETS

In section 1.1 the terms contributing to the total magnetic free energy of a body were examined. By using perfect specimens, such as thin platelets, it should prove possible to correlate observed structures and their behaviour with theoretically calculated variations in this total energy. However, the observations mentioned in this chapter will show that neither conventional domain theory nor micromagnetics is sufficiently sophisticated to cope with such a

problem.

The theory of domains, in which regions of uniform magnetisation are separated by thin transition regions of known energy, has already been shown to have limitations when ripple or stripe domains in thin films are considered, section 1.3.8. However, these are not the only limitations. It sheds no light on the processes leading to the nucleation of domains on decrease from saturation, or during low field variations. The stray field above a specimen has usually fallen below that necessary to gather colloid long before a specimen is saturated, and the final approach to saturation is usually by rotation, where domain theory is of no help.

Earlier calculations have shown that as the anisotropy of a material decreases the domain wall width increases, which in the limit leads to domain walls of infinite thickness. De Blois (1968a), however, has made colloid observations of wall structures in platelets of almost zero anisotropy. With no crystallographic easy directions the magnetisation in the centre of the platelet was found to curve gradually in its path from one "domain" to another, but near the edge was constrained by demagnetising fields to lie parallel with it.

Two further important features of platelet behaviour which fall outside the framework of conventional domain theory are the role played by point singularities, and the rotation of magnetisation at the edge of platelets. In both of these case examples a localised divergence of the magnetisation occurs. Singularities within the magnetisation of the platelet are involved in its nucleation as the platelet cools below the Curie temperature. They are also seen to play an important role in the structure and formation of walls, in addition to the already familiar cross-tie structure. Divergence of the magnetisation occurs at the base of echelons, see FIGS. (5.7 and 8), and other wall structures of a platelet in zero field, and to a greater degree when fields are applied. However, details of these and other features will emerge during discussions in this chapter.

An alternative approach to the study of magnetisation distribution has been by micromagnetics, Brown (1962, 1963) and Shtrikman and Treves (1963). In micromagnetics the magnetisation is described by a vector field of constant magnitude, but whose direction varies with position. Domains and domain walls, when they exist, should emerge naturally as regions in which the spatial variation of the magnetisation is respectively very slow and very rapid. Actual magnetic states might be calculated by searching for a minimum of the free energy, with the external field as a parameter. However, this approach is not yet sufficiently sophisticated to make it usefully applicable to domain wall problems.

Brown (1945) has discussed the weaknesses of the domain concept and cited the example of the deviation from saturation of an ideal ellipsoid as being outside its limits. However, it remains the only approach on which useful discussions can be based, and has yielded reasonably good agreement with experiment. This approach will be used, and its limitations will become apparent.

5.1.1 Domain Formation in Platelets

The Curie temperatures of Fe/Ni and Ni/Co alloys, (Bozorth, 1951), show that platelet growth in the Fe/Ni system or in the Ni/Co system up to 30% Co occurs above this temperature. At higher Co percentages, although growth occurs below this temperature, the arguments outlined below for the formation of domains in platelets still apply.

In section 1.1.6 several magnetic terms were seen to contribute to the total free energy of a platelet, but the relative importance of these terms does not remain constant with temperature. Domains only form in a platelet as it cools to room temperature at the end of a growth period. Directly after cooling through the Curie temperature the anisotropy is negligible and the magnetostatic fields at the platelet edge constrain the magnetisation to follow a smooth path around the platelet, roughly parallel to the nearest edge. This

requires the creation of a circle Bloch line at the centre of the platelet.

As the anisotropy energy increases in magnitude with decreasing temperature it becomes relatively more important at the expen . of the magnetostatic energy. The magnetisation in the central regions of the platelet turns towards the forming easy axes, <100> in platelets with positive anisotropy and <110> in those with negative anisotropy. The subsequent behaviour thereafter is straightforward for platelets with positive anisotropy and <100> edges, or the <110> edge of a negative anisotropy material. The magnetisation for the most part already lies along easy axis and the rotation at corners forms 90° domain walls, and a classic four domain closure structure is formed. If the platelet is rectangular the Bloch line can form a 180° wall and the structure remains similar, FIG. (5.1).

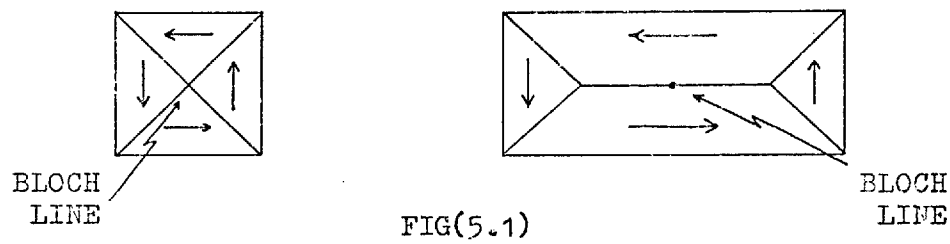

FIG(5.1)

In platelets with negative anisotropy and <100> edges, or a <110> edge in a positive anisotropy material the development of the domain structure is more interesting. The magnetisation near the edge does not easily turn away from the edge towards easy directions because of the surface magnetic charge density this would create at the edge. However, the total energy is lowered by decreasing the anisotropy energy at the expense of forming a volume charge density near the 'walls' of a 'tulip' pattern which forms, FIG.(5.2a).

At the corners this <100> edge magnetisation leads to the formation of diagonal 90° walls, which further from the corners may develop into 180° walls. With further cooling reverse edge domains nucleate at the base of the tulip structure, FIG.(5.2b) and as the

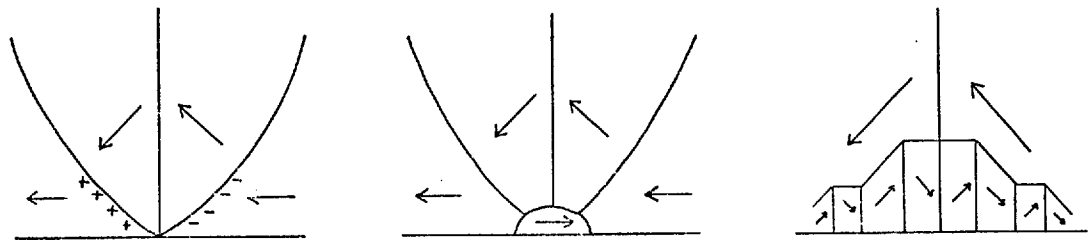

(a) TULIP (b) (c) ECHELON

FIG.(5.2)

anisotropy becomes still more important this reversed region enlarges and sub-divides to form an echelon structure of 90° walls, FIG.(5.2c). Finally, at room temperature, apart from the edges of the platelet, the only significant contribution to the energy comes from domain walls. At the edges alternating surface pole distributions exist, together with some curling of the magnetisation at the ends of walls.

This hypothetical development of domain structures has not been confirmed by observations at elevated temperatures. However, FIG.(1.1) showed a large variation in the magnetocrystalline anisotropies of the Fe/Ni and Ni/Co systems. De Blois (1968a) has recorded structures at room temperature with a wide range of anisotropies and in this way the changing conditions with decreasing temperature have been effectively simulated at room temperature.

The virgin domain patterns observed in platelets taken directly from the furnace often give a clear indication of how the structure was formed. FIG.(5.3) shows the domain structures which have formed in a trapezoidal and two triangular platelets of nickel with (001) faces.

The trapezoid, FIG.(5.3a), is bounded by 2 [110] , a [$\bar{1}$00] and a [010] edges and is 2200 Å thick. The magnetisation forms a simple closure structure in the centre with echelons of reversed magnetisation along the <100> edges. There is little colloid collection at the base of the echelons, showing that flux closure outside the platelet is low. Instead, small closure domains are seen to exist at the base of the

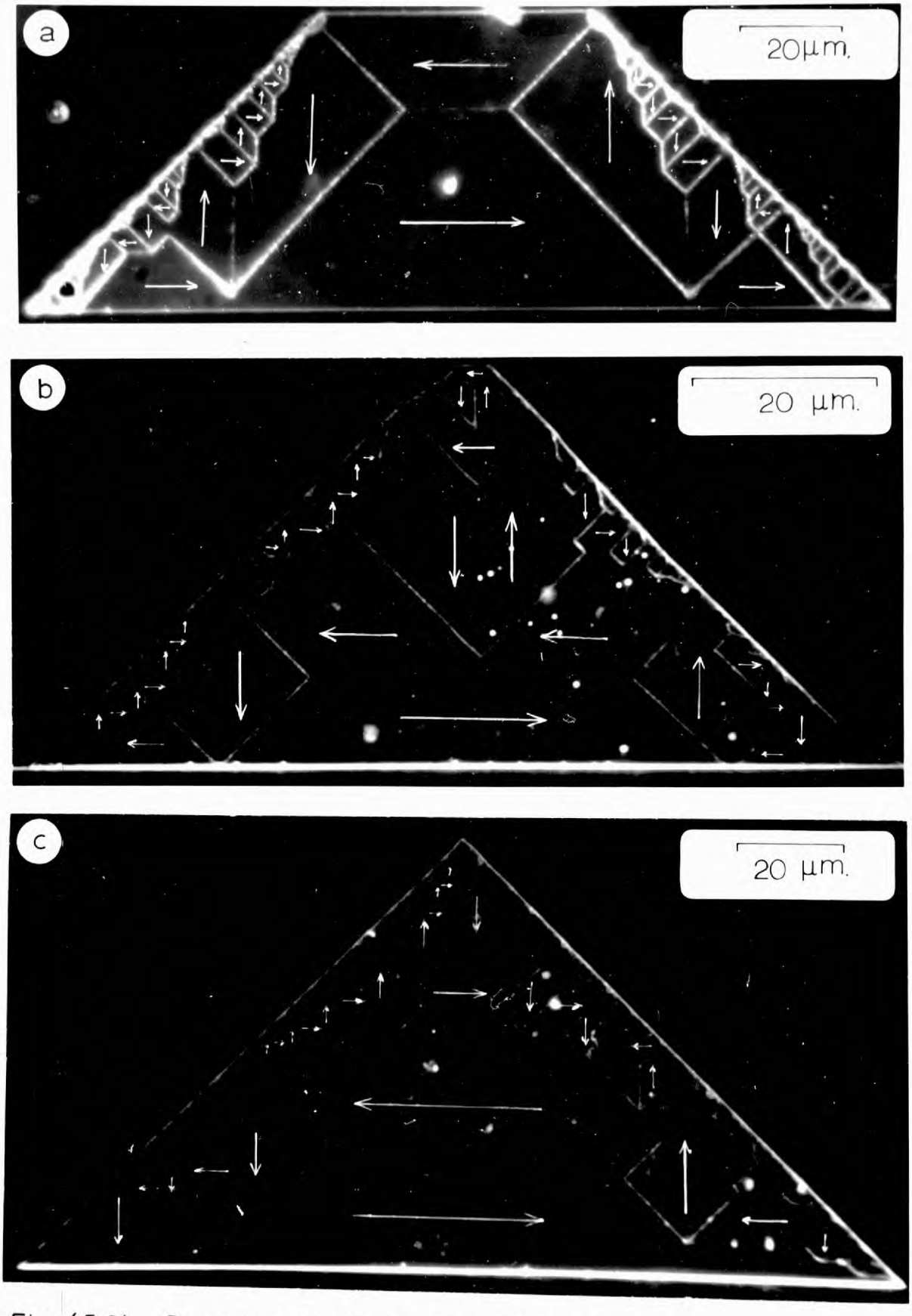

Fig. (5.3) Domain structures in nickel crystals

echelons where the magnetisation lies in a hard direction, parallel with the platelet edge. The symmetry of the domain structure gives further indication of the perfection of the crystal and the near stability of this particular domain configuration.

Crystallographically, the triangle of FIG.(5.3b) is similar to the trapezoid (a) but the [$\bar{1}$00] and [010] sides are continued to the apex. A simple circulation of magnetisation is again seen at the base of the platelet, but a vertical extension is also present involving two 180° walls. The larger of these was probably nucleated at an earlier stage of domain development from the meeting of spikes (see section 5.2) which had grown out from opposite sides. The echelon structure at the base formed at a later stage, as the domains settled into a rectangular array. There are minor circulations at the edges of the platelet but these just help to provide complete internal closure and can be neglected.

Finally, the triangle, FIG.(5.3c), 3050 Å thick, shows the presence of two horizontal 180° walls which indicates that during the cooling a second circle Bloch line must have nucleated, nearer the apex, with an opposite sense of rotation.

5.1.2 Configuration of Domain Structures

The domain structure of a rectangular nickel platelet 2550 Å thick is seen in FIG.(5.4a), and a diagrammatic explanation below it, (b). The magnetisation shows a net circulation about the long invisible 180° wall to the left of centre, with reverse closure domains formed about the corners so that the net magnetisation in any direction will be zero and thus produce no external magnetic field. The symmetry of the pattern about lines bisecting the corner will also be noted.

The central 180° wall is almost invisible by the colloid technique as are many, but not all, of the others. The invisible 180° walls are indicated in FIG.(5.4b). There are two possible orien-

a

b

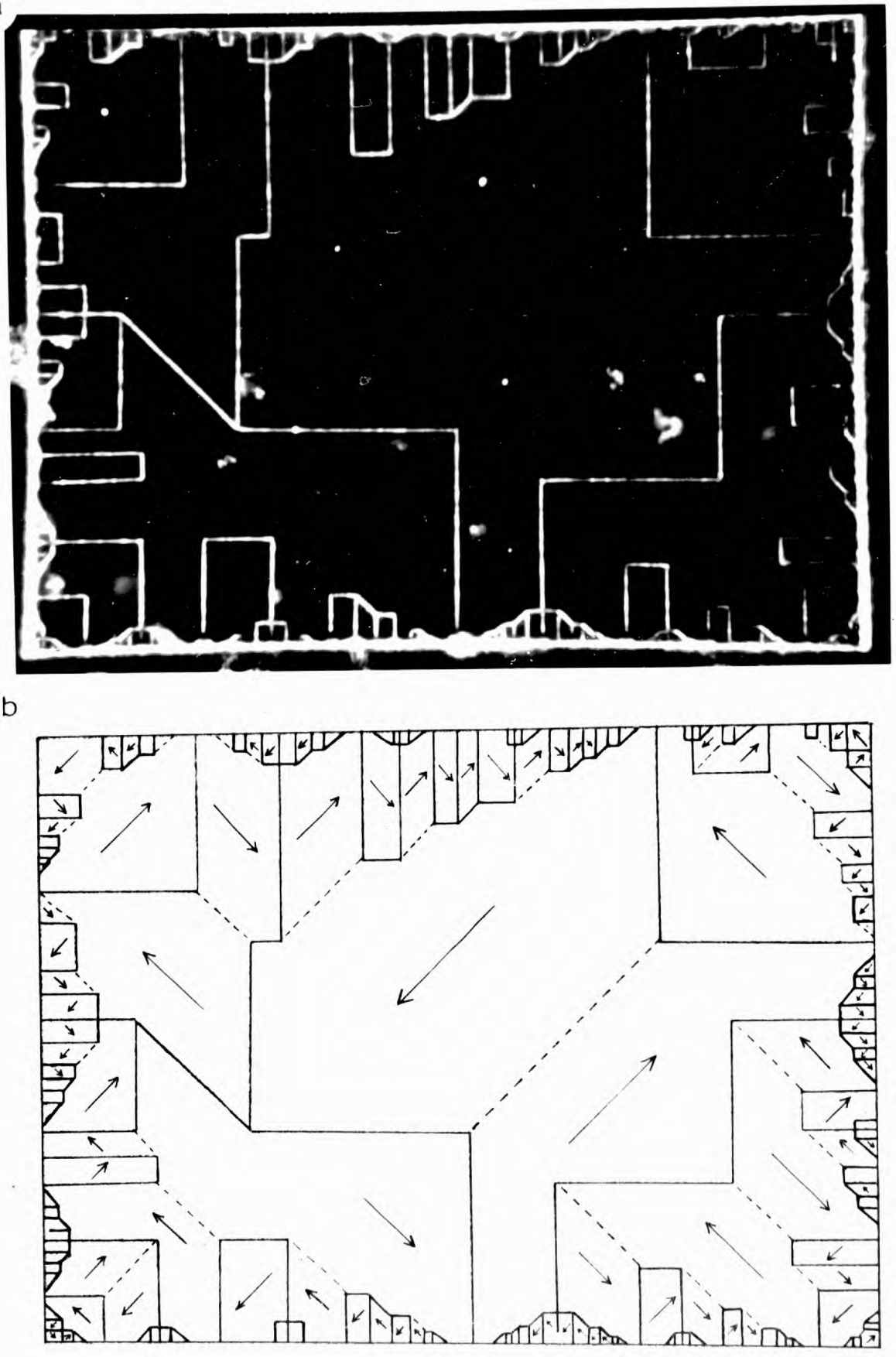

10 µm

Fig. (5.4) Interpretation of domain structure

tations for 180° walls but the invisibility is not a function of orientation, as is seen by comparing the three 180° walls on the right hand side of the platelet. However, it may be connected with the end structure, as we shall see shortly.

Gondo (1962) from his observations on thin iron films has distinguished between two types of 90° wall intersections, A and B, according to the flux closure around them, FIG.(5.5)

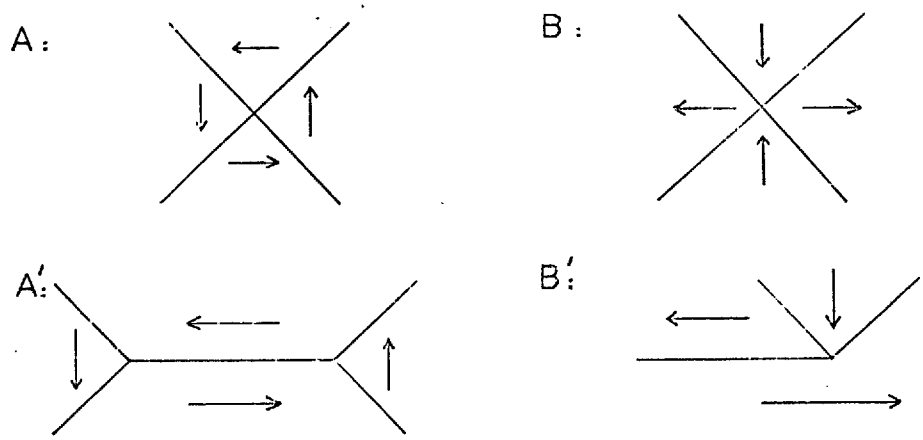

FIG.(5.5) WALL INTERSECTIONS

These configurations also appeared in a modified form which included a 180° wall, A' and B'.

Gondo suggested that the colloid collections above 180° walls in type A' structures were fainter than above those in type B' because the spin directions at a type A' wall junction would favour deviation into a Néel type wall near the centre.

The structural form of the bright metastable walls in platelets is still in question but they probably have at least a partially Néel structure because the Néel wall has a greater stray field than the Bloch. In agreement with Gondo's observations a bright wall is never observed to form where it is terminated at either end by an A' type intersection, which would require the formation of a circle Bloch line, FIG.(5.6a). They may, however, form with a cross Bloch line, as in (b), or where there is no line at all, as in (c) and (d).

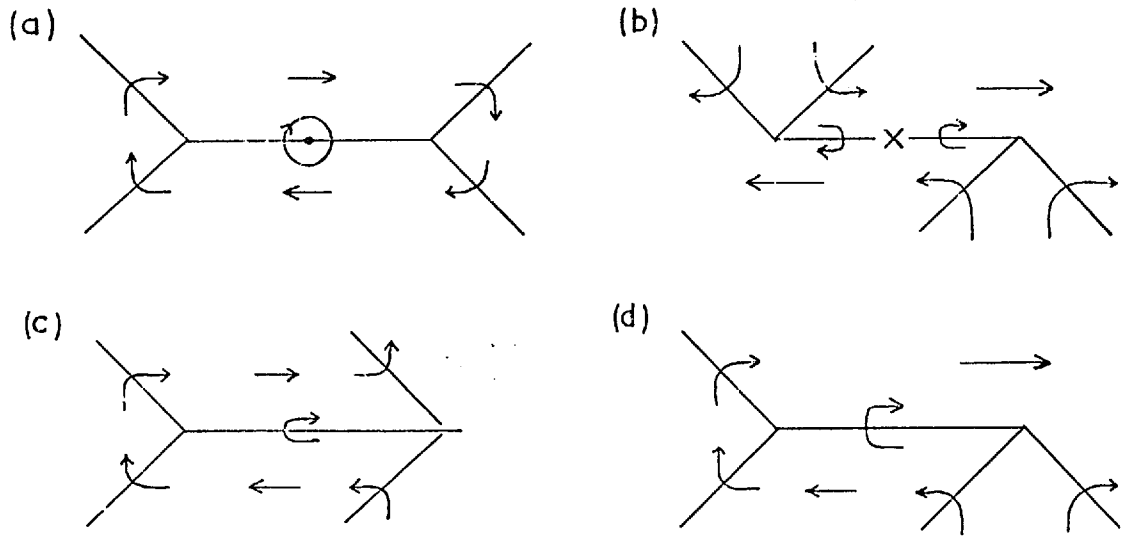

FIG.(5.6) 180° WALL INTERSECTIONS, De Blois (1968)

It could be that the bright wall is of pure Néel type which does not form in the presence of a circle Bloch line. This, however, is unlikely because such walls are observed to form in platelets far thicker than would be expected to support a Néel type structure. The structure must thus be more complex and a mixed Néel-Bloch character has been suggested, De Blois (1966).

The computer calculation of an intermediate wall structure by Torok et al (1965) showed in the case of uniaxial anisotropy a gradual transition from a Néel to Bloch structure with film thickness, with all Bloch walls of not exactly 180° having an intermediate structure.

In platelets the two wall types coexist over a range of thicknesses, but the bright 180° wall is a metastable structure and with a moderate disturbance, on first applying fields, snaps into a faint wall. The inference from this would be that the bright wall is pure Bloch and metastable, and transforms into the faint intermediate structure when sufficient energy is supplied. This, however, runs contrary to all previous experience of the fields above Bloch walls, and to La Bonte's recent calculation (1969). The intermediate wall

structure in platelets cannot therefore be that proposed by Torok et al because bright and faint walls are observed to coexist over a large thickness range.

De Blois (1968) reports the rarity of bright walls up to 1800 Å which would be more consistent with a transition in wall structure with thickness rather than a continuation of the Néel wall structure. He has also observed that double 180° walls, Williams and Sherwood (1957), Kaczer (1958) and La Bonte and Brown (1966), may be formed in an apparently continuous process from bright 180° walls, which in turn are formed from the interaction of 90° domain walls. Double Néel walls if so formed would be expected to annihilate each other. These observations indicate a Bloch type of wall.

This uncertainty illustrates the limitations of the Bitter technique, and an electron microscopic investigation of these wall structures by low angle diffraction at high accelerating voltages might prove very profitable. Theoretically, a numerical wall calculation on the basis of the rather unusual anisotropy configuration of these platelets would also be rewarding.

Counterflow closure patterns of magnetisation in the form of echelon structures are to be seen along the edges and at the corners of rectangular platelets, FIG.(5.4), and along the <100> edges of triangles, FIG.(5.3). This type of reverse closure structure was first observed, in bulk single crystals of iron, with much larger dimensions, Martin (1957) and Bloor and Martin (1959). It has also been observed in single crystal iron film by Lorentz Microscopy, Michalak and Glenn (1961).

Lorentz microscopy observations of the echelons in platelets have shown how the internal closure of the magnetisation is achieved.

The magnetisation is seen to curl around the bottom of every alternate 90° wall, FIG.(5.7). A short wall is formed on either side which meets the edge at an angle α, shown, where α is about 50°.

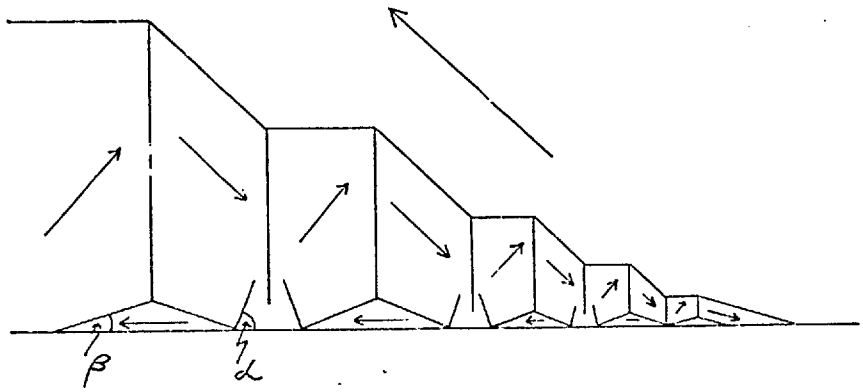

FIG.(5.7) THE ECHELON STRUCTURE

Within the confines of these two walls the magnetisation lies parallel with the edge. Magnetostatic energy is thus decreased at the expense of anisotropy energy. Curling of the magnetisation has previously been observed in thin films less than 550 Å thick, Hornreich (1963), but although this upper thickness limit is considerably lower than the platelet thickness the situation is more favourable. With a magnetocrystalline easy axis out of the plane it becomes easier for the magnetisation to tip and the curl to occur in three dimensions. The angle of 50° suggests that a certain pole density has formed at the walls, but this is of opposite sign on either side of the 90° wall. The closure structure at the base of the other alternate set of 90° walls is slightly different and consists of small reverse closure triangles, whose sides make an angle β of about 20° with the edge.

FIG.(5.8) shows the closure structure on a [100] edge at the corner of a triangular nickel platelet. The faintness of the 180° walls will be noticed and the small size of the structure at the bottom of the echelons, it is in fact barely visible. Instead, slightly excessive colloid collections are seen where the magnetisation must be curling at the bottom of the walls. The regularity of these echelons is a commonly observed feature.

FIG.(5.9) shows the end of a blade-shaped platelet of Ni/Co, with positive anisotropy and a whisker extension along the [110] straight edge. A [110] axis field has been applied and removed to

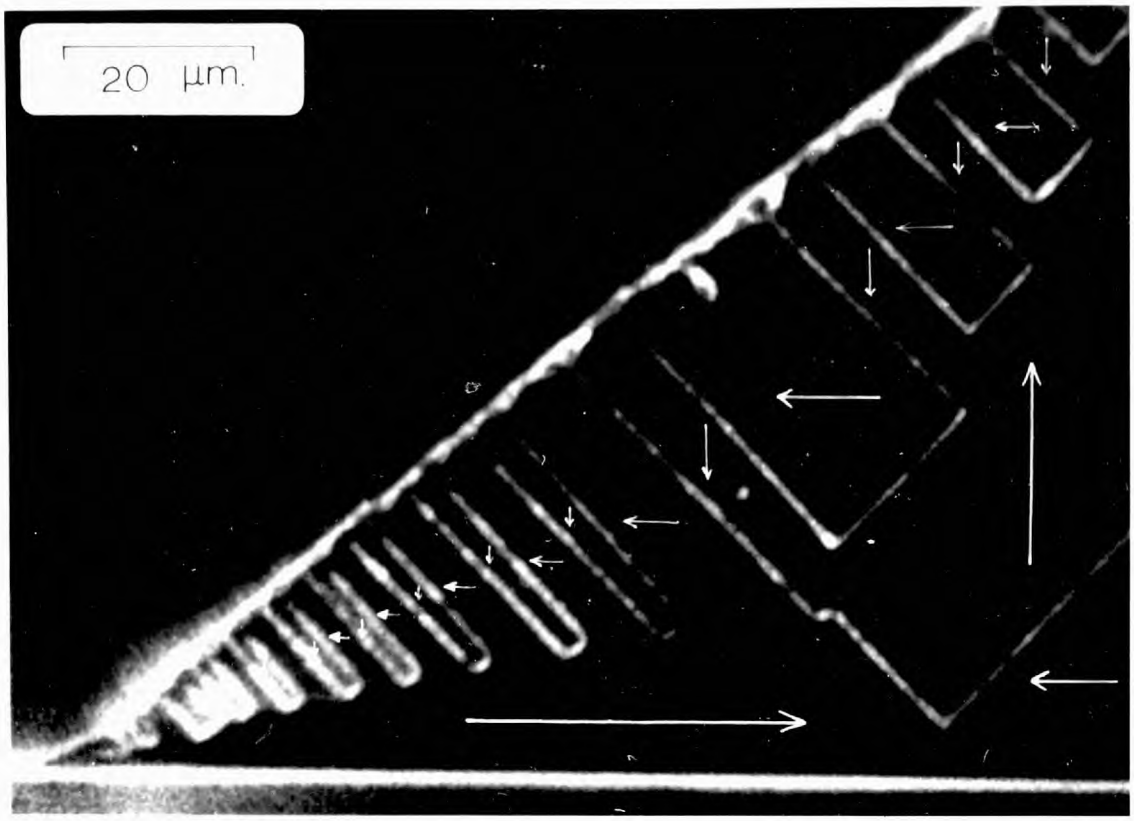

Fig. (5.8) Echelon structure in triangular platelet

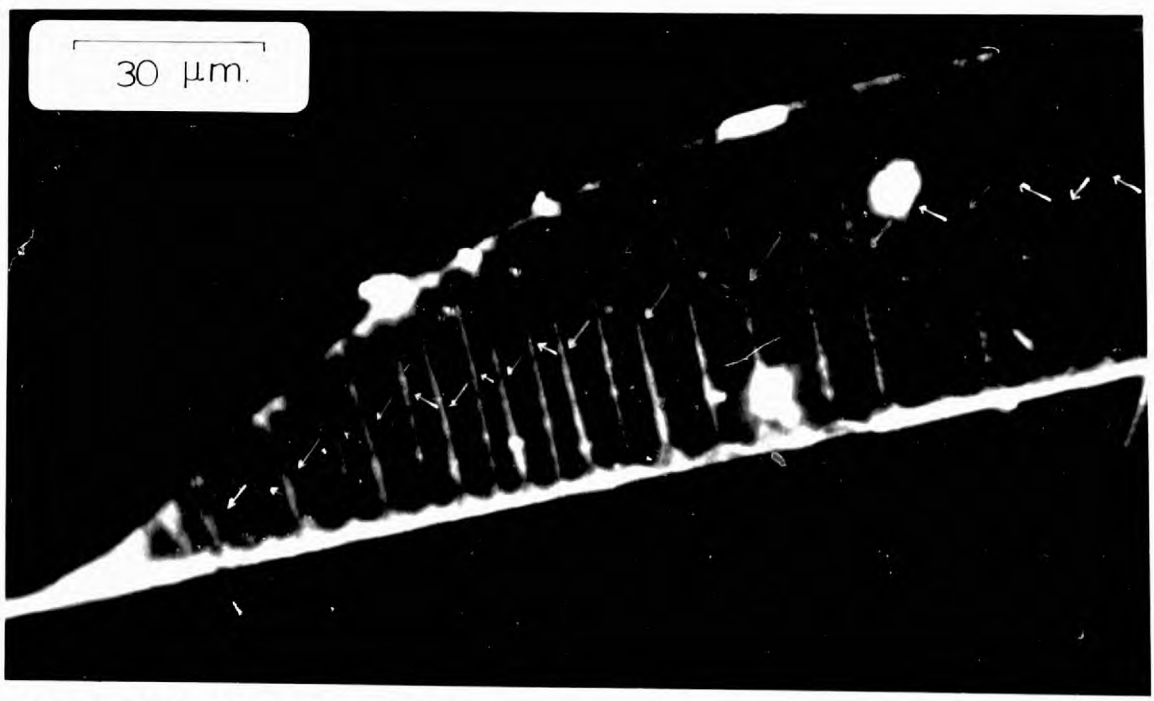

Fig. (5.9) Magnetisation in blade shape platelet.

give the observed structure which is seen to consist of successive 90° walls, allowing the magnetisation to lie along the platelet in easy <100> directions. Closure structures now are seen to form along the [110] edge without the echelons but with the alternating α and β closure domains. With the numerically lower anisotropy value, see FIG.(1.1) the closure structures are seen in a magnified scale.

The curving edge shows how as the edge changes from lying along a [110] axis to being along a [100] the closure structure disappears and the 90° domain walls adopt a spike configuration, see section 5.2, so that the magnetisation outside of these spikes lies almost continuously along the edge.

5.1.3 Domains in Low Anisotropy Alloys

A reduction in the magnetocrystalline anisotropy of a platelet causes the exchange energy to become relatively more important and the wall width and size of domain closure pattern to increase. FIG.(5.10) shows some examples of domain structures which are typical of platelets with low anisotropies in the Ni/Co system. Unfortunately, in the Ni/Co system, unlike the permalloy system studied by De Blois (1968a), the magnetostriction constants do not fall to zero at compositions of zero anisotropy. The role that magnetostriction plays in influencing the domain patterns is uncertain and conventional domain theory is uninformative in these types of materials.

The end of a rectangular platelet, FIG.(5.10a), shows that although the anisotropy is still negative, as seen by the magnetisation directions in the centre, the magnetisation at the edge remains closely parallel with the edge in all places. 'Tulip' patterns are seen especially at the corners, however they are often incomplete showing how the magnetisation is turning, but so gradually that the colloid does not collect. The magnetisation directions can be inferred, in the absence of colloid collections from experience of

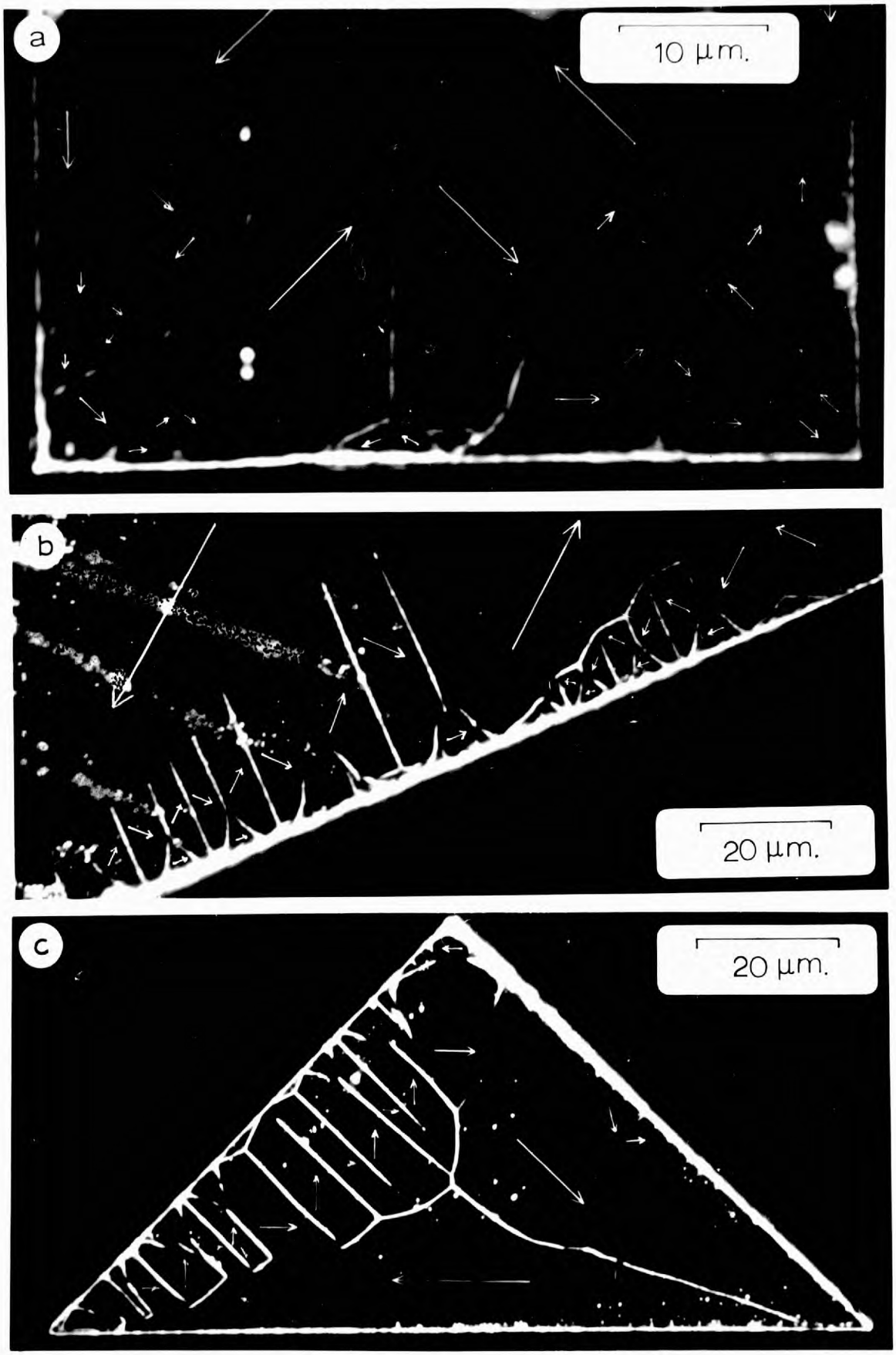

Fig. (5.10) Domains in low anisotropy platelets

domain structures in platelets with larger anisotropies.

The edge echelon structure of another low anisotropy platelet is seen in FIG.(5.10b). The walls between the magnetisation in the main domains and in the closure echelons are completely invisible in the lower set of echelons. In the upper set, however, the alternate segments of 180° and 90° walls which separate the main domain magnetisation from the reverse closure in more anisotropic materials have transformed into a continuous wall.

Finally, FIG.(5.10c) shows a triangular platelet with a compositional variation across it. Echelons are seen to have formed on the L.H. [100] edge where the anisotropy is still negative, but not on the equivalent R.H. [100] edge. Instead, just one wall is seen to bisect the lower corner and the magnetisation on either side of it lies parallel to the adjacent edge so that the wall is no longer a true 180° wall. Other low anisotropy platelets have also exhibited the wandering of long walls as seen in FIG.(5.10c).

5.2 PLATELET BEHAVIOUR IN MAGNETIC FIELDS

The domain structures which exist in platelets in zero field after a magnetic field has been applied and removed are not necessarily similar to those observed in a virgin platelet. It has been suggested earlier (section 5.1.1) that before locking into its final structure the magnetisation circulates around the platelet as it cools from the Curie temperature. On decreasing from saturation in a magnetic field, however, there will be a tendency for the magnetisation to lie along the field direction, especially if this is one of low anisotropy. Thus although the net magnetisation in zero field will, if there is no remanence, be zero, the structure of the domains need not be identical with that observed in the virgin state.

Many domain structures can satisfy low anisotropy energy and complete flux closure but the domain wall energy will vary according

to how this is achieved, and the zero field structures will not therefore have equivalent energies. It would, however, be virtually impossible to calculate whether a given zero field structure represents a stable equilibrium configuration for the particular shape and size of platelet in which it exists. Experience has shown that, with facilities for applying fields in only one direction, once the topology of the virgin domain structure has been broken it is often impossible to return to that same structure.

By photographically recording the domain structure present in a crystal when a given field was applied it was possible to observe the domain structure as the platelet was cycled around a hysteresis loop. This has been done with many crystals and in a few selected examples with sufficient detail to allow an M-H loop for the crystal to be plotted. This type of analysis has been made by Gemperle (1966) during his study of iron platelets, and will be referred to later.

5.2.1 Wall Movement and Hysteresis

The behaviour of a typical Ni rectangle under hard and easy axis fields is seen in FIGS.(5.11 and 5.12). The specimen seen in FIG.(5.11a) in its virgin state is the same platelet discussed in FIG.(5.4). A hard axis [100] direction field was applied and the domain structure in a field of 3.7 oe is seen in (b). A rearrangement of the domain walls took place facilitating the growth of the two sets of domains with magnetisation components parallel with the field direction at the expense of the other two sets of domains with magnetisation anti-parallel with the field. Two 90° walls stretched almost the entire width of the platelet. At the top of the R.H. one there was a gathering of colloid on either side of the wall. The edge closure structure separated and, what would otherwise have been a rather large edge pole distribution was broken up by spike domains so that there was a lower overall magnetostatic field at the edge, but at the expense of forming a small volume pole distribution along the spike wall, FIG.(5.13). This volume distribution appeared because

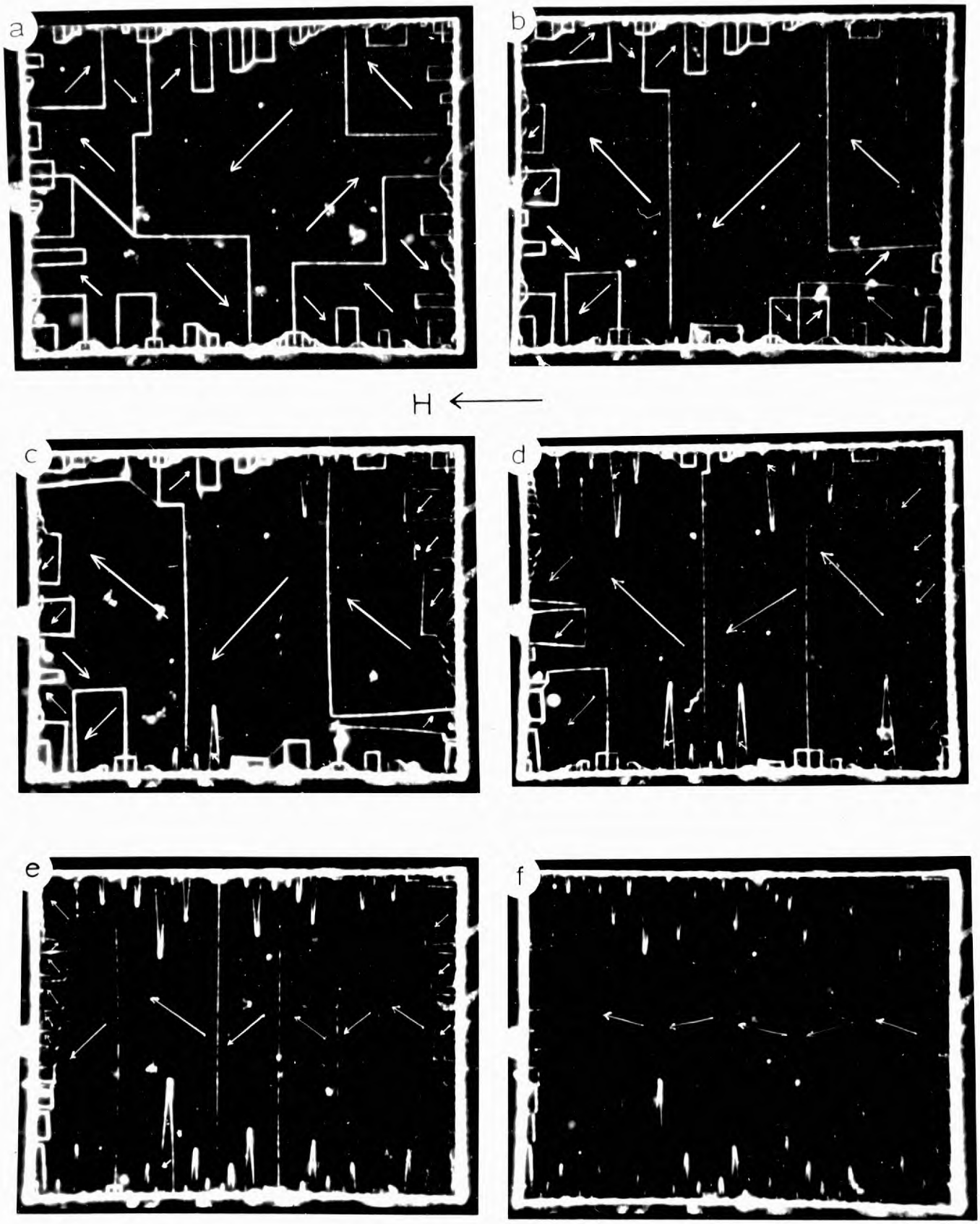

Fig. (5.11) Application of hard axis field

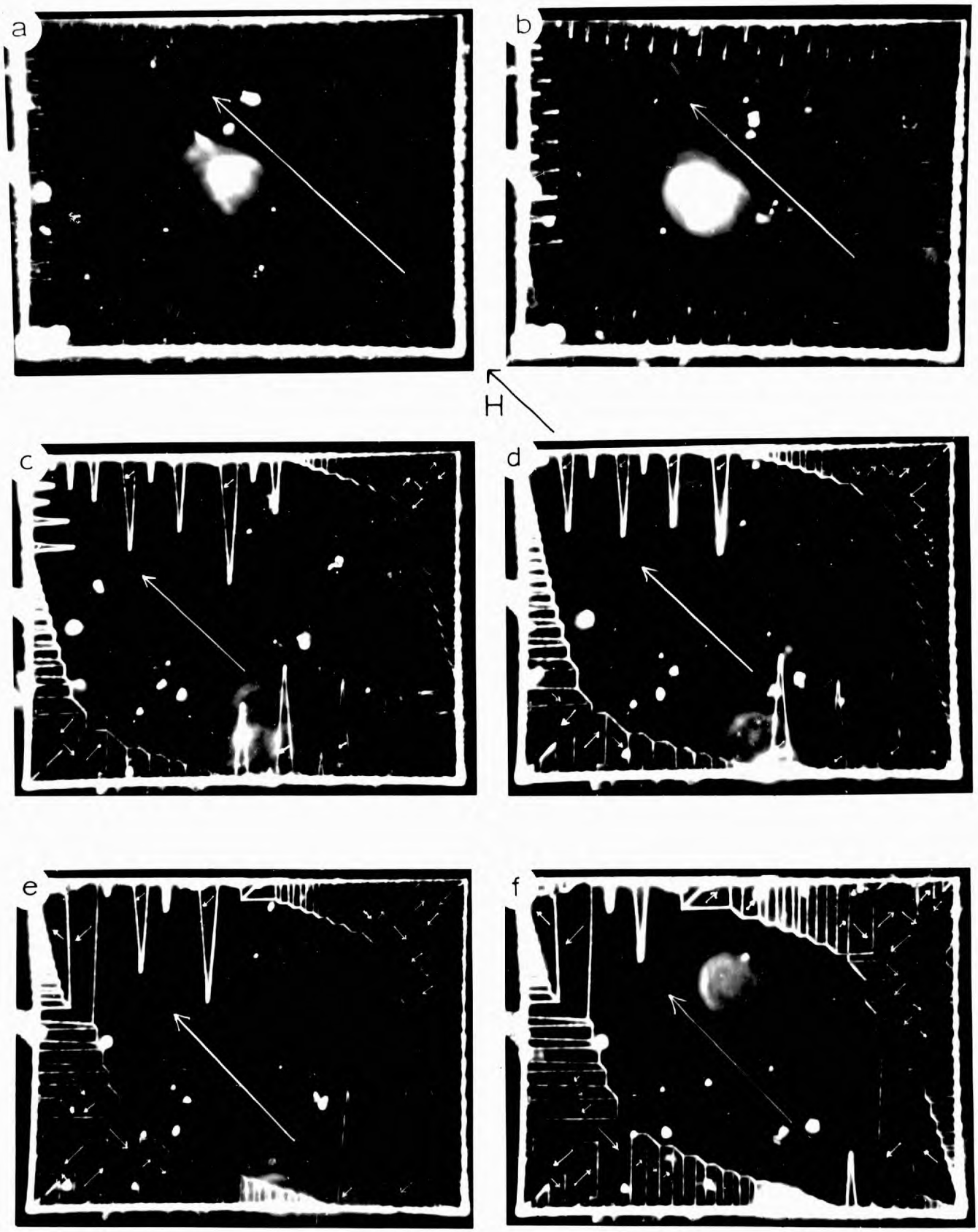

Fig. (5.12) Application of easy axis field

the walls that form the spike domains did not exactly bisect the magnetisation directions on either side.

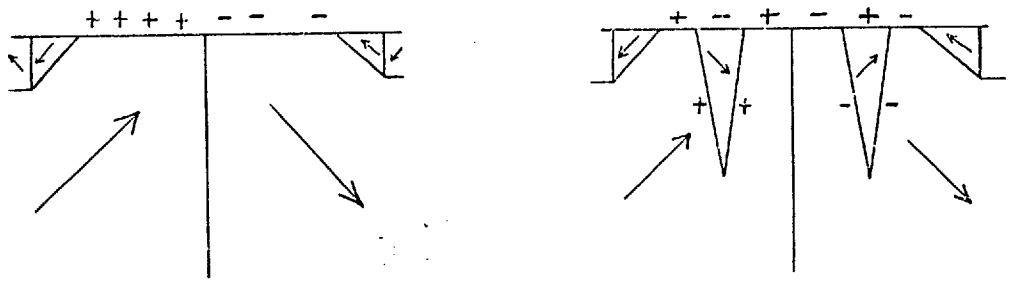

FIG.(5.13) SPIKE FORMATION

These spikes enlarged at 6.3 oe, FIG.(5.11c), and also appeared at the bottom of the other 90° wall. More spikes are seen at 10.7 oe (d). At 21.1 oe (e) the magnetisation formed a 'zig-zag' down the entire length of the platelet apart from the two ends. Small edge closure domains existed at the base of the 90° walls and the overall magnetostatic edge field lowered by the presence of spike domains all along these edges. At either end a reverse circulation closure structure existed and its formation from the bending of end echelon structures, present at lower fields, is clearly visible in the photograph. At 44 oe, FIG.(5.11b), these end structures shrank somewhat, but more important the 90° walls across the platelets almost disappeared, (one is just visible on the R.H. side of the photograph).

At this stage, and even before, saturation was achieved, not only by the movement of domain walls but also by rotation of magnetisation within the domains. At a field of 110 oe the grease securing the platelet to the substrate was no longer able to hold the platelet against the field torque and the platelet rotated so that the field became directed along the [110] axis. In this direction the platelet appeared saturated.

The behaviour of this same platelet in a decreasing easy axis field is seen in FIG.(5.12). At 22 oe (a) spikes, which were approximately uniform in length, formed on the [100] edge decreasing

the edge field. Gaps in the colloid collection at the edges, corresponding to the positions of the spikes in the platelet show how the stray field was locally decreased. An echelon structure (only just visible) was also nucleated at the bottom L.H. and top R.H. corners. As the field decreased to 16 oe, FIG.(5.12b), the echelon structure increased in area and the spikes in length but fewer in number. This process continued in decreasing fields with the spikes becoming larger, but fewer in number, and the reverse echelons expanding from the two corners, as seen in FIG.(5.12c) at 6.6 oe and (d) at 5.9 oe.

Substructures formed at the base of the spikes to decrease their own edge field, which for these low external fields had become too large. Each end of the echelon terminated in a spike which, as the echelons increased in size, moved with it, and simultaneously changed size until a different end structure was formed, FIG.(5.12d). The symmetry of the echelons is apparent and their corner structure formed thus:

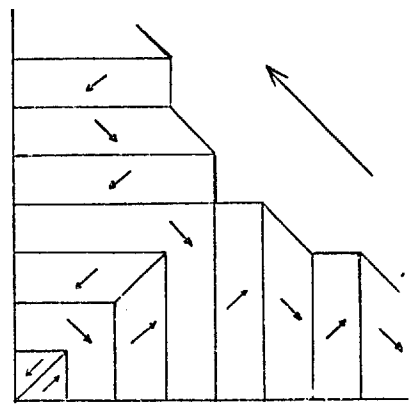

FIG.(5.14) CORNER STRUCTURE

The effect of a spike meeting an opposite echelon was to finally split the main domain in the centre of the platelet, FIG.(5.12e), at 4 oe and lead to the zero field closure pattern. The bending of the 90° walls away from the [100] direction, just after a spike broke into the echelon structure on an adjacent side, is seen in FIG.(5.12f) at 3.2 oe.

As the magnetisation directions are known, and do not vary through the thickness of the platelet, it was possible to obtain a M against H plot from the vector sum of the domain magnetisation components in the field direction. This could be done by measuring the area of domains in a given direction at some particular field, either by drawing the pattern on squared paper and summing the squares, or by cutting up the paper domains and weighing together those with similar magnetisation directions. This latter method was found to be more satisfactory. (The magnetisation always lies along <110> directions, thus for an easy axis loop the magnetisation lying along the perpendicular easy axis can be neglected. For a hard axis loop the magnetisation always lies at 45° to the field, with components either parallel or anti-parallel).

Using this method, magnetisations were found for the series of domain photographs in FIGS.(5.11 and 5.12) and the resulting easy and hard axis magnetisation curves are seen in FIG.(5.15). This method could not be continued to fields much above 10 oe for a hard axis loop because the magnetisation in every domain lay at 45° to the hard axis and rotation occured within the domains. At low fields the component of magnetisation in the field direction is the measured area of the forward oriented domains, minus that of the reverse domains, multiplied by cos 45. If rotation is neglected the normalised magnetisation in the field direction can never exceed cos 45, i.e. 0.707. This is indicated in FIG.(5.15). However rotation does occur and an assumed magnetisation curve is also shown in FIG.(5.15), with saturation finally occurring at over 100 oe.

FIG.(5.16) shows the behaviour of a trapezoidal Ni platelet 2500 Å thick in a [110] easy axis field, both increasing and decreasing, with the hysteresis loop from these pictures shown in FIG.(5.17). Interesting features of the loop are the low coercivity, $\sim$ 1 oe, the saturation at about 70 oe, the apparently linear change of magnetisation with field up to 7 oe, and the similarity with the easy axis curve, FIG.(5.15), from the Ni rectangle. This last observation,

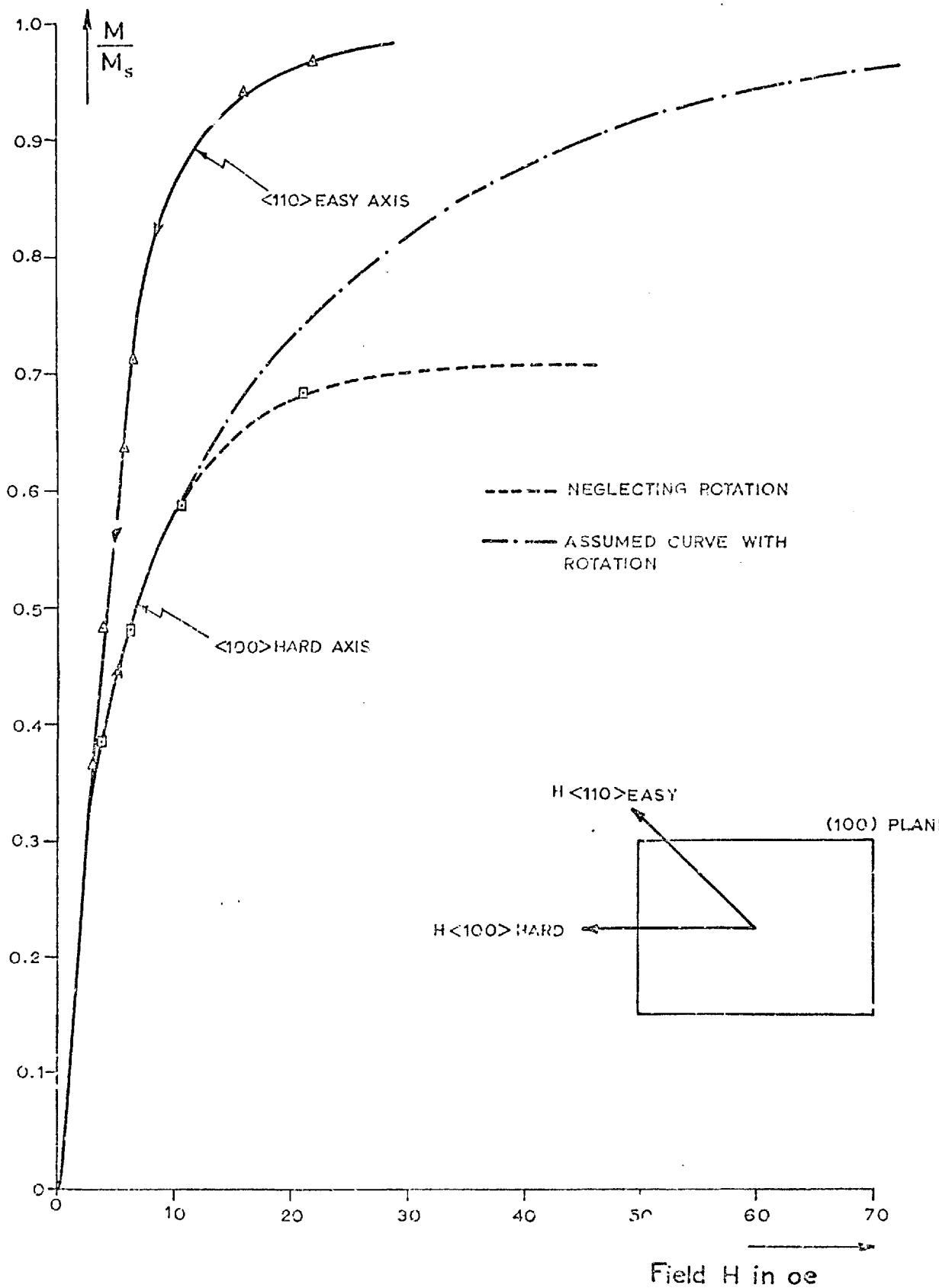

Fig. (5.15) Magnetisation curve of a rectangular nickel platelet

although perhaps not very surprising, is interesting. It shows that when the easy axis hysteresis loop of the entire platelet is considered the shape of the corners, such as the apex of a triangle have little influence on the overall behaviour of the platelets.

If it is assumed that the relationship between the magnetisation and the applied field is similar to that of an ellipsoid then $M(H) - H/(1/\chi + N)$ where χ is the susceptibility and N the demagnetising factor. For these specimens $\chi \gg 1$ and the expression reduces to $M(H) = H/N$. By assuming $M_s(Ni) = 484$ emu. we can find N from the tangent to the magnetisation curves of FIGS.(5.15 and 5.17). In the low field linear region $N \sim 0.02$. This value increases in stronger fields as the demagnetisation effect of the end planes becomes more effective. The magnetisation curve is thus controlled by the demagnetisation effects and depends on the shape of the crystal.

As the field in FIG.(5.16) was increased the structure rearranged slightly (a)$\rightarrow$(b), then the two 180° walls moved towards the edges of the platelet as the centre domain grew, bowing a little during the process. At 6.2 oe, FIG.(5.16d), the bottom wall reached the edge and broke on the L.H. side, but still remained along the edge and joined with the forming spike on the R.H. side. This happened with the top wall at 10.4 oe, FIG.(5.16e), where the low angle between the platelet edge and the wall is seen. Spikes formed down either edge (f) and finally shrank as the platelet saturated.

In decreasing fields the spikes grew out, FIG.(5.16g), until two met and nucleated a 180° wall (h). This structure expanded until the tip reached the bottom of the crystal, whereupon a triangular closure domain formed (i), which expanded causing the 180° wall to shrink back to a circle Bloch line (j). A further decrease in field, FIG.(5.16k), caused the two sides of the wall intersection to separate causing the Bloch line to form a 180° wall perpendicular to the previous one. This is an example of the important role that magnetic singularities, such as Bloch lines, play in the behaviour of domains in these crystals.

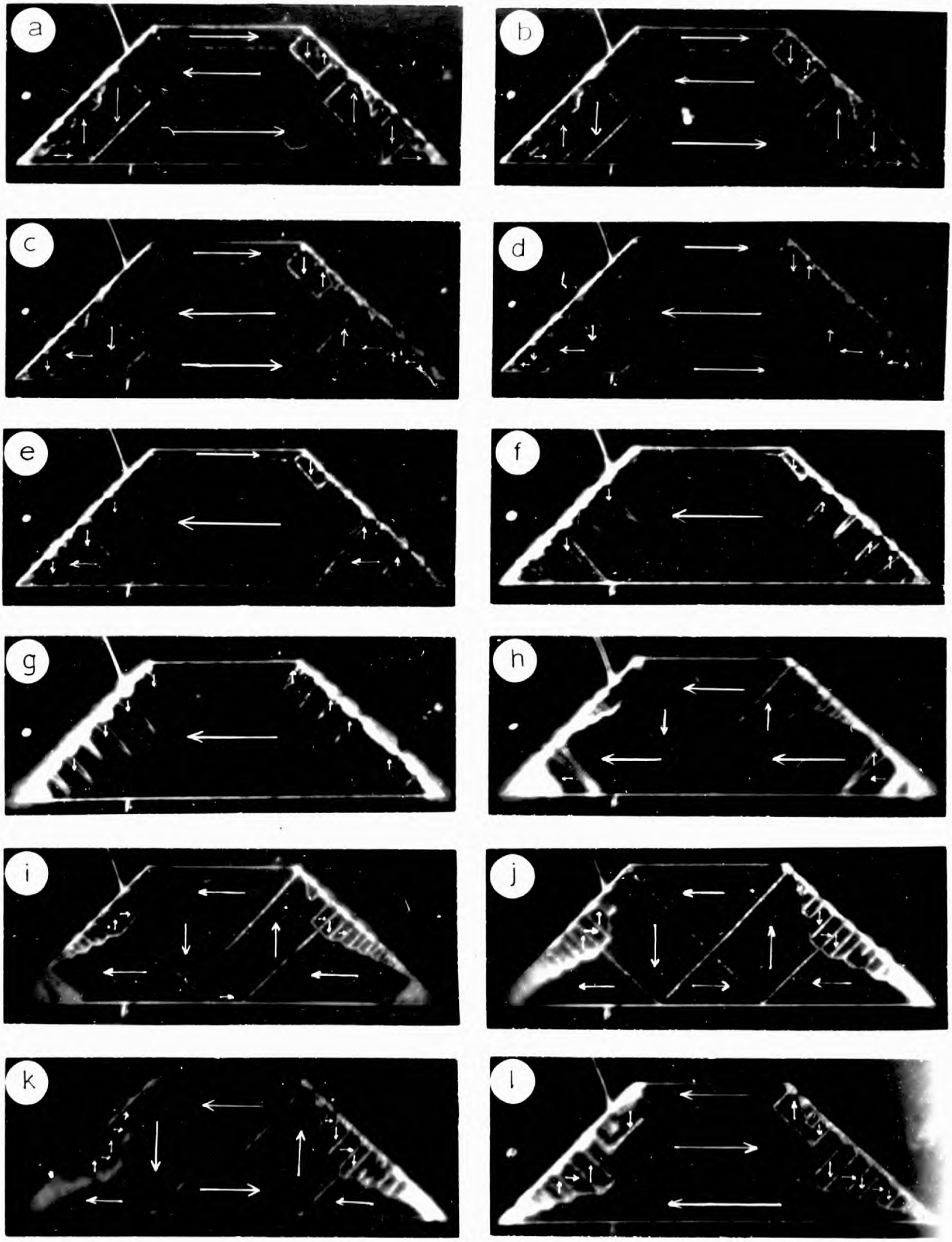

Fig. (5.16) Hysteresis loop on nickel platelet

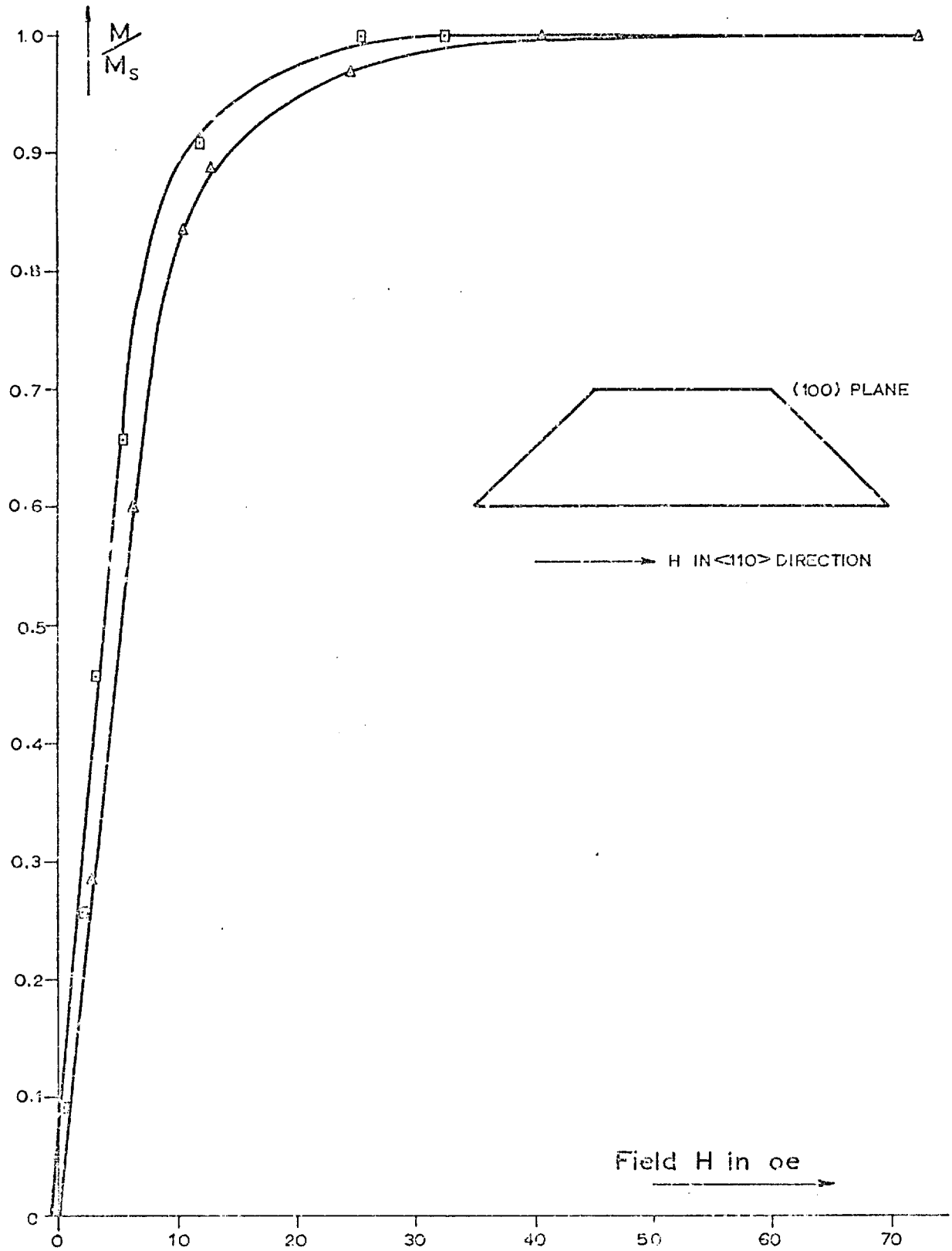

Fig. (5.17) Hysteresis loop from nickel platelet

At almost zero field, FIG.(5.16l), the structure rearranged so that there were once again two 180° walls across the platelet. Differences will be noticed, however, with structure, FIG.(5.16a). The topological structure changes occurred with very little energy change and do not appear to have an effect on the hysteresis loop.

Magnetisation curve studies by Gemperle (1966) on iron platelets showed that in fields up to 50 oe the initial configuration of the domain structure remained unbroken, with the domain walls bent and consequently charged by the action of the magnetic field. De Blois noted a maximum of 11.4 oe for this to occur in positive anisotropy Ni/Co platelets. At Higher fields the instability introduced by increased wall charges caused the structure to rearrange itself in a complicated Barkhausen jump, clearly visible on the magnetisation curve. Before this occurred the susceptibility of the wall motion was reduced to as low as 10 by the pinning of the wall by the corners. By simultaneously photographing the domain pattern on both surfaces Gemperle and Kaczer (1969) were able to show that the angle which the domain wall made with the plane of the crystal also changed during the application of fields, reaching a minimum just before the jump occurred.

The absence of similar jumps occurring in the behaviour of Ni platelets is due, partly to the more complex domain structure, and partly to the different anisotropy which affects the corner structure.

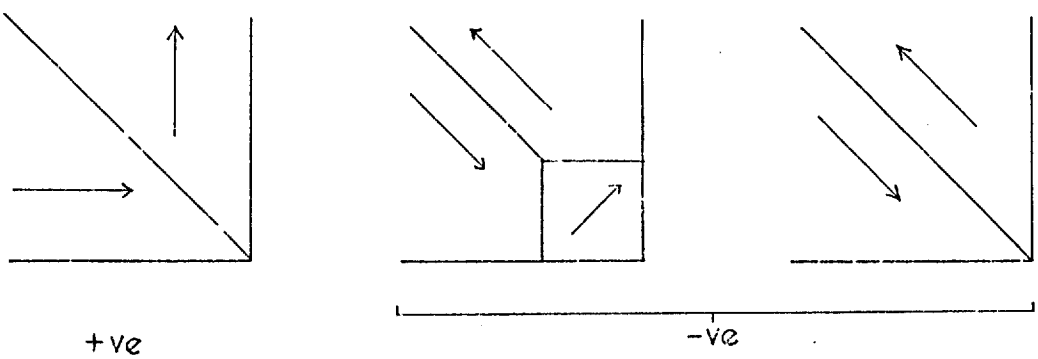

FIG.(5.18) CORNER STRUCTURES

It is immediately apparent that for the applied field direction shown in FIG.(5.18) that the corner of a positive anisotropy platelet provides a stronger pinning centre for domain walls than either of the negative anisotropy alternatives. However, because of the increased complexity of the structures found in negative anisotropy platelets rearrangement of the domain structures can occur by many smaller jumps. The effect of the weaker pinning in these platelets can be seen in FIG.(5.16, d & e) and although this may lead to jump in the hysteresis loop these are too small to be detected by this method.

5.2.2 Saturation and Nucleation

One of the less tractable problems in magnetism is that of domain nucleation. A basic assumption of nucleation theory is that a specimen starts from complete saturation, but certainty of the absence of nuclei of reversed magnetisation is difficult to achieve.

In 1945 Brown had shown theoretically that for an ideal ellipsoidal specimen whose long axis coincided with the easy axis of the material and the applied field, no nucleation could occur until a reverse field had reached a value greater than $2K/M_s - NM_s$, where N is the demagnetising factor. However, comparison of the measured coercive force of Ba $Fe_{12}O_{19}$ and Mn Bi had shown that the measured values were far lower, a situation known as Brown's paradox. One possible explanation is that the experimental results came from specimens not fully saturated so that the observed coercivity corresponded to the growth of residual domains rather than the nucleation of new ones. Shur et al (1960) in observations on Mn Bi particles 10-15 μm across measured a coercive field of a few hundred oersteds after saturation with a 5 k.oe field (a field which ought to be sufficient), but a field of a few thousand oersteds after saturating with 20 k.oe. However, they were unable to repeat these experiments with 50 μm diameter specimens.

The role of the edges and corners of a specimen must be very important. Shtrikman and Treves (1960) suggested that the limitation in Brown's approach was that if a single crystal with sharp corners was considered, the demagnetising field of a uniformly magnetised specimen would no longer be uniform, and this would result in much higher local demagnetising fields. Near sharp corners these fields would tend to especially high values and hence neglect would lead to large disagreements even when $K \gg M_s^2$. In his review of nucleation theory Aharoni (1962a) even suggested that saturation was unattainable in finite applied fields. He also concluded (1962b) that small regions of reversed magnetisation could not be formed by thermal agitation.

Certain support for the work of Shtrikman and Treves came from the coercive field measurements on Fe whiskers by De Blois and Bean (1959) who found the field value in the centre of a long whisker to be not significantly less than $2K/M_s$ in the centre of the whisker and to decrease substantially towards the tip. They were also able to associate regions of lower coercivity with visible defects on the surface. This was extended by Aharoni and Neeman (1963) who associated this reduction in the coercive field with the volume of the defects. A statistical treatment of these nucleation results was attempted by Brown (1962).

Sherwood et al (1959) found that single crystals of orthoferrite had high coercive fields which reduced when scratched to almost zero, suggesting that magnetisation reversal started at local defects and was not a function of the dimensions of the specimen, (see below). Kooy and Enz (1960) in their work on $BaFe_{12}O_{19}$ showed that a given crystal had nucleating sites each with its own coercive field, but it was not possible to predict on any occasion at which of the sites nucleation would occur.

No satisfactory theory of coercivity yet exists and a complete mathematical solution will only be obtained by solving Brown's

equations for a crystal with sharp corners. This is currently too difficult. Any theory has also to account for the coercivity of small particles, which despite Sherwood's work on bulk specimens, many workers have measured as being proportional to the reciprocal of their radii, Luborsky (1961).

An indication of the saturation field of platelets can be obtained from careful observations of their domain structures. By saturating a platelet then reducing the field until a domain structure formed at the corner, it was possible to know if the reverse nuclei had been driven out of the specimen. If the magnetisation direction of the corner closure structure was identical with the rest of the crystal the reverse nuclei could be assumed to have been driven out by the saturating field. But if the corner closure structure was still in opposition to the net magnetisation then the reverse nuclei probably persisted even at high fields. The two possible results in decreased field are seen in FIG.(5.19).

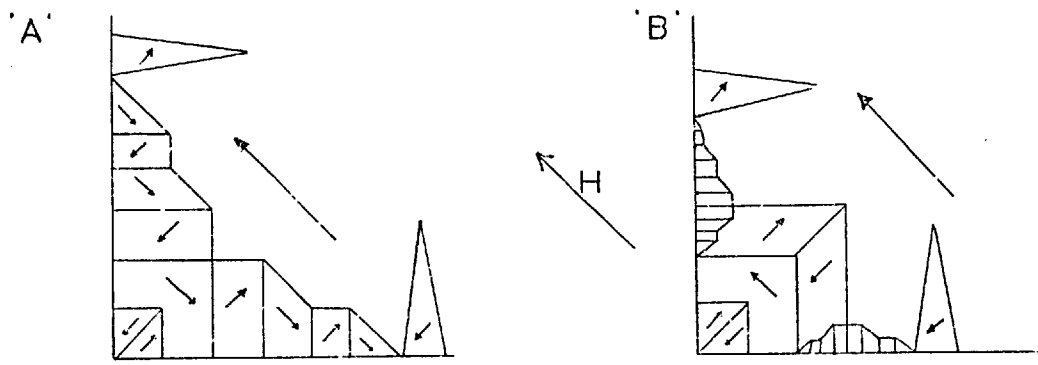

FIG.(5.19) CORNER STRUCTURES ON DECREASE FROM SATURATION

In forming type 'A' structures the reverse nuclei had not previously been removed, but type 'B' was formed after the platelet had been fully saturated. Experiments of this type on Ni crystals have shown a variation in the necessary saturating field from corner to corner, but the range is 350-400 oe, and the value of $2K/M_s$ is 235 oe for Ni. De Blois (1968a).

The importance of the corners is emphasised when the behaviour

of trapezoidal platelets is considered. With an easy axis field, nucleation was found to occur on the edges, with the formation of spike domains. Above 80 oe. the colloid cloud showed no local indentations and it is thought that the platelet was completely saturated at this field. It would thus appear that the absence of the apex made a significant difference.

For these and previous observations the field required for complete saturation was critically dependent on the perfection and shape of the edges and corners, probably down to the atomic level with any imperfections contributing to lower the saturation and coercive fields.

5.2.3 Surface Pinning

A frequently observed effect in the movement of domain walls towards the edges of platelets has been the phenomena of surface pinning. Referring again to FIG.(5.16) the two flanking echelon structures of (c) are seen connected by a 180° Bloch wall. When the field was increased to 6.2 oe (d) the L.H. structure broke and formed a spike domain, but the R.H. structure remained intact with the 180° wall disappearing into the edge of the platelet, as seen in FIG.(5.20).

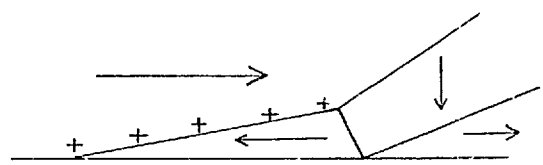

FIG.(5.20) DISAPPEARANCE OF 180° WALL

A similar feature is seen in FIG.(5.16e). The field has increased to 10.4 oe and the R.H. corner structure has disappeared to leave the 180° wall lying along the edge of the platelet. Observations on other platelets have shown that if at this stage the field was decreased this 180° wall would, over a field change of a few tenths of an oersted, completely separate from the edge in a Barkhausen jump.

Another example of this effect was noticed to occur between (k) in FIG.(5.16) where one 180° Bloch wall crossed the platelet, and (l) where there were two. At a certain field the left hand 90° walls lifted away from the edge but remained connected to it by a 180° wall, FIG.(5.21).

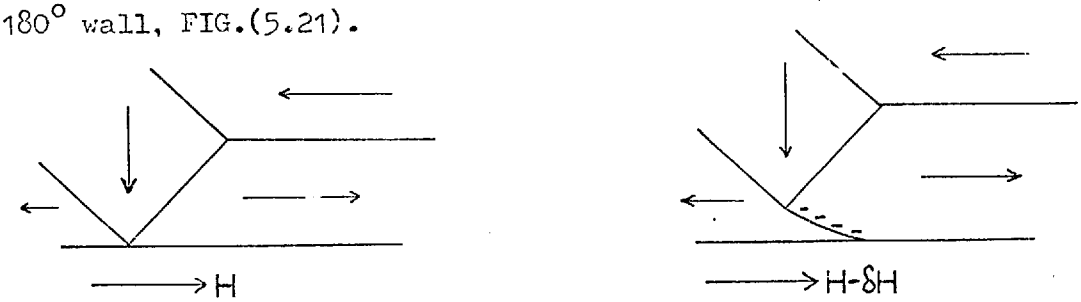

FIG.(5.21) FORMATION OF 180° WALL

But this stage only existed briefly, for with a further small field change a Barkhausen jump occurred with the 180° wall suddenly separating from the edge and moving across the platelet to give a structure more related to (l).

Further observations of this type of effect have been made on positive anisotropy platelets. Gemperle (1966), it will be recalled, observed a bowing of the domain walls of structure (a) in FIG.(5.22) when a field was applied to give structure (b). A further field

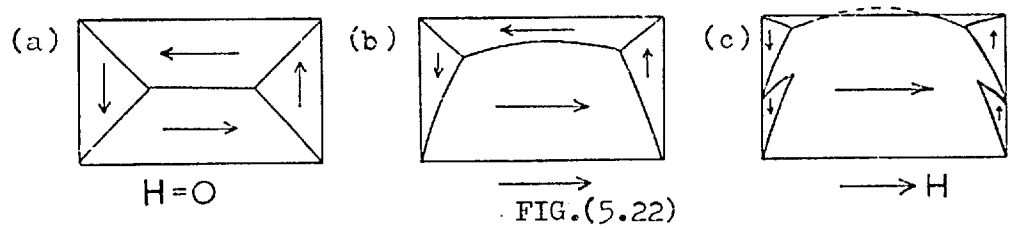

FIG.(5.22)

increase, he found, caused a major Barkhausen jump to occur and the 180° wall to disappear. However, De Blois (1967) managed to position a wall against the edge of a platelet, FIG.(5.22c), so that even although the projection of the arcs extended outside the edge of the platelet the wall did not part. When the field was decreased the walls moved away from the edge to form the previous structure.

From these observations it can be seen that a Bloch wall can exist against the edge of a platelet and not unwind, thus the spins at the edge must be rotationally restrained. This surface pinning of spins may play an important role in determining the domain behaviour and nucleation of platelets, and is related to the surface pinning thought to occur in spin wave resonance experiments. (See Weber (1968) for an introduction into this literature).

5.2.4 Néel Strip Structures

Lee (1953) and Bates (1964) have shown that to calculate the magnetisation curves for single crystals, especially in weak fields, an accurate knowledge of their domain structure is required. There have, however, been very few domain structures observed which also allow exact theoretical checks to be made. One of these, a block in the form of a long rectangular bar where the primary domains are packed in concertina fashion, FIG.(5.23), was first proposed by Néel (1944) and has been confirmed in essentials by many subsequent workers.

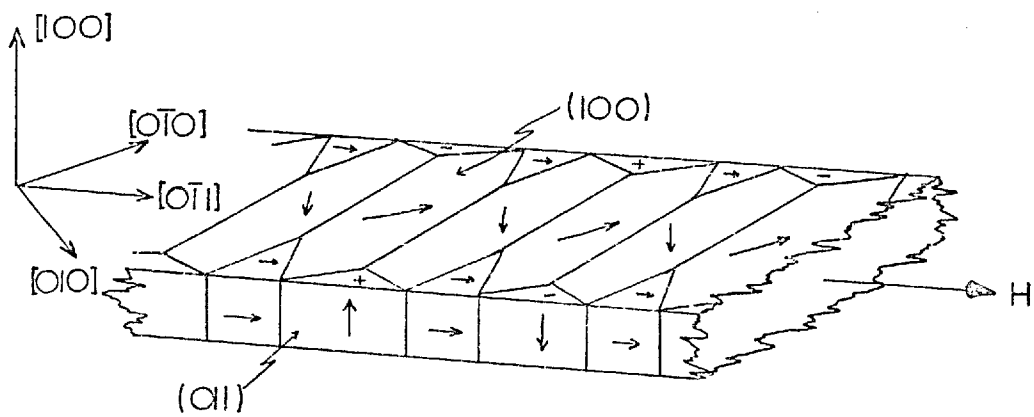

FIG.(5.23) NÉEL STRIP

In the general case of such a Néel strip the sides and orientation of the block are as shown in FIG.(5.23) with the magnetisation turned slightly from the <100> easy directions by the field H to make an angle θ ($<45^{\circ}$) with the [0$\bar{1}$1] direction. Closure is made by sets

of 'p' and 'q' triangular closure domains with the magnetisation directed in and out of the plane respectively. Good agreement has been obtained using iron crystals but the exact nature of the closure structures has not always been certain.

Rectangular platelets with <100> edges, {100} surfaces and negative anisotropy can, if thin enough, be suitable specimens. De Blois (1968b) has made such studies and found the observed spacing four times smaller than his calculation for a 87% Ni/Fe platelet of 1950 Å thickness. These permalloy platelets have also shown a variety of possible closure structures.

A specimen of Ni (dimensions 90x20x0.39 μm) in which a Neel strip was induced is seen in FIG.(5.24f). A zero field structure is seen in FIG.(5.24a) with the walls almost exclusively 90° and a large number of circle Bloch lines present down the centre of the platelet. When a [100] hard axis field of 3.6 oe was applied (b) those domains with components of magnetisation favourably oriented grew at the expense of those on the opposite side of the platelet. The extent of the movement is clearly shown by the central 90° walls, being largest away from the end, where the demagnetising field is lowest. At 11.3 oe FIG.(5.24c) the wall has moved completely out of the platelet, except near the end, to leave single 90° walls stretched across the width of the platelet. If any closure domains existed, they were too small to resolve.

At higher fields, as we have previously noted with hard axis fields, rotation of the magnetisation occurred and the colloid disappeared as the angle that the magnetisation made with the wall increased. This process is seen at 24 oe, FIG.(5.24d), and at 49 oe (e), with the spikes shrinking at yet higher fields to leave a saturated platelet. A most interesting feature of FIG.(5.24d) is the distribution of spikes about alternate 90° walls, this will be discussed later. On decreasing from a high field the structure, FIG.(5.24f), formed at 8.3 oe and developed into the zero field

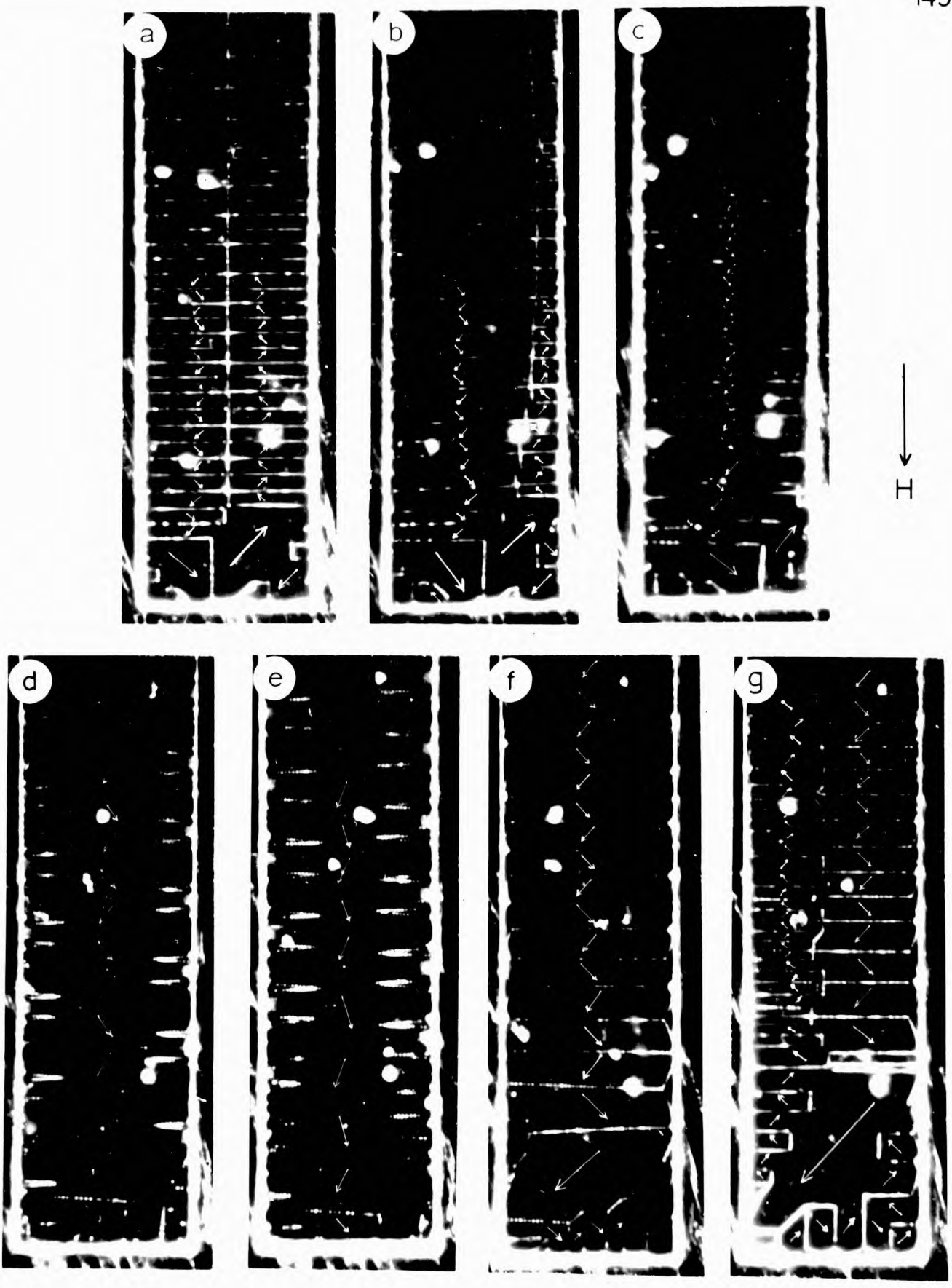

Fig. (5.24) Application of hard axis field.

structure seen in (g). The structure of (f) is suitable for Neel strip calculations. With a specimen of this thickness (3,800 Å) 'q' domains become energetically unfavourable and the structure used for analysis of FIG.(5.12f) is shown in FIG.(5.25)

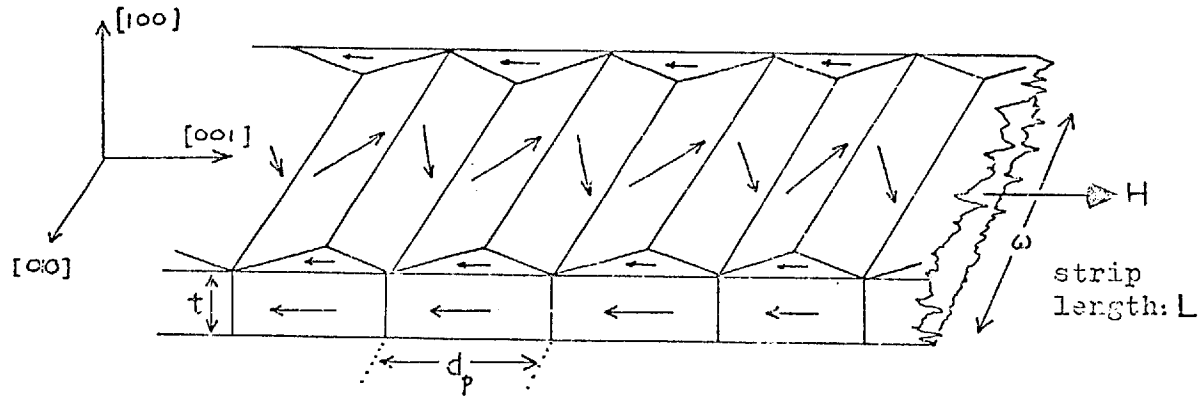

FIG.(5.25) NÉEL STRIP ANALYSED IN APPENDIX (C)

It should be noted that despite the different orientation of the strip the easy <110> axes bear a similar relationship to the edges. The closure domains have a spacing d_p equal to twice that of the main walls, and the normal component of magnetisation is continuous across all walls. An expression for d_p is derived in Appendix (C) as:

$$d_p^2 = \frac{-8\gamma_\omega}{K_1 \sin 2\theta(\cos\theta+1)(3\cos\theta-2)} \qquad (C.3)$$

where θ is related (see Appendix (C)) to the applied field by the formula

$$H_{eff} M_s = 2K_1 \cos\theta \cos 2\theta \qquad (C.1)$$

For the purposes of calculating the demagnetising field of the strip the value of θ can be taken as 45°.

Hence the pole strength at either end is $M_s \cos 45\ (t \times \omega)$ and thus the demagnetising field in the centre is

$$H_{demag} = 2\left[\frac{M_s \cos 45\ (t \times \omega)}{(L/2)^2}\right] = 4\sqrt{2}\, M_s \frac{t\omega}{L^2}$$

which for the dimensions of this Ni strip gives H_{demag} = 2.4 oe and the effective field in the centre of the strip of FIG.(5.12f) is H_{eff} = 8.3 - 2.4 = 5.9 oe.

Solving equation (C.1) graphically using this value for H_{eff} gave θ as 44°, thus justifying the initial assumption.

Equation (C.3) was solved with this value of θ, taking K_1 as 5.7×10^4 ergs/cm^3 and γ, the wall energy density as 1 erg/cm^2.

The result gave d_p = 5.0 µm.

Direct measurement from FIG.(5.24f) gave d_p = 3.0 µm.

An alternative closure structure, FIG.(5.26), was considered, again with the normal component of magnetisation continuous across all walls, but it predicted a spacing of 9.6 µm suggesting that it

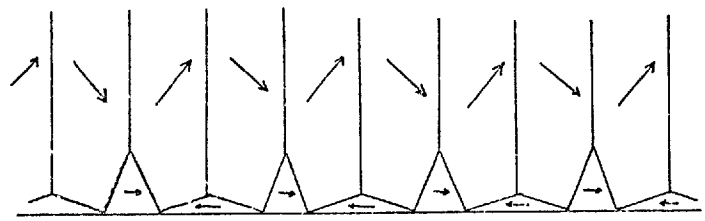

FIG.(5.26) ALTERNATIVE CLOSURE STRUCTURE

was unlikely. Possible reasons for the disagreement between the theoretical and experimental values for d_p are: the use of an incorrect value for γ, errors in the measurements made, or inaccuracies in the model used. Although the value of γ has been much questioned (see section 1.5), the value used in this platelet, of 3,800 Å thickness, cannot be so incorrect as to account for the disagreement, and would have to be 0.3 ergs/cm^2 to allow the results to agree.

Differentiating expression (C.3) for d_p^2 with respect to θ it was found that the error in d_p was as high as 2 µm/degree at this value of θ. The estimation of the field value which determines θ thus becomes a critical quantity and may have led to the disagreement.

There are also limitations in the model used for the closure structures. Although in essence they are probably as assumed for the calculation, their wall energies have been neglected and so has the possibility of any curling at the base of the main walls. With these limitations in mind the disparity in the results becomes more understandable.

Finally, if this closure structure is also assumed to have existed in FIG.(5.24c) the formation and distribution of the spike domains in (d) can be understood. As the field increased the angle of the magnetisation in the main domains decreased and the closure domains shrank, FIG.(5.27). Curling could easily occur at the base

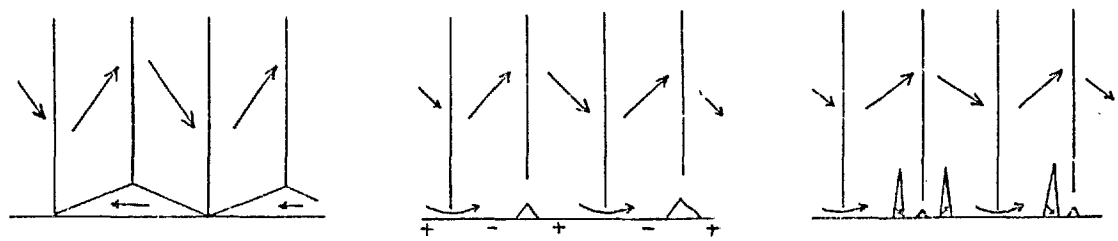

FIG.(5.27)

of the walls between the closure domains, but not near the closure domains themselves. This would have left a large surface pole density which by the formation of the spike domains on either side of the closure domain was dispersed in the body of the crystal.

5.3 WALL STRUCTURES IN PLATELETS

The structure of domain walls in thin films has been extensively investigated as a function of film thickness, composition, growth conditions and applied field history. A widely used model to explain these types (due to Middelhoek) and its limitations, was discussed in section 1.3. The thickness ranges over which different workers have claimed wall types to exist have shown a variation and a certain amount of overlap. However, the extent to which this is due to imperfections and unknown structural parameters resulting from

different preparation conditions is not clear. The near perfection of platelets together with their known physical and ferromagnetic parameters reduce these limitations and should enable more precise checks to be made on the ranges and the extend to which overlapping represents intrinsically allowed metastable structures.

Domain studies have been made on Ni and Ni alloy platelets with thicknesses ranging from just over 500 Å to over 10 μm. This provides a continuous span in observations of intrinsic domain wall types from the Néel and Cross-tie structures of thin films to the Bloch walls of bulk specimens found in positive anisotropy materials, or the complex stripe structures of negative anisotropy materials, which are the subject of Chapter 6.

From a correlation of the thickness and composition measurements by the electron microprobe with the type of wall structure observed by colloid technique it has been possible to make a plot of the platelet 180° wall structures. This is seen in FIG.(5.28), being a modified and updated plot of that due to De Blois (1968a).

Above 1500 Å the wall types found in virgin platelets were either pure Bloch or a combination of Bloch and the bright metastable walls. The metastable walls, whose structure was discussed in section 5.1.2, usually disappeared on application of a field leaving the faintly visible pure Bloch walls. Below 800 Å only Néel walls have been seen. Between 800 and 1500 Å a complicated transition exists, with different structures having similar energies, so that several structures can coexist simultaneously in the same platelet. In both Ni/Co and permalloy platelets all three types have been seen to coexist along the same 180° wall.

Unfortunately, information is sparse on the thinner platelets because of the difficulties in producing and handling them without introducing any strain. The thinnest specimen used in the current investigation was 860 Å thick but only showed Bloch walls. Although FIG.(5.28) applies to the Permalloy system a similar plot could be

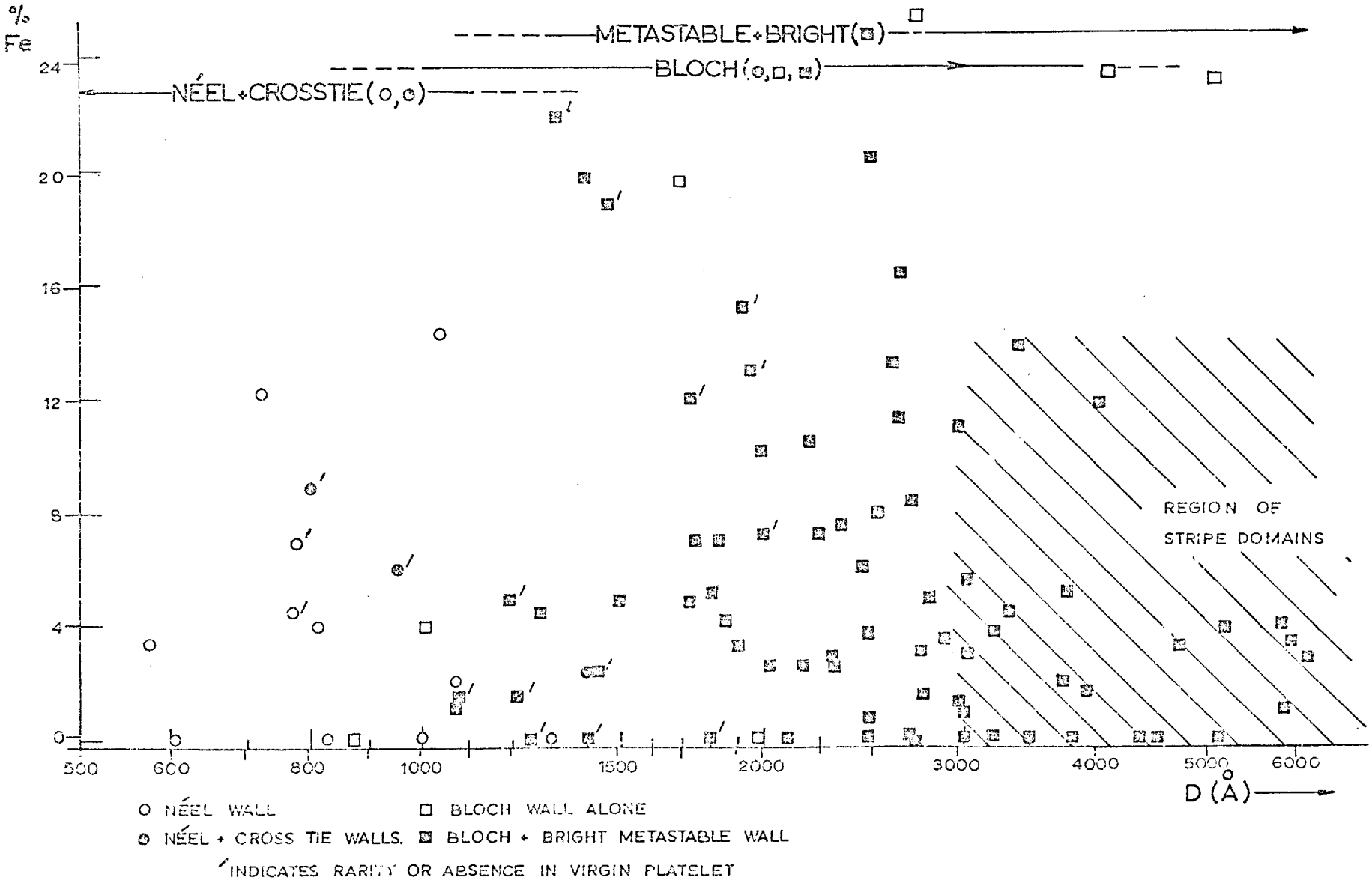

Fig.(5.28)180° Wall types in platelets as function of thickness and composition.

constructed for Ni rich platelets in the Ni/Co system. Wall structure variations in pure Fe and Co are unknown because they have never been grown thin enough to show these interesting transitions. The more exotic transition structures are usually more readily visible in platelets with lower anisotropies in either the Ni/Fe or Ni/Co systems.

The Bitter patterns from cross-tie walls in platelets appeared to indicate a completely different structure to those in uniaxial films and have been given the name 'beaded', but in fact these are now thought to be basically the same. The wall is broken into segments by alternate circle and cross Bloch lines. The circle Bloch lines appeared as absences in the colloid collection along the wall and the cross lines as tiny circles of colloid around a colloid-free region. The long tails associated with the cross Bloch lines in thin evaporated films were not visible. An additional feature not seen in evaporated films was the flanking of a circle Bloch line by two cross lines to form a set of three Bloch lines constituting a winding, attracting, group normal to the cross-tie wall.

The motion of Bloch lines along domain walls in fields applied normally to the walls is thought to contribute to the phenomenon of Creep (see Kayser (1967) and Torok et al (1969)) by increasing those parts of the wall with magnetisation rotations favourable to the field direction, at the expense of those against. This action has been observed in Ni/Co platelets as well as films, De Blois (1968a). In thicker platelets Bloch lines have also been seen in the middle of stripe patterns where they could be moved independently of the pattern itself.

The wall structures that exist in these platelets, especially in the region 800-1500 Å, are seen to be more varied than a simple Middelhoek calculation would suggest. The recent calculations of wall configurations by La Bonte (1969) and Hubert (1969) have shown the complex nature of the Bloch and Néel walls and have served to lessen the differences between the two extreme rotations that had been

considered by Middelhoek. In this region, therefore, energy differences between these more complex wall structures must be small and degeneracy is probably a more accurate description than coexistance for the variety of structures observed.

CHAPTER 6

DOMAIN STRUCTURES IN THICKER PLATELETS

INTRODUCTION

In Chapter 5 the properties of the domain structures in thin platelets were examined and reference was made to the complications which arise when the thickness of a platelet is increased. Kittel (1946) first showed that for a given anisotropy an upper thickness limit exists for planar magnetisation configurations. With anisotropy easy axes at 35.3° to the plane of the platelets this has been found to occur at about 4000 Å with the adoption of stripe domain configurations. The formation and behaviour of these patterns are discussed in the second part of this chapter following a review of earlier stripe domain work on thin films, a subject which has been of interest because of its potentialities in magneto-optical displays, Spain and Fuller (1966).

6.1 STRIPE DOMAINS IN THIN FILMS

6.1.1 Stripe Domains in Normal Incidence Films

Kittel (1946) had shown that the magnetic structure of a thin film depended on the ratio k of the demagnetising to anisotropy fields, ($k = 2\pi M_s^2/K$). For values of $k \ll 1$ the film consisted of a single domain magnetised perpendicular to the film plane and for $k \gg 1$ the magnetisation lay in the plane of the film. Between these two extremes a transitional structure was shown to exist by Kaczer et al (1963), who theoretically investigated a magnetically uniaxial unbounded film with an easy axis normal to the film in which the

magnetisation oscillated sinusoidally about the plane of the film. The magnetisation was made to satisfy the well-known Euler's equations and a general expression derived for its energy. This was found to depend on the material parameter k, the thickness of the film and the angle of maximum deflection ϕ_o. The spacing of the resulting 'stripe domains' was related to ϕ_o by the equation

$$d = 2\sqrt{\frac{A}{K}}\,\mathcal{K}(\sin\phi_o) \qquad (6.1)$$

where $\mathcal{K}(\sin\phi_o)$ is an elliptic integral of the first kind.

The first observation of stripe domains was made by Spain (1963) on a 80.5:17.5:2, Ni:Fe:Co film of 1900 Å thickness, and striations seen in the Bitter pattern with a period of 8800 Å. These stripes had formed parallel with the magnetisation and showed extreme stability and uniformity. Spain suggested that the pattern arose from an oscillation of the magnetisation about the plane of the film. The same films also showed rotatable initial susceptibility (of type R.I.S. 1) and a coervice field of 20 oe. In R.I.S. 1 films, after high field saturation χ_{init} parallel to the field is zero and χ_{init} perpendicular a maximum. R.I.S. 2 films show different properties, see Cohen (1962).

One of the essential differences between stripe domains in films and platelets lies in the origin of the out of plane anisotropy. In platelets it arises crystallographically from the 35.3° angle that the four <111> easy axes make with the (100) plane, and the difficulty arises in the interpretation of the observed patterns in terms of magnetostatic and anisotropy energies. In films, however, an anisotropy axis is formed normal to the plane of the film and the difficulty arises in knowing its magnitude, variation and possible origins.

The conditions found for the presence of stripe domains in thin films were in agreement with Lehrer's observations on the incidence

of R.I.S. and "mottled" film behaviour (1963), and Hubert and Smith's report (1959) that isotropic strain in the plane of a film created a normal easy axis. The strong compositional dependence of the critical thickness, t_c, suggested that strain and magnetostriction played important roles.

Simultaneous with Spain's observations, workers at the Hitachi laboratories, Japan, had observed stripe domains in permalloy films, Saito et al (1964a), as well as iron and cobalt, Sugita et al (1964 & 1965a). They had also made calculations for the 'critical thickness' above which stripes formed and the stripe spacing, by minimising the exchange, anisotropy and magnetostatic energies. Saito et al (1964b).

Unlike Kaczer's sinusoidal distribution a saw tooth magnetisation variation was assumed by Saito et al (1964b), of maximum excursion ϕ_o and half wavelength d, in a film of thickness t and normal anisotropy axis, value K, see FIG.(6.1). No lateral variation was assumed to occur with $(M_s)_x = 0$. From this model Saito et al (1964b) derived expressions for the critical thickness,

$$t_c = 27 \left(\frac{8}{\pi^2}\right)^2 \left(\frac{AM_s^4}{K^3}\right)^{\frac{1}{2}} \qquad (6.2a)$$

and for the stripe spacing

$$d = 2\left(\frac{\pi^2}{8}\right)^{\frac{2}{3}} \left(\frac{At}{M_s^2}\right)^{\frac{1}{3}} \qquad (6.2b)$$

However, observations of stripe spacing showed it to be several times smaller than the theoretical value, with a $t^{\frac{1}{2}}$ dependence. The possibility of K arising from an isotropic strain was investigated, but agreement was not found to be good. In weak fields the orientation of the domain walls remained unchanged and the uniaxial easy axis existing along the directions of the stripes rotated with the stripes into any field direction.

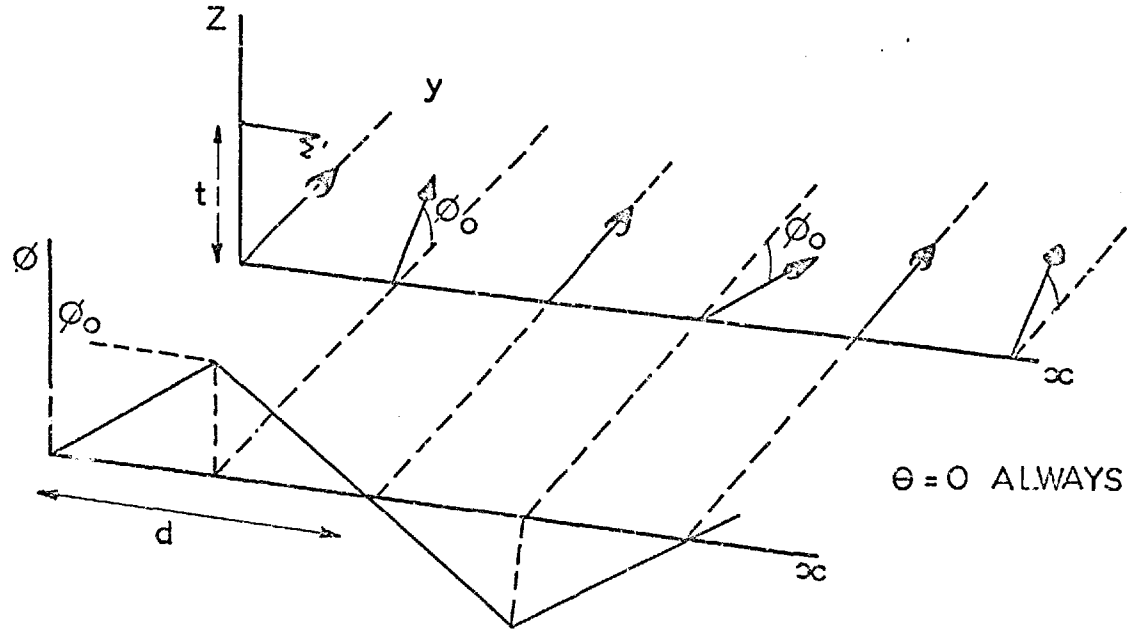

Fig. (6.1) Stripe domains (after Saito)

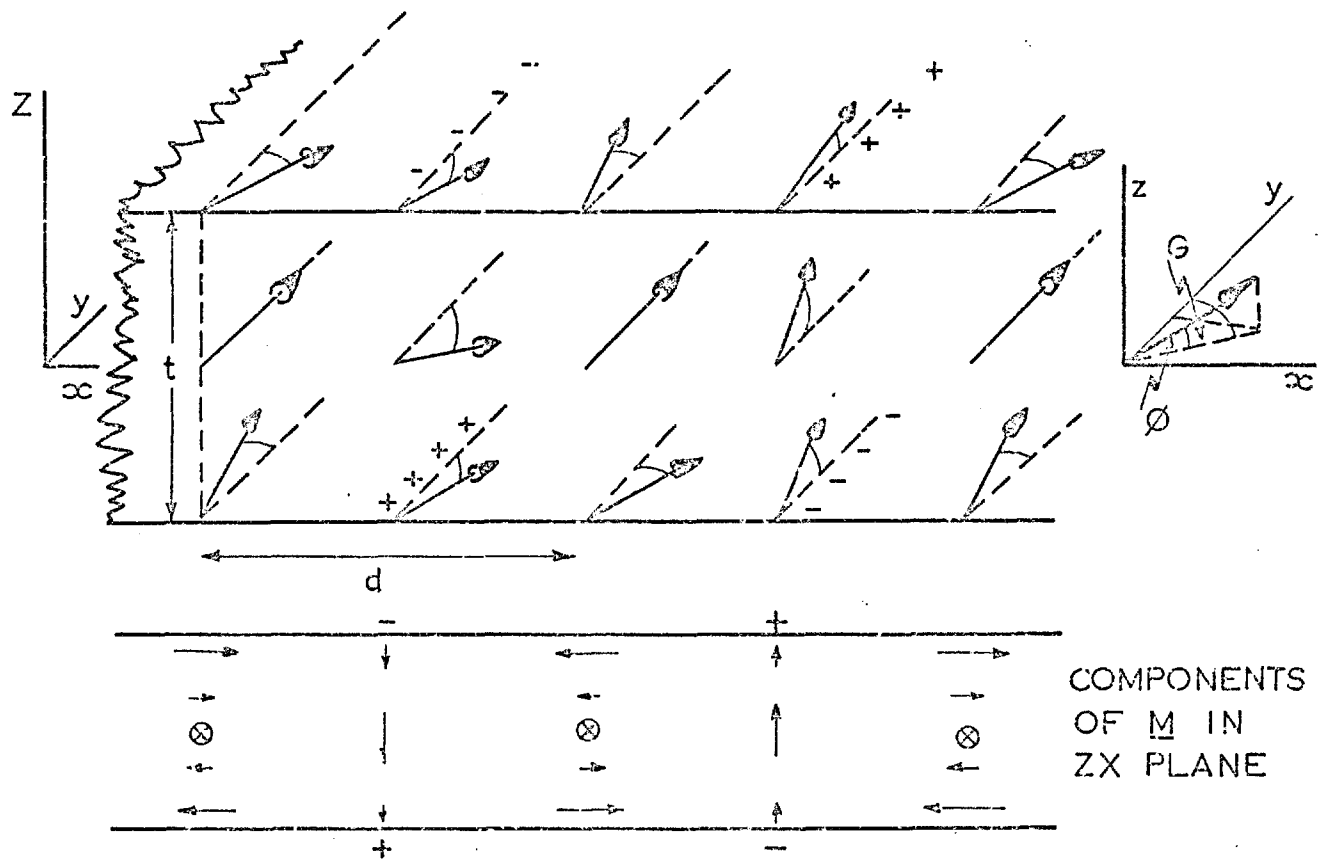

Fig. (6.2) Stripe domains (after Muryama)

Saito's model appeared to fit the observed properties of the B-H loop and the magnetoresistance measurements. It was substantially confirmed by the first Lorentz microscope investigation made on a 95:5 Ni:Fe film of 1200 Å thickness by Koikeda et al. (1964).

The relaxation phenomena which had been observed earlier in films displaying mottling and R.I.S. was associated with the movement of stripe domains by Sugita and Fujiwara (1965). They found reversal to occur by a nucleation of stripe domains in the new field direction and their movement across the film in a 'creep' type action.

Studies by Wade and Silcox (1966) had indicated that vapour deposited films contained voids and formed a columnar structure. Thus the anomalous perpendicular anisotropy causing stripe domains was attributed by Lo and Hanson (1967) to a shape anisotropy

$$K_s = \frac{2\pi M_s^2 D^4}{(D+d)^4} - K_\perp \qquad (6.3a)$$

(where $K_\perp$ is a perpendicular anisotropy due to the columnar structure defined by Iwata et al (1966))
and a magnetostrictively induced anisotropy

$$K_\sigma = \frac{-\frac{3}{2}\sigma\lambda D^2}{(D+d)^2} \qquad (6.3b)$$

D is the columnar grain diameter (independent of thickness) and d is the grain boundary layer thickness.

The critical thickness in Saito's model was then given by

$$t_c = 2500\, M_s^3 \left(\frac{D}{D+d}\right)^6 (K_s + K_\sigma)^{-\frac{3}{2}} \qquad (6.4)$$

From a t_c against composition plot, K_s was found to be an order of magnitude larger than K_σ at 85% Ni suggesting that the perpendicular anisotropy arose from shape anisotropy at low anisotropy compositions, but strain induced anisotropy became significant in Ni

rich regions. These results were substantially corroborated by Fujiwara et al (1965) and Sugita et al (1967).

The spin configurations considered so far have been assumed and, by the discrepancy between the observed and calculated stripe spacings, have obviously not satisfied minimum energy considerations. Saito (1966) modified the model to a less restricted case by allowing the $\underline{M}$ vector to vary in the manner of a modified μ^* correction, Williams et al (1949), thus allowing a certain amount of internal closure by decreasing the magnetostatic energy at the expense of the anisotropy and exchange energies. He assumed that no magnetic charges existed except on the surface and that the spin configuration was described by a sinusoidal function. This model gave much improved agreement with the experimental results.

This work was extended to a full micromagnetic calculation with solutions precisely satisfying a set of Euler's equations by Murayama (1966). The determined state had a lower energy than any other provided that the state was fully expressible in two functions, one corresponding to a μ^* correction and the other to a flux closure property.

The coordinate system adopted was taken at the centre of the film, see FIG.(6.2), with the x axis perpendicular and the y axis parallel with the stripes, and the z axis normal to the film. Murayama considered three cases:-

MODEL I	$\phi = \phi(x)$	$\theta = \text{const.} = 0$
MODEL II	$\phi = \phi(x,z)$	$\theta = \text{const.} = 0$
MODEL III	$\phi = \phi(x,z)$	$\theta = \theta(x,z)$

A uniform distribution in the y direction was assumed.

Model I is seen to correspond with Saito's model, where variation with z is ignored, and Model II results from the application of a μ^* correction to Model I. Model III, seen schematically in

FIG.(6.2) for a film with perpendicular anisotropy is the distribution with minimum energy formed when the magnetisation directions were allowed to vary freely over the xz plane, with a general orientation towards the y direction. The magnetisation components in this zx plane are also shown in FIG.(6.2) and the structure is seen to consist of a series of circle Bloch lines of alternate rotation directions lying in the centre of the film, with a certain amount of flux closure between these. With these models the domain spacings at the critical thickness were found to be

$$d \simeq \pi \left[2 \frac{A}{2\pi M_s^2} t \right]^{\frac{1}{3}} \qquad \text{for MODEL I} \qquad (6.4,\text{I})$$

$$d \simeq \sqrt{t} \left[\pi^2 \frac{A}{2\pi M_s^2} \right]^{\frac{1}{4}} \qquad \text{for MODEL II} \qquad (6.4,\text{II})$$

and

$$d \simeq \sqrt{t} \left[\pi^2 \frac{A}{K\ 2\pi M_s^2} (K+2\pi M_s^2) \right]^{\frac{1}{4}} \qquad \text{for MODEL III} \qquad (6.4,\text{IIIa})$$

with

$$t_c \simeq 2\pi \sqrt{\frac{A}{K}} \qquad (6.4,\text{IIIb})$$

Equation (6.4,I) is very close to the result in equation (6.2b) for a saw tooth distribution. Model II was found to resemble Kittel's parallel strip multidomain model without closure domains, and Model III coincided with this model, retaining the closure domains, if the wall energy was put equal to $\sqrt{AK}$, (Kittel's closure domains having width $\propto (\gamma/K)^{\frac{1}{2}}$ and Murayama's with width $\propto (\gamma/2\pi M_s^2)^{\frac{1}{2}}$.)

Unlike Model I, Model III was found to fit the observed variation of stripe spacing as a function of film thickness very well. In agreement with Kittel, Murayama found that if $K < 2\pi M_s^2$ the parallel strip multidomain structure was a higher energy state than the closure structure but when $K \sim 2\pi M_s^2$ this preference vanished and Models I and II became equally favoured to III. The effect of $K > 2\pi M_s^2$ was not

studied because Murayama's treatment was only valid when $K < 2\pi M_s^2$. It will be noticed that the thinnest film in which stripe domains are expected is roughly as thick as a Bloch wall with magnetostatic energy neglected.

In 1967 Murayama investigated a fourth model

MODEL IV $\quad \phi = \phi(x,y,z) \quad \theta = \theta(x,y,z)$

He found, however, that at the critical thickness the lowest energy configuration contained no modulation in the y direction. This may not be the case at greater thicknesses but Murayama's treatment was limited to critical cases and can give no guide at high thicknesses, being outside the limits of its application.

Finally, stripe domains have been reported in thicker permalloy films, t = 2.5 - 10 μm, by Krinchik (1968). The structure proposed (FIG.(6.3)) from high resolution Kerr work has a form, as might be expected, mid-way between the Kittel closure structure and Murayama's Model III. The magnetisation lies at angles ψ and ϕ to those of a true Kittel structure.

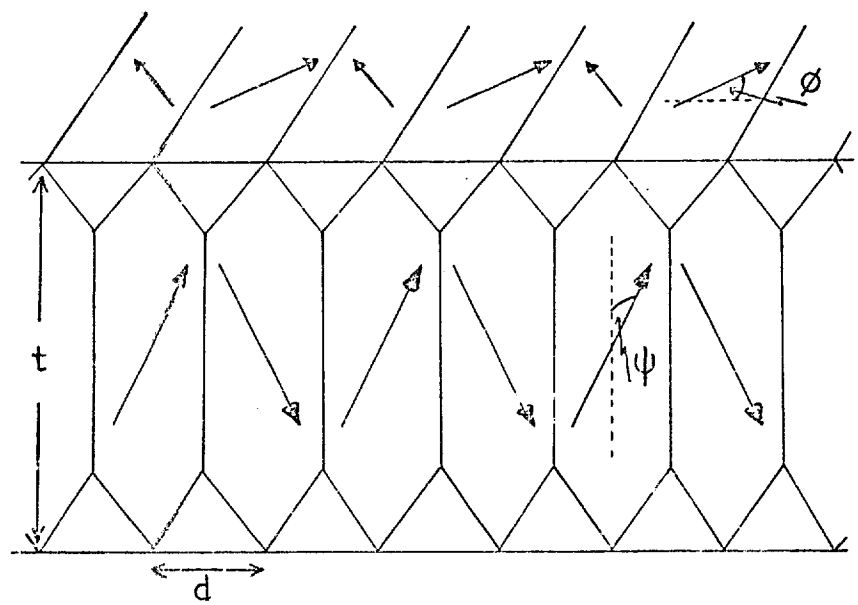

FIG.(6.3) STRIPE STRUCTURE (AFTER KRINCHIK)

t	d	ϕ	θ	ψ
2.5 μm	0.7 μm	37°	52°	8°
10 μm	2.5 μm	18°	46°	4°

The measured values for d and ϕ for the extremes of thickness are tabulated together with values for θ and ψ which Krinchik estimated from his Kerr effect studies. The dimensions of this configuration in contrast to Murayama's are now partly dictated by the formation of definite domain walls. Murayama's Model III was seen in FIG.(6.2) to have a series of Bloch lines running parallel with the stripes through the thickness of the film. Thus Krinchik's model is related to Murayama's by the extension of these Bloch lines into walls.

6.1.2 Stripe Domains in Oblique Incidence Films

The first observation of stripe domains in films evaporated at an oblique incidence to the substrate was made by Baltz (1966). He found that thick films of permalloy, evaporated at angles of incidence of 60°-80°, exhibited stripe domains which ran parallel to the easy axis of the film (induced by the oblique incidence evaporation) and perpendicular to the vapour stream.

A completely new type of stripe domain was observed in thicker films independently by Tatsumoto et al (1968) with the Bitter technique and Pulchalska and Ferrier (1967) by Lorentz microscopy. Tatsumoto found in 76:24, Ni:Fe films that only the Saito type domains existed near saturation and only the new type near remanence. The coexistance of both types was observed during a critical stage of the magnetisation process, corresponding to discontinuities in the magnetisation.

Pulchalska and Ferrier investigated permalloy films with thicknesses up to 3000 Å, evaporated at varying angles of incidence. Below 40° only the Saito type stripes were present, with the domain magnetisation aligned perpendicular to the incident vapour stream by the oblique incidence anisotropy, see Metzdorf and Wiehl (1966) and

Crowther and Cohen (1967).

Above 50° the stripe domains lay parallel with the incident vapour stream in a more regular structure ($d \sim 3500$ Å) and showed greater contrast on the Lorentz micrographs, leading to the name of 'strong stripes'. It is these that were observed by Talsumoto et al. At higher angles of incidence (70° and 80°) the stripes became more complicated although still basically unidirectional.

Ferrier and Pulchalska (1968) reported investigations on the strong stripe structures establishing details of the spin configurations by low-angle diffraction (Ferrier and Murray (1966)) as a complete circulation of a component of the magnetisation, perpendicular to the average magnetisation direction, about the in-plane component in the direction of the weak stripes. The average magnetisation in the weak stripes did not lie in the plane of the films but varied from domain to domain, and 360° walls formed from Néel lines in the Bloch walls to help equalise the magnetostatic fields. These 360° walls were also found completely isolated in the middle of a domain and were thought to have nucleated on a film imperfection or inclusion, to lower the free pole density in that domain.

At higher angles of incidence the increased surface pole density led to the establishment of a complete strong stripe structure. This is seen in FIG.(6.4) where one component of the magnetisation vector can be imagined as circulating around the in-plane axial component. The 180° walls separating a domain containing strong stripes from a reverse magnetised domain are also seen to have degenerated into 90° walls and Bloch lines.

In walls where the magnetisation in the weak stripes on either side made the same average angle with the film plane 360° walls formed within the 180° walls and expanded equally into the domains on either side.

The structure proposed for these stripe domains by Tatsumoto et al

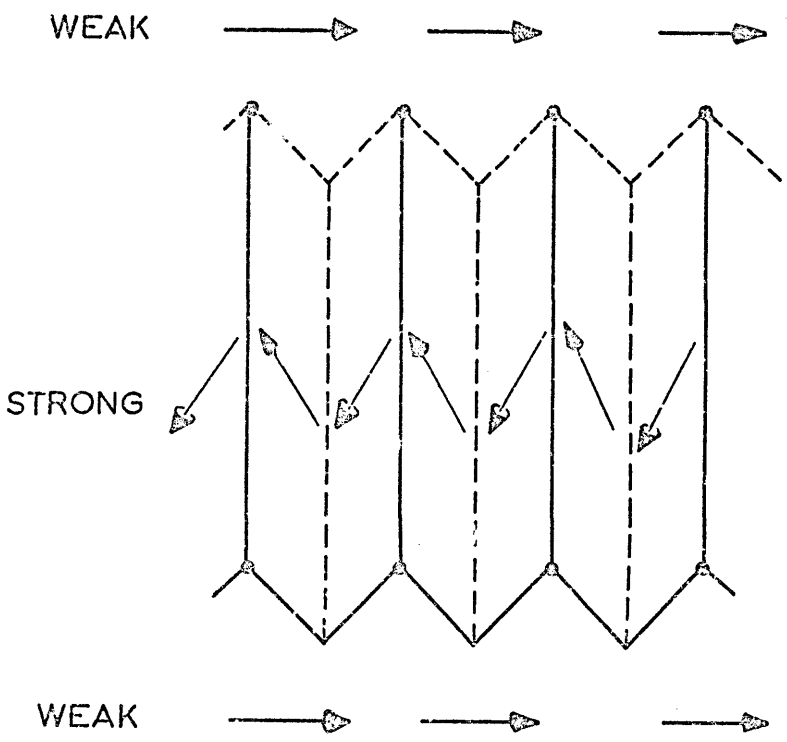

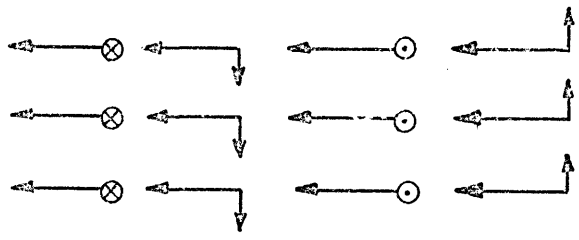

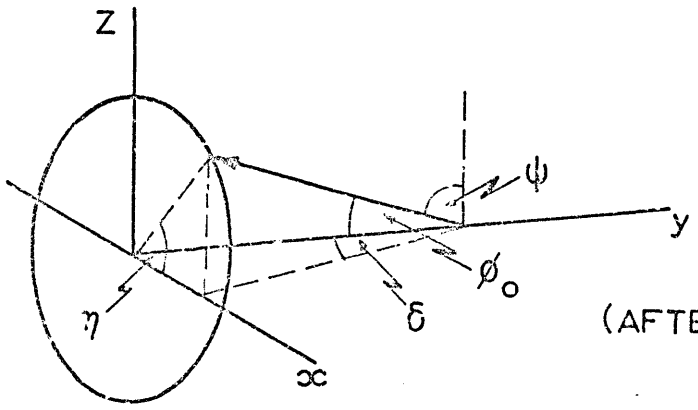

Fig. (6.4) 'Strong' Stripe Domains

was similar, but it ignored the presence of a constant in-plane component of magnetisation and in so doing was in clear disagreement with the low angle diffraction pictures.

An analysis of the strong stripe domain structure was made by Sukiennicki (1968), and the angles used are seen in FIG.(6.4). The magnetisation was assumed to make a constant angle ϕ_o with the y-axis and an angle ψ with the z axis. The magnetisation component which spiralled around the y axis was taken to make a linearly varying angle η with the x axis in the zx plane. With the wavelength of the structure given by L, $\eta = (2\pi/L)y$, where L = 2d, twice the spacing of the lines of Bitter colloid. By minimising the total energy density (including terms both for in-plane and perpendicular anisotropies) Sukiennicki determined:

$$d \left(= \frac{L}{2} \right) = \left[\frac{2\pi^2 A t}{M_s^2} \right]^{\frac{1}{3}} \qquad (6.5a)$$

and

$$t_c = \left[\frac{36\pi^2 A M_s^4}{(K_\perp - K_{11})^3} \right]^{\frac{1}{2}} \qquad (6.5b)$$

The spacing d was in generally good agreement with the experimental results although three or four times too small. K_{11} had been found as 8×10^4 ergs/cm^3 and for these films the expression for the critical thickness appears correct if the unknown $K_\perp$ is taken as being greater than 8×10^5 ergs/cm^3. From the work of Sugita et al (1967) this was not an unreasonable value. Sukiennicki also showed that the proposed structure was energetically favourable to the weak Saito stripes if the anisotropies were as expected.

Limitations on the model were the assumptions that η was a linearly dependent function of y and ϕ_o was independent of z. A non linear variation of η and a variation of ϕ_o leading to a dispersion of the surface magnetisation at the expense of anisotropy, exchange and volume poles (after Murayama's treatment) would probably have been

energetically more favourable. It is clear, however, that the strong stripes formed when $K_{\perp}$ was sufficiently large that the ϕ_o of the Saito stripes would have approached 90°.

6.1.3 Stripe Domains in Iron Foils

In (001) films with <100> easy axes stripe domains would not be expected in single crystals of iron. However, foils were prepared with a strong (111) texture by Bourret and Dautreppe (1966) and examined by Lorentz microscopy to show stripe domains. The walls separating the Weiss domains were either 180° or 120° or 60° and were directed along the [110] or [112] axes. The stripes lay parallel with the magnetisation directions and appeared at a critical foil thickness of 1300 Å, with a spacing d of 1000 Å. Observations were made on foil thicknesses up to 4000 Å where the stripe spacing was observed to be 4500 Å. The interpretation of these structures was basically an angled Saito weak stripe structure, see FIG.(6.5).

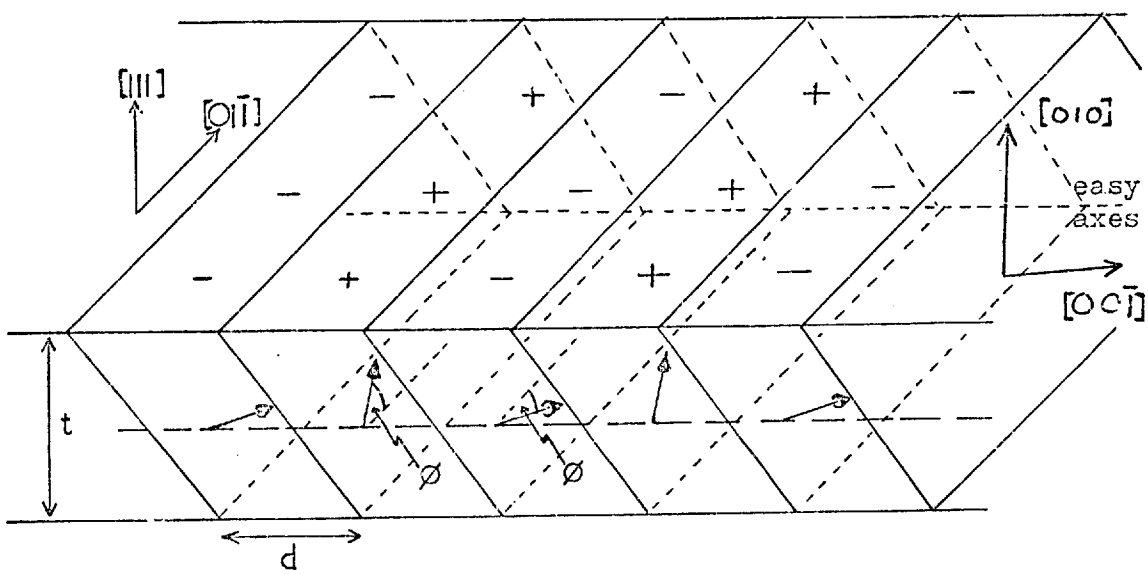

FIG.(6.5) STRIPE DOMAINS IN (111) IRON FOILS
(AFTER BOURRET & DAUTREPPE)

The magnetisation, whilst being generally directed towards the

[01$\bar{1}$] direction, is seen to oscillate in a (100) plane approaching the two easy axes [00$\bar{1}$] and [010] that lie in that plane. The concept of magnetisation zones perpendicular to the plane of the foil has to be abandoned with the plane of oscillation making an acute angle with the plane of the foil, and by so doing avoiding the formation of a volume pole density.

The magnetostatic energy was approximated by a μ^* correction and an expression for the total energy minimised with respect to ϕ and d. The result showed that this oscillation was energetically favourable for foils thicker than 1250 Å with an amplitude ϕ of about 30°, varying little with foil thickness. The stripe spacing d was predicted to increase linearly with foil thickness, but at a rate far below that observed experimentally, giving a d value of just over 2000 Å for a foil of 4000 Å thickness.

A full micromagnetic treatment has not been applied to these foils, but Bourret and Kleeman (1967) extended the μ^* correction to this particular geometry. The equations required numerical solution and gave good agreement with experimental results for the critical thickness, but the dependence of the stripe spacing d on the foil thickness was far too low. This probably arose from a linearisation of the equations at an earlier stage in the calculations. However, it is interesting to note that at the critical thickness the angle ϕ was found not to tend to zero, but to about 20°. Thus any use of small angle approximations for the determination of the critical thickness in this type of geometry is fundamentally wrong.

6.1.4 The Application of Micromagnetics to Stripe Domains

Before considering the properties of stripe domains in thin platelets the application of micromagnetics to stripe domain calculations is considered.

Exact solutions of Brown's equations of micromagnetism are difficult to obtain because of complexities arising from the expression

for the stray field energy and from the limitation that the squares of the direction cosines of the magnetisation vector must at all times sum to unity,

$$\sum_{i=1}^{3} \alpha_i^2 = 1$$

In a limiting case of $M_s^2 \longrightarrow \infty$, whilst the other physical parameters remained finite, the magnetisation configuration would be such as to avoid the formation of stray fields. Thus in this limiting case:

$$\begin{aligned} \text{div } \underline{M} &= 0 \\ \underline{M} \cdot \underline{n} &= 0 \text{ on all surfaces} \end{aligned} \qquad (6.6)$$

where $\underline{n}$ is the vector surface normal.

A classical Bloch wall in an infinite body is an example of such a distribution. Hubert (1969) applied the limitations of equations (6.6) to situations in thin films with the restriction that $k \gg 1$ ($k = 2\pi M_s^2/K$). The opposite limit with $k \ll 1$ is suitably covered by the μ^* method. Hubert found that a micromagnetic configuration satisfying equation (6.6) did not in general fulfil Brown's equations and although micromagnetic equations allowing (6.6) were formulated they were not easy to solve for any but linear cases. Hubert restricted himself to approximations by a Ritz's method. However, this approach has been most important in providing an upper bound to the energy of any real micromagnetic configuration.

An example of such a result was seen in section 1.5 considering the theoretical models for Bloch walls. It was seen that La Bonte's two dimensional construction of a Bloch wall fell below Hubert's upper limit, whereas all previous models had had higher energies, see FIG.(1.10).

Hubert applied equations satisfying zero stray field not only to Bloch and Néel walls but also to ripple and stripe structures. Considering once again the critical case, the critical film thickness

below which no stripes would be stable t_c, in a film with a uniaxial anisctropy normal to the film plane, was found to be:

$$t_c = \frac{2\pi}{\left[1 - \frac{HM_s}{2K}\right]} \sqrt{\frac{A}{K}} \qquad (6.7a)$$

H being applied in a direction parallel with the stripes and

$$d = \left[\frac{2K - HM_s}{2K + HM_s}\right]^{\frac{1}{2}} t_c \qquad (6.7b)$$

which for $K/2\pi M_s \longrightarrow 0$ is seen to be in agreement with the result of Murayama, see equation (6.4,IIIb) and of Holz and Kronmüller (1969), (see below).

Numerical calculations were also performed for the stripe domains seen in iron foils, to give the critical thickness as

$$t_c = 6.83\left(\frac{A}{K_1}\right)^{\frac{1}{2}} \qquad (6.8a)$$

and the stripe spacing at that thickness as

$$d = 7.77\left(\frac{A}{K_1}\right)^{\frac{1}{2}} = 1.11\ t_c \qquad (6.8b)$$

Holz and Kronmüller (1969) treated the nucleation of stripe domains by considering the critical parameters for which the magnetisation began to rotate out of the film plane. Because at this stage the magnetisation direction only deviated slightly from the film plane the problem could be treated by linearized micromagnetic equations. (Murayama's paper was criticised for violating the micromagnetic surface conditions and this was avoided in Hubert's work).

Solving the resulting equations, they were able to characterise materials by the parameter k, mentioned before ($k = 2\pi M_s^2/K$).

(a) When $k > 1$ and $t < t_c$ the magnetisation lay in the film plane with the domains separated by either Néel or Cross-tie walls.

(b) When $k > 1$ and $t > t_c$ a stripe structure formed, and as t increased above this thickness a continuous transition from stripe to bulk domain structures occurred (note the work of Krinchik, section 6.1.1).

(c) When $k < 1$ the magnetisation was independent of the thickness of the film, lying parallel or anti-parallel with the easy axis down to values of t = 0. (Domain structures in these materials are established by the nucleation of reversed domains at imperfections and dislocations.

A plot of t_c and d_c as functions of 1/k displayed these three regions graphically and from the positions of the 1/k values of the transition ferromagnets the critical thicknesses were found to be

$$\begin{aligned} t_c^{Ni} &= 2780 \text{ Å} \\ t_c^{Fe} &= 1320 \text{ Å} \\ t_c^{Co} &= 233 \text{ Å} \end{aligned} \qquad (6.9)$$

At large values of k, t_c was found to approach the value $2\pi(\frac{A}{K})^{\frac{1}{2}}$, in agreement with Murayama's result.

The relative insensitivity of t_c to M_s for $k \gg 1$ implied that the formation of stripe domains occurred by a stray-field free magnetisation process, Hubert (1969). With decreasing M_s values the stray field increased in importance.

To obtain agreement with Saito's experimental results for t_c and d a perpendicular anisotropy of 60% of Saito's value had to be used, which may well be acceptable.

A check was also made on the stripe domains in (111) plane iron foils, see section (6.1.3). The value Bourret and Dautreppe had used

for the exchange constant (0.8×10^{-6} ergs/cm) was considered too low. Using a value of 2×10^{-6} ergs/cm the critical thickness was found to be

$$t_c = 6.225\left(\frac{A}{K_1}\right)^{\frac{1}{2}} \qquad (6.10a)$$

and

$$d = 1.11\, t_c \qquad (6.10b)$$

in excellent agreement with equations (6.8).

The numerical value for t_c of 1320 Å was too high for Bourret's experimental results. The value of d (2930 Å) at this thickness showed even greater disparity but this was probably because d was a sharply varying function of t at this thickness. The disagreement of the value of t_c itself is probably to be found in the initial assumption of Holz and Kronmüller's equations, that because they were considering only critical conditions linear equations could be used. However, it will be recalled from the work of Bourret and Kleeman that even at the critical thickness the maximum spin deflection was $\sim 20^{\circ}$. It unfortunately looks as if non linear equations will be necessary.

The approach adopted by these authors is obviously very powerful and has scope for further development being limited exclusively by the ability to handle the complex mathematical functions. A similar approach to the strong stripe structures would also be very desirable.

6.2 STRIPE DOMAINS IN PLATELETS

Observations of stripe domains in platelets with negative magnetocrystalline anisotropy have been reported by De Blois (1965 and 1968a). Several types of stripe pattern have been observed, varying with the thickness and composition of the platelets. The minimum anisotropy <111> axes point out of the plane of the platelets at 35.3° and the magnetisation turns towards these directions when the anisotropy energy is sufficiently lowered at the expense of the

exchange and magnetostatic energies. The <111> directions lie in the {110} and {112} planes, there being a set of six of the former and four of the latter. With the exception of the 109° rotations in the {110} planes, rotation from one <111> direction to another involves only a small anisotropy barrier, thus leading to the multiplicity of possible stripe structures. These are described in section 6.2.1 below.

6.2.1 Platelet Stripe Structures

Type I stripe domains have been found in platelets which exhibit pseudo-positive anisotropy, that is platelets with compositions of low, but nevertheless still negative magnetocrystalline anisotropy which show structures normally associated with platelets of positive anisotropy. In the thicker platelets the 180° domain walls lie along the <100> direction and the 90° walls along the <110> directions with the Bitter patterns from the stripes lying parallel with the hard <100> directions. This configuration can easily be explained by analogy with the stripe domains in iron foils, see section 6.1.3, and reference to FIG.(6.5).

If the stripes are assumed to slant through the platelet in {110} planes then the magnetisation in a given domain can oscillate on a 109° arc between two <111> directions, but giving a net component in a <100> direction. Thus if the surface Bitter pattern shows a net [100] magnetisation, the magnetisation in one stripe might lie in a $(0\bar{1}1)$ plane having a [111] direction and in the adjacent stripes would lie in parallel $(0\bar{1}1)$ planes but oriented towards the $[1\bar{1}\bar{1}]$ direction. It is unlikely that the magnetisation actually rotates as far as the <111> direction in any of the stripes because the surface pole fields would reduce this angle, in the manner of a μ^* correction.

This structure, although hypothesised from colloid work has been confirmed by x-ray diffraction topography.

Type II stripes are seen as striations in the colloid which they

do not gather nearly as readily as the other types of stripe domains. They have often been seen in platelets together with Type III stripes, see for example FIGS.(6.8 & 9). The structure is thought to be similar to that of the Saito stripes with the net magnetisation oriented in a <110> direction with an oscillation of the magnetisation vector on a 71° arc in the (110) plane towards the [111] and [11$\bar{1}$] directions. The structure of the Type II stripes is probably modified in the same way that Murayama's treatment, see FIG.(6.2), modified the Saito stripe structure. Thus the stripes essentially consisted of a set of Bloch lines running through the platelet in the <110> direction with the surface magnetisation acting as a closure structure. The internal flux closure produced by this arrangement is high and accounts for the poor colloid collection.

Type III stripes collect colloid far more strongly than Type II yet fit with little disturbance into the <110> closure structures familiar from Chapter 5. The boundary between Type III and Type II stripe domains in zero field has been found to lie approximately along <100> directions indicating the normal component of magnetisation across the boundary to be constant. The stripes themselves lie almost, but not exactly, parallel with a [100] direction despite the fact that the magnetisation vector oscillates in a (110) plane towards [111] and [11$\bar{1}$] directions.

De Blois (1968a) noticed a small change in the magnitude of the net magnetisation associated with the structural change between Type II and Type III stripes. A compatible structure could be constructed, however, by assuming (a) the normal component of magnetisation to remain constant across the boundary between the two types, (b) the magnitude of the net magnetisation in the Type III stripes to be a little smaller than in Type II, and (c) a slight divergence of the magnetisation to occur near the boundary in Type II stripes to lower the normal component across the walls. Type III stripes tend to form parallel with an edge, or step in an echelon structure, leading to a

smaller divergence of the magnetisation than if Type II stripes were to gradually change direction in these same regions.

Type IV stripes are not uniform through the thickness of the platelet and are confined to the thicker specimen. The structure is thought by De Blois (1968a) to consist of helical rotations of the magnetisation vector through 71°, parallel to a $\{110\}$ plane, from one $\langle 111 \rangle$ direction to another. If, for example, the net magnetisation is along the [110] direction then the magnetisation vector in one stripe can be taken as rotating clockwise in a $(\bar{1}01)$ plane from the $[111]$ direction at the top to the $[1\bar{1}1]$ direction at the bottom. The magnetisation vectors in the neighbouring stripes on both sides then point towards the $[\bar{1}1\bar{1}]$ direction at the top and rotate clockwise in a (011) plane to point towards the $[11\bar{1}]$ direction at the bottom.

These changes in orientation from the top to the bottom surfaces of the platelet can be visualised with the help of FIG.(6.6a). The magnetisation in a given stripe rotates from the direction T1 at the top to B1 at the bottom of the stripe. In the neighbouring stripes on either side the magnetisation at the top points in the direction T2 and rotates in a different (110) plane to B2 at the bottom. The stripe domain walls lie in the (110) plane containing T1 and B2.

The resulting stripe domain pattern at the top and bottom of the crystal as seen from above is shown in FIG.(6.6b). This structure, like those of Murayama and Krinchik provides an increased degree of local flux closure.

De Blois (1968a) has reported a few observations made on the behaviour of these stripes under in-plane magnetic fields. The effect of the field on the stripe pattern was found to be directionally dependent. In some directions alternate stripes became very faint or even disappeared, thus effectively doubling the spacing without altering the stripe structure, and in other directions the brightness remained unchanged but the stripes became asymmetrically spaced.

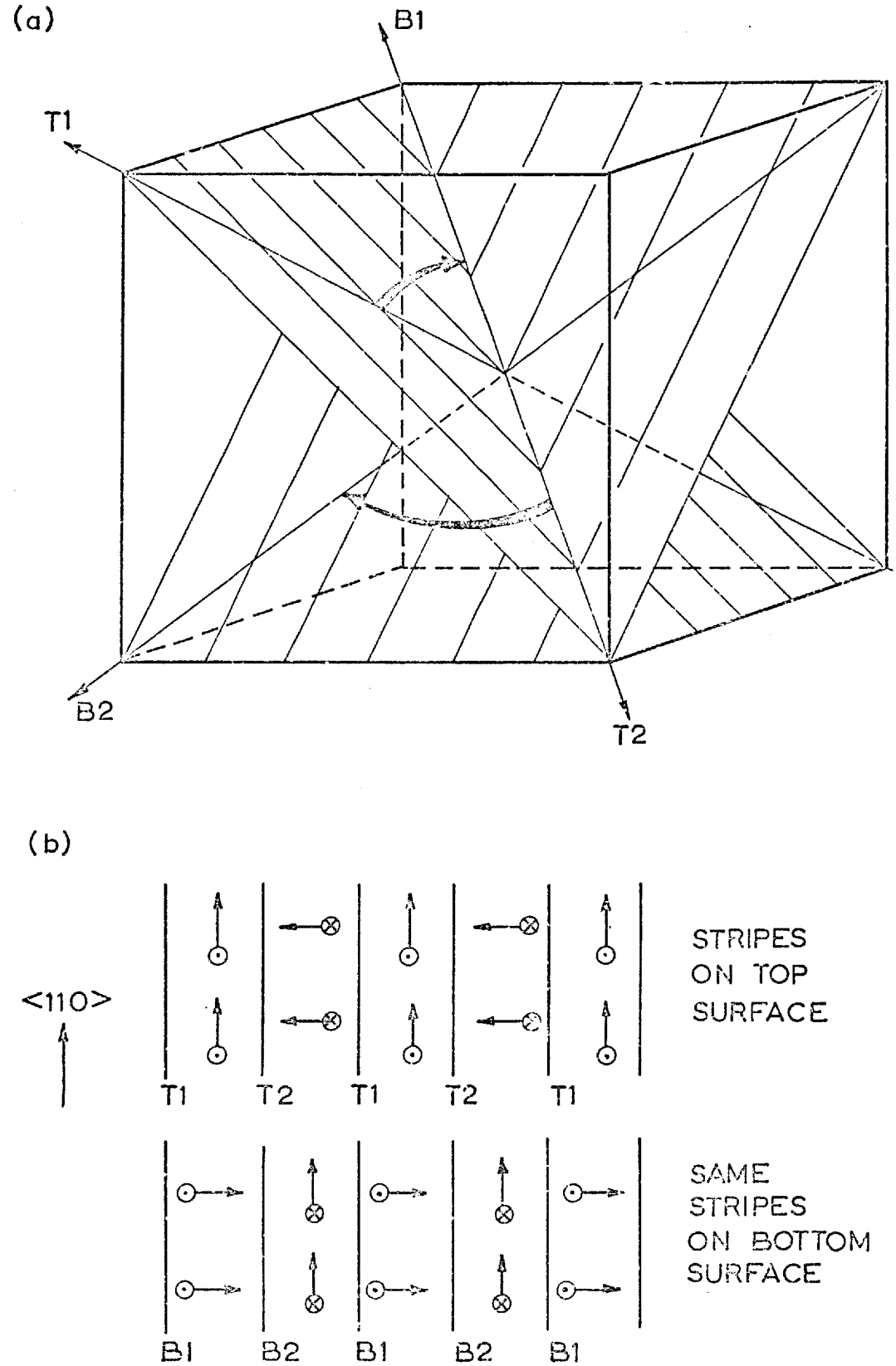

Fig. (6.6) Stripe domains type IV (after De Blois)

The 180° wall in Type IV stripes has been explained as a rotation of the in-plane component of the magnetisation through 180° (over a distance where a 90° rotation normally occurs) with the vertical component reversing sign in the normal way, as seen in FIG.(6.7).

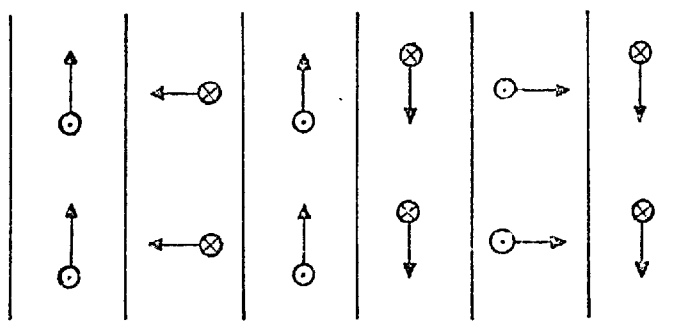

FIG.(6.7) 180° WALL IN STRIPE IV DOMAINS

The presence of a 180° wall cannot therefore of itself be detected, with a colloid technique, by its increased local field.

No calculations have yet been made either to determine theoretically the equilibrium stripe spacing or to give any indication of the critical thickness at which these stripes form.

Type V stripes (not classified by De Blois) have only been seen in the small triangular edge closure domains of platelets. The structure of these is thought to resemble the strong stripe domains observed by Ferrier and Pulchalska (1968). In both cases it will be noticed that the out of plane anisotropy is not normal to the plane, but for different reasons. In films a uniaxial anisotropy arises from the oblique incidence evaporation, but in platelets the origin is crystallographic. This helical rotation of the magnetisation allows a region of flux closure with net magnetisation parallel with the edge to still exist and to form a stripe pattern in thicker platelets.

The possibilities offered by these five stripe models must be considered in the sections following, describing observations made on several platelets.

6.2.2 Observations on Mixed Stripe Structures

The coexistence of several stripe structures is seen in FIG.(6.8b) on a (100) plane of a nickel crystal with <100> edges. The thickness of this platelet is not known exactly, however from the Lorentz investigations it would seem to be less than 4000 Å. This particular platelet had a shape similar to those previously seen in FIG.(3.5c), but this is of no importance in considering the fine magnetic structure.

The structure of the main domains seen in FIG.(6.8b) formed a familiar closure pattern, but the striated colloid collections within these domains suggested the existence of a weak type II stripe structure. This was further confirmed by Lorentz microscopy. FIG.(6.8a)*, a Lorentz micrograph taken in the Fresnel mode at 500 kV, shows a 180° wall near the centre of the platelet with the fine oscillation from the stripes on either side. The stray field from these oscillations is too weak to gather significant amounts of colloid, and although the magnification of FIG.(6.8a) is not known the stripe spacing is thought to be less than 5000 Å.

Small echelon structures only exist near the corners of the platelet and are formed with a separate type of stripe domain, most readily visible in the right hand corner. The small size of these domains complicates their stripe pattern but one of a type III structure would seem the most likely. Triangular closure domains along the top edge show a type V structure, which will be mentioned again later.

The effect of an easy axis applied field on this platelet is seen in FIG.(6.9). During this series of photographs the platelet was free to rotate in the colloid so that the field was known to be

---

*FIG.(6.8a) was obtained by Dr. I.E. Pulchalska using the high voltage microscope of the Cavendish Laboratory, Cambridge.

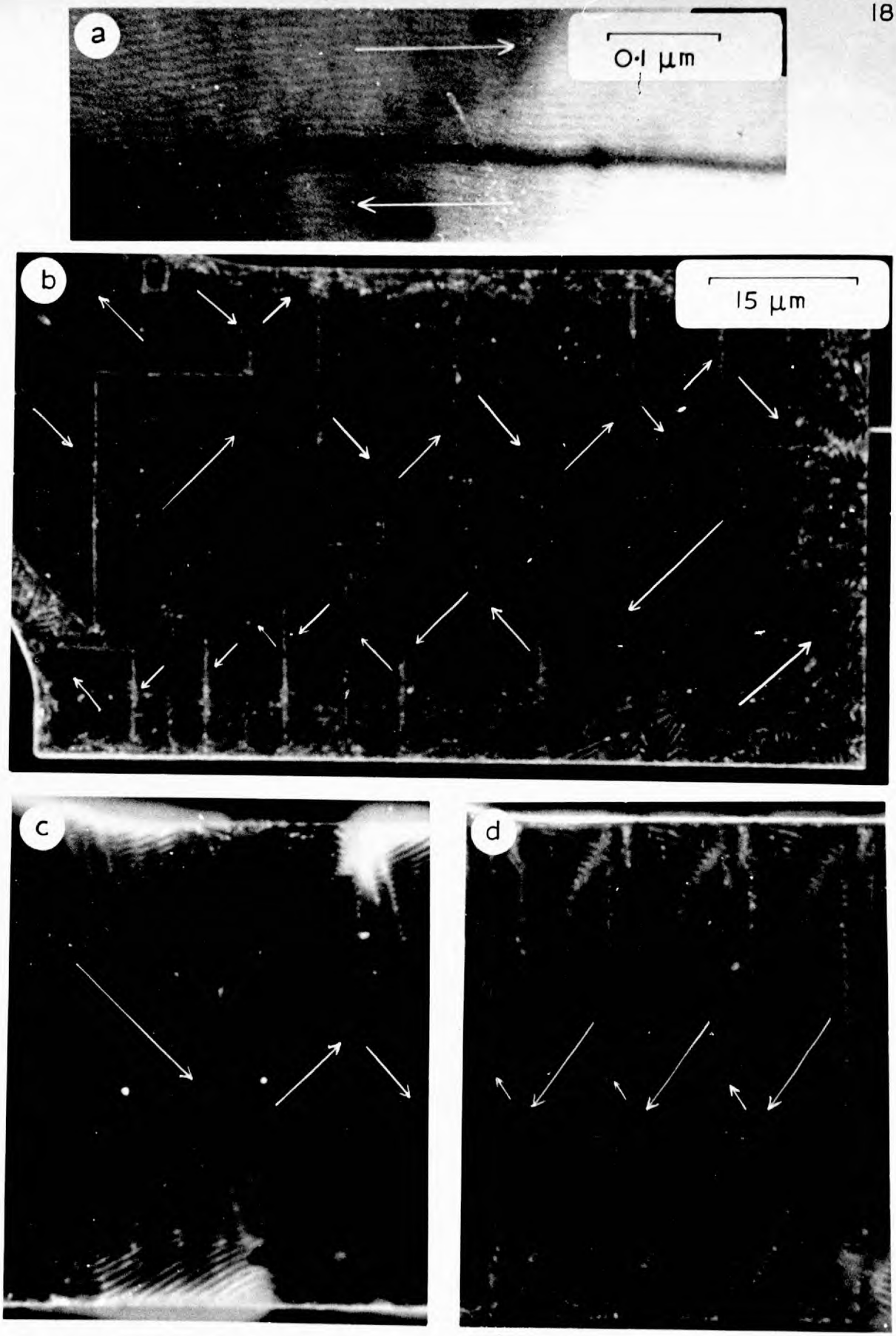

Fig. (6.8) Mixed stripe structures

applied exactly along the easy axis and strain was unlikely to have affected the domain pattern. A frequently observed feature of platelets with stripe domains was the poor definition of the zero field structures, which is why the photograph preceding FIG.(6.9a) was omitted.

This photograph, FIG.(6.9a), shows the pattern in a field of 27 oe where 90° walls were seen to stretch across the width of the crystal as the magnetisation 'zig-zagged' along its length. Weak type II stripes were clearly visible but did not show a uniform direction in any domain. Instead they showed a waving variation within the domain and a general rotation away from the field direction. At the edges of the domains with magnetisation lying in the field direction sudden changes occurred to a stronger stripe structure, which made an angle of between 15° and 20° with the platelet edge and which, judging by the colloid collection, had a large stray field.

It is possible that these edge areas were formed by type III stripes. (The boundary conditions between type II and type III were discussed in section 6.2.1). It is further possible that the type III structures formed because no closure structures (familiar in thinner platelets) existed at the edge, and the edge stray field from the type III stripes was lower than from the type II. Then in order to maintain a constant normal component of magnetisation across the boundary between the two stripe regions, a torque was exerted on the type II stripes causing them to deviate and the boundary to adjust and adopt an equilibrium angle. This angle was not necessarily constant because of the changing effective magnetic field in the proximity of the edge.

The effect of progressive increases in the magnetic field are seen in FIG.(6.9b) at 60 oe, (c) at 83 oe and (d) at 107 oe. In (b) most of the 90° walls had shrunk to spike domains although faint colloid collections could still be seen across the platelet in four

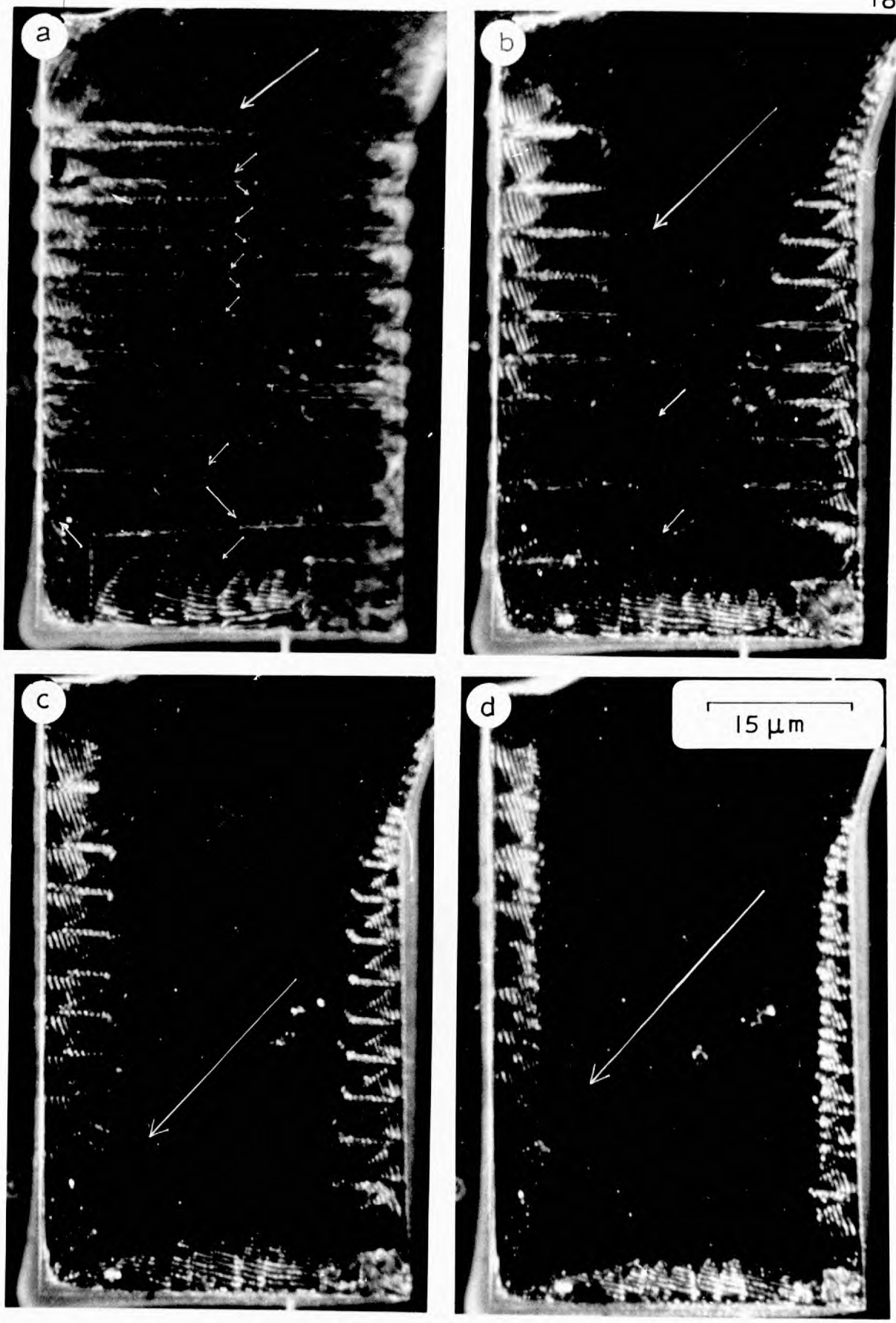

Fig. (6.9) Application of easy axis field

places, indicating the remains of possible double walls. The striations from the type II stripes decreased, and with the decrease in the 90° walls also rotated back to a more normal angle of about 45° with the <100> edges. The volume of the type III stripes increased along all the edges, where they formed a very regular pattern. The spike domains themselves were narrow (~2 μm wide) and showed a similar periodic spacing, in the colloid collection along their walls, to the stripes. In FIG.(6.9c & d) the spikes shrank back and merged with the strong stripe domains.

During these processes it is interesting to note how the colloid distribution along the edge of the platelet became more uniform with increasing field, as the edge became entirely flanked by the type III stripes. With increasing field gaps also appeared in the colloid stripe formation. In some circumstances this might have been attributed to a lack of colloid particles, but this does not apply here and suggests that the magnetisation was lying in the plane of the platelet with a certain amount of curling occurring near the edge. It is possible that the platelet was of such a thickness that the stripe domains were only just stable, and their very presence was influenced by the local magnetic field conditions.

Two further interesting observations are seen in FIG.(6.8c & d). Part of the platelet is shown in (c) in a decreasing field of 27 oe, i.e. a similar field to that of FIG.(6.9a). The tips of the type III stripe regions stretched right out into the type II regions and very large colloid clouds gathered where these same fields ended at the edges. Finally, FIG.(6.8d) shows the effect of a 61 oe field across the opposite diagonal of the platelet. The 90° walls stretched across the platelet and a fascinating boundary shape formed between the two types of stripes.

The shape of this boundary between the type II and type III stripe regions may be influenced by restrictions on the free movement of the domains along the edge itself. It can be seen that the 90°

walls did not always make direct intersections with the edge and small spike domains may have existed, thus distorting the local field. If, as suggested above, the transition between the stripe types is affected by the local field, then the presence of the spikes may, by distorting the field, have given the stripe boundary this shape.

6.2.3 Stripe Behaviour in Magnetic Fields

Observations have been made on several Ni crystals with thicknesses in the region of 6,000 Å whose stripe domains have shown similar behaviour. One of these, a kite-shaped platelet with rectangular dimensions 98x90x0.64 μm. is discussed in detail. The virgin structure of this platelet is seen in FIG.(6.10a) and a demagnetised pattern at higher magnification in FIG.(6.10b).

Careful inspection of FIG.(6.10a) enabled overall magnetisation directions to be ascribed to the domains by analogy with the closure structures familiar from thinner platelets. The presence of 180° walls was often marked by a line of colloid separated from the stripe pattern, this can be seen clearly in FIG.(6.10b), but the 90° walls were not always so apparent.

If the magnetisation directions have been ascribed from the overall flux closure pattern in the platelet, as has been done here, the relationship between the stripes and the magnetisation directions in the main domains is established. Each of the main domains consisted of several stripe regions where the stripes made an angle of 80° with the net magnetisation and 8° with the nearest [100] direction. The stripe spacing remained very uniform with a 0.8-0.9 μm. separation. The effect of applying magnetic fields, see below, showed the magnetisation direction not to be constant in a given domain but to vary slightly (as shown by the dashed arrow in FIG.(6.10b)) creating a low angle wall between the various stripe regions in one domain. It is seen, therefore, that the magnetisation distribution over most of the platelet can be explained by a structure based on the type III stripe

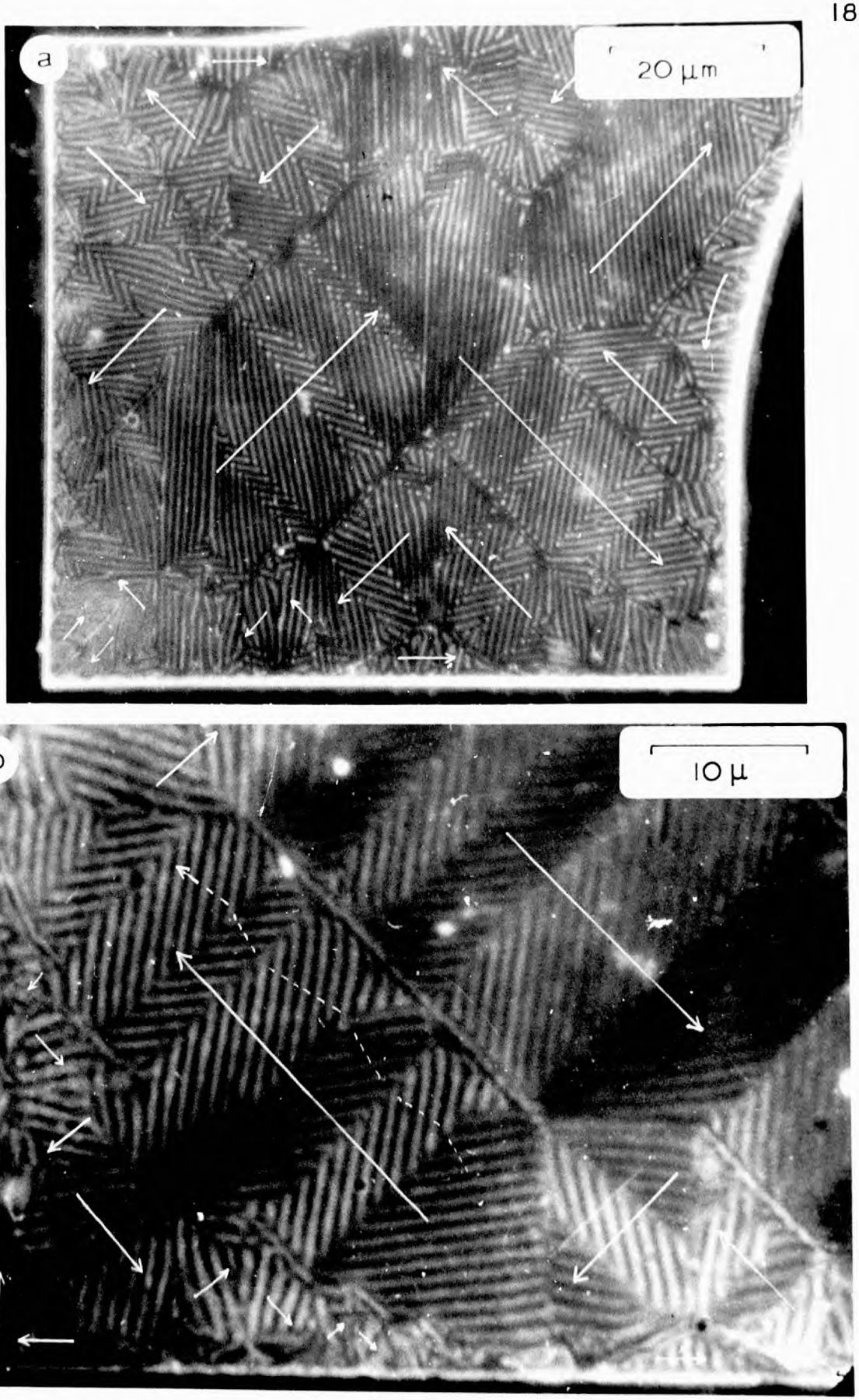

Fig. (6.10) Platelet showing Type III stripe domains

domains.

Where the magnetisation changed fairly rapidly over small areas, near the edges of the platelet, the stripe pattern was more complex. This can be seen along the bottom edge and the left-hand corner of FIG.(6.10b). At the base of some of the echelon structures small triangular regions were visible in which the magnetisation lay parallel with the edge of the platelet. The stripes, however, were normal to the platelet edge, which could only be explained satisfactorily if they were assumed to be type V.

(a) Easy Axis Fields

The effect of an easy [110] axis field is seen in FIG.(6.11), with the initial zero field structure after demagnetisation shown in FIG.(6.11a). The main domains stretched across the platelet, but these were normal to the easy axis along which the platelet had been demagnetised. On several occasions when this was repeated the same structure formed, indicating its particular stability in this crystal. The dark field illumination was slightly off-set in this picture to increase the contrast and emphasise the presence of similarly oriented stripe regions.

With the applied field directed towards the bottom left-hand corner only small areas of the platelet had favourably oriented initial magnetisation directions (notice especially the echelon structures on the upper left-hand side and the lower right-hand side). These areas became enlarged at 8 oe, FIG.(6.11b) while areas with reverse magnetisation shrank and the remaining areas with neutral magnetisation directions adjusted to accommodate these changes. This process is seen in a more advanced stage at 16.5 oe in FIG.(6.11c).

The two stripe orientations in the main transverse easy axis domains did not behave equivalently under the magnetic field, but one orientation grew at the expense of the other, indicating a slightly off-set orientation of the net magnetisation within each stripe

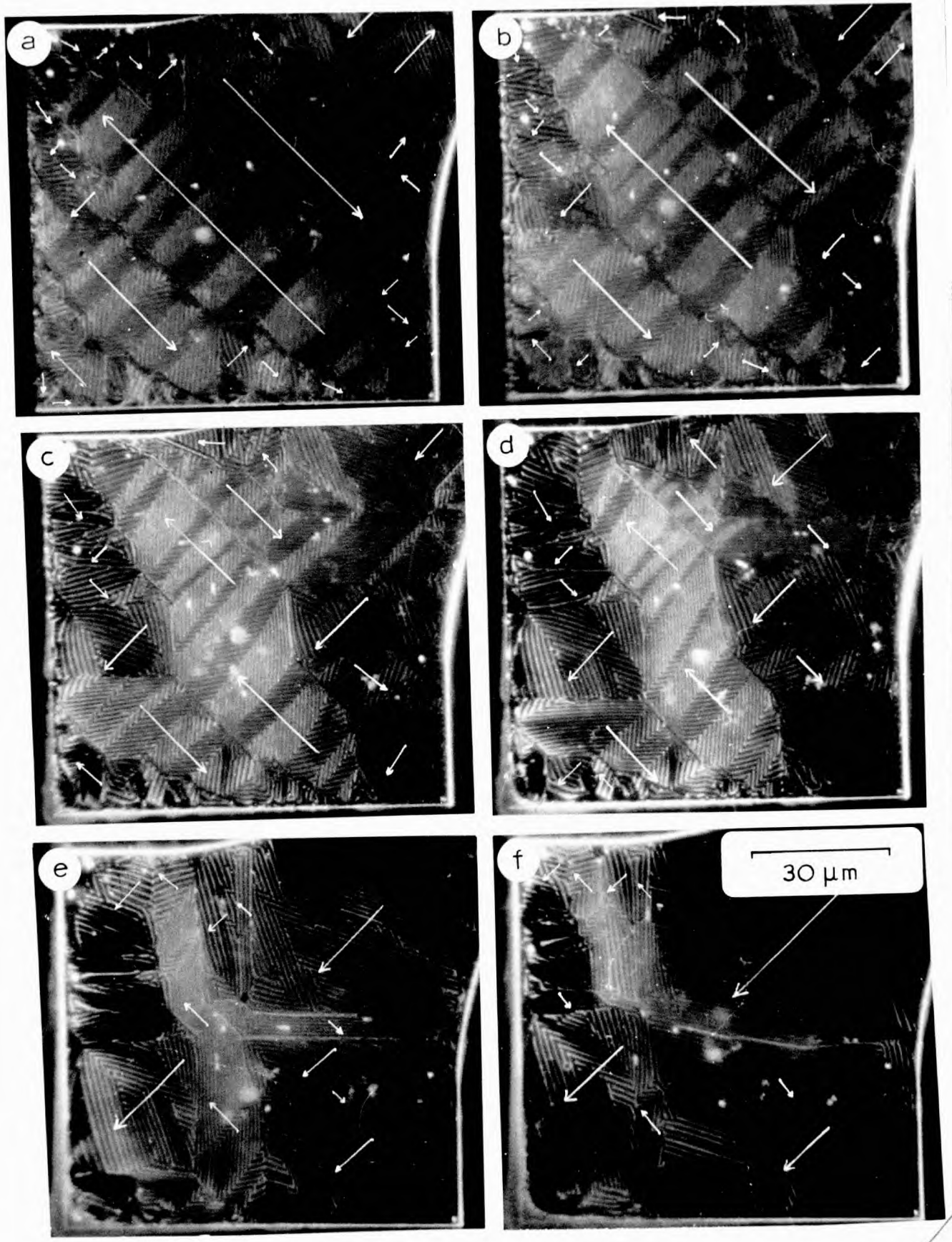

Fig. (6.11) Application of easy axis field

sector, see FIG.(6.12).

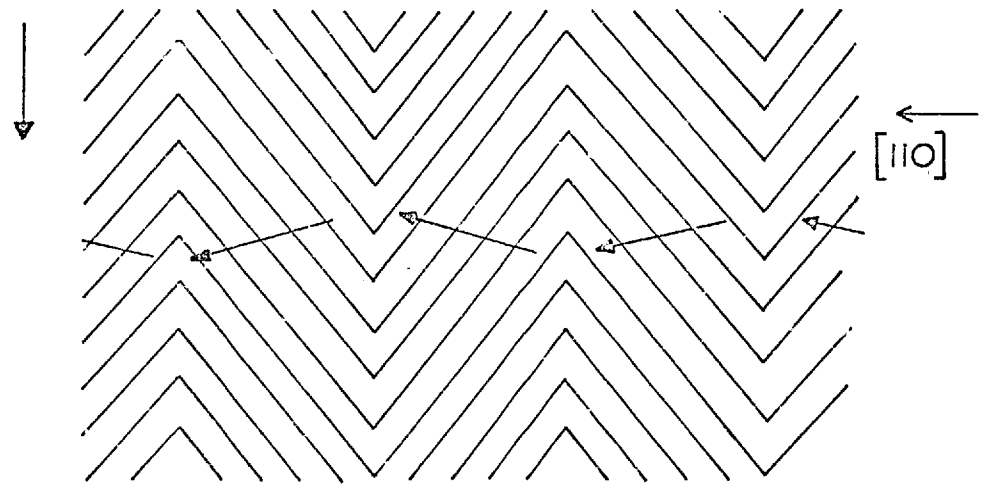

FIG.(6.12) SUBDIVISION OF DOMAINS WITH TYPE III STRIPES

The 90° rotations which subdivided the closure echelons were not visible as distinct walls even in zero field. As the field increased the division became even more complicated and the echelons on both the left-hand and right-hand sides of FIG.(6.11c) showed a complex stripe pattern with the stripes bending through angles of up to 20°, and even subdividing. The net result of this was to increase the magnetisation volume favourably oriented towards the field direction.

A further three photographs were taken at 26 oe, FIG.(6.11d), 41.5 oe, (e), and 59 oe, (f), and show a continuation of the above process. In (e) it was still just possible to correlate various regions of the platelet to determine how the existing structure had been reached, but in (f) this was no longer the case. At higher fields the stripe formation seen in the top right-hand corner of (f) formed across the entire platelet.

The behaviour in higher fields is seen more clearly in FIG.(6.13) which shows two pictures taken from a set on a separate but almost identical platelet, at 44 oe, (a), and 55 oe, (b) Long sweeping

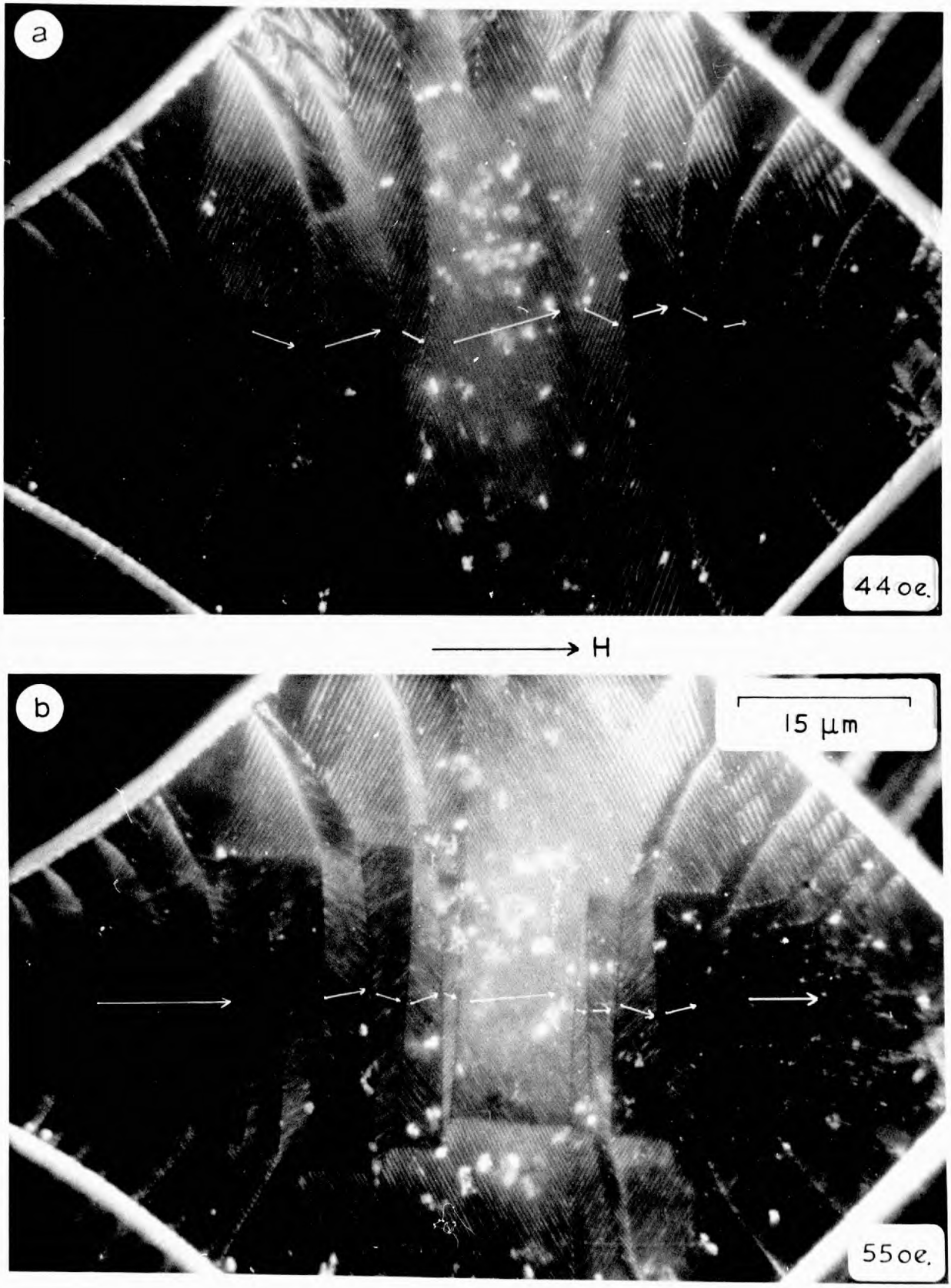

Fig. (6.13) Type III stripes in higher easy axis fields

stripe areas crossed the platelet, FIG.(6.13a), and the angle between stripes in adjacent sections decreased to about 65°. The stripe width varied from about 0.9 μm. in the centre of the platelet to 1.3 μm. at the edges. It would appear that the decreased angle made with the field direction was unstable, and with a further increase in field, a slight rearrangement occurred to give low angle stripe boundaries of up to 20°, see FIG.(6.13b).

The stripes finally just faded away at higher fields. The beginning of this can be seen on both the left-hand and right-hand sides of this photograph. At higher fields the size of the stripe-less area slowly increased until only small edge stripes remained. Visual observations could only be made to 160 oe. where some stripes still remained. It is interesting to note that thinner platelets showed no evidence of domain structure in comparable easy axis fields although reverse nuclei probably still existed, as has already been discussed. To check whether these were freak conditions the platelet was removed and inserted in a 10 k oe field, subsequent observation showed the stripes to have returned and their behaviour to remain unaltered.

(b) Hard Axis Fields

Starting from a magnetic structure identical with that of FIG.(6.11a) the effect of a hard [100] axis field was investigated on the same platelet. The observed movement of the stripe domains is seen in FIG.(6.14) in a field of 16 oe, (a), 31 oe, (b), 49 oe, (c), 65 oe, (d), 85 oe, (e), and 120 oe, (f). The field was applied in a direction from the top to the bottom in these photographs.

Unlike the case in the easy axis field none of the domains had its magnetisation oriented in the field direction, but the left-hand and right-hand structures both showed favourable orientations and expanded. The beginnings of this at 16 oe can be seen in FIG.(6.14a). On the left-hand side a triangular closure domain with type V stripes

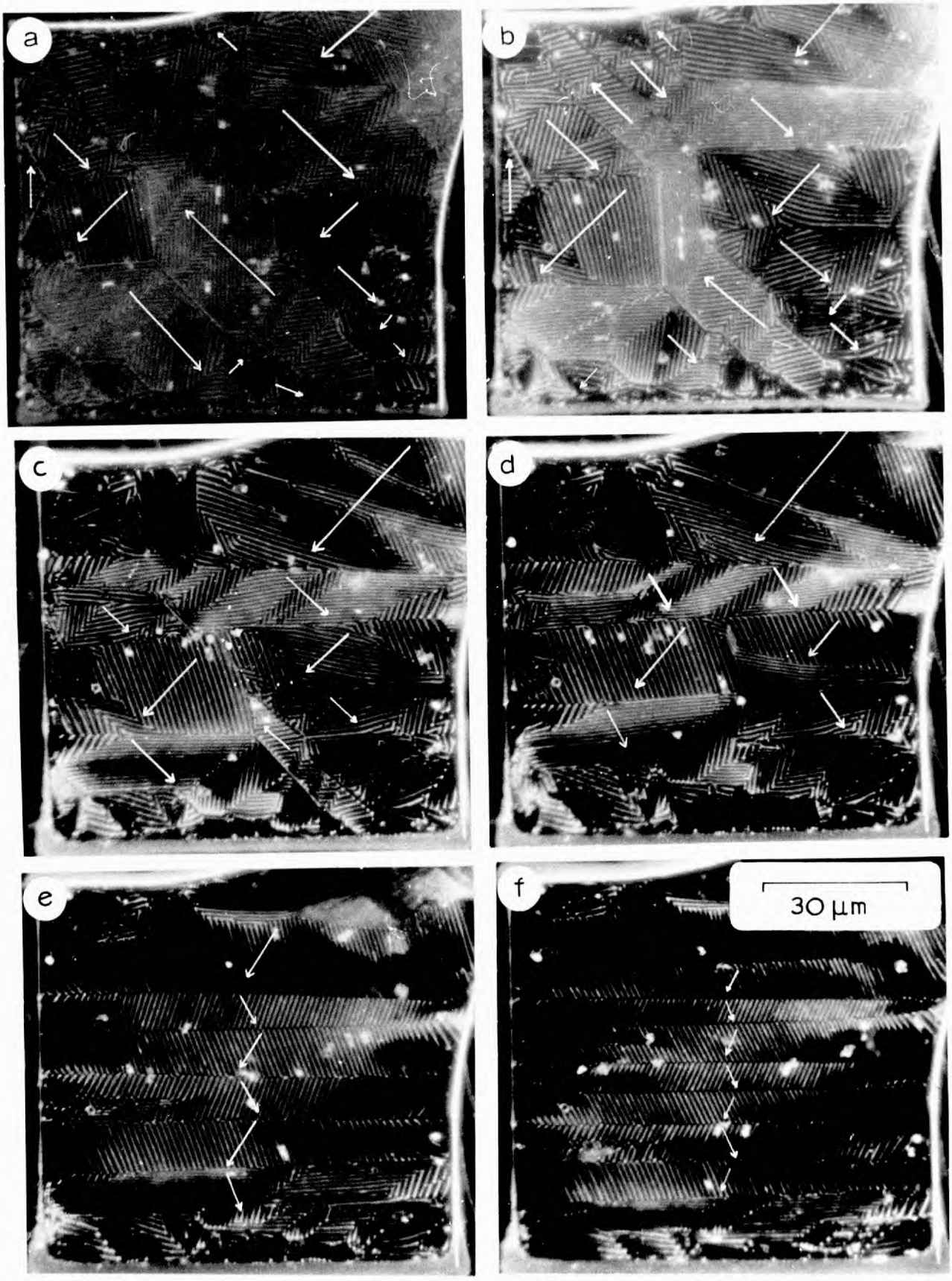

Fig. (6.14) Application of hard axis field

can be clearly seen, but with reversed magnetisation it shrank in higher fields.

The two main domains of the opposite echelons displaced the stripe domains existing in the centre of the platelet and met under an applied field of 49 oe, FIG.(6.14c). Smaller regions in (b) with stripes in the appropriate orientation also expanded at the expense of the horizontal stripes. This process continued and is seen at 65 oe, (d), and 85 oe, (e), where a very regular stripe structure covered the centre of the platelet. The behaviour of the bottom of the platelet is too complex to interpret, and with the minima in the anisotropy, the magnetic field and the magnetostatic energies all oriented in different directions, this is hardly surprising. Finally, (f) at 120 oe shows a further division of the stripes at higher fields.

The angle that these stripes made with the applied field direction as a function of that field is shown in FIG.(6.15). In the low fields this angle was taken from the stripes in the main domain of the left-hand echelon structure. The angle that the stripes made with the field would seem from these results to have increased linearly with field. An error of $\pm 2^{\circ}$ is shown in FIG.(6.15), being representative of the accuracy in setting the protractor used to measure the stripe angle. In addition to this it will be noticed that a slight angular variation also occurs along the length of the stripes in a given area, presumably in response to changing values of the local field.

Three photographs were taken in decreasing field immediately afterwards, and the stripe angles from these are also shown in FIG.(6.15). The fact that these lie on a lower curve can be tentatively explained by the sequence of measurement. The angles taken from FIG.(6.14) in increasing field were measured on a specimen that had just been demagnetised along a [110] direction, whereas those in decreasing field were from a specimen that had been saturated

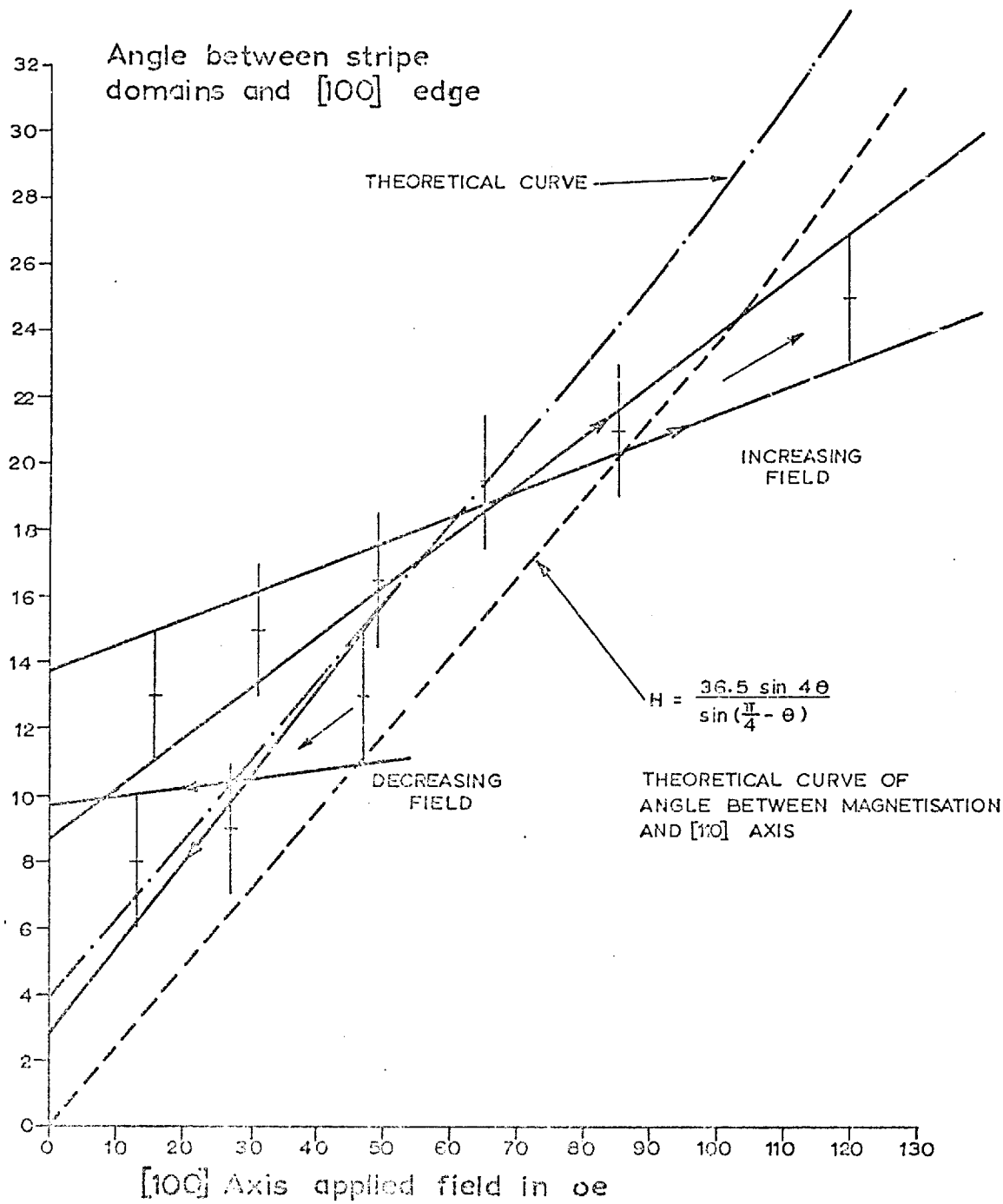

Fig (6.15) Stripe angle as function of hard axis field.

in a [100] direction. It is thus possible that the surrounding areas, having different magnetisation arrangements, had produced different local torques on the magnetisation in either case.

A basis for an explanation of the increase in the angle between the stripes and the [100] direction has been advanced by Leaver (1969). He considered the rotation of the magnetisation from the <111> directions by a field applied in the [100] direction, but at the same time constrained the magnetisation to maintain a constant angle ϕ with the [001] direction. He equated the field torque on the magnetisation with the rate of change of the anisotropy energy due to the angular rotation (see Appendix 'D') and found that the field excitation could be expressed by the equation

$$H = \frac{36.5 \sin 4\theta}{\sin (\frac{\pi}{4} - \theta)} \qquad (D.4)$$

where θ is the angle between the planar component of the magnetisation and the [110] direction.

This function is also plotted in FIG.(6.15) and is seen to be almost linear. The structures seen on this platelet have also been seen on much thicker platelets (see section 6.2.4) where the anisotropy is more important than the magnetostatic energy, which suggests that in zero field the magnetisation is already oscillating between <111> directions. Thus if the stripe structure itself tends to maintain the magnetisation angle ϕ with the [001] direction, the application of a field causes rotation of the stripe pattern as the magnetisation structure rotates towards the (100) plane in the field direction, pulling the stripes towards the [110] direction.

The theoretical values of H in FIG.(6.15) would be depressed slightly when the demagnetising field is considered, thus bringing the gradient into better agreement with the observed values. This field varies according to the position in the platelet of the region where the behaviour of the stripes is being studied.

A similar expression to equation D.4 can also be derived for the application of an easy axis field normal to the initial magnetisation direction. However, it is apparent from FIG.(6.11) that in this case the greater part of the magnetisation re-alignment is achieved by domain wall motion rather than by rotation.

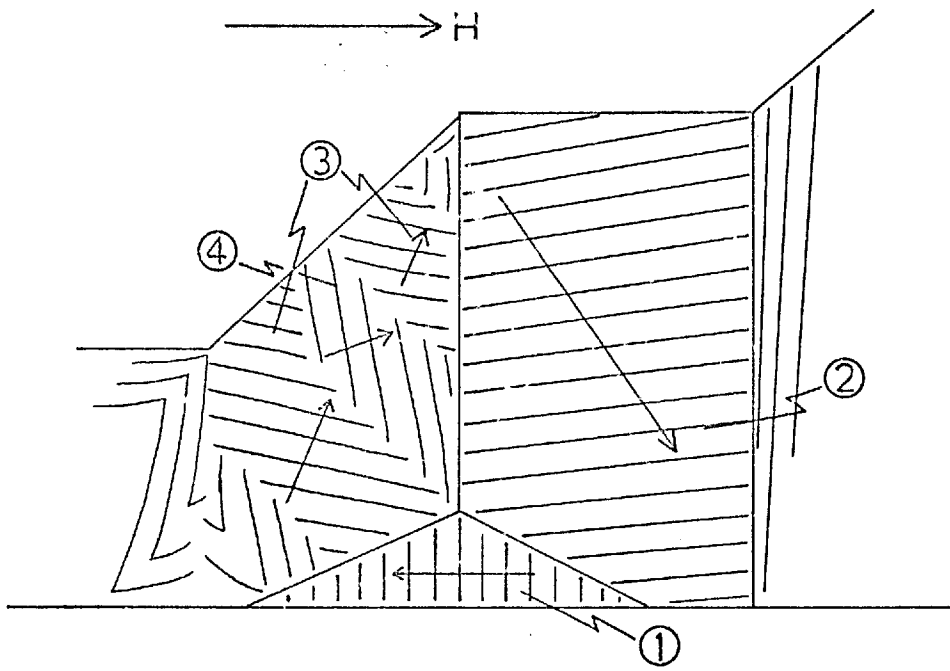

FIG.(6.16) ECHELON STRUCTURE IN STRIPE DOMAINS

Evidence from the application of an easy axis field, FIG.(6.11), has already suggested that the magnetisation in the various stripe regions within one domain is offset from the [110] direction. This was shown diagrammatically in FIG.(6.12). Further evidence for this is seen in FIG.(6.16) which is a representation of part of the left-hand side of FIG.(6.14a). In this diagram the triangular reverse closure domain (1) is thought, as in the thinner platelets, to have its net magnetisation lying parallel with the edge and must therefore have a type V stripe structure. The domain walls bounding this region will bisect the magnetisation directions on either side if no charges are formed along them and the planar components of magneti-

sation in each domain are equal. This therefore fixes the magnetisation directions in the type III stripe regions. Thus, a relationship between the magnetisation and stripes is established, and is seen in FIG.(6.16) to agree with the previous suggestion, shown in FIG.(6.12).

The magnetisation in region (2) of FIG.(6.16) makes an angle of 5° with the [110] direction and 60° with the stripes in that section. Thus, to get a true comparison between the theoretical and experimental curves in FIG.(6.15) for this particular region a -5° correction should be applied to the theoretical curve. Remembering that in this region the magnetisation makes a 60° angle with the stripes, the theoretical curve can be converted to represent the angle between the stripes and the field. This would then predict an angle of $+10^{\circ}$ for the zero field angle with the same slope as the curve representing equation D.4. Displacing the curve by $+4^{\circ}$, as shown in FIG.(6.15), brings it into better agreement with the range of experimental points, however the slope remains in error. This suggests that the magnetisation and the stripe pattern may not be as rigidly coupled as has been implied, and relative rotation may occur with the magnetisation turning away from the <111> directions and into the plane of the platelet.

Alternatively, it must be remembered that the rotational theory in Appendix 'D' has assumed that the entire magnetisation lies in the <111> direction, whereas in any real stripe structure other magnetisation directions are also present. If the effect of a complete distribution rotating were considered, the equilibrium between the torque and rate of change of anisotropy energy might not be the same. This would lead to a different dependence of the stripe angle on the applied field than given by equation (D.4) and might be in better agreement with the experimental results.

Region (3) in FIG.(6.16) is equivalent to region (2) and behaves in the same manner, but the magnetisation in region (4)

points 10° nearer to the field direction than in regions (2) or (3). With the increase in field the stripes in this region rotated until they lay normal to the field direction, see FIG.(6.14d). The stripe spacing had decreased and the magnetisation probably made an angle of 25° with the field direction. Further rotation of region (4) appeared blocked by the nature of the structure and the type (2) and (3) regions continued to grow at its expense, until only they existed. A change in the stripe spacing of the type (4) regions in FIG.(6.16) was also observed and may have occurred through a magnetisation rotation away from the <111> directions. The effect of the blocking of the stripe rotation and the change in spacing precludes the application of the above theory to these type (4) regions. Further details of this blocking are described in section 6.2.5.

6.2.4 Stripe Domains in Very Thick Platelets

Observations have also been made of stripe domains in platelets more than an order of magnitude thicker than those discussed in section 6.2.3. Two photographs of the virgin stripe structures in a triangular platelet, which was approximately 9 μm. thick but not of constant thickness, are seen in FIG.(6.17). The first (a) shows what is clearly an echelon structure on a [100] edge of the platelet, and the second (b) shows an enlarged view of a central domain area, with a similar structure to the area at the top right-hand corner of (a).

The central structure (b) shows what must have been two 180° walls extending vertically across the field of view, although there was effectively no colloid collection along them but a very precisely defined gap in the stripe pattern. Small triangular closure domains with an absence of stripe domains were visible on either side of these walls, although detailed examination of the original negative showed these to be smaller than the photograph suggests. Although shown clearly in FIG.(6.17b) the small triangular regions are not unique

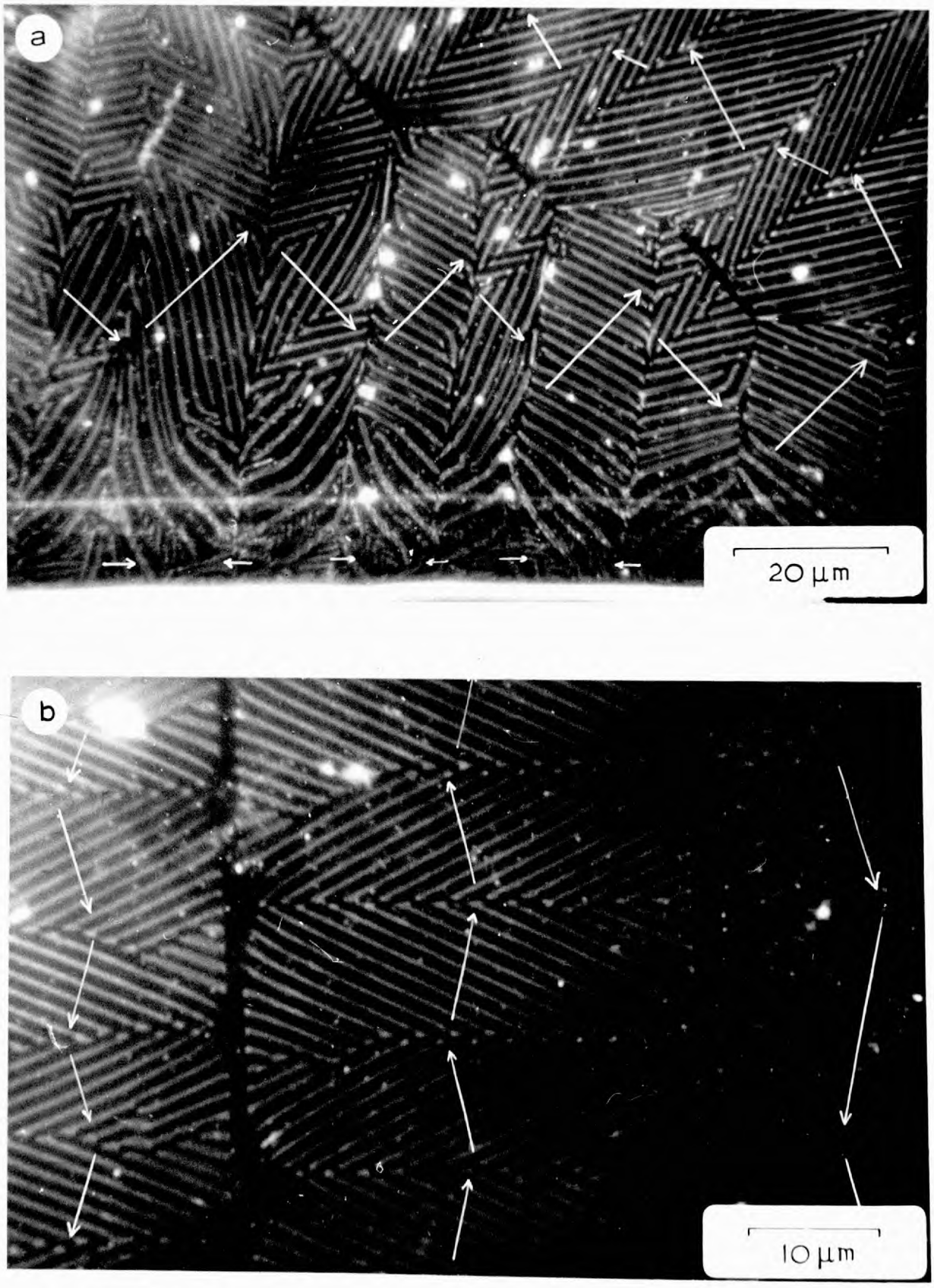

Fig. (6.17) Stripe domains in very thick platelets

to these very thick platelets and reference to the work on thinner platelets confirms their presence in platelets where the 180° walls are visible, see FIG.(6.10, 11 & 14). However, none of the observations that have been made have given any definite indications of the magnetisation directions in these very small regions. The acute angle between the stripe sections in any domain was 53° and the spacing 1.5 μm.

The stripe structure in the echelons was more complex than in the centre of the platelet, especially near the edge. Examination under an optical microscope showed that there was a thickening of the platelet along the [100] edge shown and the line across the bottom of FIG.(6.17a) was a real thickness contour on the crystal. At this edge the platelet was 9 μm. thick and decreased to 6-7 μm. in the centre. A significant increase in the stripe spacing could be seen with the appearance of a second weaker stripe between the strong stripes and near the very edge a complete set of fine stripes, showing the greatly increased width of the main stripes. Distinct closure domains were generally not visible and the complexity of the pattern was probably due in part to the increased magnetic freedom with the thicker edge, and in part to the amount of flux closure that was being achieved within the stripe patterns.

The top wall of the echelon structure in FIG.(6.17a) consisted of alternate 180° and 90° wall structures. It will be noticed that, in a similar manner to FIG.(6.17b), colloid failed to collect along the 180° boundary and the 90° wall was hardly visible except from the alternate intermeshing of the stripes. It would seem that this type of stripe pattern can accommodate a 90° magnetisation change within its structure but not the change required for a 180° wall.

The application of an easy axis field to another thick triangular platelet is seen in FIG.(6.18). The platelet measured 280 μm. along the hypotenuse and was 13 μm. thick. The four photographs were

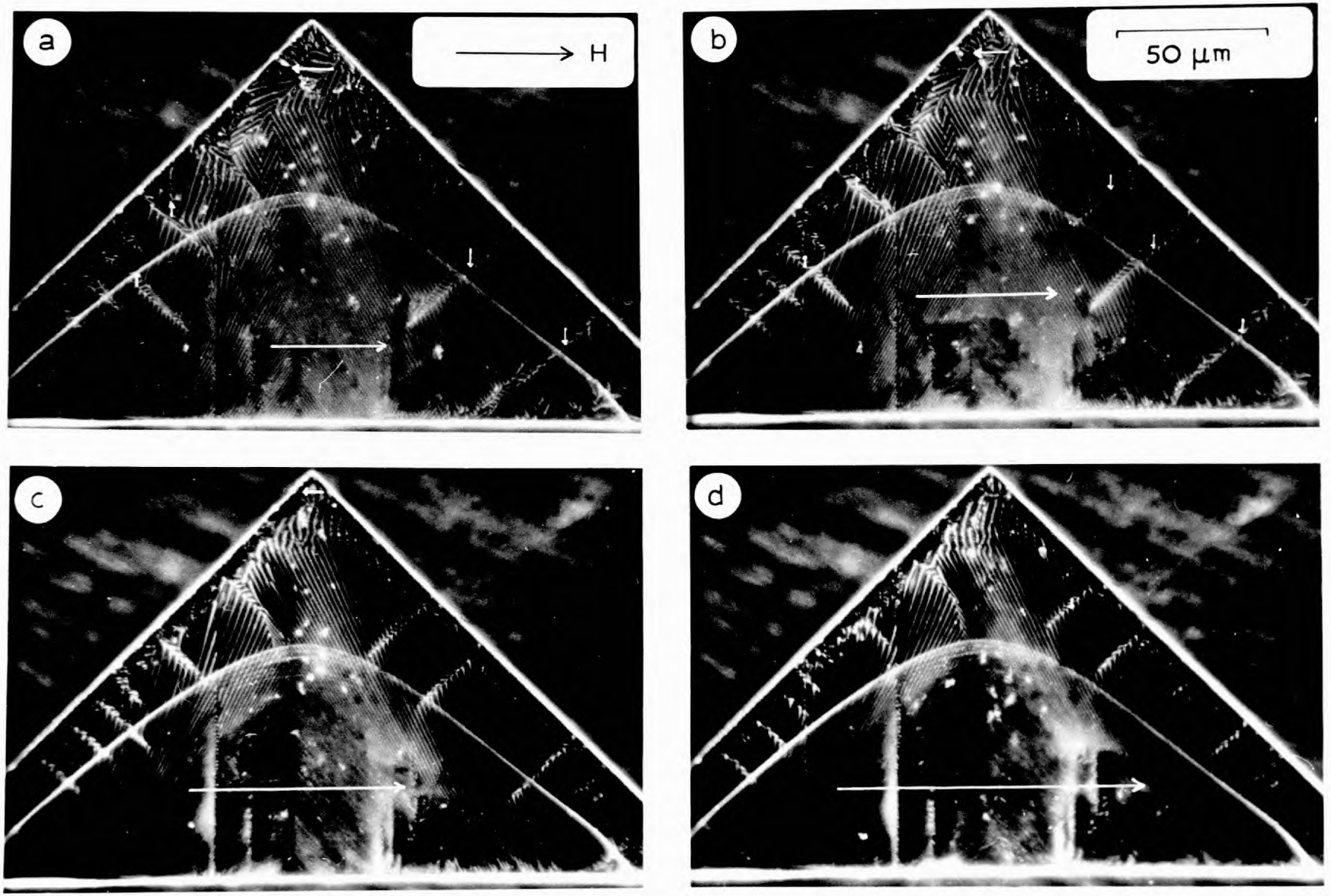

Fig. (6.18) Application of easy axis field in thick platelets

taken from a set and show the behaviour at intermediate fields 47 oe, (a), 58 oe, (b), 83 oe, (c), and 105 oe, (d).

Three features were immediately apparent. The major growth step and a series of minor ones inside it, which crossed the centre of the platelet in an arc, were at no time seen to have any effect on the behaviour of the stripes and could be ignored. Thus at these dimensions the thickness of the platelet was not critical in determining the behaviour of the stripes. Several vertical lines, parallel with the [110] direction appeared on all pictures. They appeared not to be structural, but exerted a large influence on the local stripe structure. Finally, the appearance and behaviour of spike domains forming on the [100] edges, then shrinking to disappear at higher fields, showed identical overall behaviour with that familiar from studies on thinner platelets, without stripe domains.

At 47 oe, FIG.(6.18a), two spikes had formed on the right-hand edge of the platelet and three on the left-hand side, with a fourth just emerging in the stripe pattern. The stripe angles both inside and out of these spikes fitted the now familiar type III description, but the pattern at the apex and along the top of the right-hand side showed great complexity and a wide spacing. Due to the proximity of the edge the effective field in these regions was lower but the kinks and terminations of the stripes were fascinating although unexplained. Another interesting region was the low angle stripe boundary near the centre of the hypotenuse of the platelet, formed by successive spikes terminating.

An increase in field to 58 oe, FIG.(6.18b), caused the spikes to decrease in size but increase in number, and the reverse closure complex to be pushed further towards the apex. This process was taken a stage further in a field of 83 oe, (c), with most of the platelet covered by large sweeping stripe domains. The effect of the vertical lines, mentioned earlier, showed very strongly, but the

stripes also underwent slight directional changes for no apparent reason. At occasional places across the platelet regions existed where the stripes completely disappeared, presumably because the magnetisation then lay entirely within the platelet plane. At 105 oe, FIG.(6.18d), the stripeless areas dominated the platelet but stripes still persisted at the apex. Eventually at higher fields these too should disappear. Again it will be noticed that these fields are much nigher than those required to remove domains from thin platelets.

Bearing in mind the greater thicknesses of these platelets it is perhaps rather surprising that a type III structure seems to fit their behaviour. This, however, cannot be certain because no sophisticated quantitative calculations have been performed. The possibility of structures similar or related to those discussed by Krinchik (1968), see FIG.(6.3), should not be overlooked.

6.2.5 Complexities in Stripe Structures

Detailed observations of flux reversal showed many features of stripe domains in platelets which are not understood. These are discussed in this section in conjunction with colloid pictures of stripe domains taken at higher magnification.

The domain photographs seen in FIG.(6.19) were taken from the centre of a long rectangular nickel platelet of dimensions 440 x 27.5 x 0.66 μm. The virgin pattern from a central region of this platelet can be seen in FIG.(6.19a). The magnetisation followed a zig-zag path along the [110] directions in the centre of the platelet. Reverse flux closure was achieved by triangular regions containing type V stripes, seen clearly on the left-hand edge.

Several features seen in FIG.(6.19a) are of interest. In section 6.2.4 the absence of colloid collections along the 180° domain boundaries was noted. In this photograph from a thinner platelet the termination of the stripes on either side of the wall is clearly visible, with a gap before the colloid collection along the

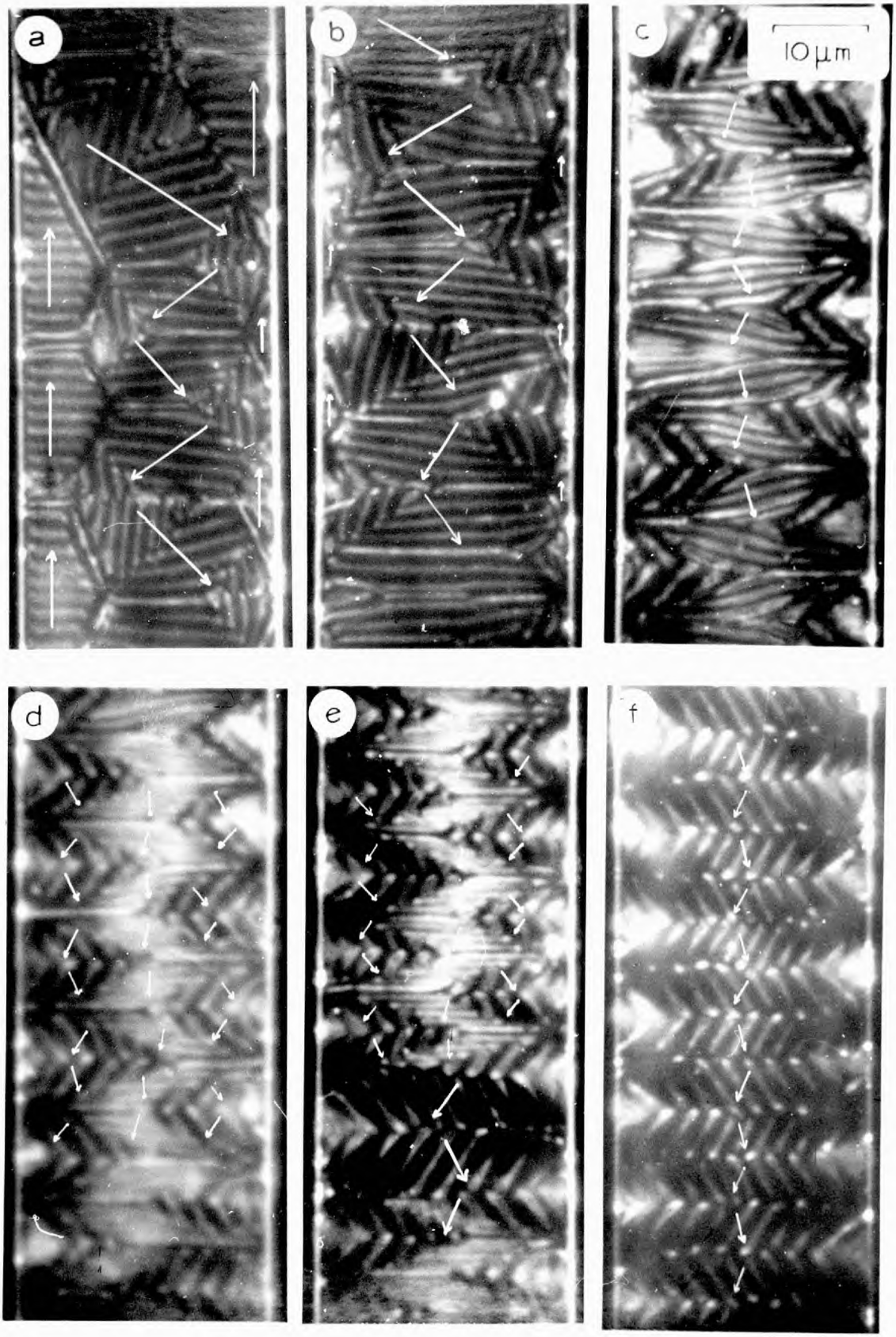

Fig. (6.19) Detailed behavior of stripes with hard axis field.

wall itself. A slight increase in the colloid collection was sometimes visible at the end of the stripes. This is possibly where the magnetisation was locally rotating more rapidly to lie in the platelet plane. The 180° walls, although necessary from the overall flux pattern within the platelet do not therefore seem to fit well with the oscillations of the stripe domains. This can also be seen in FIG.(6.10).

The forward magnetisation in FIG.(6.19a) appeared to be divided by 90° walls across the width of the platelet. At one end the stripes lay parallel with these walls but at the other had diverged to leave a triangular closure region where the stripes lay almost in the [100] direction. This occurred at opposite ends on alternate walls and must have been important for flux closure. Again, regions like this can be found by referring to FIGS.(6.10 & 11) where stripe domains, although not of the type V lay in a [100] direction normal to the edge but rotated to connect with [100] stripes parallel with the edge. These particular regions played an important part during the application of hard axis fields.

In a field of 6.0 oe, FIG.(6.19b), the reverse triangles with type V domains had shrunk and the closure areas of the main domains expanded. The entire structure is now seen to resemble a Néel strip with a degree of rotation of the magnetisation occurring in the expanded closure areas. Another interesting feature, visible in the photograph, was the splitting of the colloid collection along some of the stripes. At this thickness it was not thought to arise from free poles on the under face of the platelet, as had been observed in thinner platelets, Gemperle and Kaczer (1969).

At higher fields 16 oe, FIG.(6.19c), 25 oe, (d), and 37 oe, (e), these closure areas continued to grow, with the volume of the central domains decreasing. At the same time the spacing of the stripes in this central region decreased, whilst they showed an increased tendency

to lie normal to the field direction and to split. This was unexpected as these regions already had a magnetisation component in the field direction. It would seem therefore that this structure was incapable of rotating fully into the field direction, being in some manner blocked, and therefore had to be displaced by the closure areas, which were apparently more free to expand.

This observation together with the behaviour seen in FIG.(6.14) suggests that the stripes which lie almost normal to the applied field direction show an increased resistance to rotation. This may be because stripe rotation is restrained by the overall magnetic structure of the neighbouring domains and only rotation of the magnetisation within the stripes is possible. Thus the closure domains with the intermeshing of the stripes in the two halves may provide a 'flexible joint' in the magnetisation structure and expand into the centre of the platelet, as seen in FIG.(6.19). The increased magnetic field also caused the spacing of the central stripes to decrease, where the magnetisation was probably locally rotating independently of stripes, and causing the stripes to split.

Finally, at 49 oe, FIG.(6.19f), the particular area shown contained only stripes originating from the closure domains. A light gathering of colloid showed areas where a small divergence of the magnetisation occurred at the edge of the platelet, but, in the main, the magnetisation must have been directed along the [100] axis. The angle that the stripes made with the field direction was, at 30°, much higher than angles previously measured for this field, i.e. about 16° at 49 oe. It could, however, be that the details of the stripe structure were different from that of FIG.(6.14e & f). The spacing of the stripes in the hard axis field in that platelet was 1 μm. whereas the ones seen in FIG.(6.19f) had a spacing of about 2 μm, i.e. twice as wide. A far larger displacement than would seem probable is required to make the theoretical curve in FIG.(6.15) fit this value, again indicating that perhaps these stripes are not exactly of the

same type as those discussed earlier.

Gaps in the colloid between successive orientations of the stripes could be clearly seen, as well as a non-uniformity in the colloid collection. This again indicates the complexity of the structures, even in higher fields.

As an interesting comparison FIG.(6.20a) shows the corner of a platelet 6,200 Å thick in a field of 27 oe applied along the easy axis. A close-up of part of it is seen in FIG.(6.20b). The overall magnetisation directions were certain from familiarity with thinner platelets, with spike domains formed from the edges, and triangular closure domains at the base of the spikes. Yet within this arrangement the stripe domains could be seen to execute very complex variations for no apparent reason.

Observations were also made on both sides of a platelet with stripe domains. Unfortunately, these observations could not be made simultaneously but were achieved by completely immersing a freely suspended platelet in colloid sandwiched between two microscope cover slips, spaced apart with grease. Successive observations were made on either face of the platelet, inverting the specimen under the microscope. These showed a similar overall structure on either face, as seen in FIG.(6.21a & b), but with slight variations in detail.

A 180° wall, if visible on one face, was also visible on the other. The absence of colloid in some of the triangular closure regions, which has already been commented on, occurred on both faces. A slight displacement of the stripes on one face compared with the other was possible but not completely proved. The nature of the stripe pattern in corresponding regions was similar although in detail there may have been differences. These differences are at the limit of resolution of the colloid and may even have arisen from slight obstructions to the free flow of colloid over both faces.

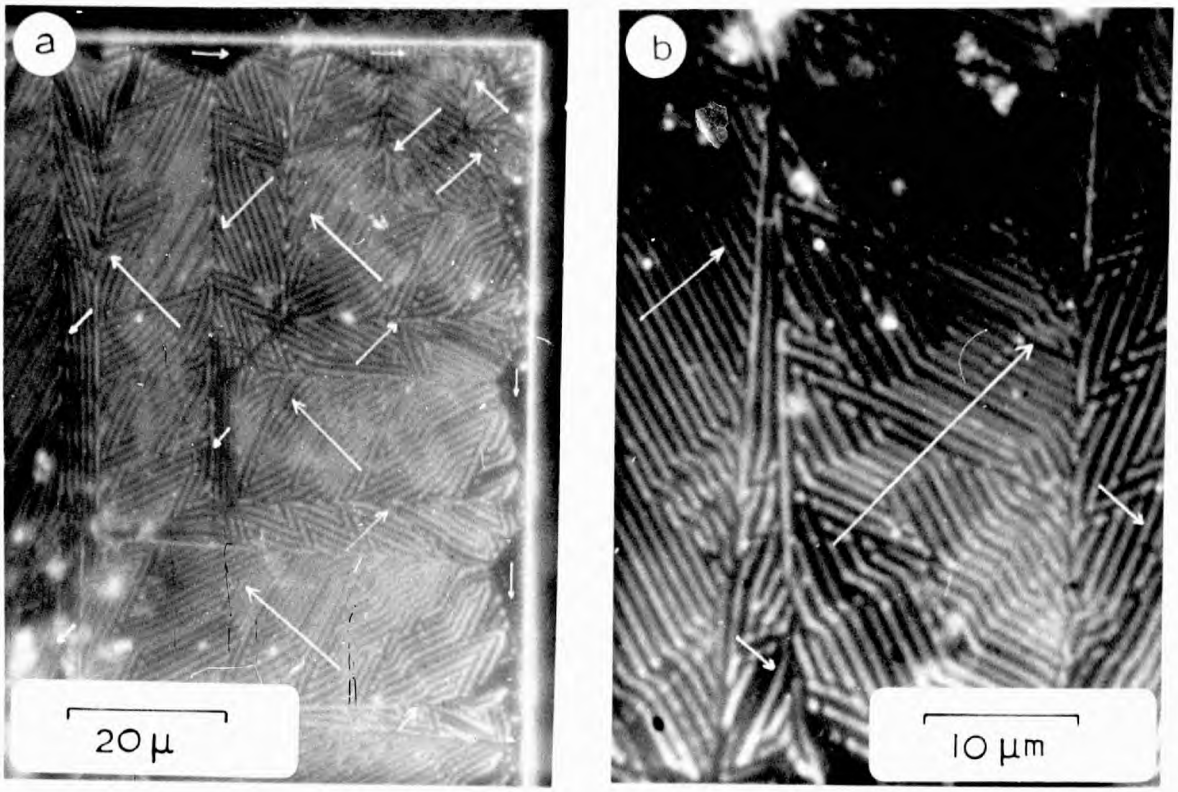

Fig. (6.20) Spike domains in stripe platelets

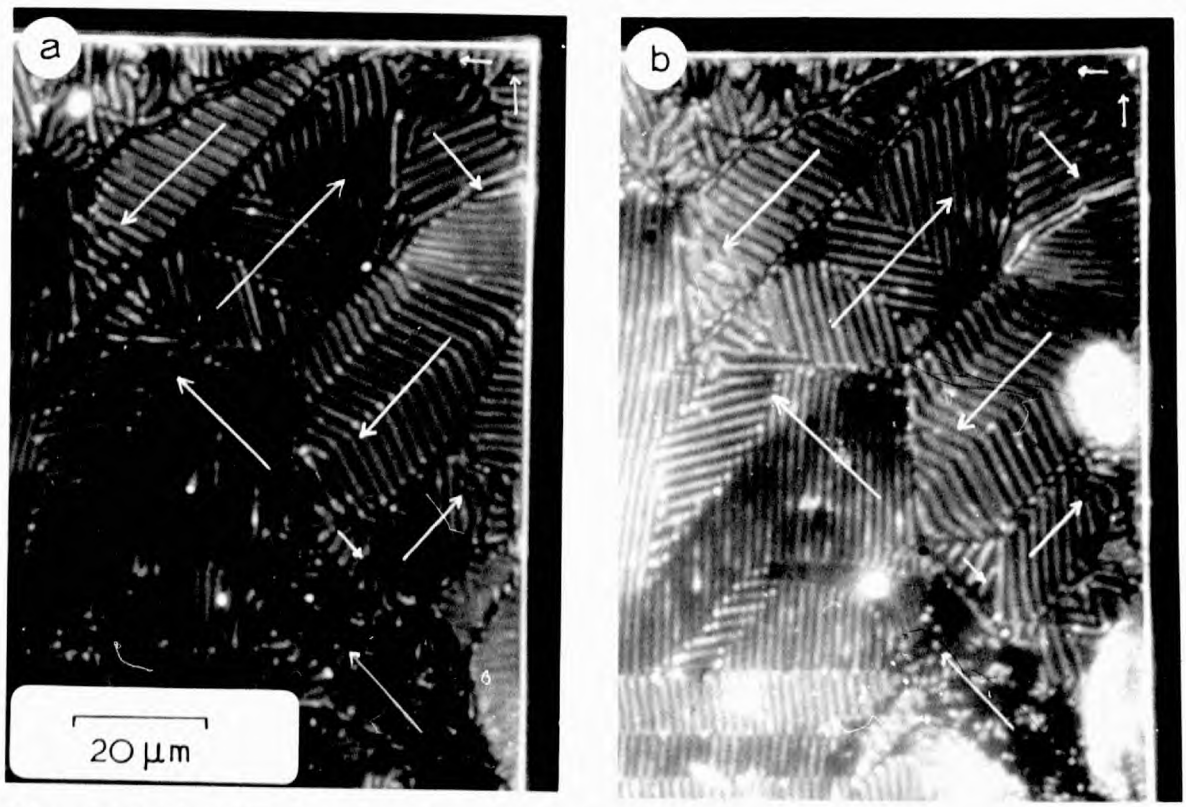

Fig. (6.21) Stripes on opposite faces of one platelet

6.2.6 Summary of Stripe Observations

Earlier sections have attempted to fit a crude model to explain the many varied stripe structures observed in platelets. De Blois (1968a) had observed the type IV structures in thicker platelets. No evidence of this structure has been found. The best approximation is the type III structure with magnetisation oscillating about the plane of the platelet angled at something near 45° to the colloid collections, however such a description is still obviously insufficiently sophisticated.

In zero field the flux closure patterns can be correlated with familiar structures in thin platelets. Yet the domains themselves are often subdivided into regions containing similar stripes, but in different orientations, and the stripes in the sub-domains can show angular variations of up to 20°. At the same time the stray field produced and the change in orientation between two sets of adjacent stripes in neighbouring domains separated by a 90° wall may be no greater than within the same domain. This, however, is not the case when the domains are separated by a 180° wall, and a distict break exists in the colloid pattern.

There is little change in structure through the thickness of the platelet in the thinner stripe bearing platelets. The fact that structures in platelets an order of magnitude thicker appear to be similar suggests that this may also be the case with these. At the bottom end of the thickness range the type III structures are found to be compatible with the type II Saito stripes, and at the top end of the range the circle Bloch lines, which probably exist through the centre of the platelet, expand to become Bloch walls.

The behaviour under both easy and hard axis fields is very complex. In the case of the former, long sweeping stripes form across the platelet with decreasing separation in increasing fields, until they finally disappear. The field necessary to saturate a

stripe bearing platelet in the easy axis is much higher than for a thin platelet and approaches the anisotropy field value. In the case of hard axis fields short sections of stripe domain form making an angle with the field direction which is a function of the applied field. These sections of stripes become shorter with increasing field.

No model has been found which adequately fits the many characteristics observed. The stripe patterns seen over quite large areas, in high fields or zero field, suggest that they may be formed by a reasonably simple magnetisation distribution. In this distribution the mean magnetisation is loosely coupled to the stray field pattern and its net direction lies somewhere in the region of 45° to the stripe direction. The first step to an understanding of these complex stripe structures requires a micromagnetic calculation but more limitations must first be put on possible models to enable this to be done. As these structures have been observed on nickel any calculation will probably have to include magnetostrictive terms.

CHAPTER 7

MAGNETOSTATICS IN PLATELETS

INTRODUCTION

In section 1.1 of this thesis the terms which contribute to the magnetic free energy of a body were examined and an expression obtained for the total energy. Various terms in the expression are dominant according to the size, shape and nature of the material body being considered. In the case of the ferromagnetic platelets studied in this thesis the magnetostatic energy played an important part in determining their behaviour, seen clearly in the observations reported in Chapters 5 and 6. Unfortunately, the magnetostatic energy of these platelets is difficult to evaluate and makes direct comparison between their observed behaviour and any theoretical models complex, an exception being the Néel strip treated in section 5.2.4.

The magnetostatic energy was shown in section 1.1.4 to consist of two terms, that arising from the applied field, $\underline{H}_o$, and that from the material itself, $\underline{H}'$, so that

$$\underline{H} = \underline{H}_o + \underline{H}' \qquad (7.1)$$

and

$$E_H = -\mu_o \int (\underline{H}_o + \tfrac{1}{2}\underline{H}') \cdot \underline{M}\, d\tau \qquad (1.7)$$

Unlike $\underline{H}_o$, $\underline{H}'$ usually lies in a direction such that $\underline{H}' \cdot \underline{M}$ is negative.

The Maxwell equations for the magnetostatic field are:

$$\text{curl } \underline{H} = 0 \tag{7.2}$$

$$\text{div } \underline{B} = 0 \tag{7.3}$$

$$\underline{B} = \mu_o (\underline{H} + \underline{M}) \tag{7.4}$$

in M.K.S. units

and from (7.3) and (7.4)

$$\text{div } \underline{H} = - \text{div } \underline{M} \tag{7.5}$$

Because the curl of the magnetic excitation is at all times zero it is possible to express $\underline{H}'$ as the gradient of the magnetic scalar potential

$$\underline{H}' = - \text{grad } \phi \tag{7.6}$$

and from equations (7.5) and (7.6)

$$\nabla^2 \phi = \text{div } \underline{M} \tag{7.7}$$

With the potential itself expressed as a combination of surface and volume pole densities, as seen earlier

$$\phi = \frac{1}{4\pi} \int_S \frac{\underline{M} \cdot d\underline{s}}{r} - \frac{1}{4\pi} \int_V \frac{\text{div } \underline{M}}{r} \, d\tau \tag{1.5}$$

With the volume integral taken over the entire volume of the specimen and the surface integral over the entire outside surface. In principle therefore the magnetostatic energy of any charge distribution may be calculated by first evaluating the magnetic scalar potential ϕ using equation (1.5), determining $\underline{H}'$ from ϕ using equation (7.6), and finally combining $\underline{H}'$ with $\underline{M}$ according to equation (1.7) to give the magnetostatic energy.

Alternatively we may write

$$E_H' = - \tfrac{1}{2} \mu_o \int_V \underline{H}' \cdot \underline{M} \, d\tau \tag{1.6}$$

which by using equation (7.6) becomes

$$E_H' = \tfrac{1}{2} \mu_o \int_V \text{grad } \phi \cdot \underline{M} \, d\tau$$

and can be rewritten as

$$E_H' = \tfrac{1}{2}\mu_o \int_V \text{div}\,(\phi\,\underline{M})\,d\tau \;-\; \tfrac{1}{2}\mu_o \int_V \phi\ \text{div}\,\underline{M}\,d\tau$$

which by using Gauss's theorem becomes

$$E_H' = \tfrac{1}{2}\mu_o \int_S \phi\,\underline{M}\cdot\underline{ds} - \tfrac{1}{2}\mu_o \int_V \phi\ \text{div}\,\underline{M}\,d\tau \qquad (7.8)$$

In magnetostatic calculations $\underline{M}$ is usually assumed to be uniform within the specimen so that the second term may be neglected.

Thus

$$E_H' = \tfrac{1}{2}\mu_o \int_S \phi\,\underline{M}\cdot\underline{ds} \qquad (7.9)$$

$$\text{or}\quad E_H' = \tfrac{1}{2}\mu_o \int_S \phi\,\sigma\,ds$$

where $\sigma = \underline{M}\cdot\underline{n}$

In this chapter a short review is given of the methods that have been used to evaluate magnetostatic energies. This is followed by a description of an incomplete attempt that has been made to evaluate the magnetostatic energy of a platelet, entirely numerically, and to incorporate this in a total energy expression. One of the simplest examples of the movement of domains is seen in FIG.(7.1). It should be possible to predict this observed behaviour from a minimisation of the fundamental expressions for the various energy terms involved. However, this has not yet provided definite answers.

7.1 EVALUATION OF MAGNETOSTATIC ENERGIES

Reference has already been made in section 1.1.4 to the evaluation of magnetostatic energies of specimens whose shape can be approximated by that of an ellipsoid. However, such calculations are of limited range and of little interest in explaining domain behaviour. Other approaches have therefore been made in attempts to enable domain

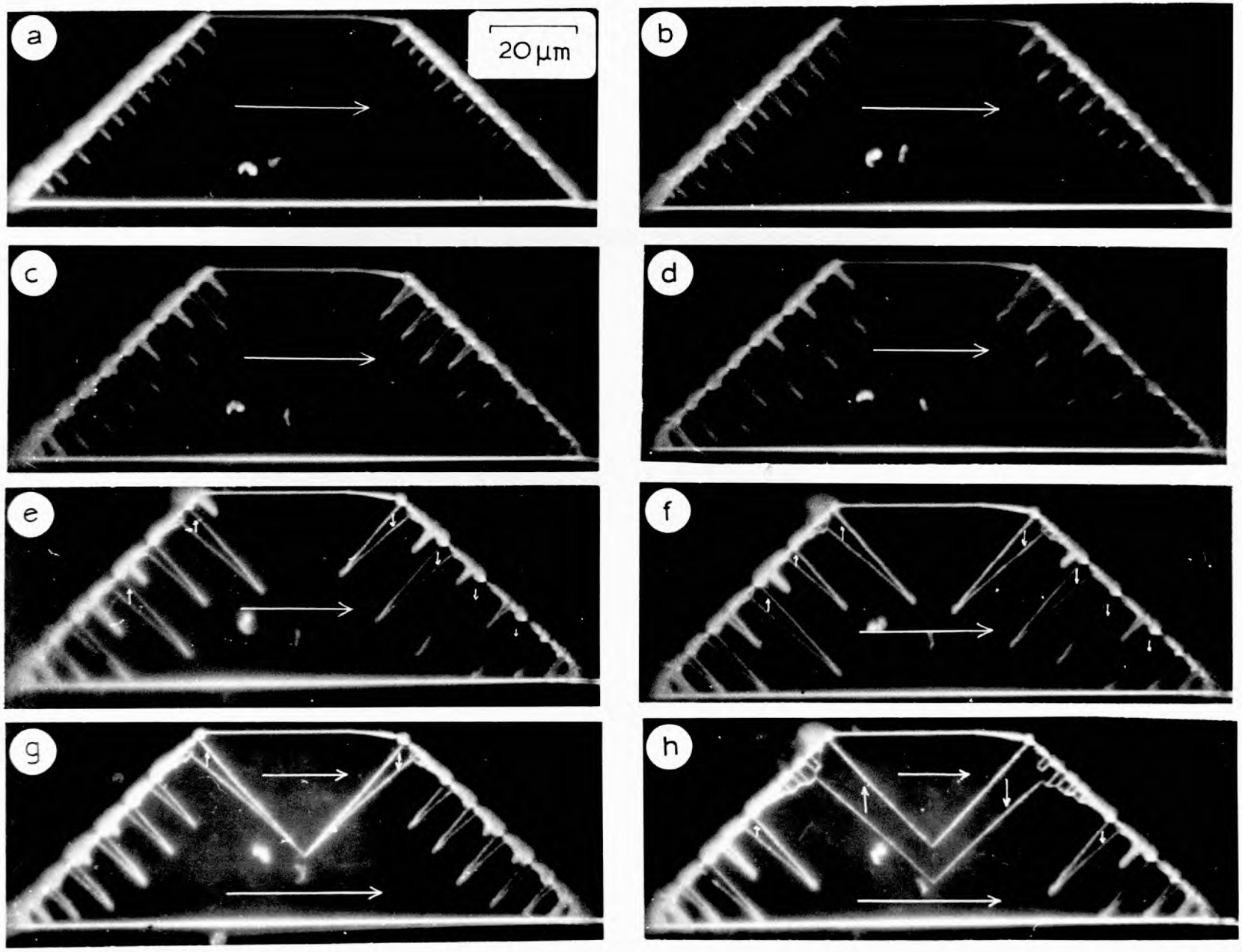

Fig. (7.1) Growth of Spike Domains

calculations to be put on a stronger theoretical foothold.

7.1.1 Fourier Methods

One important technique has been the application of Fourier methods in evaluating the energies of infinite periodic domain structures. This was first applied to the important problem of a thin plate with parallel strip domains, see FIG.(7.2), by Kittel (1946).

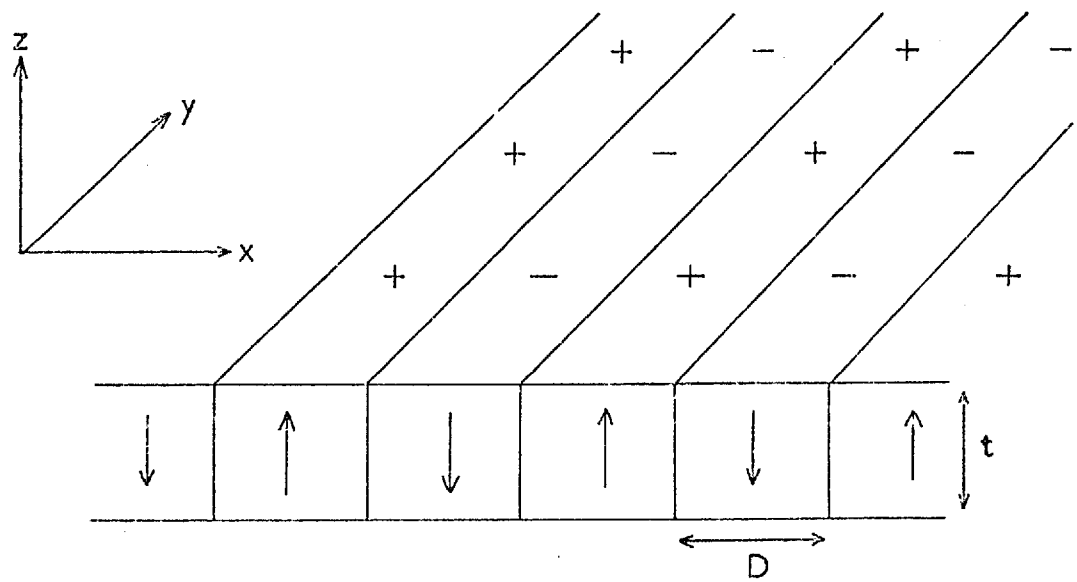

FIG.(7.2) THIN PLATE WITH STRIP DOMAINS

Kittel calculated the magnetostatic energy density per unit area of a single plane of alternating strips as

$$E_H' = 0.8525\ M_s^2\ D \qquad (7.10)$$

For a thin plate he took the value as being double that for one surface, i.e. $1.71\ M_s^2\ D$. This only strictly applicable when $t \gg D$ and interactions between the surfaces can be neglected. Malek and Kambersky (1958) included this interaction and determined the energy per unit area as:

$$E_H' = \frac{16\, M_s^2\, D}{\pi^2} \sum_{n}^{\infty} \frac{1}{n^3}\left(1 - 1^{-\frac{n\pi t}{D}}\right) \qquad (7.11)$$

where n is odd.

As $t \longrightarrow \infty$ equation (7.11) becomes equal to (7.10).

Silcox (1963) considered the case when both the magnetisation and easy axis were inclined to the plate normal but the expression required an experimentally measured parameter to generate the results. A completely theoretical expression was derived by Jakubovics (1966b) which was confirmed by Lorentz microscopy observations made on cobalt foils.

By expanding the potential in two Fourier series taking different forms inside and out of the plate, after Goodenough (1954), Kooy and Enz (1960) investigated the energy of reverse domains in a partially magnetised plate. They also considered the case of a single reversed cylindrical domain in an infinite plate.

The double Fourier series, suggested by Kittel (1949) was used by Spacek (1959) to calculate the magnetostatic energy of several different infinite strip, checkerboard and echelon structures on a single plane, all of which had zero overall charge. Simple and complex honeycomb structures were evaluated by Kozlowski and Zietek (1966) and concentric squares by Di Chen (1967).

7.1.2 Direct Integration

In crystals where the domain structure is large in relation to the size of specimen, which can no longer be regarded as infinite Fourier methods are no longer suitable. It therefore becomes necessary to use numerical methods to evaluate the integral of equation (7.9). Rhodes and Rowlands (1954) considered the problem of a bounded thin plate, i.e. similar to that shown in FIG.(7.2) but only containing a few domain walls in total. They expressed the mutual energies of two

parallel surface charge distributions as

$$E_{r_1} = \mu_o \iint \sigma_2 \, \phi_2 \, (x_2 y_2) \, dx_2 \, dy_2 \qquad (7.12)$$

$$\phi_2 = \iint \frac{\sigma_1}{r_{12}} \, dx_1 \, dy_1$$

i.e. ϕ_2 is the scalar potential at some point on surface (2) due to the integrated charge distribution of surface (1). The interaction energy between charge distributions is positive if they are of the same sign and negative if of opposite sign.

A calculation of this type was used by Craik and McIntyre (1967) to evaluate the critical size for the adoption of a single domain state by a rectangular block, as a function of its aspect ratio and of the ambient field.

In a review of the magnetic domain structures of small crystals by Craik (1970) this approach was extended to evaluate the equilibrium number of domains in a small uniaxial crystal as a function of its dimensions. This gave the interesting result that above certain ratios of crystal dimensions only odd numbers of domains are predicted. Craik also showed that in a very simple case the equilibrium position for a domain wall in a crystal need not leave the crystal in a demagnetised state.

7.1.3 The μ^* Correction

A decrease in magnetostatic energy can occur in crystals with out of plane easy axes by a rotation of the magnetisation away from these axes and into the plane of the crystal. The surface pole density is reduced at the expense of introducing anisotropy energy and a volume pole distribution, and thus is more likely to occur in materials with low anisotropy. Corrections of this type are generally known as μ^* corrections and were first used by Williams et al (1949). They derived an expression for the effective permeability normal to

the easy direction as

$$\mu^* = 1 + \left[\frac{2\pi M_s^2}{K}\right] \qquad (7.13)$$

(The permeability parallel with the easy direction is assumed unity since the magnetisation in that direction cannot be changed appreciably).

This allows the total energy of the system to be written as $\frac{1}{2}\int \sigma\phi \, ds$, where σ is the surface charge density on the assumption of infinite anisotropy, and ϕ is the potential at the surface evaluated from a charge density σ on a material with permeability μ^*.

By using this technique Fox and Tebble (1958) investigated energy reductions in high crystalline anisotropy materials as a function of the angle made with the basal plane. It has also been applied to the open Kittel type structure in uniaxial materials, and to the magnetostatic field in thin plates showing stripe domains, as was seen in section 6.1.

7.2 NUMERICAL APPROACH TO DOMAIN BEHAVIOUR IN PLATELETS

Although the methods described in section 7.1 have been useful in evaluating the magnetostatic energies of periodic magnetisation distributions they are unsuitable for the situations that exist in thin platelets with planar domain configurations. Often no symmetry or periodicity exists in the platelets and an attempt has therefore been made to evaluate the energy completely numerically.

Sommerfeld (1952) considered the case of a cylindrical bar magnet of length 2l and evaluated the magnetostatic potential produced by a uniform pole density on the circular faces at either end. He showed clearly the relationship between the magnetic excitation, H', the field, B, and the magnetisation M. This is shown in FIG.(7.3) where the field quantities are given as functions of position along the

axis of the magnet.

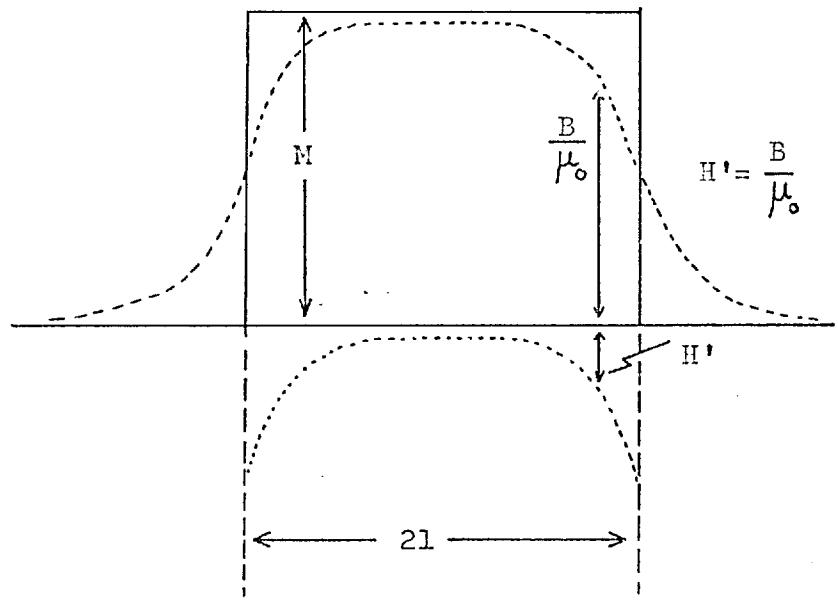

FIG.(7.3) DEMAGNETIZATION OF A UNIFORMLY MAGNETIZED BAR

The magnetisation is zero outside the body of the magnet and has a constant value M inside. The magnetic excitation H' is at all times negative inside the bar and thus has a demagnetising action with a very small value in the centre, but increasing to reach a value of $-M/2$ at either end. At the surface itself H' becomes $+M/2$, with a discontinuity M, and thereafter outside the body follows the magnetic field values, being related by $B = \mu_o H$. The magnetic field itself attains almost the full magnitude $\mu_o M$ at the centre of the bar, but is only half as large at the ends, and is of course continuous, in keeping with the boundary conditions at the surface.

This approach was extended by O'Dell (1960) who studied the magnetic excitation inside a cylindrical thin ferromagnetic film. The geometry of this situation was such as to give an expression for the magnetic potential ϕ and excitation H'. The expression for ϕ was valid at any point within the film, except within a distance t of the end, where t was the thickness of the film, because the integrand for

ϕ contained a singularity at this point. The excitation within the neighbourhood of either end was calculated from a separate expression which ignored the contribution from the opposite end and avoided the singularity, but was only valid near the one end. This limitation on the general expression for the potential is important in the platelet work considered below.

A set of photographs, FIG.(7.1), had been obtained recording one of the simplest domain movements observed in platelets, and the work below is an initial investigation of this behaviour.

The formation and behaviour of spike domains, near to saturation in increasing and decreasing fields applied along the easy axis of a platelet, has already been noted in Chapter 5. FIG.(7.1) shows in detail a decrease from saturation in a (100) plane trapezoidal platelet. Initially the large stray field which had existed along both of the [100] edges at saturation was lowered by the formation of numerous small spike domains, seen at 21 oe. in FIG.(7.1 a). These grew out, and at the same time decreased in number at 16 oe. (b) and further 11 oe. (c). At this stage, however, only some of the spikes continued to enlarge whilst others shrank, 8 oe. (d), continuing at 6 oe. (e). With a further decrease in field to 4.9 oe. (f) the spikes themselves became so wide that small closure structures formed at their own base. At 4.85 oe. the uppermost spikes on either side extended until they touched, and the remainder collapsed back FIG.(7.1g). Finally with a further slight decrease in field to 4.8 oe. the Bloch line which must have existed at this tip extended to form a vertical 180° Bloch wall, seen in (h).

Thus initially many spikes formed along the sides of the platelet, to lower the magnetostatic field on the <100> edges. With decreasing fields some spikes continued to grow and others to shrink, with the total number of spikes gradually decreasing, until eventually the configuration was changed by the formation of the 180° wall. As the process was performed quasi-statically over a period of several

minutes, this behaviour was assumed to represent successive equilibrium structures. Although initially a larger number of reverse domains were nucleated observations have shown that it is unfavourable for these all to grow. This type of behaviour has not previously been reported and is still unexplained. If it is assumed, and it would seem reasonable to do so for this type of behaviour has been seen on many occasions, that the platelet is always in its lowest free energy state, then energy minimisation calculations should give a prediction as to spike length and behaviour. This is investigated below.

7.2.1 Evaluation of Magnetostatic Field of Saturated Platelet

The magnetostatic potential at any point inside a saturated trapezoidal platelet seen in FIG.(7.4 a) is given by

$$\phi(z,x) = \frac{1}{4\pi}\int_{S_1}\frac{\underline{M}_s\cdot\underline{n}_1}{r_1}\,ds_1 + \frac{1}{4\pi}\int_{S_2}\frac{\underline{M}_s\cdot\underline{n}_2}{r_2}\,ds_2 \qquad (7.14)$$

If the magnetisation is assumed uniform throughout, the demagnetising field at the point (z,x) is given by

$$H'_x(z,x) = -\frac{\partial\phi}{\partial x} \quad \text{and} \quad H'_z(z,x) = -\frac{\partial\phi}{\partial z}$$

The total demagnetising energy of the platelet is then given by

$$E_{H'} = \tfrac{1}{2}\mu_o \int_{\substack{\text{volume of}\\ \text{platelet}}} H'_z M_s \, d\tau \qquad (7.15)$$

($\underline{H}'_x\cdot\underline{M}_s$ being zero at every point).

Alternatively, the platelet can be imagined as consisting of a series of n parallel bars all having the same uniform magnetisation and cross section, as seen in FIG.(7.4 b). The total surface area of the end has been reduced by $\frac{1}{\sqrt{2}}$, if faces normal to the x-direction are disregarded, therefore $\underline{M}_s$ is replaced by $\sqrt{2}\,\underline{M}_s$ to compensate for this change.

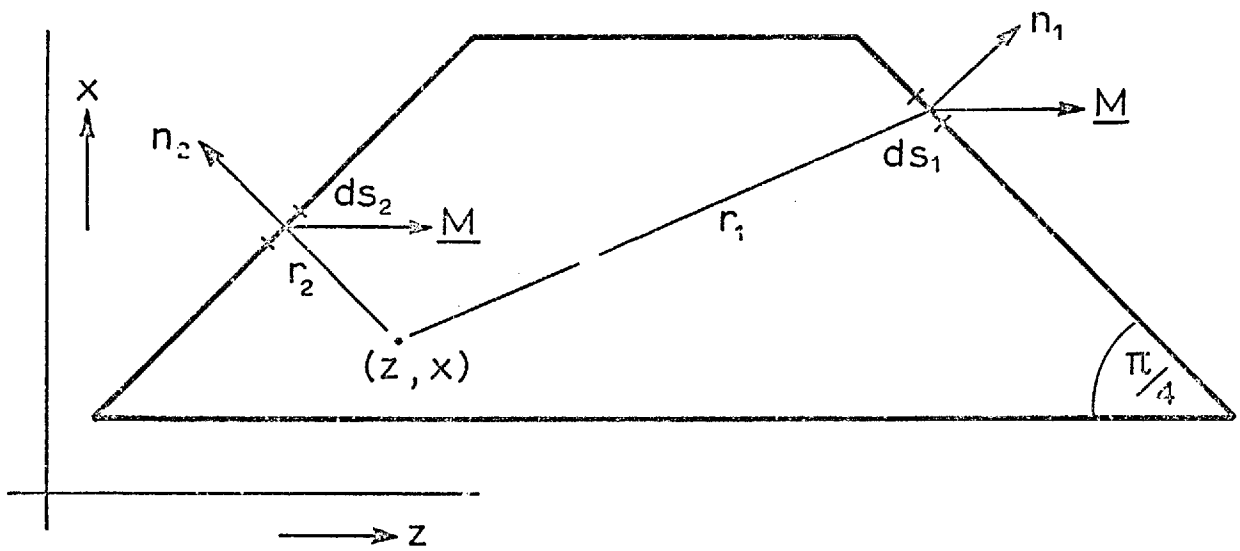

Fig. (7·4 a) Geometry used for saturated platelet

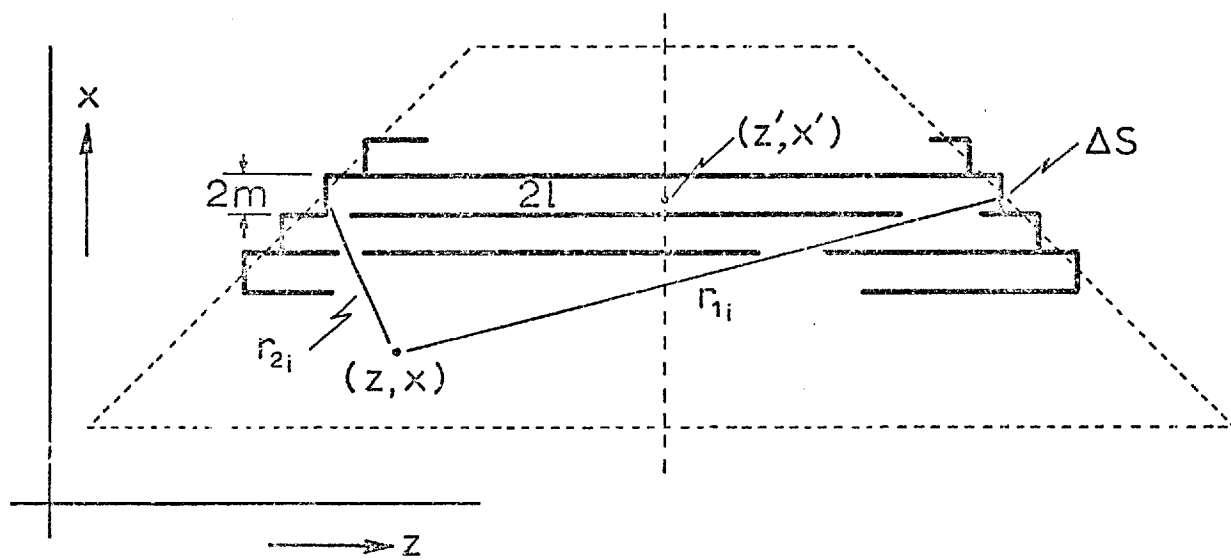

Fig. (7·4b) Synthesis of platelet by strips

The potential at any point can now be written as the summation of the potentials produced by each strip separately at that point

$$\phi\,(z,x) \;=\; \sum_{i\,=\,1}^{n} \left[\frac{1}{4\pi} \int \frac{M_s \Delta S}{r_{1i}} - \frac{1}{4\pi} \int \frac{M_s \Delta S}{r_{2i}} \right] \qquad (7.16)$$

where ΔS is the cross-sectional area of a strip.

The demagnetising energy at the point (z,x) remains as $\frac{1}{2}\,\mu_o\, H'_z(z,x)\, M_s$. If the platelet is thin any variation in r_{1i} and r_{2i} through the thickness of the platelet can be neglected when integrating over the end surfaces. Using the symbols defined in FIG.(7.4 b) the potential at (z,x) can be written as

$$\phi\,(z,x) \;=\; \sum_{i\,=\,1}^{n} \frac{M_s}{4\pi} \int_{x'-m}^{x'+m} \left\{ \frac{t\,dx''}{\left[(z'+l-z)^2+(x''-x)^2\right]^{\frac{1}{2}}} - \frac{t\,dx''}{\left[(z'-l-z)^2+(x''-x)^2\right]^{\frac{1}{2}}} \right\} \qquad (7.17)$$

It is more convenient to differentiate this expression with respect to z before evaluating the integral and this gives $H'_z(z,x)$.

Rearranging equation (7.15) using (7.17) the demagnetising energy can be rewritten in summation form as

$$E_{H'} \;=\; \tfrac{1}{2}\,\mu_o\, M_s \sum_{x} \sum_{z} H'_z(z,x)\, \delta z\, \delta x \qquad (7.18)$$

(the summation being carried out over all co-ordinates (z,x) inside the area of the platelet).

This expression is not valid within distances $\sim t$ from the edge of the platelet and such regions are omitted in evaluating equation (7.18).

The accuracy with which the bars substitute for the edge distribution increases with the number of bars, i.e. as the end steps

degenerate into a slope.

A simulation of a saturated trapezoidal platelet of base length 150 μm, height 50 μm and thickness 0.2 μm was made using strips of 1 μm width, i.e. putting n = 50. The value of $H_z(z,x)$ was determined over a mesh of co-ordinates, and at each co-ordinate was taken to be the value appropriate to the surrounding 25 sq. μms. A computer program was written which evaluated the ratios $H'_z(z,x)/M_s$ and $H'_x(z,x)/M_s$ over this mesh of co-ordinates using equation (7.17). The scalar product $\frac{1}{2}\mu_o \underline{M}_s.\underline{H}'_x(z,x)$ was at all times zero because $\underline{M}$ was assumed to lie uniformly along the z axis, and the product $\frac{1}{2}\mu_o \underline{M}_s.\underline{H}'_z(z,x)$ was at all times negative because the demagnetising field opposed the magnetisation. The value of $\underline{M}_s$ for Ni is 5.5×10^5 amps/m, and for a platelet of this volume (10^{-15} m^3) the total demagnetising energy given by equation (7.18) is found to be 3.9×10^{-13} joules. The applied field necessary to saturate the platelet was taken as 5×10^{-3} wb/m^2 making the applied field energy 2.75×10^{-12} joules.

With the magnetisation lying entirely along the [110] direction the cosines of the magnetisation vector are $\alpha_1 = \frac{1}{2}$, $\alpha_2 = \frac{1}{2}$ and $\alpha_3 = 0$. Taking the value K_1 from section 1.1.2 as -5.7×10^3 joules/m^3 this gives the total magnetocrystalline anisotropy energy of the platelet as 1.42×10^{-12} joules. If saturation is achieved entirely by wall motion, as happens when an easy axis field is applied, the anisotropy energy can be regarded as constant, and can therefore be neglected. If rotation occurs this is no longer true and allowance would have to be made for this energy change.

In addition to calculating the total energy of the platelet the computer program enabled the magnetic excitation to be plotted as a function of position at any point in the platelet. A typical result of the computations is seen in FIG.(7.5). The plots show the variation of H_z and H_x, normalised with respect to M_s, along a centre axis of the platelet, AB, parallel with the z axis. They are included to

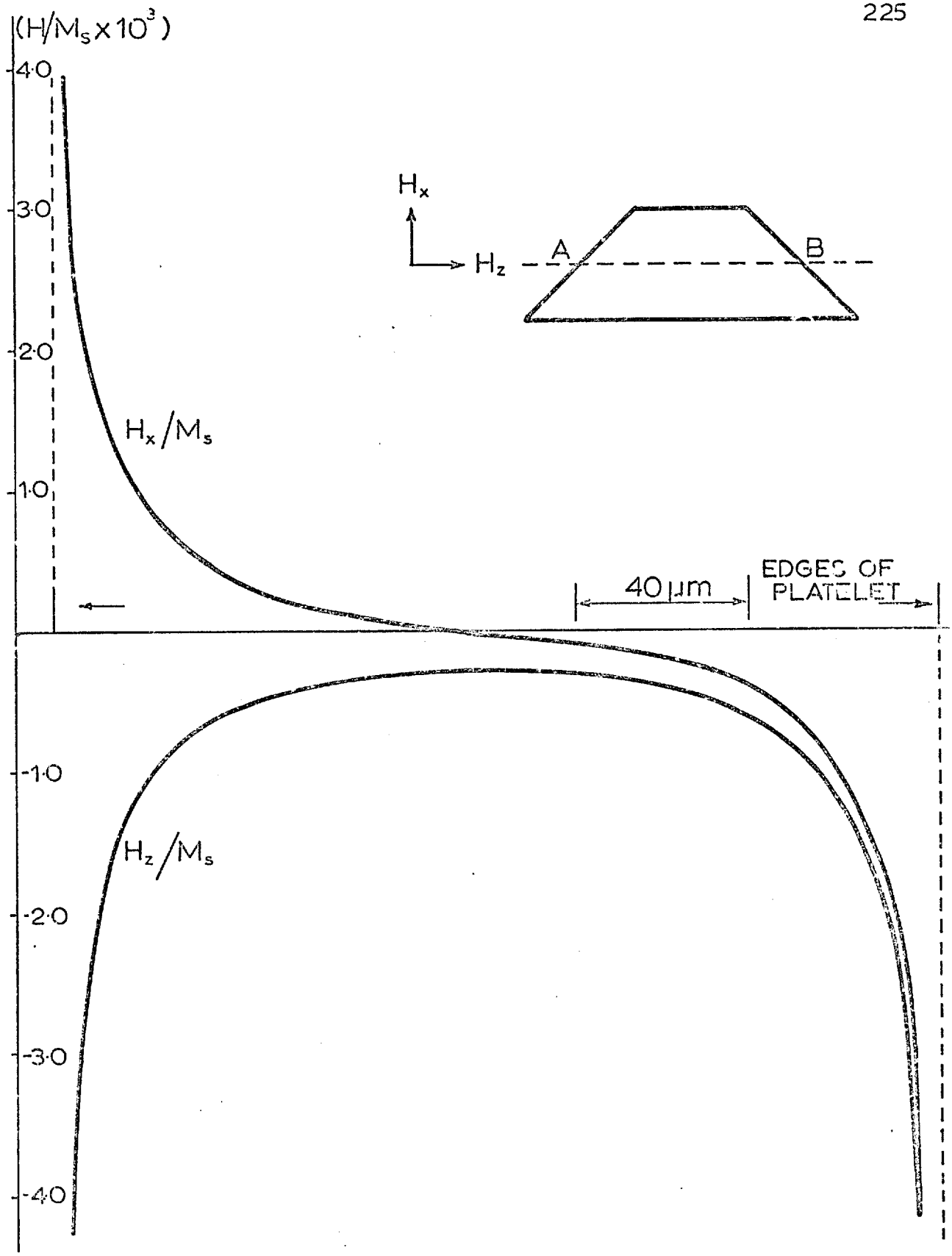

Fig. (7·5) Variation of H_z and H_x along centre of trapezoid platelet parallel with z-axis (A-B)

demonstrate the degree of variation within the platelet, with the largest contributions arising near the pole densities at either end. Little variation occurred in the excitation in a line close to and parallel with the pole densities at either end. It began to increase locally in the region of the corners, but these areas are in any case outside the limitations of the model.

7.2.2 Platelet With Mixed Edge Distribution

In the previous section the magnetostatic potential at any point in a saturated platelet was found by a summation process. This may have appeared cumbersome for the saturated platelet whose edge contributions could have been determined by direct integration, however, it has a wider flexibility.

When reverse domains form at the platelet edge the charge distribution is no longer of uniform sign. This can be easily reproduced in the summation process because any combination of positive and negative contributions can be included whereas direct integration would have been impossible. The effect of the formation of any distribution of reversed domains on the magnetostatic field from the edge is thus easy to study.

The effect of a non-uniform edge charge distribution resulting from spike formation is seen in FIG.(7.6). The variation of H_z across the width of the platelet is plotted for two cases. These are shown with a dotted line in the case of a saturated platelet and with an interrupted line for a non-uniform charge distribution. Two scans across the width are given for each case, the first, 'A', is made at a distance equivalent to 3 μm from the edge and the second, 'B', at 8 μm.

In the saturated platelet H_z does not vary substantially across the width of the platelet although it does increase towards the end marked X^1. At 8 μm from the edge it has a value $\frac{1}{4}$ of its value at 3 μm. Regions of reversed edge charge were included at locations

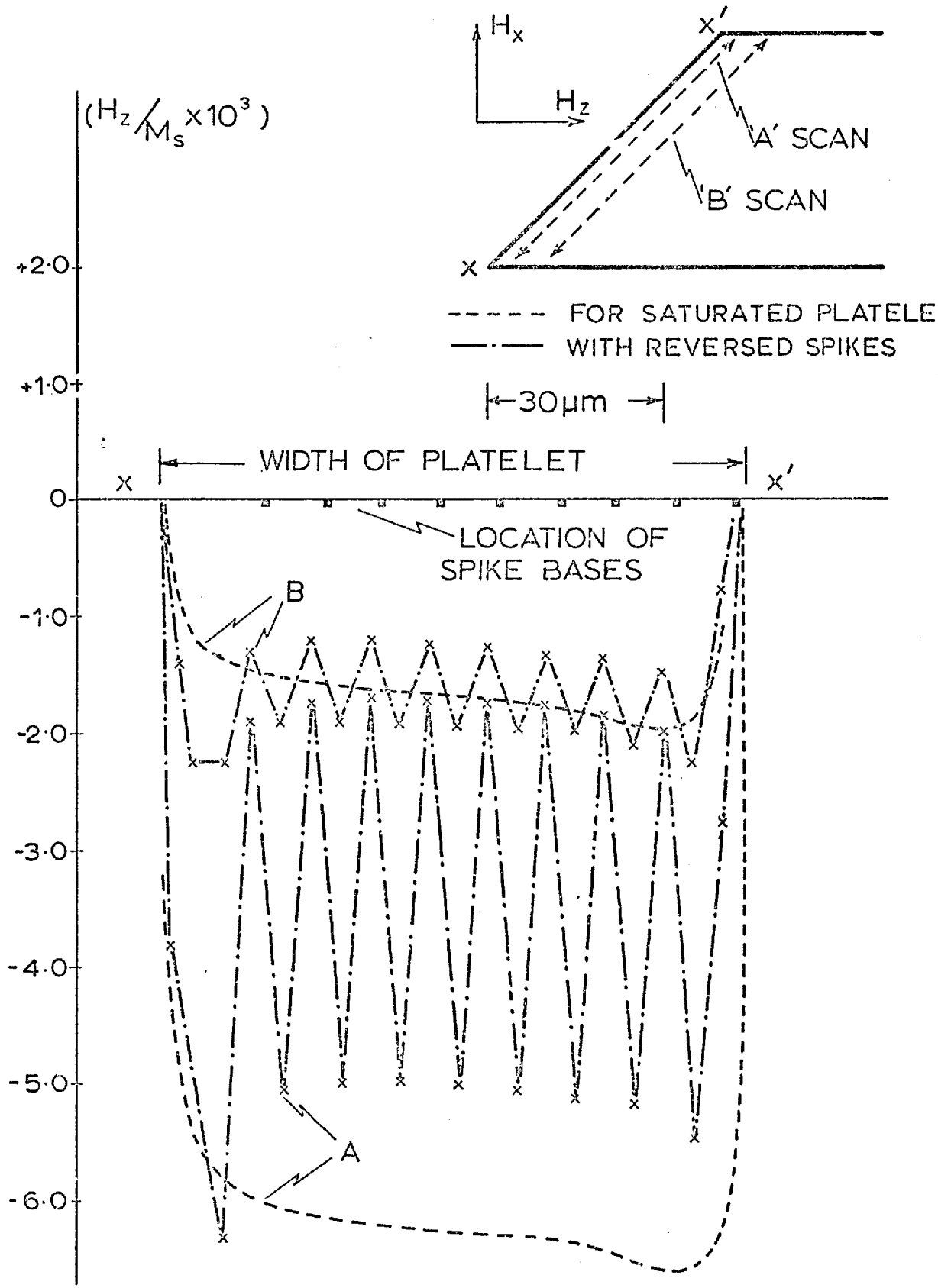

Fig. (7·6) Variation of H_z with and without reversed spikes.

indicated on the axis in FIG.(7.6) and their effect seen by the shape of the solid curve. Emphasis should not be placed on the detailed shape of this curve because it is to an extent dictated by the resolution of the evaluation points.

The 'A' scan at 3 μm shows an average H_z value with reversed charges half as large as that of the saturated platelet. The 'B' scan at 8 μm however, shows negligible change in its average value as the localised effect of the reversed regions begin to even out.

7.2.3 Energies in Platelet With Spike Domains

Both H_z/M_s and H_x/M_s were seen in FIG.(7.5) to fall to low values in the centre of the platelet away from the edge charges. Calculations can therefore be simplified by assuming that the field at any point in the platelet arises only from the nearest edge, the contribution from the far edge being neglected. Having made this change it is also more convenient to rotate the orientation of the platelet within the co-ordinate system. The geometry of this new position is shown in FIG.(7.7).

When a platelet with spike domains is considered the magnetostatic potential at any point (z,x) can be divided into two contributions, that from the edge charges, and that from the 90° walls which do not lie exactly along the <100> directions.

If the edge is subdivided into n equal segments, each of edge area ΔS whose charge can be positive or negative, the contribution to the potential at (z,x) from these edge charges can be expressed as

$$\phi_E(z,x) = \sum_{i=1}^{n} \frac{(\pm)_i}{4\pi} \int \frac{(M_s/\sqrt{2})\Delta S}{r_i} \qquad (7.19)$$

where r_i is the distance from the i'th segment to the point of evaluation (z,x).

Again, any variation in r_i through the thickness of the platelet

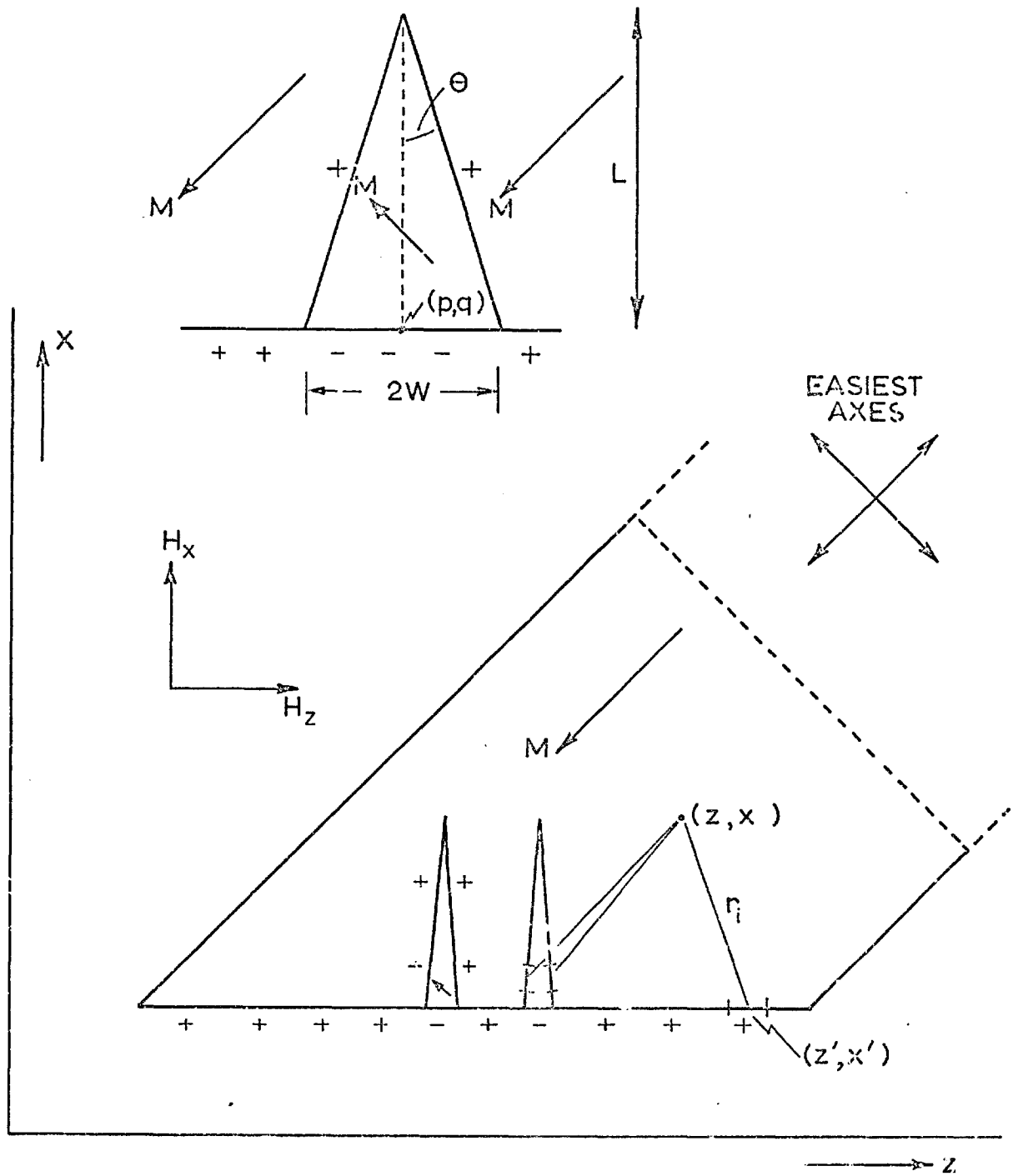

Fig. (7·7) Geometry used to evaluate energy of platelet with spike domains

is neglected and equation (7.19) becomes:-

$$\phi_E(z,x) = \sum_{i=1}^{n} \frac{(\pm)_i}{4\pi} \int_{z'-1}^{z'+1} \frac{t\, dz''}{\left[(z-z'')^2+(x-x')\right]^{\frac{1}{2}}} \qquad (7.20)$$

This expression is differentiated with respect to z and x to give $(H'_z)_E$ and $(H'_x)_E$ at every point and this field, resulting from the edge charges, is assumed applicable over the local area $\delta z\, \delta x$.

The potential at the same general point (z,x) from the charged spike domain walls may also be evaluated. The reason for their charge may be understood by reference to FIG.(7.8)

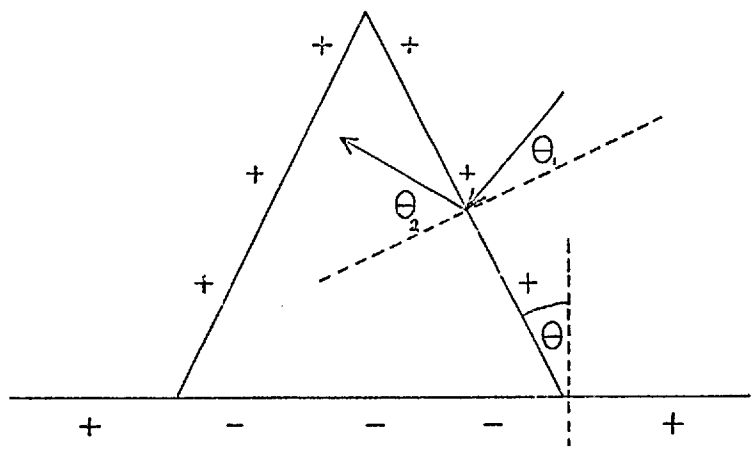

FIG.(7.8) CHARGE FORMATION ON SPIKES

The magnetic charge formed per unit length of the wall is given by :-

$$(M_s \cos\theta_1 - M_s \cos\theta_2)\, t$$

But $\theta_1 = (45 - \theta)$ and $\theta_2 = (45 + \theta)$ and the expression therefore simplifies to

$$\sqrt{2}\, M_s\, t \sin\theta$$

It is apparent that the sign of the charges on either spike wall

are identical, and opposite to the edge charges at the base of the spike.

The potential at the point (z,x) from a spike of base width 2ω and length L can be written as

$$\phi_s(z,x) = \frac{1}{4\pi} \frac{\sqrt{2}\, M_s\, t \sin\theta}{\cos\theta} \int_0^L \left[\frac{1}{r_{s1}} + \frac{1}{r_{s2}}\right] dx \qquad (7.21)$$

where r_{s1} and r_{s2} are the distances from the two area elements of length $\frac{dx}{\cos\theta}$ on either spike wall.

The quantities sin θ and cos θ in equation (7.21) can be expressed in terms of ω and L, and r_{s1} and r_{s2} as f (z,x,p,q,ω & L). This enables the magnetostatic potential at (z,x) from one spike of length L, semi-base width ω, and base co-ordinates (p,q) to be evaluated. The expression is differentiated with respect to z and x, before evaluating the integral, to give $(H'_z)_s$ and $(H'_x)_s$ at any point from this one spike. This field at (z,x) will in general arise from contributions from several spike domains and the appropriate values for r_{s1} and r_{s2} must be substituted in equation (7.21) to enable the contribution from each of the spikes to be included in the total value for $(H'_z)_s$ and $(H'_x)_s$.

If the case of a platelet with n spike domains is considered, with a certain fixed edge distribution the total demagnetising field at the point (z,x) is given by

$$\left.\begin{aligned} H'_z(z,x) &= (H'_z)_E + \sum_n (H'_z)_s \\ H'_x(z,x) &= (H'_x)_E + \sum_n (H'_x)_s \end{aligned}\right\} \qquad (7.22)$$

where n sums the contributions from all the spikes.

The total magnetostatic energy can no longer be found by an expression directly analogous to (7.18) because M_s does not bear the identical relationships to H'_z and H'_x over the entire platelet. This

is illustrated in FIG.(7.9).

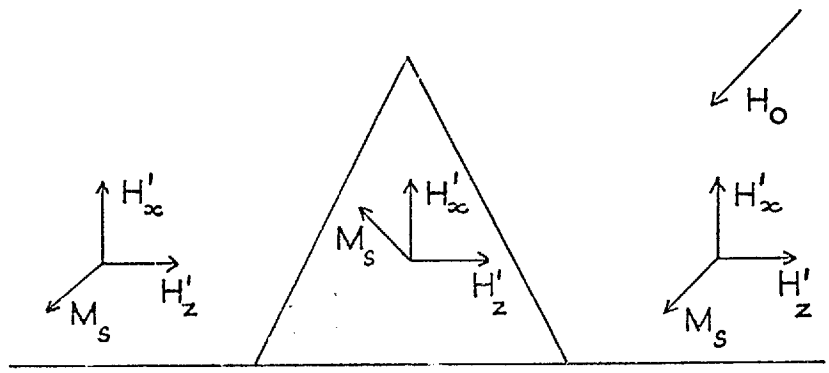

FIG.(7.9) RELATIONSHIP BETWEEN M_s AND FIELD

For locations outside the spikes the total magnetostatic energy is

$$E_{H'} = \tfrac{1}{2}\mu_o \sum_{\substack{x \\ \text{outside} \\ \text{spikes}}} \sum_{z} \left[M_s H'_z(z,x) \cos 135 + M_s H'_x(z,x) \cos 135 \right] \delta z \, \delta x \qquad (7.23)$$

and for locations inside the spikes

$$E_{H'} = \tfrac{1}{2}\mu_o \sum_{\substack{x \\ \text{inside} \\ \text{spikes}}} \sum_{z} \left[M_s H'_z(z,x) \cos 135 + M_s H'_x(z,x) \cos 45 \right] \delta z \, \delta x$$

By adding together these two expressions for the areas where each is appropriate the total magnetostatic energy of the platelet is obtained. This is the value appropriate for a platelet with a given edge distribution and spikes defined by parameters ω and L, where the values for ω correspond to the chosen edge distribution.

Other terms in this expression for the total energy of the platelet are more easily calculated. The applied field energy $\int \underline{M}_s . \underline{H}_o \, d\tau$ is constant over the entire volume of a saturated platelet. When spikes are formed the magnetisation within the spikes lies normal to the applied field, and thus $\underline{M}_s . \underline{H}_o = 0$ in these regions. This can

be seen in FIG.(7.9). The effective volume over which $\underline{M}_s \cdot \underline{H}_o = M_s H_o$ is taken as the volume of the platelet excluding the volume of the spike domains.

The wall energy can easily be calculated as the product of the total spike wall area and the assumed energy density of these walls. For convenience this energy density is taken as 1 erg/cm^2.

The anisotropy energy of the platelet does not effectively change with the presence of the spike domains because the magnetisation remains in the same relative orientation to the <111> directions.

A computer program was written which enabled the applied field, the magnetostatic and the domain energies to be calculated for a given spike distribution present in the platelet.

One investigation has considered a trapezoidal platelet with base 150 μm, width 50 μm, and thickness 0.2 μm, containing 10 spikes of base width 2 μm on the <100> faces. The computer program evaluated the energy contributions to the total energy of the platelet as the length of these spikes changed from 1 to 20 μm. The variation of the various terms with spike length are shown in FIG.(7.10) for an applied field of 15 oe.

The magnitude of the applied field energy decreased as the length of the spikes increased because a smaller volume of the platelet had magnetisation lying along the field direction. The wall energy showed an expected linear increase with spike length and the magnetostatic energy a decrease which was only linear above 8 μm length. The resulting value for the total energy showed a slow change with length and a shallow minimum at about 3 μm.

Comparison can be made here with FIG.(7.1 b) where, for an almost identical field, the spikes had an observed average length of about 7 μm. Two factors may account for this difference. The photograph shows a slightly greater number of spike domains and the

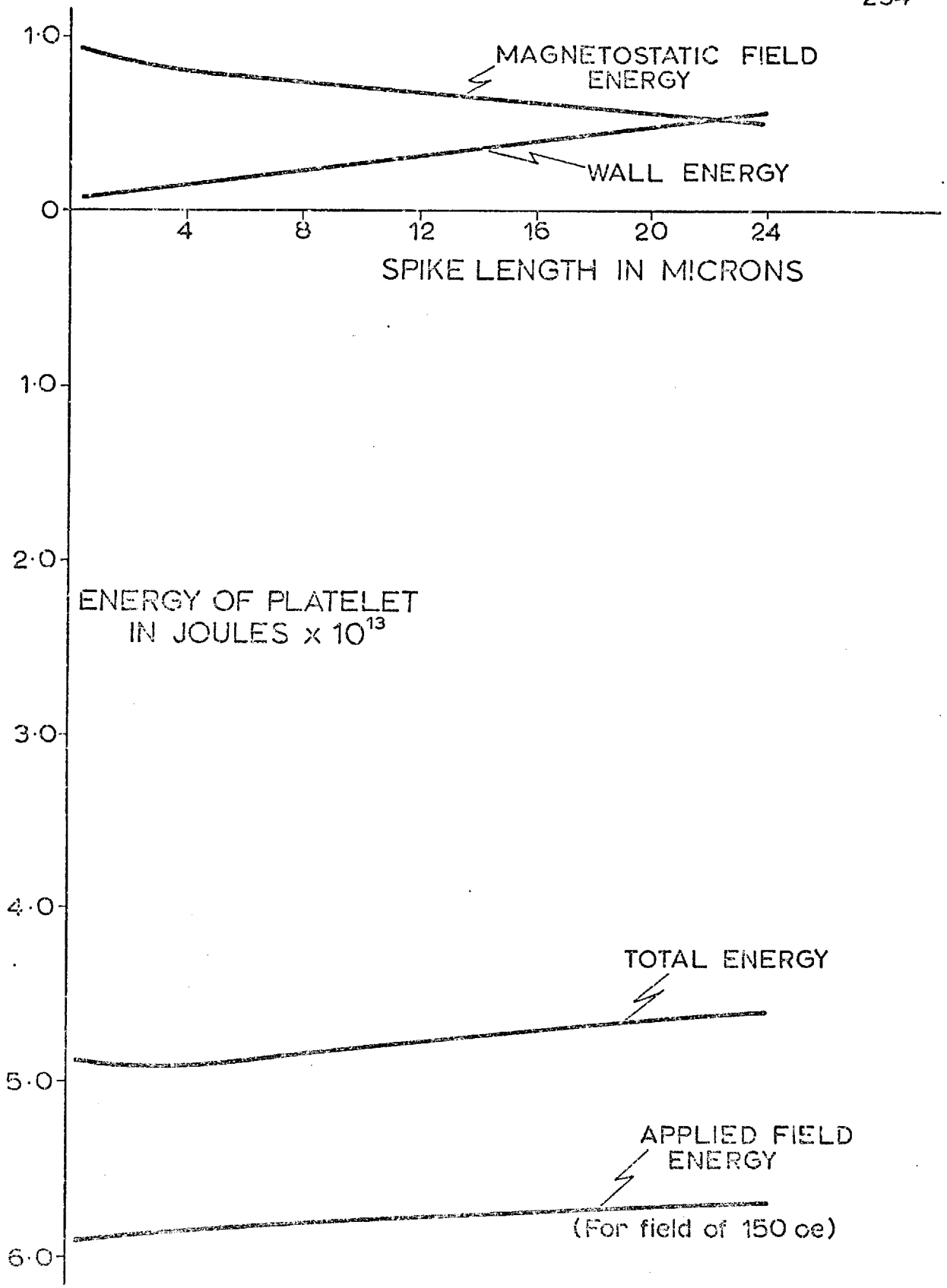

Fig. (7·10) Energy of platelet as function of spike length

presence of these might displace the position of the energy minimum. In addition the colloid particles between the spikes are seen to have collected over the edges of the platelet itself, suggesting a possible rotation of the magnetisation out of the platelet plane. To incorporate this effect local anisotropy energy changes would also have to be calculated. This would be difficult, but their omission may account for the difference between the two results.

Several precautions had to be taken during computation to ensure that no evaluations of the magnetostatic fields were made at locations on or very near to the spike walls. Due account was also taken in the summations of the difference in the magnetostatic field energies inside and out of the spikes, following equation 7.23 and FIG.(7.9).

The base widths of the spikes were chosen and then two parameters external to the computer program remained to be fixed, the wall energy of the spike walls and the value of the applied field. If these were kept within the limits of reasonable expectation the minimum in the total energy remained shallow, as shown in FIG.(7.10). This small change makes an investigation of the energy changes associated with the relative changes in spike lengths with field, as seen in FIG.(7.1), a dubious proposition.

The physical interpretation of FIG.(7.10) is of an interchange of magnetostatic energy with wall energy in the platelet as the spikes increase in length. This shift is recorded in the overall energy changes within the platelet. However, the change is localised and becomes masked by the larger volume of the platelet which remains virtually unaffected by these changes. It will be recalled from FIG.(7.6) that although at 3 μm from the edge the average internal field in a platelet with reversed domains was substantially lower than in a saturated platelet, at 8 μm. this difference was much less. This suggests that if an explanation of the spike domain behaviour in FIG.(7.1) is to be sought from an energy stand point attention should be paid to the local energy changes occurring near the platelet edge

rather than searching for a minimum in the overall free energy of the platelet.

Domains were introduced in Chapter I as being the result of two opposing requirements in a magnetic body. Their presence enables the total magnetic free energy to be reduced to a minimum value while maintaining low exchange, anisotropy and magnetostatic energy simultaneously. FIG.(7.1) shows some of the simplest domain configurations that have ever been observed, yet the mathematical analysis of the behaviour of these spikes by a consideration of the free energy is not straightforward.

It is stressed that this work is incomplete but the indications are that it might be more informative to consider the energy changes occurring in restricted regions or else to work in terms of the field forces acting between the spike domain walls in the platelet.

CHAPTER 8

CONCLUSIONS

8.1 SUMMARY

In Chapters 5 and 6 of this thesis observations on the domain properties of ferromagnetic crystals have been reported. In negative anisotropy platelets with (100) faces the domain structure is critically dependent on crystal thickness. At thicknesses less than 4000 Å planar domain configurations exist, but with increasing thickness the anisotropy, with easy axes in the <111> directions, becomes increasingly important. Structures in these thicker platelets thus arise from a balance, mostly between the anisotropy and magnetostatic energies, and form the stripe patterns discussed in Chapter 6.

The small size of these platelets causes their behaviour to be substantially influenced by the magnetostatic fields arising from the edges of the platelets. It is this same demagnetising field that accounts for the nature of the virgin domain structure, and the formation of echelon structures on <100> edges in negative anisotropy platelets or <110> edges on positive anisotropy platelets. In platelets with low anisotropy the magnetostatic energy becomes relatively more important and wall structures form in configurations which avoid the formation of any edge fields, and for this reason sometimes adopt unusual angles.

The degree of perfection of the platelets is high and, unless the platelets have been damaged in some way, structural considerations can be ignored when considering the movement of domain walls. Quasi-

static field observations show that saturation of a platelet by an in plane easy axis field is achieved almost exclusively by domain wall motion. The shape of the M against H plot shows that the behaviour of the platelet is largely controlled by the demagnetising field, making the final approach to saturation slow. Under a hard axis field wall motion first occurs by domains with a magnetisation component in the field direction growing at the expense of those with only a component in the reverse direction. However, above about 10 oe rotation begins to occur making the measurement of M against H plots from the domain areas impossible for the hard axis fields.

Very seldom has it been possible to give a quantitative interpretation of the observed behaviour because of the impossibility of obtaining an expression for the magnetostatic energy. An exception to this is the observations made on an induced Néel strip structure in a long rectangular platelet where the longitudinal demagnetising field could be easily calculated. The evaluation of magnetostatic energies and its possible application to explain some of the behaviour observed in platelets was outlined in Chapter 7. Situations of interest in this work often cannot be treated in analytic terms and the application of numerical methods has been suggested. The calculation of the magnetic excitation for a given situation by this method is comparatively simple, but rather inflexible in coping with changing domain structures, thus limiting its own application.

Magnetisation situations of interest which exist in observed platelet behaviour are usually too complex to enable a micromagnetic approach to be adopted. Alternatively the domain approach, and the numerical treatment of the magnetostatic field do not consider non-uniform magnetisation rotations and are thus often erroneous in their predictions. The magnetic energies in a platelet can often be very locally distributed as was seen in Chapter 7, making the quantitative interpretation of behaviour difficult, except in specialised cases.

In Chapter 5 the wall structures which exist in the platelets

and their variation with thickness and composition are seen to be more prolific and complex than the variation encountered in thin films. In the thickness range in which these variations are seen the differing wall structures must have very similar energies. Bloch lines play an important part, both in the initial formation of the domain structure and in the complexities that exist in the walls themselves where transitions between wall types occur. Of particular interest is the bright meta-stable wall structure which is frequently seen in the virgin domain structures, see for example FIG.(5.4). Its structure is still uncertain.

Many of the remarks made above on the behaviour of domains in thin platelets also apply to thicker platelets, where an additional complication is added by an oscillation of the magnetisation about the plane of the platelet. This decreases the anisotropy energy but at the same time establishes a vertical magnetostatic field. In the transition from planar to stripe configurations several types of oscillation exist, which are to a certain extent functions of platelet thickness. For example, the TYPE II stripe oscillations are only seen at the bottom of the thickness range. However, great similarities exist in the structures in platelets 6000 Å thick, and those an order of magnitude thicker at 6 μm. This suggests that the TYPE III structure thought to exist over this range is stable and is largely controlled by the anisotropy energy. Many details of behaviour were seen in Chapter 6 which are not adequately explained and a quantitative model is required for the TYPE III structure.

Finally, reference is made to Chapter 3 where the production of these platelets was considered. The bromide of the required metal alloy is placed in a wet dilute stream of hydrogen, where it is reduced to give tiny platelets of the metal itself. To obtain the platelet growth habit a low supersaturation is required to suppress two dimensional nucleation. This is obtained by using a low transport rate by careful choice of the reactions used. An analysis of the

thermodynamics of the possible transport reactions within this system corroborates the experimental findings. The growth mechanism of the platelet habit is difficult to explain but it would seem that, especially in the case of the triangular platelets, it is coupled with the growth of whiskers by a screw dislocation mechanism.

8.2 POSSIBLE DEVELOPMENTS

The small size of these platelets and the difficulty of their growth restricts any technological application and outweighs advantages otherwise gained from their perfection. An extension of the range of compositions investigated might be interesting, but is limited by difficulties of crystal growth. If this is confined to the current process, permalloy compositions can be produced but the number of independent parameters affecting growth is high, hence reproducibility is difficult to achieve. Alternative processes for producing platelets will be worth investigating in a search for a simpler system if the platelets are required in any number. The very nature of their non-epitaxial production which gives the platelets their high perfection is a severe disadvantage in any possible application.

As an extension of the present work further observations on the occurrence and behaviour of stripe domains are obviously required. In this direction, work was started towards adding the facility of applying magnetic fields normal to the platelet plane, during observations in the optical microscope. The effect of a vertical field should give further information on the magnetisation distribution within the stripe pattern. It might be useful to confirm by torque magnetometry whether the anisotropy values are as expected, but this may prove difficult with the small volume of material and the large shape anisotropy. In addition there is no underlying physical reason why any other anisotropy should exist.

The lack of a quantitative model to adequately explain the

behaviour of the stripe domains was evident in discussions in Chapter 6. A micromagnetic calculation based on the TYPE III stripes would be most interesting. However, reference to other similar calculations shows that this would not be easy and in any case a more detailed knowledge of the structure, in the form of a phenomenalogical model is needed before this can be attempted.

This additional information might come from the use of Lorentz microscopy together with low angle diffraction techniques. This, by necessity, will have to be done with high energy electron beams. Typical examples of the operation of the Cavendish 750 kV microscope in the Foucault and Fresnel mode are seen in FIG.(8.1).

The tip of a triangular nickel platelet is seen in FIG.(8.1a). The presence of a possible whisker thickening down one edge is clearly visible, as are other structural features which have not yet been explained. The whisker edge is a [110] edge and the other thought to be a [120] edge. The abrupt join to a [100] edge is seen in FIG.(8.1b), taken on the same platelet. The domain patterns of (a) and (b) do not correlate with those familiar from colloid work and are rather similar to the domains seen in uniaxial polycrystalline films. The change in pattern could result from strain present in the platelet, arising during mounting, or from the effect of vertical fields from the microscope objective lens. This latter case is thought to be more likely and the presence of this field could make Lorentz observations misleading.

A further illustration of this is seen in FIG.(8.1c) which shows the presence of reversed spikes of magnetisation at the edge of a platelet. The micrograph was taken with the microscope operated in the Fresnel mode and a field of 45 oe applied in the platelet plane. The magnetisation in the spikes is reversed by about 180° and thus shows a greater similarity with formations in uniaxial films than with the 90° spikes seen on platelets with the Bitter colloid technique, for example FIG.(7.1).

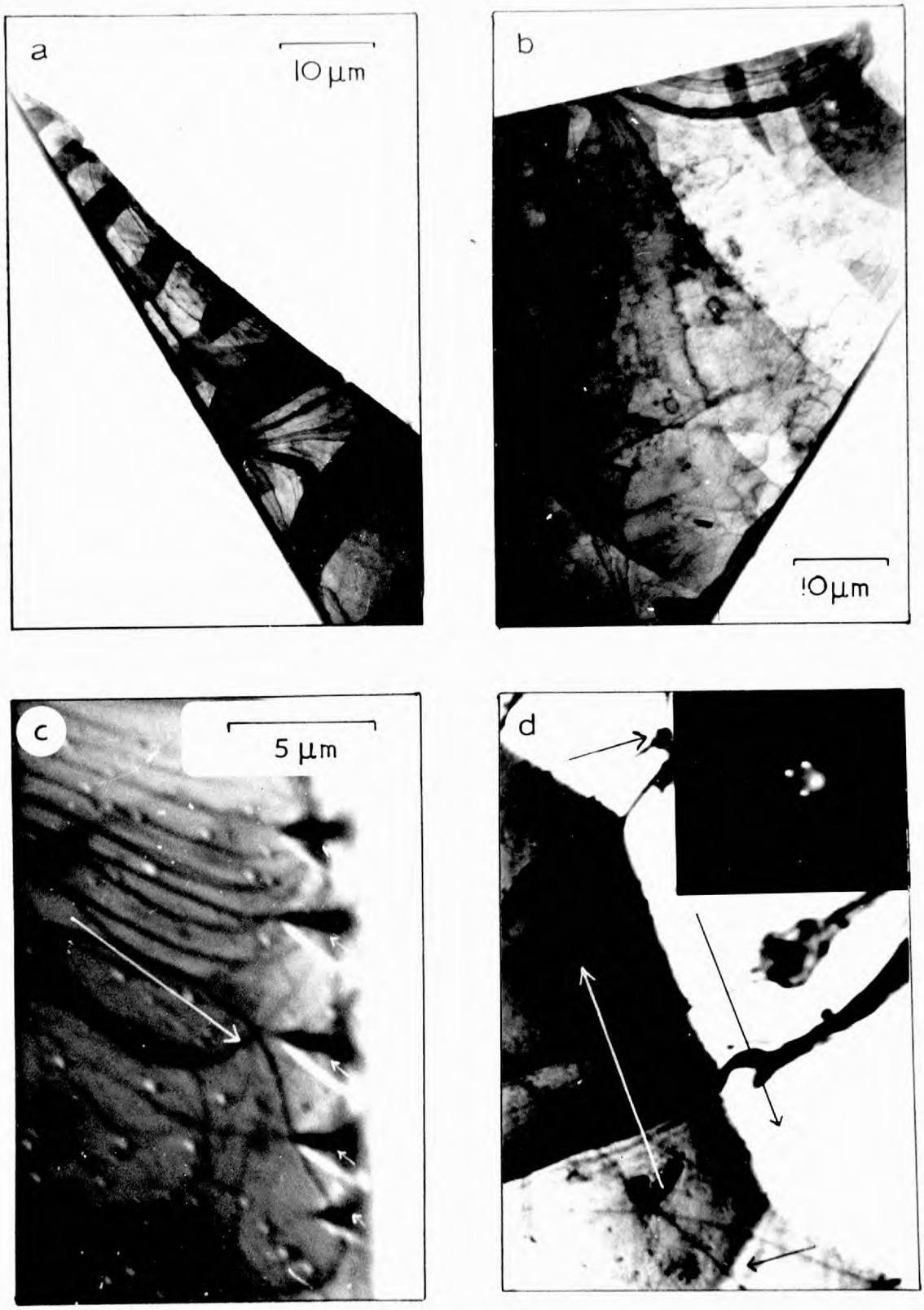

Fig. (8.1) High voltage Lorentz Micrographs from platelets

Finally, an area showing the flux closure circulation of the magnetisation is seen in FIG.(8.1d). This was taken in the Foucault mode and inset is seen the diffraction pattern produced by the magnetic splitting of the centre spot by the four domains in this area of the platelet.

Electron microscopy may also be useful in giving some guide to the structure of the meta-stable intermediate walls. It is possible to compare the electron beam intensity distribution measured at the photographic plate with that expected from the transmission of an electron beam through a given structure. The comparison of the observed distribution with one calculated from a theoretical model would provide a good check on the model itself, although this is not easy. A similar treatment could also be applied to walls in thinner platelets.

APPENDIX A

Calculation of the energy of a 180° wall in the (110) plane of a thin film with negative cubic magnetocrystalline anisotropy

(1) Bloch Wall

FIG (A.1) shows the co-ordinate system used for the calculation.

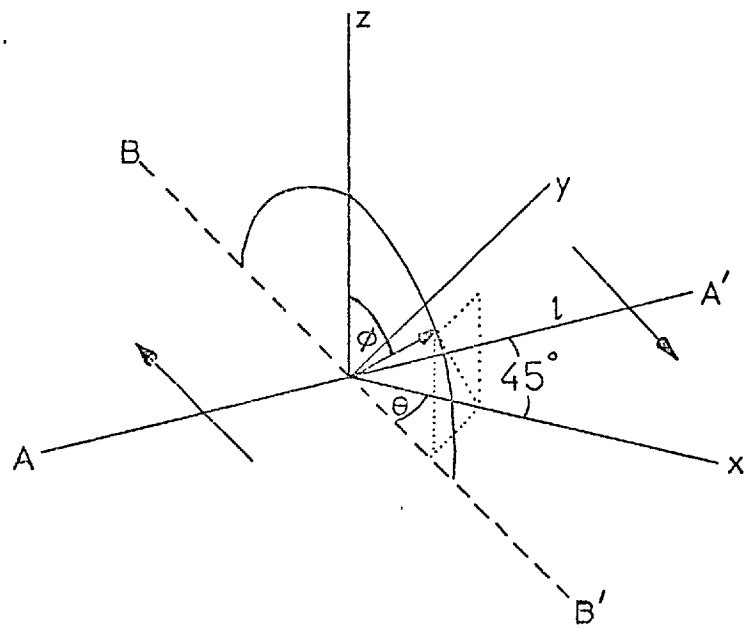

FIG (A.1)

The wall is considered to extend from $l = -\frac{a}{2}$ to $l = +\frac{a}{2}$ along the axis AA' shown.

From FIG (A.1) we can express the direction cosines of the M vector in terms of the angles θ and Ø:

$$\alpha_1 = \sin \phi \cos \theta$$

$$\alpha_2 = -\sin \phi \sin \theta$$

$$\alpha_3 = \cos \phi$$

M remains in the BB'Z plane, angled such that $\theta = \pi/4$ always.

Thus, ignoring K_2, the anisotropy energy can be written as:

$$E_K = \frac{K_1}{4} (\sin^4 \phi + \sin^2 2\phi)$$

This can be averaged over the wall width:

$$\frac{1}{a} \cdot \frac{K_1}{4} \int_{-a/2}^{a/2} (\sin^4 \phi + \sin^2 2\phi) \, dl = + \frac{7K_1}{32}$$

The expressions for exchange and magnetostatic energy will be identical with the expressions for a Bloch wall in a uniaxial thin film (Middelhoek 1961).

Thus we can write:

$$\gamma_{B\pi} = A(\frac{\pi}{a})^2 a + \frac{7}{32} K_1 a + \frac{\pi a^2}{(a + t)} M_s^2$$

which is equation (1.23).

(2) Néel Wall

FIG (A.2) shows the co-ordinate system used for the calculation.

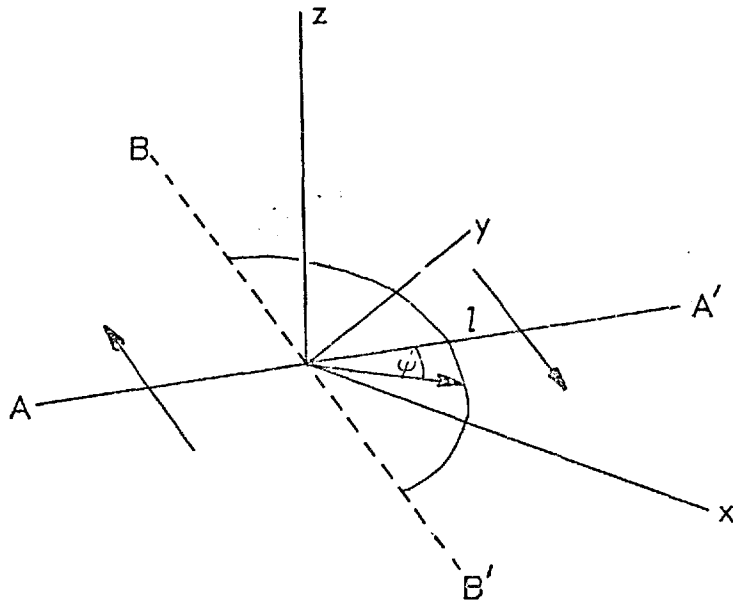

FIG (A.2)

Again the wall is considered to extend from $l = -\frac{a}{2}$ to $l = +\frac{a}{2}$ along the axis AA' shown.

$\emptyset$ is re-defined from the Bloch wall case as seen in FIG (A.2) and now the direction cosines of the $\underline{M}$ vector become:

$$\alpha_1 = \cos(45 - \emptyset)$$

$$\alpha_2 = \cos(45 + \emptyset)$$

$$\alpha_3 = 0$$

M remains in the BB'AA' plane.

Again, ignoring K_2 the anisotropy energy can be written as:

$$E_K = \frac{K_1}{4}(\cos^2 2\emptyset)$$

This is averaged over the wall width:

$$\frac{1}{a} \cdot \frac{K_1}{4} \int_{-a/2}^{a/2} \cos^2 2\phi \, dl = \frac{K_1}{8}$$

And, as before, the expressions for exchange and magnetostatic energy are identical with those of a Néel wall in a uniaxial thin film.

Hence:

$$\gamma_{N\pi} = A\left(\frac{\pi}{a}\right)^2 a + \frac{1}{8} K_1 a + \frac{\pi a t}{(a + t)} M_s^2$$

which is equation (1.24).

APPENDIX B

Preparation of colloidal magnetite (Bitter Colloid)

The method used in the production of colloid for the work reported in this thesis is given. The important points are underlined.

3 gms of hydrated $FeCl_3$ and 1.54 gms of hydrated $FeSO_4$ were dissolved in distilled water and the total volume of solution made up to 150 ml. 2.5 gms of NaOH were dissolved in 50 ml of distilled water and the solution brought to the boil.

The iron solution was stood between the poles of a 1.5 Kgauss permanent magnet and heated. The NaOH solution was allowed to drip in slowly while the solution was constantly stirred.

A dense brown-black precipitate formed

$$FeSC_4 + 2NaOH \longrightarrow Fe(OH)_2 + Na_2SO_4$$

$$FeCl_3 + 3NaOH \longrightarrow Fe(OH)_3 + 3NaCl$$

$$Fe(OH)_2 + 2Fe(OH)_3 \longrightarrow \downarrow Fe_3O_4 + 4H_2O$$

The solution was now boiled, whilst remaining in the magnetic field. This accelerates the ageing and polarises the chains as mentioned in the text. Boiling might continue for $\frac{1}{2}$, 1 or 2 hours.*

Boiling was stopped, the solution allowed to separate out and then decanted. Distilled water was added to the precipitate which

---

*The two colloids used in this work had had 1 and 2 hour boils.

was stirred so that all was thoroughly washed. It was again allowed to settle and then decanted and rewashed, the process being repeated three times. The pH of the last rinse was very carefully adjusted to pH5 by the addition of N/100 HCl.

The time required to settle the solution increased markedly with each rinse. In this respect it was found advantageous to stand the beaker above an inhomogeneous magnetic field so that magnetic as well as gravitational forces caused settling.

After the last rinse the slurry was added to 1 litre of $\frac{1}{2}\%$ Teepol solution with pH 5.0-5.2. This slurry was dispersed into a colloidal form by stirring with a 1" diameter paddle for several minutes at 4000 r.p.m. The solution was allowed to settle overnight in a weak magnetic field. If the process had behaved well a black colloid would remain above any settling which occurs. This colloid turns to a claret colour as oxidation occurs, and after a day or two can be used for domain observations.

APPENDIX C

Calculation of Equilibrium Domain Configuration in a Néel Block

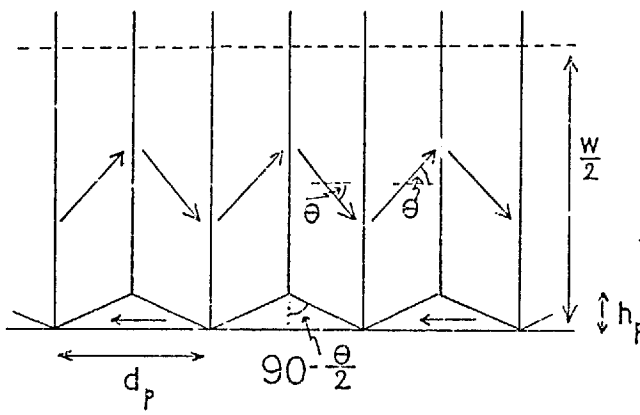

A Néel Block with only reversed 'p' closure domains
Length, L; Width, W; Thickness, t.

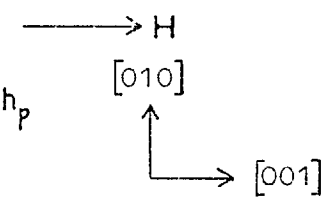

With the application of a magnetic field in the [001] direction the magnetisation turns away from the <110> directions rotating against the magnetocrystalline anisotropy to make an angle θ with the [001] axis. The rotation is assumed to be such that the normal component of magnetisation remains continuous across the boundary.

Magnetic energy in the main domains

$$E = K_1 \cos^2\theta \sin^2\theta - M_s H \cos\theta$$

$$= \frac{K_1}{4} \sin^2 2\theta - M_s H \cos\theta$$

$$\frac{\partial E}{\partial \theta} = K_1 \sin 2\theta \cos 2\theta + M_s H \sin\theta$$

$$= 0 \text{ when E reaches a minimum value, giving}$$

$$M_s H = -2K_1 \cos\theta \cos 2\theta \qquad (C.1)$$

The energy minimum is then

$$E_{min} = \frac{K_1}{4} \sin^2 2\theta + 2K_1 \cos^2\theta \cos 2\theta$$

$$= K_1 \cos^2\theta(2-3 \sin^2\theta)$$

Free-pole effects at the edges are reduced by the formation of 'p' closure domains, again with the normal component of magnetisation continuous across the boundary.

The energy/unit volume of the 'p' closure domain is

$$K_1 \cos^2 \frac{\pi}{2} \cos^2 0 + M_s H = M_s H = - 2K_1 \cos\theta \cos 2\theta$$

Hence the energy of formation of the 'p' domains/unit volume is

$$E_p = - 2K_1 \cos\theta \cos 2\theta - K_1 \cos^2\theta \, (2-3 \sin^2\theta)$$

which simplifies to

$$E_p = - K_1 \cos\theta \, (\cos\theta + 1)^2(3 \cos\theta - 2) \qquad (C.2)$$

The dimensions of the closure domains are d_p, t and

$$h_d = \tfrac{1}{2} d_p \cos(90 - \frac{\theta}{2}) = \tfrac{1}{2} d_p \tan\frac{\theta}{2} = \frac{\tfrac{1}{2} d_p \sin\theta}{(1 + \cos\theta)}$$

and hence the volume of these domains is

$$v_p = \tfrac{1}{2} d_p h_p t = \frac{\tfrac{1}{4} d_p^2 t \sin\theta}{(1 + \cos\theta)}$$

hence the energy of formation of a closure domain is

$$E_p v_p = \frac{- d_p^2 t \sin\theta K_1 \cos\theta \, (\cos\theta + 1)^2(3 \cos\theta - 2)}{4(\cos\theta + 1)}$$

$$= d_p^2 t K_p \quad \text{where } K_p = - \tfrac{1}{8} K_1 \sin 2\theta(\cos\theta + 1)(3 \cos\theta - 2)$$

The total energy of the Néel block/unit area of section t d_p is

$$E_N = \frac{1}{t d_p}\left[2\,\gamma\omega\, t + 2 d_p^{\,2}\, t\, K_p + \omega\, d_p t\, K_1 \cos^2\theta(2-3\sin^2\theta)\right]$$

where γ is the wall energy density, and assuming $\omega \gg d_p$ so that the closure domain walls are neglected.

$$\frac{\partial E_N}{\partial d_p} = -\frac{2\gamma\omega}{d_p^{\,2}} + 2K_p$$

which reaches a minimum when $\frac{\partial E_N}{\partial d_p} = 0$

i.e. when $d_p^{\,2} = \frac{\gamma\omega}{K_p}$

resubstituting, the equilibrium value for d_p is given by

$$d_p^{\,2} = \frac{-8\gamma\omega}{K_1 \sin 2\theta\,(\cos\theta + 1)(3\cos\theta - 2)} \qquad (C.3)$$

APPENDIX D

Rotation of Type III Stripe Domains under Applied Fields

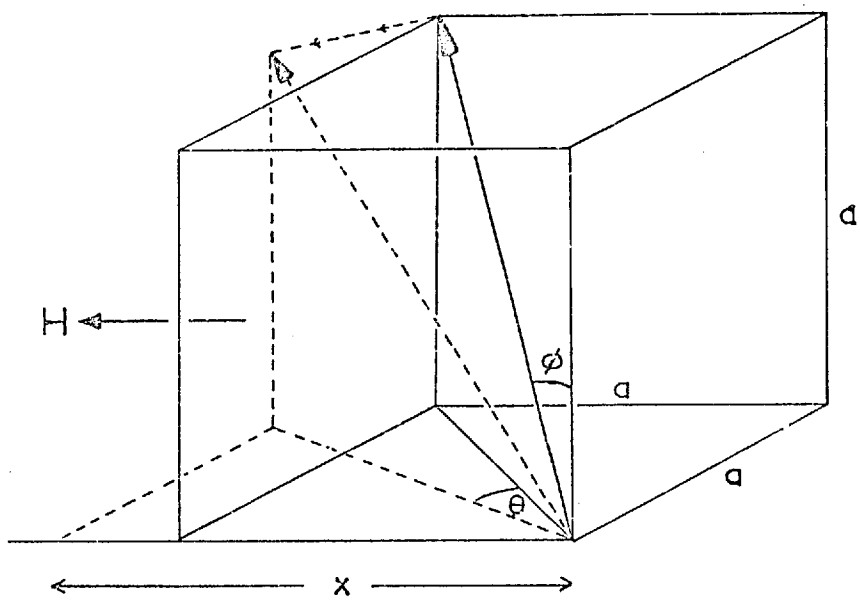

For the purpose of this calculation the presence of any non <111> direction magnetisation components from the oscillation of the magnetisation towards different <111> directions is ignored. Initially it is assumed to all lie in the [111] direction and the application of a [100] axis field causes the magnetisation to rotate towards the plane containing this direction, but with the angle ϕ remaining constant.

It will be noticed that $\cos \phi = \alpha_3 = \frac{1}{\sqrt{3}}$

where α_1, α_2 and α_3 are the direction cosines of the magnetisation.

The anisotropy energy/unit volume is expressed as

$$E_K = K_1(\alpha_1^2\alpha_2^2 + \alpha_2^2\alpha_3^2 + \alpha_3^2\alpha_1^2) + K_2(\alpha_1^2\alpha_2^2\alpha_3^2) + \ldots\ldots$$

which using $\alpha_3^2 = \frac{1}{3}$ simplifies to

$$E_K = K_1\left[\alpha_1^2\alpha_2^2 + \frac{1}{3}(\alpha_1^2 + \alpha_2^2)\right] + \frac{1}{3}K_2\alpha_1^2\alpha_2^2$$

But $\sum_{i=1}^{3} \alpha_i^2 = 1$ hence $\alpha_1^2 + \alpha_2^2 = \frac{2}{3}$

$$E_K = (K_1 + \frac{1}{3}K_2)\,\alpha_1^2\alpha_2^2 + \frac{2}{9}K_1$$

$$= -(K_1 + \frac{1}{3}K_2)(\alpha_1^4 - \frac{2}{3}\alpha_1^2) + \frac{2}{9}K_1 \qquad (D.1)$$

The projected angle of rotation is given by θ

where $\cos(\frac{\pi}{4} - \theta) = \frac{x}{a\sqrt{2}}$

thus $\alpha_1 = \frac{x}{a\sqrt{3}} = \sqrt{\frac{2}{3}}\cos(\frac{\pi}{4} - \theta)$

and $\alpha_2 = \sqrt{\frac{2}{3}}\sin(\frac{\pi}{4} - \theta)$

Hence E_K can be expressed in terms of this angle as

$$E_K = -(K_1 + \frac{1}{3}K_2)\left[\frac{4}{9}\cos^4(\frac{\pi}{4} - \theta) - \frac{4}{9}\cos^2(\frac{\pi}{4} - \theta)\right] + \frac{2}{9}K_1$$

Differentiating this expression with respect to θ we get

$$\frac{\partial E_K}{\partial \theta} = -\frac{4}{9}(K_1 + \frac{K_2}{3})\left[4\cos^3(\frac{\pi}{4} - \theta)\sin(\frac{\pi}{4} - \theta) - 2\cos(\frac{\pi}{4} - \theta)\sin(\frac{\pi}{4} - \theta)\right]$$

which simplifies to

$$\frac{\partial E_K}{\partial \theta} = -\frac{2}{9}\left(K_1 + \frac{K_2}{3}\right) \sin 4\theta \qquad (D.2)$$

With the field along the [100] axis in the plane of the platelet, the torque exerted on M due to the field is

$$\underline{M} \wedge \underline{H} = M H \alpha_1$$

$$= \sqrt{\frac{2}{3}}\, M H \sin\left(\frac{\pi}{4} - \theta\right) \qquad (D.3)$$

But $$\frac{\partial E_K}{\partial \theta} = \underline{M} \wedge \underline{H}$$

hence

$$-\frac{2}{9}\left(K_1 + \frac{K_2}{3}\right) \sin 4\theta$$

$$= \sqrt{\frac{2}{3}}\, M H \sin\left(\frac{\pi}{4} - \theta\right)$$

using the values for K_1 and K_2 cf Franse and De Vries (1968) quoted in Chapter 1. This equation reduces to

$$H = \frac{36.5 \sin 4\theta}{\sin\left(\frac{\pi}{4} - \theta\right)} \qquad (D.4)$$

REFERENCES

AHARONI, A. Rev. Mod. Phys. 34 227 (1962a).

AHARONI, A. J. Appl. Phys. 33 1324 (1962b).

AHARONI, A. J. Appl. Phys. 37 3271 (1966a).

AHARONI, A. J. Appl. Phys. 37 4615 (1966b).

AHARONI, A. J. Appl. Phys. 38 3196 (1967).

AHARONI, A. J. Appl. Phys. 39 861 (1968).

AHARONI, A. and NEEMAN, E. Phys. Lett. 6 241 (1963).

ALCOCK, C.B. and JEFFES, J.H.E. Trans. Instn. Min. Metall. 76 C246 (1967).

ALLAN, W.J. and WEBB, W.W. Acta. Met. 7 646 (1959).

ANDRÄ, W. Ann. Phys. Leipzig 17 233 (1956a).

ANDRÄ, W. Ann. Phys. Leipzig 17 78 (1956b).

ARGYRES, P.N. Phys. Rev. 97 334 (1955).

AUBERT, G. J. Appl. Phys. 39 504 (1968).

BACIGALUPI, J.J. J. Appl. Phys. 34 999 (1963).

BALTZ, A. J. Appl. Phys. 37 1485 (1966).

BANBURY, J.R. and NIXON, W.C. J. Sci. Inst. 44 889 (1967).

BARKHAUSEN, H. Phys. Zeits. 20 401 (1919).

BARNETT, M.E. and NIXON, W.C. J. Sci. Inst. 44 893 (1967).

BASTERFIELD, J. and PRESCOTT, M.J. J. Appl. Phys. 38 3190 (1967).

BATES, L.F. Proc. Phys. Soc. 84 625 (1964).

BATES, L.F. and SPIVEY, S. Brit. J. Appl. Phys. 15 705 (1964).

BERGMAN, W.H. Z. Ang. Phys. 8 559 (1956).

BEYERSDORF, K. Glas und Hochvakuum Technik 2 8 (1952).

BHIDE, V.G. and SHENOY, G.K. J. Appl. Phys. 34 1778 (1963).

BIRSS, R.R. Adv. in Phys. 8 252 (1959).

BITTER, F. Phys. Rev. 38 1903 (1931).

BLACKBURN, W.J.S. and FERRIER, R.P. J. Appl. Phys. 39 1163 (1968).

BLACKMAN, M. and GRUNBAUM, E. Proc. Roy. Soc. A241 508 (1957).

BLOCH, F. Z. Physik. 74 295 (1932).

BLOIS, M.S. J. Appl. Phys. 26 975 (1955).

BLOOR, D. and MARTIN, D.H. Proc. Phys. Soc. 73 695 (1959).

BOBECK, A.H., FISCHER, R.F. and PERNESKI, A.J. I.E.E.E. Trans. MAG 5 544 (1969).

BOERSCH, H., HAMISCH, H., WOHLLEBEN, D. and GROHMANN, K. Z. Physik 164 55 (1961).

BOERSCH, H., HAMISCH, H., GROHMANN, K. and WOHLLEBEN, D. Z. Physik 167 72 (1962).

BOERSCH, H. and LAMBECK, M. Z. Phys. 177 157 (1964).

BONGERS, P.F. I.E.E.E. Trans. MAG 5 472 (1969).

BONSE, U., HART, M. and NEWKIRK, J.B. Advances in X-Ray Analysis 10 1 (1967).

BOURRET, A. and DAUTREPPE, D. Phys. Stat. Sol. 13 559 (1966).

BOURRET, A. and KLEMAN, M. Phys. Stat. Sol. 23 207 (1967).

BOZORTH, R.M. Ferromagnetism, Van Nostrand (1951).

BRENNER, S.S. Acta. Met. 4 62 (1956).

BRENNER, S. and SEARS, G.W. Acta. Met. 4 268 (1956).

BROWN, W.F. Rev. Mod. Phys. 17 15 (1945).

BROWN, W.F. Magnetostatic Principles in Ferromagnetism, North Holland (1962a).

BROWN, W.F. J. Appl. Phys. 33 3022 (1962b).

BROWN, W.F. Micromagnetics, Interscience, J. Wiley (1963).

BROWN, W.F. and LA BONTE, A.E. J. Appl. Phys. 36 1380 (1965).

BUCKLEY, H.E. Crystal Growth, J. Wiley, N.Y. (1951).

BURTON, W.K., CABRERA, N. and FRANK, F.C. Phil. Trans. Roy. Soc. A243 299 (1951).

CALLEN, E. J. Appl. Phys. 39 519 (1968).

CAREY, D. and ISAAC, E.D. Magnetic Domains and Techniques for their Observation, E.U.P. (1966).

CASTAING, R. and DESCAMPS, J. J. Phys. Rad. 16 304 (1955).

CECH, R.E. Acta. Met. 7 787 (1959).

CECH, R.E. Acta. Met. 9 459 (1961).

CHANG, H. and FETH, G.C. I.E.E.E. Trans. Communications & Electronics 83 706 (1964).

CHANG, H. and LIN, Y.S. I.E.E.E. Trans. MAG 3 653 (1967).

CHIKAWA, J. and NAKAYAMA, T. J. Appl. Phys. 35 2493 (1964).

CHIKAZUMI, S. Physics of Magnetism, J. Wiley (1964).

COHEN, M.S. J. Appl. Phys. 33 2968 (1962).

COHEN, M.S. I.E.E.E. Trans. MAG 1 156 (1965).

COHEN, M.S. J. Appl. Phys. 38 4966 (1967).

COHEN, M.S. Chapter X, Thin Film Phenomena, ed. Chopra, K.L., McGraw Hill (1969).

COLEMAN, R.V. Met. Rev. 9 261 (1964).

COLEMAN, R.V. and CABRERA, N. J. Appl. Phys. 28 1360 (1957).

COLEMAN, R.V. and SCOTT, G.G. Phys. Rev. 107 1276 (1957).

COLEMAN, R.V. and SCOTT, G.G. J. Appl. Phys. 29 526 (1958).

COLEMAN, R.V. and SEARS, G.W. Acta. Met. 5 131 (1957).

COOPER, R.W., PEARSON, R.F., VAN HEEK, H. and PAGE, J.L. I.E.E.E. Trans. MAG 5 472 (1969).

COSSLETT, V.E. Contemp. Phys. 9 333 (1968).

CRAIK, D.J. Proc. Phys. Soc. B69 647 (1956).

CRAIK, D.J. Contemp. Phys. 11 65 (1970).

CRAIK, D.J. and GRIFFITHS, P.M. Proc. Phys. Soc. B70 1000 (1957).

CRAIK, D.J. and GRIFFITHS, P.M. Brit. J. Appl. Phys. 9 279 (1958).

CRAIK, D.J. and McINTYRE, D.A. Proc. Roy. Soc. A302 99 (1967).

CRAIK, D.J. and TEBBLE, R.S. Ferromagnetism & Ferromagnetic Domains, North-Holland (1965).

CROWTHER, T.S. and COHEN, M.S. J. Appl. Phys. 38 3 (1967).

DE BLOIS, R.W. J. Appl. Phys. 36 1647 (1965).

DE BLOIS, R.W. J. Vac. Sci. & Tech. 3 146 (1966).

DE BLOIS, R.W. General Electric Report AFCRL-67-0107 (1967).

DE BLOIS, R.W. General Electric Report AFCRL-68-0414 (1968a).

DE BLOIS, R.W. J. Appl. Phys. 39 442 (1968b).

DE BLOIS, R.W. and BEAN, C.P. J. Appl. Phys. 30 S 225 (1959).

DE BLOIS, R.W. and GRAHAM, C.D. J. Appl. Phys. 29 931 (1958).

DEY, S.K., BOWMAN, H.J. and BOOTH, A.D. J. Phys. E. (J. Sci. Inst.) 2 162 (1969).

DI CHEN J. Appl. Phys. 38 1309 (1967).

DIETZE, H.D. and THOMAS, H. Z. Phys. 163 523 (1961).

DILLON, J.F. J. Appl. Phys. 29 539 (1958a).

DILLON, J.F. J. Appl. Phys. 29 1286 (1958b).

DILLON, J.F. Annual Report of the Smithsonian Institution, p.385 (1960).

DILLON, J.F. J. Appl. Phys. 39 922 (1968).

DOVE, D.B. J. Appl. Phys. 34 2067 (1963).

DUPOUY, G. and PERRIER, F. J. de Microscopy 1 167 (1962).

ELLINGHAM, H.J.T. J. Soc. Chem. Ind. 63 125 (1944).

ELMORE, W.C. Phys. Rev. 51 982 (1937).

ELMORE, W.C. Phys. Rev. 54 309 (1938a).

ELMORE, W.C. Phys. Rev. 54 1092 (1938b).

ELMORE, W.C. Phys. Rev. 58 640 (1940).

ESHELBY, J.D. J. Appl. Phys. 24 176 (1953).

ESHELBY, J.D. Phil. Mag. 3 440 (1958).

FAUST, J.W. and JOHN, H.F. Trans. Met. Soc. A.I.M.E. 233 230 (1965).

FELDTKELLER, E. Symposium on the Electric and Magnetic Properties of Thin Metallic Layers (Louvain 1961) p.98.

FELDTKELLER, E. Z. Angew. Phys. 15 206 (1963).

FELDTKELLER, E. Z. Angew. Phys. 19 530 (1965).

FELDTKELLER, E. and FUCHS, E. Z. Angew. Phys. 18 1 (1964).

FELDTKELLER, E. and LIESK, W. Z. Angew. Phys. 14 195 (1962).

FELDTKELLER, E. and STEIN, K.U. Z. Angew. Phys. 23 100 (1967).

FELDTKELLER, E. and THOMAS, H. Phys. Kondens. Materie. 4 8 (1965).

FERRIER, R.P. Bull. Soc. fr. Min. Crystal. 90 464 (1967).

FERRIER, R.P. and MURRAY, R.T. J. Royal Microscopical Soc. 85 323 (1966).

FERRIER, R.P. and PUCHALSKA, I.B. Phys. Stat. Sol. 28 335 (1968).

FITZGERALD, A.G., MANNAMI, M., POGSON, E.H. and YOFFE, A.D. J. Appl. Phys. 38 3303 (1967).

FOWLER, C.A. and FRYER, E.M. Phys. Rev. 86 426 (1952).

FOWLER, C.A. and FRYER, E.M. J. Opt. Soc. America 44 256 (1954a).

FOWLER, C.A. and FRYER, E.M. Phys. Rev. 94 52 (1954b).

FOWLER, C.A. and FRYER, E.M. Phys. Rev. 104 552 (1956).

FOWLER, C.A., FRYER, E.M. and TREVES, D. J. Appl. Phys. 31 2267 (1960).

FOWLER, C.A., FRYER, E.M. and TREVES, D. J. Appl. Phys. 32 2965 (1961).

FOX, M. and TEBBLE, R.S. Proc. Phys. Soc. 72 765 (1958).

FRAIT, Z., FRAITOVA, D., KOTRBOVA, M. and HAUPTMAN, Z. Czech. J. Phys. B16 837 (1966).

FRANK, F.C. Disc. Faraday Soc. 5 48 (1949).

FRANSE, J.J.M. Thesis, Univ. of Amsterdam (1969).

FRANSE, J.J.M. and DE VRIES, G. Physica 39 477 (1968).

FUCHS, E. Naturwissenschaften 12 450 (1961).

FUCHS, E. Z. Angew, Phys. 14 203 (1962).

FUJIWARA, H., SUGITA, Y. and SAITO, N. J. Phys. Soc. Japan 20 2088 (1965b).

FULLER, H.W. and HALE, M.E. J. Appl. Phys. 31 238 (1960a).

FULLER, H.W. and HALE, M.E. J. Appl. Phys. 31 1699 (1960b).

FULLER, H.W. and RUBINSTEIN, H. J. Appl. Phys. 30 84S (1959).

GARROOD, J.R. Proc. Phys. Soc. 79 1252 (1962).

GEMPERLE, R. Phys. Stat. Sol. 14 121 (1966).

GEMPERLE, R. and KACZER, J. Phys. Stat. Sol. 34 255 (1969).

GENOVESE, E.R. and CHANG, H. Rev. Sci. Inst. 39 733 (1968).

GILMAN, J.J. The Art & Science of Growing Crystals, J. Wiley, N.Y. (1963).

GOMI, Y. and ODANI, Y. J. Phys. Soc. Japan 15 535 (1960).

GONDO, Y. J. Phys. Soc. Japan 17 1129 (1962).

GONDO, Y. and FUNATOGAWA, Z. J. Phys. Soc. Japan 15 535 (1960).

GOODENOUGH, J.B. Phys. Rev. 95 917 (1954).

GORSUCH, P.D. A.I.M.E. Met. Soc. Conf. 8 771 (1959a).

GORSUCH, P.D. J. Appl. Phys. 30 837 (1959b).

GREEN, A. and PRUTTON, M. J. Sci. Inst. 39 244 (1962).

GREEN, A., PRUTTON, M. and CARTER, W.S. J. Sci. Inst. 40 490 (1963).

GREEN, A. and THOMAS, B.W.J. J. Sci. Inst. 43 399 (1966).

GRUNDY, P.J. Brit. J. Appl. Phys. 16 409 (1965).

GRUNDY, P.J. and TEBBLE, R.S. Advances in Physics 17 153 (1968).

HALE, M.E., FULLER, H.W. and RUBINSTEIN, H. J. Appl. Phys. 30 789 (1959).

von HAMOS, L. and THIESSEN, P.A. Zeit. für Phys. 71 442 (1931).

HARRINGTON, J.V. M.I.T. Tech. Rep., Lincoln Lab. No.166 (1958).

HAUPTMANN, Z. and SVOBODA, E. Czech. Chem. Commun. 30 1373 (1965).

HIRTH, J. and FRANK, F.C. Phil. Mag. 3 1110 (1958).

HOFFMANN, H. I.E.E.E. Trans. MAG 4 32 (1968).

HOLZ, A. and KRONMULLER, A. Phys. Stat. Sol. 31 787 (1969).

HORNREICH, R.M. J. Appl. Phys. 34 1071 (1963).

HUBERT, A. Phys. Stat. Sol. 32 519 (1969).

HUBER, E.E. and SMITH, D.O. J. Appl. Phys. 30 267 (1959).

HUBER, E.E., SMITH, D.O. and COODENOUGH, J.B. J. Appl. Phys. 29 294 (1958).

HUTCHINS, G.A. The Electron Microprobe, ed. T.D. McKinley et al, J. Wiley, N.Y. p.390 (1966).

IWATA, T., PROSEN, R.J. and GRAN, B.E. J. Appl. Phys. 37 1285 (1966).

JAKUBOVICS, J. Phil. Mag. 13 85 (1966a).

JAKUBOVICS, J.P. Phil. Mag. 14 881 (1966b).

JANAK, J.F. Appl. Phys. Letts. 9 225 (1966).

JEFFES, J.H.E. J. Cryst. Growth 3 13 (1968).

JOY, D.C. and JAKUBOVICS, J.P. Phil. Mag. 17 61 (1968).

JOY, D.C. and JAKUBOVICS, J.P. Brit. J. Appl. Phys. Ser.2 2 1367 (1969).

KACZER, J. Czech. J. Phys. 7 557 (1957).

KACZER, J. J. Appl. Phys. 29 569 (1958).

KACZER, J. and GEMPERLE, R. Czech. J. Phys. 9 306 (1959a).

KACZER, J., GEMPERLE, R. and HAUPTMAN, Z. Czech. J. Phys. 9 606 (1959b).

KACZER, J., ZELENY, M. and SUDA, P. Czech. J. Phys. B13 579 (1963).

KANAMORI, J. Magnetism 1 127 (1963) Academic Press (Ed. Rado, G.T. and Suhl, H.)

KAYSER, W. I.E.E.E. Trans. MAG 3 141 (1967).

KERR, J. Rept. Brit. Assoc. Adv. Sci. p.40 (1876).

KITTEL, C. Phys. Rev. 70 965 (1946).

KITTEL, C. Rev. Mod. Phys. 21 541 (1949a).

KITTEL, C. Phys. Rev. 76 1527 (1949b).

KITTEL, C. and GALT, J.K. Solid State Physics 3 (1956), p.437 Ferromagnetic Domain Theory.

KOIKEDA, T., SUZUKI, K. and CHIKAZUMI, S. Appl. Phys. Letts. 4 160 (1964).

KOOY, C. and ENZ, U. Philips Res. Repts. 15 7 (1960).

KOTRBOVA, M. and HAUPTMAN, Z. Czech. J. Phys. B15 64 (1965).

KOZLOWSKI, G. and ZIETEK, W. Acta Physica Polonica 29 261 (1966).

KRANZ, J. Naturwissenschaften 43 370 (1956).

KRANZ, J., HUBERT, A. and MULLER, R. Z. Phys. 180 80 (1964).

KRINCHIK, G.S. J. Appl. Phys. 39 859 (1968).

KRYDER, M.H. and HUMPHREY, F.B. J. Appl. Phys. 40 2469 (1969).

KUBASCHEWSKI, O., EVANS, E.Ll. and ALCOCK, C.B. Metallurgical Thermochemistry, Pergamon (1967).

LA BONTE, A.E. J. Appl. Phys. 40 2450 (1969).

LA BONTE, A.E. and BROWN, W.F. J. Appl. Phys. 37 1299 (1966).

LAMBECK, M. Z. Physik 179 161 (1964).

LAMBECK, M. Z. Angew. Phys. 18 506 (1965).

LAMBECK, M. I.E.E.E. Trans. MAG 4 51 (1968).

LANDAU, L. and LIFSHITZ, E. Physik. Z. Sowjetunion 8 153 (1935).

LANG, A.R. Acta. Cryst. 12 249 (1959).

LANG, A.R. and POLCAROVA, M. Proc. Roy. Soc. London A285 297 (1965).

LEAVER, K.D. Thin Solid Films 2 149 (1968).

LEAVER, K.D. Private Communication (1969).

LEE, E.W. Proc. Phys. Soc. A66 623 (1953).

LEE, E.W. Rep. Progr. Phys. 18 184 (1955).

LEHRER, S.S. J. Appl. Phys. 34 1207 (1963).

LIFSHITZ, E. J. Phys. U.S.S.R. 8 337 (1944).

LILLEY, B.A. Phil. Mag. 41 792 (1950).

LISSBERGER, P.H. J. Opt. Soc. Amer. 51 948 (1961) (2 papers).

LISSBERGER, P.H. J. Opt. Soc. Amer. 54 804 (1964).

LO, D.S. and HANSON, M.M. J. Appl. Phys. 38 1342 (1967).

LUBORSKY, F.E. J. Appl. Phys. 32 171S (1961).

McKEEHAM, L.W. and ELMORE, W.C. Phys. Rev. 46 226 (1934).

MALEK, Z. and KAMBERSKY, V. Czech. J. Phys. 8 416 (1958).

MARTIN, D.H. Proc. Phys. Soc. B70 77 (1957).

MAYER, L. J. Appl. Phys. 26 1228 (1955).

MAYER, L. J. Appl. Phys. 28 975 (1957).

MAYER, L. J. Appl. Phys. 30 252S (1959).

MAYER, L. J. Appl. Phys. 31 346 (1960).

METHFESSEL, S., MIDDELHOEK, S. and THOMAS, H. I.B.M. J. Res. Develop. 4 96 (1960).

METZDORF, M. and WIEHL, H.E. Phys. Stat. Sol. 17 285 (1966).

MICHALAK, J.T. and GLENN, R.C. J. Appl. Phys. 32 1261 (1961).

MIDDELHOEK, S. Van Soest, Amsterdam (1961), Ph.D. Thesis.

MIDDELHOEK, S. J. Appl. Phys. 33 1111S (1962).

MIDDELHOEK, S. J. Appl. Phys. 34 1054 (1963).

MOHIUDDIN, M. Brit. J. Appl. Phys. 17 789 (1966).

MOON, R.M. J. Appl. Phys. 30 82S (1959).

MORELOCK, C.R. and SEARS, G.W. J. Chem. Phys. 31 926 (1959).

MORELOCK, C.R. and SEARS, G.W. J. Chem. Phys. 34 1008 (1961).

MURAYAMA, Y. J. Phys. Soc. Japan 21 2253 (1966).

MURAYAMA, Y. J. Phys. Soc. Japan 23 511 (1967).

NABARRO, F.R.N. and JACKSON, P.J. Growth and Perfection of Crystals p.13, J. Wiley, N.Y. (1958).

NEEL, L. J. Phys. Radium 5 241 (1944).

NEEL, L. Cahiers de Phys. 25 1 (1944).

NEEL, L. Compt. Rend. 241 533 (1955).

O'DELL, T.H. I.E.E. Monograph No. 396 M (1960).

OATLEY, C.W., NIXON, W.C. and PEASE, R.F.W. Adv. Electronics & Electron Physics 21 181 (1965).

OLSON, A.L. J. Appl. Phys. 38 1869 (1967).

OLSON, A.L., OREDSON, H.N., TOROK, E.J. and SPURRIER, R.A. J. Appl. Phys. 38 1349 (1967).

OSBORN, J.A. Phys. Rev. 67 351 (1945).

PALIK, E.D. Applied Optics 6 597 (1967).

PERNESKI, A.J. I.E.E.E. Trans. MAG 5 554 (1969).

POLCAROVA, M. I.E.E.E. Trans. MAG 5 536 (1969).

POLCAROVA, M. and KACZER, J. Phys. Stat. Sol. 21 635 (1967).

POLCAROVA, M. and LANG, A.R. Appl. Phys. Letts. 1 13 (1962).

POLCAROVA, M. and LANG, A.R. Bull. Soc. fr. Min. Crystal 91 645 (1968).

PRICE, P.B. Phil. Mag. 5 473 (1960).

PRICE, F.P., VERMILYEA, D.A. and WEBB, M.B. Acta. Met. 6 524 (1958).

PRUTTON, M. Phil. Mag. 4 1063 (1959).

PRUTTON, M. Phil. Mag. 5 625 (1960).

PRUTTON, M. Thin Ferromagnetic Films, Butterworths (1964).

PUCHALSKA, I.B. and FERRIER, R.P. Thin Solid Films 1 437 (1967/8).

REGIS, M. and CALVIAC, J.C. J. Cryst. Growth 6 43 (1969).

RHODES, P. and ROWLANDS, G. Proc. Leeds. Phil. Soc. 6 191 (1954).

RICKER, Th. Phys. Stat. Sol. 30 K93 (1968).

RICKER, Th. I.E.E.E. Trans. MAG 5 179 (1969).

ROBINSON, C.C. J. Opt. Soc. Amer. 54 1220 (1964).

RODBELL, D.S. Phys. Rev. Letters 13 471 (1964).

RODBELL, D.S. Physics 1 279 (1965).

RODGERS, J.M. Proc. Int. Conf. Magnetism, Nottingham (1964) p.866.

ROESSLER, B., KRAMER, J.J. and KURIYAMA, M. Phys. Stat. Sol. 11 117 (1965).

RUBINSTEIN, H. and SPAIN, R.J. J. Appl. Phys. 31 306S (1960).

SAITO, N., FUJIWARA, H. and SUGITA, Y. J. Phys. Soc. Japan 19 421 (1964a).

SAITO, N., FUJIWARA, H. and SUGITA, Y. J. Phys. Soc. Japan 19 1116 (1964b).

SAITO, N. Ph.D. Thesis, Tokyo Univ. (1966).

SATO, H. and ASTRUE, R.W. J. Appl. Phys. 33 2956 (1962).

SATO, H., TOTH, R.S. and ASTRUE, R.W. J. Appl. Phys. 33 1113 (1962).

SATO, H., TOTH, R.S. and ASTRUE, R.W. J. Appl. Phys. 34 1062 (1963).

SATO, H., TOTH, R.S. and ASTRUE, R.W. Single Crystal Films, Pergamon Press Inc. New York (1964) p.395.

SATO, H., ASTRUE, R.W. and SHINOZAKI, S.S. J. Appl. Phys. 35 822 (1964).

SCHAFER, H. Chemical Transport Reactions, Academic Press (1964).

SCHLENKER, M., BRISSONNEAU, P. and PERRIER, J.P. Bull. Soc. fr. Min. Cristal 91 653 (1968).

SEARS, G.W. Acta. Met. 1 457 (1953).

SEARS, G.W. Acta. Met. 3 361 (1955a).

SEARS, G.W. Acta. Met. 3 367 (1955b).

SEARS, G.W. J. Chem. Phys. 25 637 (1956).

SEARS, G.W. J. Chem. Phys. 29 1045 (1958).

SEARS, G W. and COLEMAN, R.V. J. Chem. Phys. 25 635 (1956).

SHERWOOD, R.C., REMEIKA, J.P. and WILLIAMS, H.J. J. Appl. Phys. 30 217 (1959).

SHTRIKMAN, S. and TREVES, D. J. Appl. Phys. 31 147S (1960a).

SHTRIKMAN, S. and TREVES, D. J. Appl. Phys. 31 1304 (1960b).

SHTRIKMAN, S. and TREVES, D. J. Appl. Phys. 31 72S (1960c).

SHTRIKMAN, S. and TREVES, D. Magnetism 3 395 (1963).

SHUR, I.S., SHTOL'TS. E.W. and MARGOLINA, W.I. Sov. Phys. J.E.T.P. 11 33 (1960).

SILCOX, J. Phil. Mag. 8 1395 (1963).

SOMMERFELD, A. Electrodynamics. Academic Press (1964).

SPACEK, L. Czech. J. Phys. 9 186 (1959) (2 papers).

SPAIN, R.J. Appl. Phys. Letters 3 208 (1963).

SPAIN, R.J. and FULLER, H.W. J. Appl. Phys. 37 953 (1966).

STONER, E.C. Phil. Mag. 36 803 (1945).

STONER, E.C. Rep. Prog. Phys. 13 83 (1950).

STRANSKI, I.N. Z. Physik Chem. 136 259 (1928).

SUGITA, Y., FUJIWARA, H. and SAITO, N. J. Phys. Soc. Japan 19 782 (1964).

SUGITA, Y., FUJIWARA, H. and SAITO, N. J. Phys. Soc. Japan 20 469 (1965a).

SUGITA, Y. and FUJIWARA, H. J. Phys. Soc. Japan 20 98 (1965b).

SUGITA, Y., FUJIWARA, H. and SATO, T. Appl. Phys. Letters 10 229 (1967).

SUKIENNICKI, A. Phys. Stat. Sol. 29 417 (1968).

SUZUKI, T., WILTS, C.H. and PATTON, C.E. J. Appl. Phys. 39 1983 (1968).

SWALIN, R.A. Thermodynamics of Solids, J. Wiley, N.Y. (1962).

TATSUMOTO, E., HARA, K. and HASHIMOTO, T. Japan J. Appl. Phys. 7 176 (1968).

TOROK, E.J., LO, D.S., OREDSON, H.N. and SIMON, W.J. J. Appl. Phys. 40 1222 (1969).

TOROK, E.J., OLSON, A.L. and OREDSON, H.N. J. Appl. Phys. 36 1394 (1965).

TREVES, D. J. Appl. Phys. 32 358 (1961).

VOIGT, W. Magneto and Electro Optics, B.G. Teubner, Leipzig (1908).

VOLMER, M. and ESTERMANN, I. Zeit. für Phys. 7 13 (1921).

WADE, R.H. Proc. Phys. Soc. 79 1237 (1962).

WADE, R.H. and SILCOX, J. Appl. Phys. Letters 8 7 (1966).

WAGNER, R.S. and ELLIS, W.C. Appl. Phys. Letters 4 89 (1964).

WANG, F.F.Y. J. Appl. Phys. 39 865 (1968).

WARRINGTON, D.H. Phil. Mag. 9 261 (1964).

WARRINGTON, D.H., ROGERS, J.M. and TEBBLE, R.S. Phil. Mag. 7 1783 (1962).

WEBB, W.W., DRAGSDORF, R.D. and FORGENG, W.D. Phys. Rev. 108 498 (1957).

WEBER, R. I.E.E.E. Trans. MAG.4 28 (1968).

WEISS, P. J. Phys. 6 661 (1907).

WHITE, E.A.D. Acta. Cryst. 8 845 (1955).

WILLIAMS, H.J., BOZORTH, R.M. and SHOCKLEY, W. Phys. Rev. 75 155 (1949).

WILLIAMS, H.J. and GOERTZ, M. J. Appl. Phys. 23 316 (1952).

WILLIAMS, H.J. and SHERWOOD, R.C. J. Appl. Phys. 28 548 (1957).

WILLIAMS, H.J., FOSTER, F.G. and WOOD, E.A. Phys. Rev. 82 119 (1951).

WOHLLEBEN, D. Phys. Letters 22 546 (1966).

WOHLLEBEN, D. J. Appl. Phys. 38 3341 (1967).

[01$\bar{1}$] direction, is seen to oscillate in a (100) plane approaching the two easy axes [00$\bar{1}$] and [010] that lie in that plane. The concept of magnetisation zones perpendicular to the plane of the foil has to be abandoned with the plane of oscillation making an acute angle with the plane of the foil, and by so doing avoiding the formation of a volume pole density.

The magnetostatic energy was approximated by a μ^* correction and an expression for the total energy minimised with respect to ϕ and d. The result showed that this oscillation was energetically favourable for foils thicker than 1250 Å with an amplitude ϕ of about 30°, varying little with foil thickness. The stripe spacing d was predicted to increase linearly with foil thickness, but at a rate far below that observed experimentally, giving a d value of just over 2000 Å for a foil of 4000 Å thickness.

A full micromagnetic treatment has not been applied to these foils, but Bourret and Kleeman (1967) extended the μ^* correction to this particular geometry. The equations required numerical solution and gave good agreement with experimental results for the critical thickness, but the dependence of the stripe spacing d on the foil thickness was far too low. This probably arose from a linearisation of the equations at an earlier stage in the calculations. However, it is interesting to note that at the critical thickness the angle ϕ was found not to tend to zero, but to about 20°. Thus any use of small angle approximations for the determination of the critical thickness in this type of geometry is fundamentally wrong.

6.1.4 The Application of Micromagnetics to Stripe Domains

Before considering the properties of stripe domains in thin platelets the application of micromagnetics to stripe domain calculations is considered.

Exact solutions of Brown's equations of micromagnetism are difficult to obtain because of complexities arising from the expression

for the stray field energy and from the limitation that the squares of the direction cosines of the magnetisation vector must at all times sum to unity,

$$\sum_{i=1}^{3} \alpha_i^2 = 1$$

In a limiting case of $M_s^2 \longrightarrow \infty$, whilst the other physical parameters remained finite, the magnetisation configuration would be such as to avoid the formation of stray fields. Thus in this limiting case:

$$\begin{aligned} \text{div } \underline{M} &= 0 \\ \underline{M} \cdot \underline{n} &= 0 \text{ on all surfaces} \end{aligned} \qquad (6.6)$$

where $\underline{n}$ is the vector surface normal.

A classical Bloch wall in an infinite body is an example of such a distribution. Hubert (1969) applied the limitations of equations (6.6) to situations in thin films with the restriction that $k \gg 1$ ($k = 2\pi M_s^2/K$). The opposite limit with $k \ll 1$ is suitably covered by the μ^* method. Hubert found that a micromagnetic configuration satisfying equation (6.6) did not in general fulfil Brown's equations and although micromagnetic equations allowing (6.6) were formulated they were not easy to solve for any but linear cases. Hubert restricted himself to approximations by a Ritz's method. However, this approach has been most important in providing an upper bound to the energy of any real micromagnetic configuration.

An example of such a result was seen in section 1.5 considering the theoretical models for Bloch walls. It was seen that La Bonte's two dimensional construction of a Bloch wall fell below Hubert's upper limit, whereas all previous models had had higher energies, see FIG.(1.10).

Hubert applied equations satisfying zero stray field not only to Bloch and Néel walls but also to ripple and stripe structures. Considering once again the critical case, the critical film thickness

below which no stripes would be stable t_c, in a film with a uniaxial anisctropy normal to the film plane, was found to be:

$$t_c = \frac{2\pi}{\left[1 - \frac{HM_s}{2K}\right]} \sqrt{\frac{A}{K}} \qquad (6.7a)$$

H being applied in a direction parallel with the stripes and

$$d = \left[\frac{2K - HM_s}{2K + HM_s}\right]^{\frac{1}{2}} t_c \qquad (6.7b)$$

which for $K/2\pi M_s \longrightarrow 0$ is seen to be in agreement with the result of Murayama, see equation (6.4,IIIb) and of Holz and Kronmüller (1969), (see below).

Numerical calculations were also performed for the stripe domains seen in iron foils, to give the critical thickness as

$$t_c = 6.83\left(\frac{A}{K_1}\right)^{\frac{1}{2}} \qquad (6.8a)$$

and the stripe spacing at that thickness as

$$d = 7.77\left(\frac{A}{K_1}\right)^{\frac{1}{2}} = 1.11\ t_c \qquad (6.8b)$$

Holz and Kronmüller (1969) treated the nucleation of stripe domains by considering the critical parameters for which the magnetisation began to rotate out of the film plane. Because at this stage the magnetisation direction only deviated slightly from the film plane the problem could be treated by linearized micromagnetic equations. (Murayama's paper was criticised for violating the micromagnetic surface conditions and this was avoided in Hubert's work).

Solving the resulting equations, they were able to characterise materials by the parameter k, mentioned before ($k = 2\pi M_s^2/K$).

(a) When $k > 1$ and $t < t_c$ the magnetisation lay in the film plane with the domains separated by either Néel or Cross-tie walls.

(b) When $k > 1$ and $t > t_c$ a stripe structure formed, and as t increased above this thickness a continuous transition from stripe to bulk domain structures occurred (note the work of Krinchik, section 6.1.1).

(c) When $k < 1$ the magnetisation was independent of the thickness of the film, lying parallel or anti-parallel with the easy axis down to values of $t = 0$. (Domain structures in these materials are established by the nucleation of reversed domains at imperfections and dislocations.

A plot of t_c and d_c as functions of $1/k$ displayed these three regions graphically and from the positions of the $1/k$ values of the transition ferromagnets the critical thicknesses were found to be

$$\begin{aligned} t_c^{Ni} &= 2780 \text{ Å} \\ t_c^{Fe} &= 1320 \text{ Å} \\ t_c^{Co} &= 233 \text{ Å} \end{aligned} \qquad (6.9)$$

At large values of k, t_c was found to approach the value $2\pi(\frac{A}{K})^{\frac{1}{2}}$, in agreement with Murayama's result.

The relative insensitivity of t_c to M_s for $k \gg 1$ implied that the formation of stripe domains occurred by a stray-field free magnetisation process, Hubert (1969). With decreasing M_s values the stray field increased in importance.

To obtain agreement with Saito's experimental results for t_c and d a perpendicular anisotropy of 60% of Saito's value had to be used, which may well be acceptable.

A check was also made on the stripe domains in (111) plane iron foils, see section (6.1.3). The value Bourret and Dautreppe had used

for the exchange constant (0.8×10^{-6} ergs/cm) was considered too low. Using a value of 2×10^{-6} ergs/cm the critical thickness was found to be

$$t_c = 6.225\left(\frac{A}{K_1}\right)^{\frac{1}{2}} \qquad (6.10a)$$

and

$$d = 1.11\, t_c \qquad (6.10b)$$

in excellent agreement with equations (6.8).

The numerical value for t_c of 1320 Å was too high for Bourret's experimental results. The value of d (2930 Å) at this thickness showed even greater disparity but this was probably because d was a sharply varying function of t at this thickness. The disagreement of the value of t_c itself is probably to be found in the initial assumption of Holz and Kronmüller's equations, that because they were considering only critical conditions linear equations could be used. However, it will be recalled from the work of Bourret and Kleeman that even at the critical thickness the maximum spin deflection was $\sim 20^{\circ}$. It unfortunately looks as if non linear equations will be necessary.

The approach adopted by these authors is obviously very powerful and has scope for further development being limited exclusively by the ability to handle the complex mathematical functions. A similar approach to the strong stripe structures would also be very desirable.

6.2 STRIPE DOMAINS IN PLATELETS

Observations of stripe domains in platelets with negative magnetocrystalline anisotropy have been reported by De Blois (1965 and 1968a). Several types of stripe pattern have been observed, varying with the thickness and composition of the platelets. The minimum anisotropy <111> axes point out of the plane of the platelets at 35.3° and the magnetisation turns towards these directions when the anisotropy energy is sufficiently lowered at the expense of the

exchange and magnetostatic energies. The <111> directions lie in the {110} and {112} planes, there being a set of six of the former and four of the latter. With the exception of the 109° rotations in the {110} planes, rotation from one <111> direction to another involves only a small anisotropy barrier, thus leading to the multiplicity of possible stripe structures. These are described in section 6.2.1 below.

6.2.1 Platelet Stripe Structures

Type I stripe domains have been found in platelets which exhibit pseudo-positive anisotropy, that is platelets with compositions of low, but nevertheless still negative magnetocrystalline anisotropy which show structures normally associated with platelets of positive anisotropy. In the thicker platelets the 180° domain walls lie along the <100> direction and the 90° walls along the <110> directions with the Bitter patterns from the stripes lying parallel with the hard <100> directions. This configuration can easily be explained by analogy with the stripe domains in iron foils, see section 6.1.3, and reference to FIG.(6.5).

If the stripes are assumed to slant through the platelet in {110} planes then the magnetisation in a given domain can oscillate on a 109° arc between two <111> directions, but giving a net component in a <100> direction. Thus if the surface Bitter pattern shows a net [100] magnetisation, the magnetisation in one stripe might lie in a $(0\bar{1}1)$ plane having a [111] direction and in the adjacent stripes would lie in parallel $(0\bar{1}1)$ planes but oriented towards the $[1\bar{1}\bar{1}]$ direction. It is unlikely that the magnetisation actually rotates as far as the <111> direction in any of the stripes because the surface pole fields would reduce this angle, in the manner of a μ^* correction.

This structure, although hypothesised from colloid work has been confirmed by x-ray diffraction topography.

Type II stripes are seen as striations in the colloid which they

do not gather nearly as readily as the other types of stripe domains. They have often been seen in platelets together with Type III stripes, see for example FIGS.(6.8 & 9). The structure is thought to be similar to that of the Saito stripes with the net magnetisation oriented in a <110> direction with an oscillation of the magnetisation vector on a 71° arc in the (110) plane towards the [111] and [11$\bar{1}$] directions. The structure of the Type II stripes is probably modified in the same way that Murayama's treatment, see FIG.(6.2), modified the Saito stripe structure. Thus the stripes essentially consisted of a set of Bloch lines running through the platelet in the <110> direction with the surface magnetisation acting as a closure structure. The internal flux closure produced by this arrangement is high and accounts for the poor colloid collection.

Type III stripes collect colloid far more strongly than Type II yet fit with little disturbance into the <110> closure structures familiar from Chapter 5. The boundary between Type III and Type II stripe domains in zero field has been found to lie approximately along <100> directions indicating the normal component of magnetisation across the boundary to be constant. The stripes themselves lie almost, but not exactly, parallel with a [100] direction despite the fact that the magnetisation vector oscillates in a (110) plane towards [111] and [11$\bar{1}$] directions.

De Blois (1968a) noticed a small change in the magnitude of the net magnetisation associated with the structural change between Type II and Type III stripes. A compatible structure could be constructed, however, by assuming (a) the normal component of magnetisation to remain constant across the boundary between the two types, (b) the magnitude of the net magnetisation in the Type III stripes to be a little smaller than in Type II, and (c) a slight divergence of the magnetisation to occur near the boundary in Type II stripes to lower the normal component across the walls. Type III stripes tend to form parallel with an edge, or step in an echelon structure, leading to a

smaller divergence of the magnetisation than if Type II stripes were to gradually change direction in these same regions.

Type IV stripes are not uniform through the thickness of the platelet and are confined to the thicker specimen. The structure is thought by De Blois (1968a) to consist of helical rotations of the magnetisation vector through 71°, parallel to a {110} plane, from one <111> direction to another. If, for example, the net magnetisation is along the [110] direction then the magnetisation vector in one stripe can be taken as rotating clockwise in a $(\bar{1}01)$ plane from the [111] direction at the top to the $[1\bar{1}1]$ direction at the bottom. The magnetisation vectors in the neighbouring stripes on both sides then point towards the $[\bar{1}1\bar{1}]$ direction at the top and rotate clockwise in a (011) plane to point towards the $[11\bar{1}]$ direction at the bottom.

These changes in orientation from the top to the bottom surfaces of the platelet can be visualised with the help of FIG.(6.6a). The magnetisation in a given stripe rotates from the direction T1 at the top to B1 at the bottom of the stripe. In the neighbouring stripes on either side the magnetisation at the top points in the direction T2 and rotates in a different (110) plane to B2 at the bottom. The stripe domain walls lie in the (110) plane containing T1 and B2.

The resulting stripe domain pattern at the top and bottom of the crystal as seen from above is shown in FIG.(6.6b). This structure, like those of Murayama and Krinchik provides an increased degree of local flux closure.

De Blois (1968a) has reported a few observations made on the behaviour of these stripes under in-plane magnetic fields. The effect of the field on the stripe pattern was found to be directionally dependent. In some directions alternate stripes became very faint or even disappeared, thus effectively doubling the spacing without altering the stripe structure, and in other directions the brightness remained unchanged but the stripes became asymmetrically spaced.

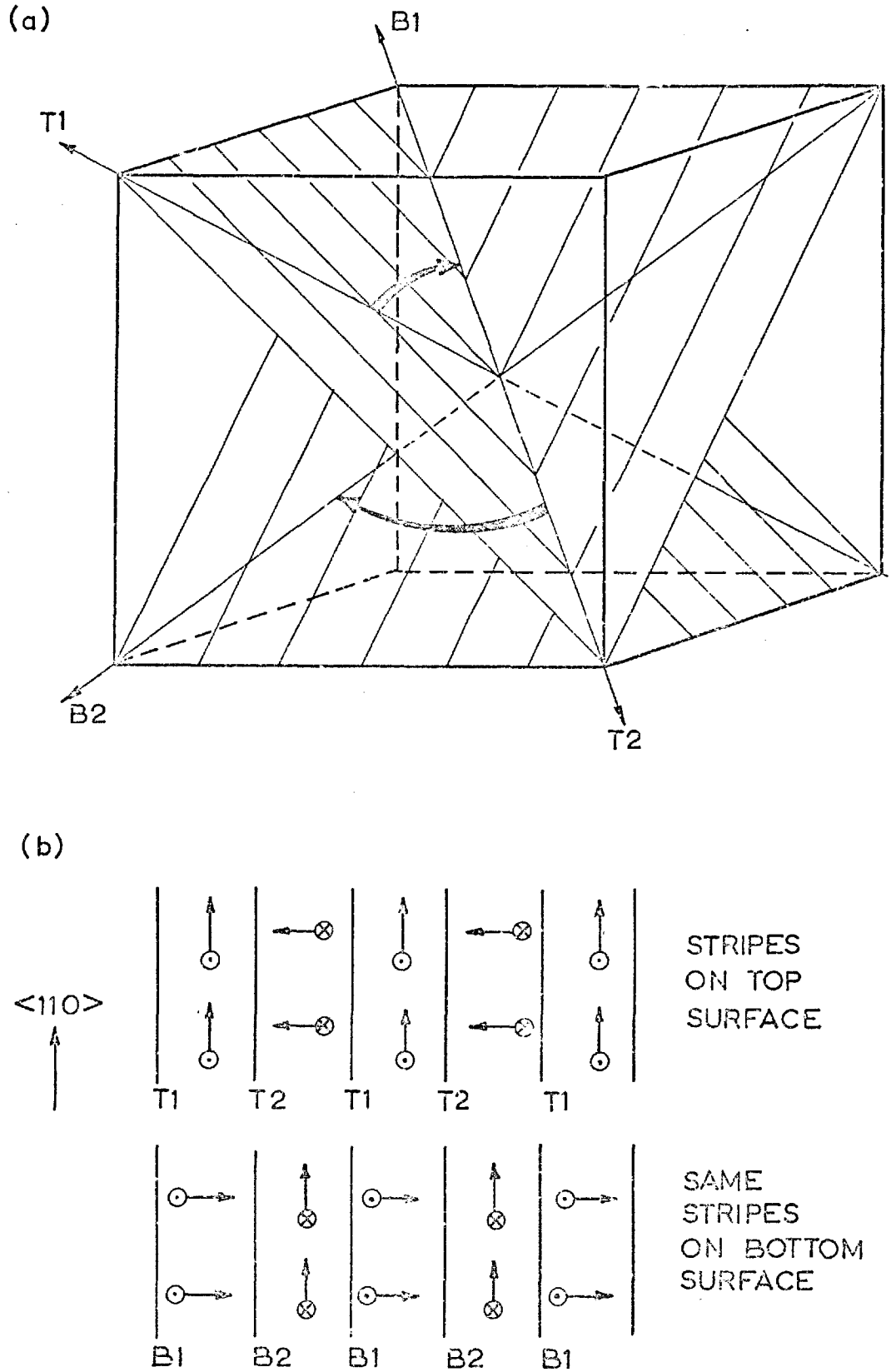

Fig. (6.6) Stripe domains type IV (after De Blois)

The 180° wall in Type IV stripes has been explained as a rotation of the in-plane component of the magnetisation through 180° (over a distance where a 90° rotation normally occurs) with the vertical component reversing sign in the normal way, as seen in FIG.(6.7).

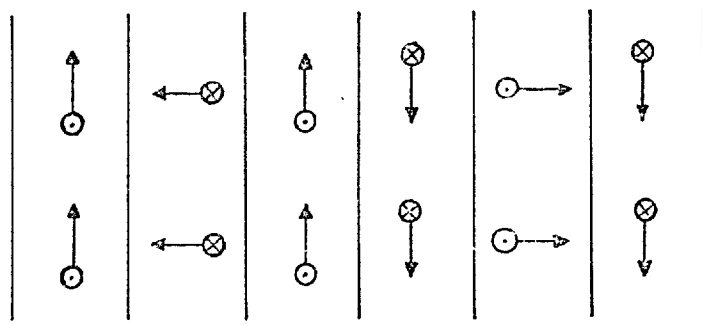

FIG.(6.7) 180° WALL IN STRIPE IV DOMAINS

The presence of a 180° wall cannot therefore of itself be detected, with a colloid technique, by its increased local field.

No calculations have yet been made either to determine theoretically the equilibrium stripe spacing or to give any indication of the critical thickness at which these stripes form.

Type V stripes (not classified by De Blois) have only been seen in the small triangular edge closure domains of platelets. The structure of these is thought to resemble the strong stripe domains observed by Ferrier and Pulchalska (1968). In both cases it will be noticed that the out of plane anisotropy is not normal to the plane, but for different reasons. In films a uniaxial anisotropy arises from the oblique incidence evaporation, but in platelets the origin is crystallographic. This helical rotation of the magnetisation allows a region of flux closure with net magnetisation parallel with the edge to still exist and to form a stripe pattern in thicker platelets.

The possibilities offered by these five stripe models must be considered in the sections following, describing observations made on several platelets.

6.2.2 Observations on Mixed Stripe Structures

The coexistence of several stripe structures is seen in FIG.(6.8b) on a (100) plane of a nickel crystal with <100> edges. The thickness of this platelet is not known exactly, however from the Lorentz investigations it would seem to be less than 4000 Å. This particular platelet had a shape similar to those previously seen in FIG.(3.5c), but this is of no importance in considering the fine magnetic structure.

The structure of the main domains seen in FIG.(6.8b) formed a familiar closure pattern, but the striated colloid collections within these domains suggested the existence of a weak type II stripe structure. This was further confirmed by Lorentz microscopy. FIG.(6.8a)*, a Lorentz micrograph taken in the Fresnel mode at 500 kV, shows a 180° wall near the centre of the platelet with the fine oscillation from the stripes on either side. The stray field from these oscillations is too weak to gather significant amounts of colloid, and although the magnification of FIG.(6.8a) is not known the stripe spacing is thought to be less than 5000 Å.

Small echelon structures only exist near the corners of the platelet and are formed with a separate type of stripe domain, most readily visible in the right hand corner. The small size of these domains complicates their stripe pattern but one of a type III structure would seem the most likely. Triangular closure domains along the top edge show a type V structure, which will be mentioned again later.

The effect of an easy axis applied field on this platelet is seen in FIG.(6.9). During this series of photographs the platelet was free to rotate in the colloid so that the field was known to be

---

*FIG.(6.8a) was obtained by Dr. I.E. Pulchalska using the high voltage microscope of the Cavendish Laboratory, Cambridge.

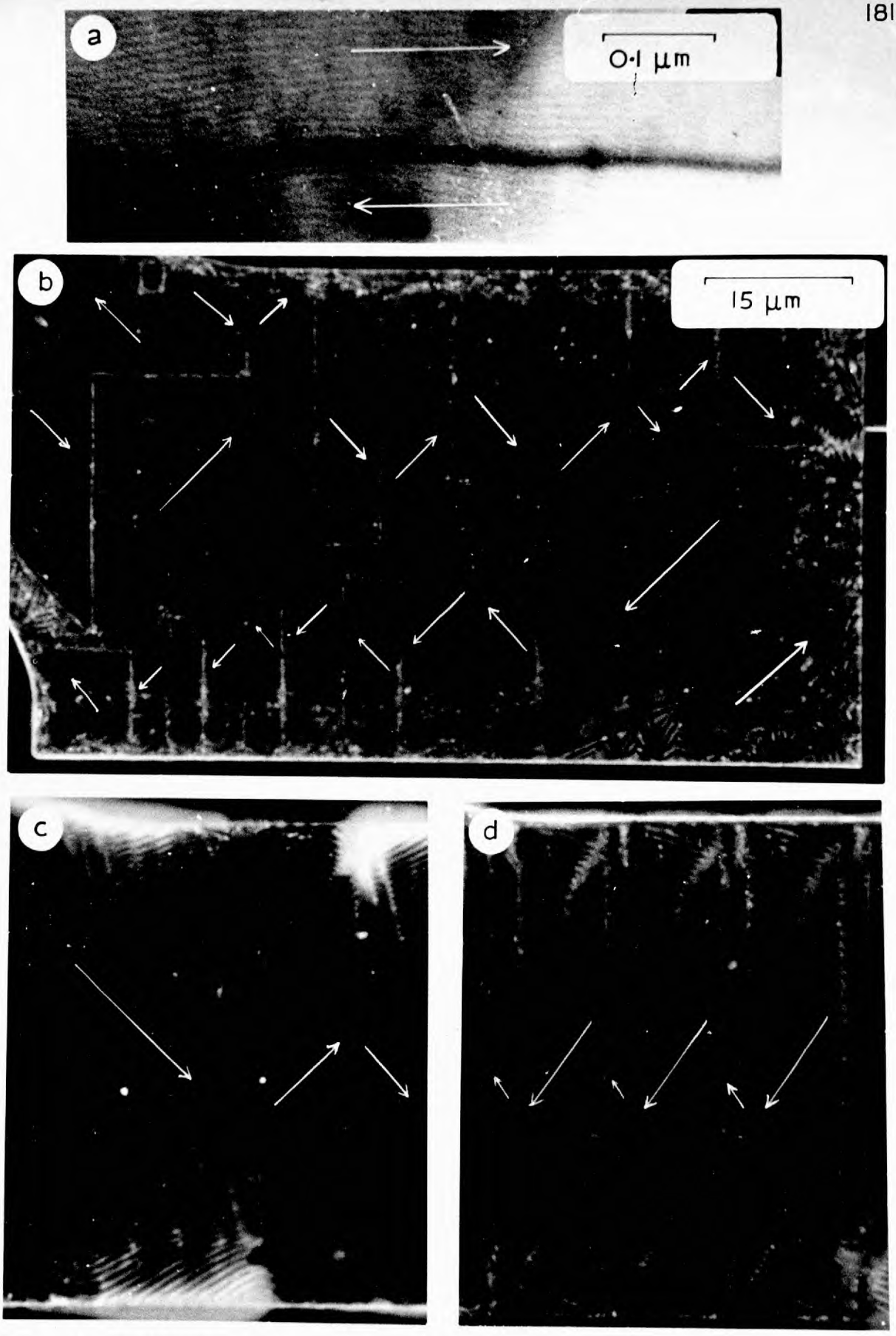

Fig. (6.8) Mixed stripe structures

applied exactly along the easy axis and strain was unlikely to have affected the domain pattern. A frequently observed feature of platelets with stripe domains was the poor definition of the zero field structures, which is why the photograph preceding FIG.(6.9a) was omitted.

This photograph, FIG.(6.9a), shows the pattern in a field of 27 oe where 90° walls were seen to stretch across the width of the crystal as the magnetisation 'zig-zagged' along its length. Weak type II stripes were clearly visible but did not show a uniform direction in any domain. Instead they showed a waving variation within the domain and a general rotation away from the field direction. At the edges of the domains with magnetisation lying in the field direction sudden changes occurred to a stronger stripe structure, which made an angle of between 15° and 20° with the platelet edge and which, judging by the colloid collection, had a large stray field.

It is possible that these edge areas were formed by type III stripes. (The boundary conditions between type II and type III were discussed in section 6.2.1). It is further possible that the type III structures formed because no closure structures (familiar in thinner platelets) existed at the edge, and the edge stray field from the type III stripes was lower than from the type II. Then in order to maintain a constant normal component of magnetisation across the boundary between the two stripe regions, a torque was exerted on the type II stripes causing them to deviate and the boundary to adjust and adopt an equilibrium angle. This angle was not necessarily constant because of the changing effective magnetic field in the proximity of the edge.

The effect of progressive increases in the magnetic field are seen in FIG.(6.9b) at 60 oe, (c) at 83 oe and (d) at 107 oe. In (b) most of the 90° walls had shrunk to spike domains although faint colloid collections could still be seen across the platelet in four

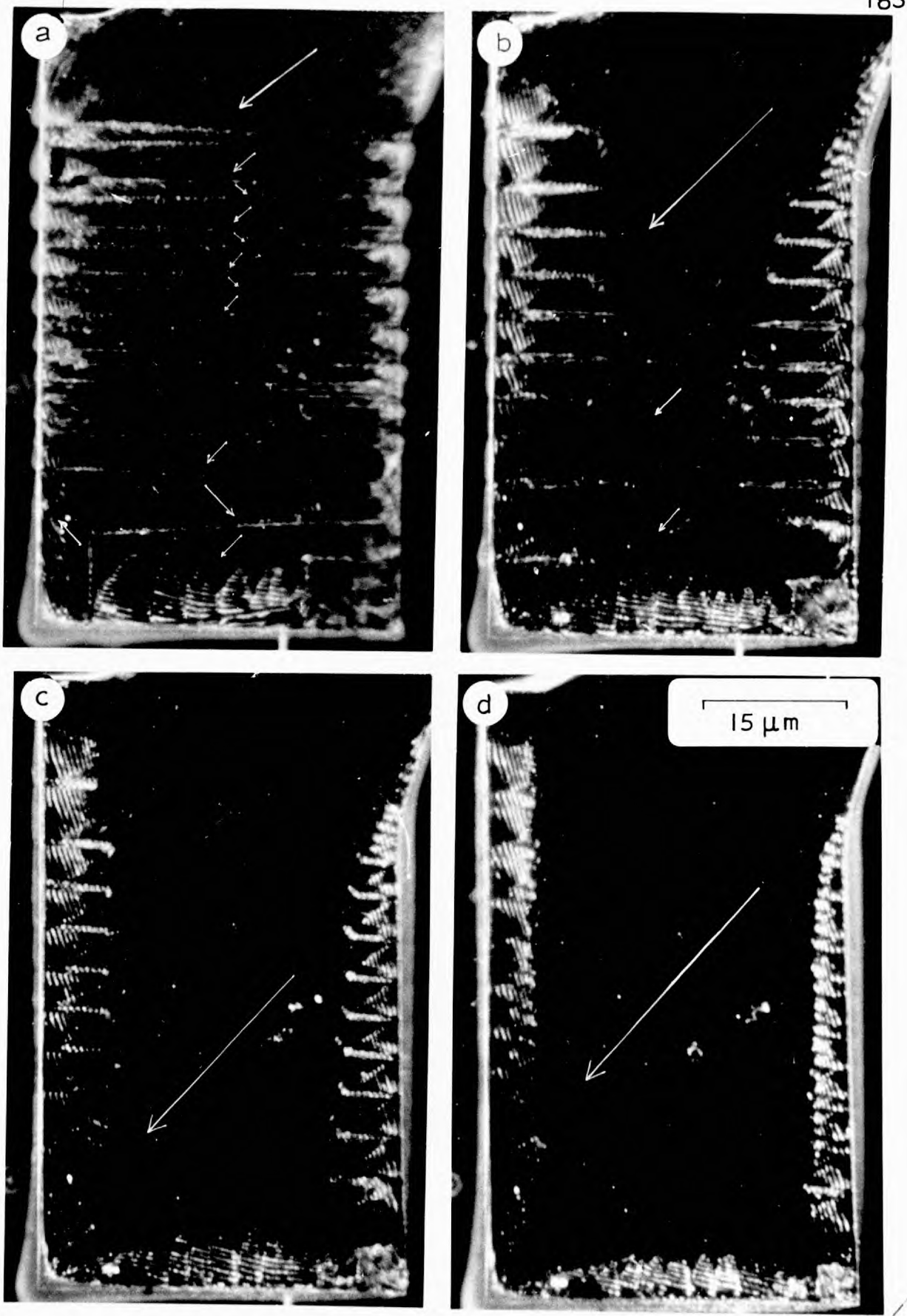

Fig. (6.9) Application of easy axis field

places, indicating the remains of possible double walls. The striations from the type II stripes decreased, and with the decrease in the 90° walls also rotated back to a more normal angle of about 45° with the <100> edges. The volume of the type III stripes increased along all the edges, where they formed a very regular pattern. The spike domains themselves were narrow (~2 μm wide) and showed a similar periodic spacing, in the colloid collection along their walls, to the stripes. In FIG.(6.9c & d) the spikes shrank back and merged with the strong stripe domains.

During these processes it is interesting to note how the colloid distribution along the edge of the platelet became more uniform with increasing field, as the edge became entirely flanked by the type III stripes. With increasing field gaps also appeared in the colloid stripe formation. In some circumstances this might have been attributed to a lack of colloid particles, but this does not apply here and suggests that the magnetisation was lying in the plane of the platelet with a certain amount of curling occurring near the edge. It is possible that the platelet was of such a thickness that the stripe domains were only just stable, and their very presence was influenced by the local magnetic field conditions.

Two further interesting observations are seen in FIG.(6.8c & d). Part of the platelet is shown in (c) in a decreasing field of 27 oe, i.e. a similar field to that of FIG.(6.9a). The tips of the type III stripe regions stretched right out into the type II regions and very large colloid clouds gathered where these same fields ended at the edges. Finally, FIG.(6.8d) shows the effect of a 61 oe field across the opposite diagonal of the platelet. The 90° walls stretched across the platelet and a fascinating boundary shape formed between the two types of stripes.

The shape of this boundary between the type II and type III stripe regions may be influenced by restrictions on the free movement of the domains along the edge itself. It can be seen that the 90°

walls did not always make direct intersections with the edge and small spike domains may have existed, thus distorting the local field. If, as suggested above, the transition between the stripe types is affected by the local field, then the presence of the spikes may, by distorting the field, have given the stripe boundary this shape.

6.2.3 Stripe Behaviour in Magnetic Fields

Observations have been made on several Ni crystals with thicknesses in the region of 6,000 Å whose stripe domains have shown similar behaviour. One of these, a kite-shaped platelet with rectangular dimensions 98x90x0.64 μm. is discussed in detail. The virgin structure of this platelet is seen in FIG.(6.10a) and a demagnetised pattern at higher magnification in FIG.(6.10b).

Careful inspection of FIG.(6.10a) enabled overall magnetisation directions to be ascribed to the domains by analogy with the closure structures familiar from thinner platelets. The presence of 180° walls was often marked by a line of colloid separated from the stripe pattern, this can be seen clearly in FIG.(6.10b), but the 90° walls were not always so apparent.

If the magnetisation directions have been ascribed from the overall flux closure pattern in the platelet, as has been done here, the relationship between the stripes and the magnetisation directions in the main domains is established. Each of the main domains consisted of several stripe regions where the stripes made an angle of 80° with the net magnetisation and 8° with the nearest [100] direction. The stripe spacing remained very uniform with a 0.8-0.9 μm. separation. The effect of applying magnetic fields, see below, showed the magnetisation direction not to be constant in a given domain but to vary slightly (as shown by the dashed arrow in FIG.(6.10b)) creating a low angle wall between the various stripe regions in one domain. It is seen, therefore, that the magnetisation distribution over most of the platelet can be explained by a structure based on the type III stripe

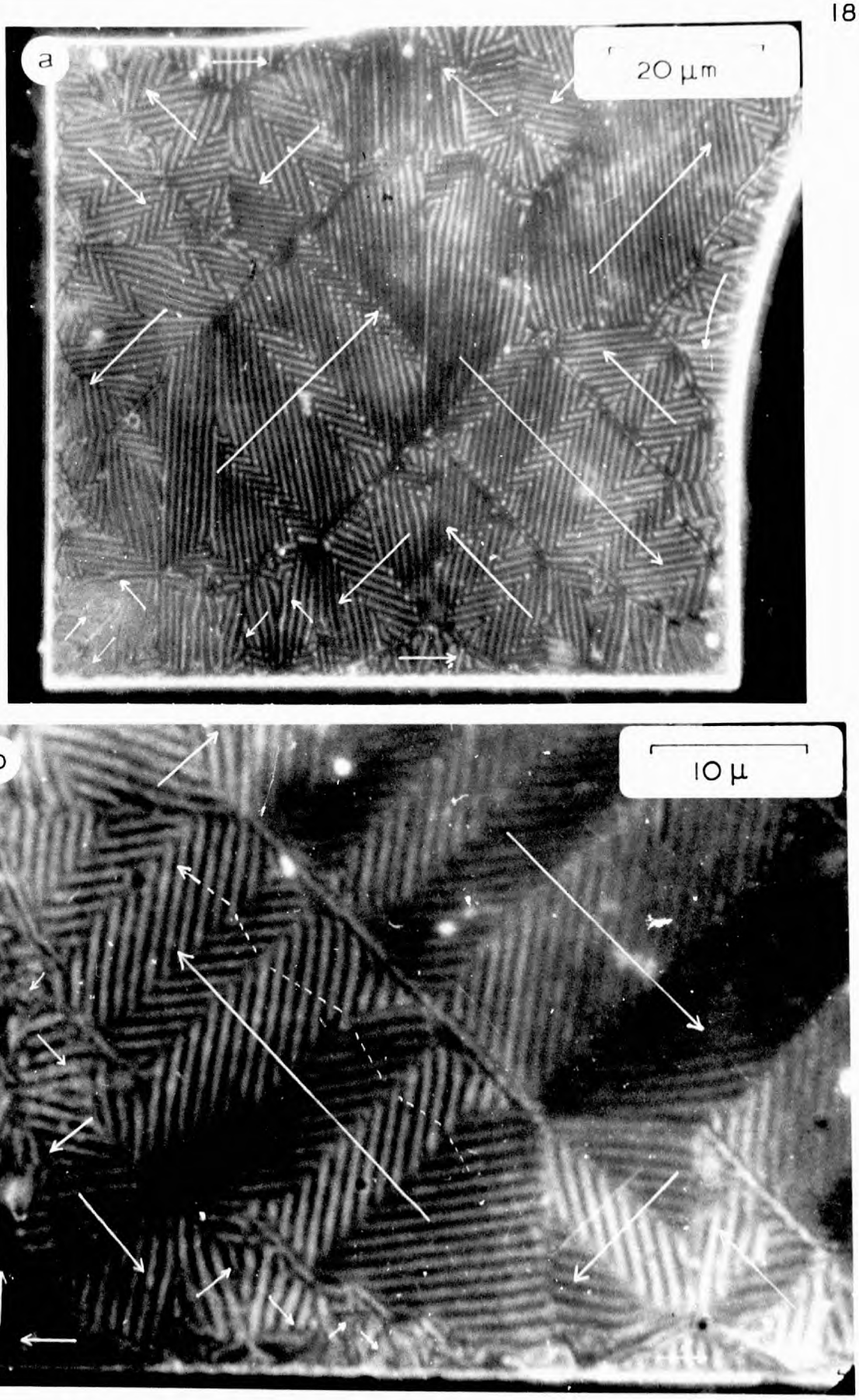

Fig. (6.10) Platelet showing Type III stripe domains

domains.

Where the magnetisation changed fairly rapidly over small areas, near the edges of the platelet, the stripe pattern was more complex. This can be seen along the bottom edge and the left-hand corner of FIG.(6.10b). At the base of some of the echelon structures small triangular regions were visible in which the magnetisation lay parallel with the edge of the platelet. The stripes, however, were normal to the platelet edge, which could only be explained satisfactorily if they were assumed to be type V.

(c) Easy Axis Fields

The effect of an easy [110] axis field is seen in FIG.(6.11), with the initial zero field structure after demagnetisation shown in FIG.(6.11a). The main domains stretched across the platelet, but these were normal to the easy axis along which the platelet had been demagnetised. On several occasions when this was repeated the same structure formed, indicating its particular stability in this crystal. The dark field illumination was slightly off-set in this picture to increase the contrast and emphasise the presence of similarly oriented stripe regions.

With the applied field directed towards the bottom left-hand corner only small areas of the platelet had favourably oriented initial magnetisation directions (notice especially the echelon structures on the upper left-hand side and the lower right-hand side). These areas became enlarged at 8 oe, FIG.(6.11b) while areas with reverse magnetisation shrank and the remaining areas with neutral magnetisation directions adjusted to accommodate these changes. This process is seen in a more advanced stage at 16.5 oe in FIG.(6.11c).

The two stripe orientations in the main transverse easy axis domains did not behave equivalently under the magnetic field, but one orientation grew at the expense of the other, indicating a slightly off-set orientation of the net magnetisation within each stripe

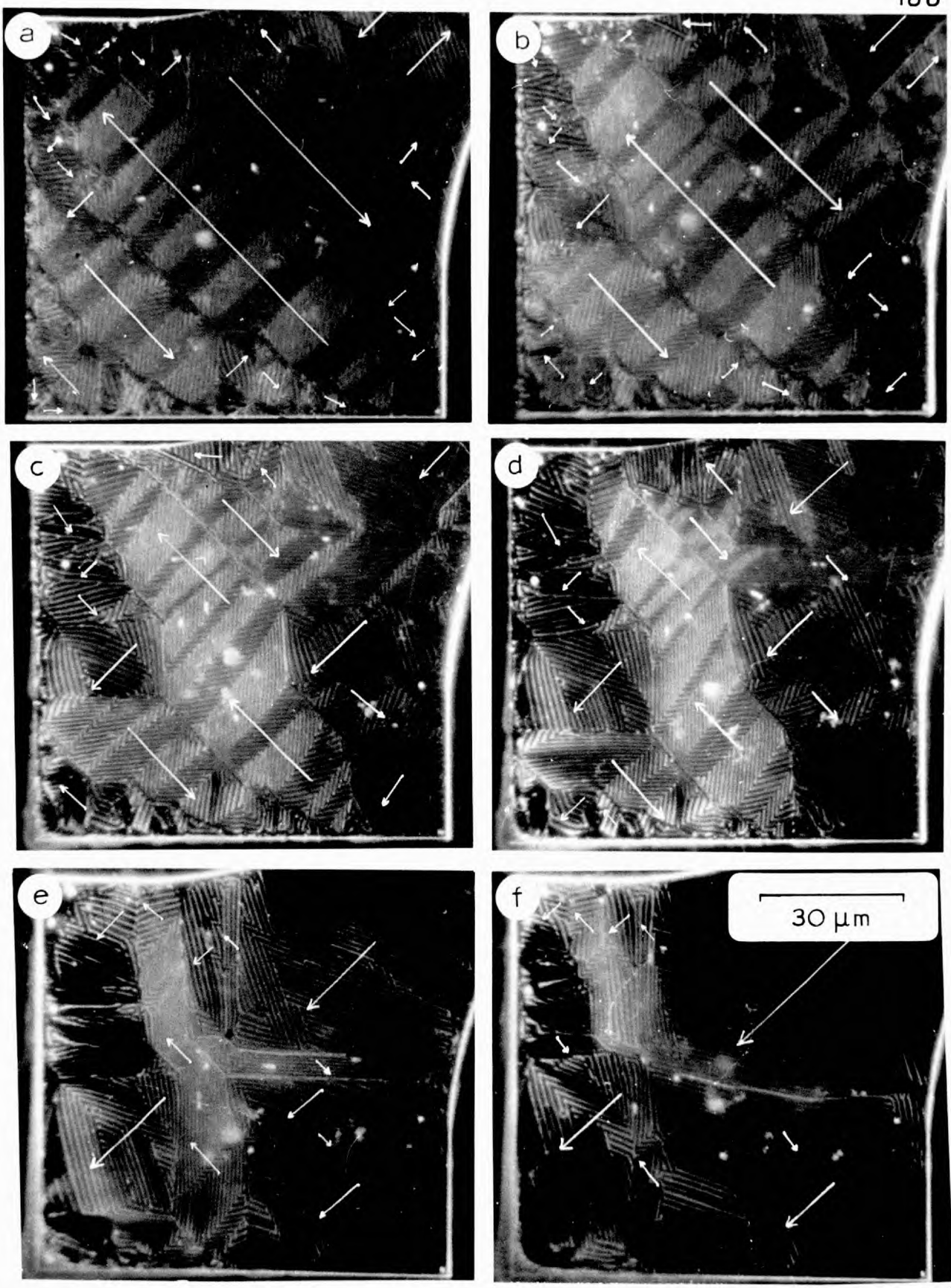

Fig. (6.11) Application of easy axis field

sector, see FIG.(6.12).

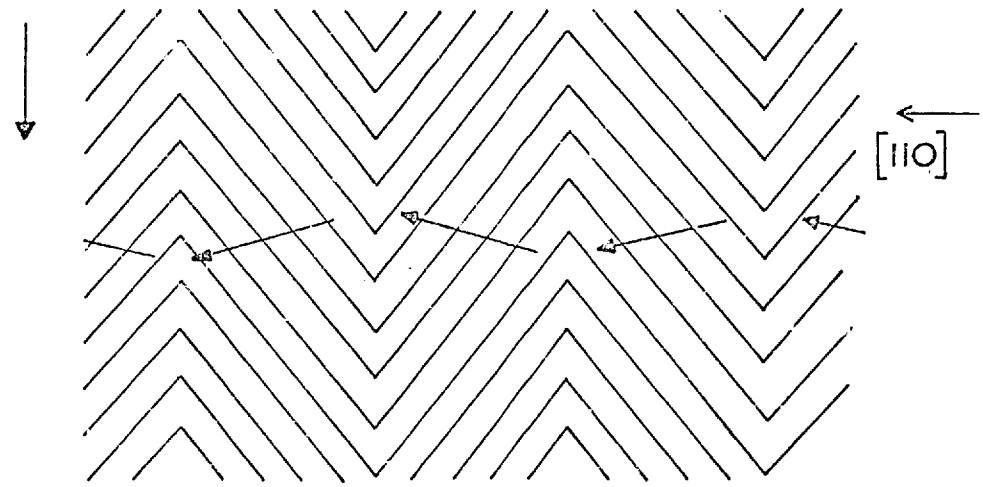

FIG.(6.12) SUBDIVISION OF DOMAINS WITH TYPE III STRIPES

The 90° rotations which subdivided the closure echelons were not visible as distinct walls even in zero field. As the field increased the division became even more complicated and the echelons on both the left-hand and right-hand sides of FIG.(6.11c) showed a complex stripe pattern with the stripes bending through angles of up to 20°, and even subdividing. The net result of this was to increase the magnetisation volume favourably oriented towards the field direction.

A further three photographs were taken at 26 oe, FIG.(6.11d), 41.5 oe, (e), and 59 oe, (f), and show a continuation of the above process. In (e) it was still just possible to correlate various regions of the platelet to determine how the existing structure had been reached, but in (f) this was no longer the case. At higher fields the stripe formation seen in the top right-hand corner of (f) formed across the entire platelet.

The behaviour in higher fields is seen more clearly in FIG.(6.13) which shows two pictures taken from a set on a separate but almost identical platelet, at 44 oe, (a), and 55 oe, (b) Long sweeping

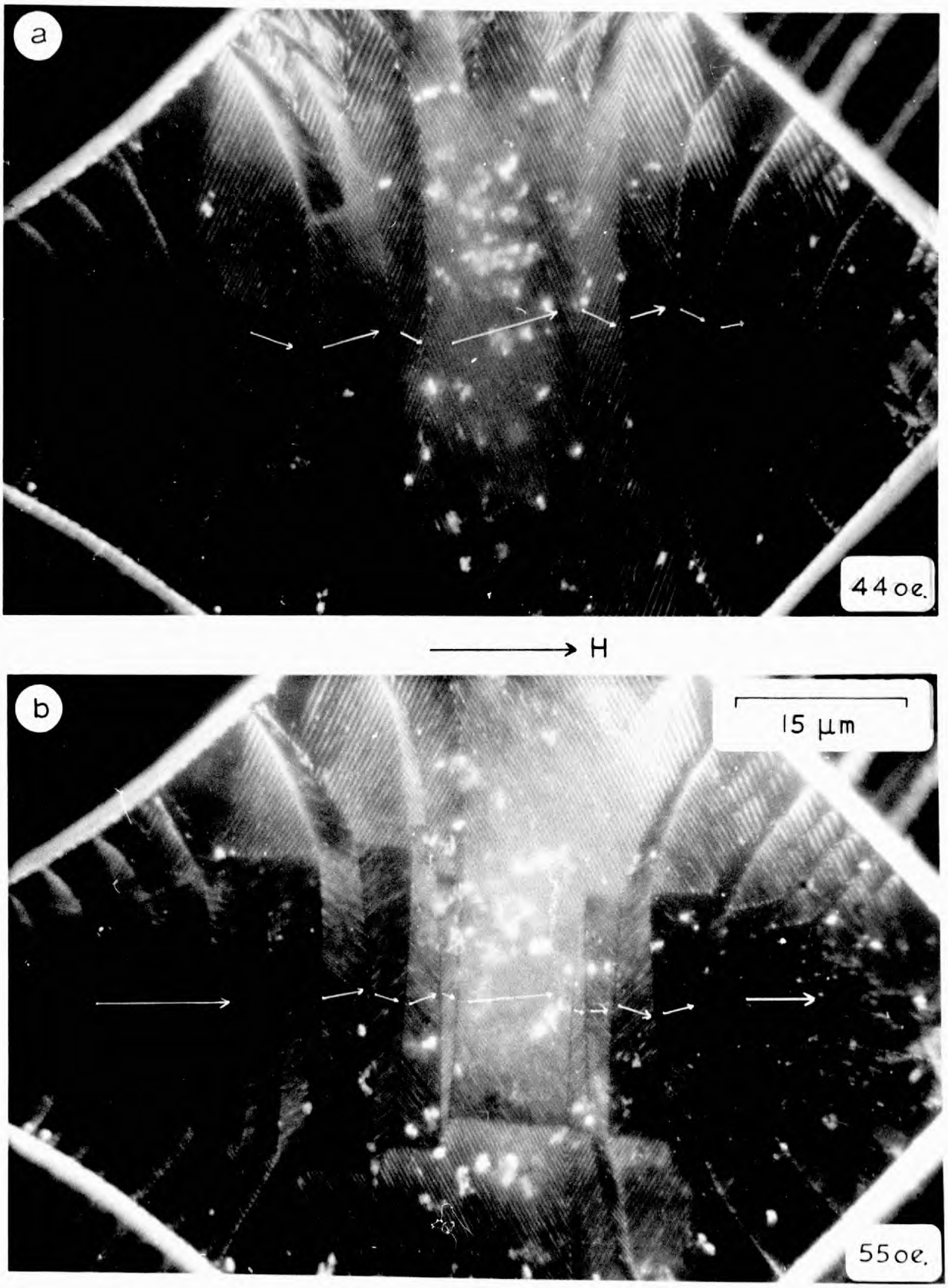

Fig. (6.13) Type III stripes in higher easy axis fields

stripe areas crossed the platelet, FIG.(6.13a), and the angle between stripes in adjacent sections decreased to about 65°. The stripe width varied from about 0.9 μm. in the centre of the platelet to 1.3 μm. at the edges. It would appear that the decreased angle made with the field direction was unstable, and with a further increase in field, a slight rearrangement occurred to give low angle stripe boundaries of up to 20°, see FIG.(6.13b).

The stripes finally just faded away at higher fields. The beginning of this can be seen on both the left-hand and right-hand sides of this photograph. At higher fields the size of the stripe-less area slowly increased until only small edge stripes remained. Visual observations could only be made to 160 oe. where some stripes still remained. It is interesting to note that thinner platelets showed no evidence of domain structure in comparable easy axis fields although reverse nuclei probably still existed, as has already been discussed. To check whether these were freak conditions the platelet was removed and inserted in a 10 k oe field, subsequent observation showed the stripes to have returned and their behaviour to remain unaltered.

(b) Hard Axis Fields

Starting from a magnetic structure identical with that of FIG.(6.11a) the effect of a hard [100] axis field was investigated on the same platelet. The observed movement of the stripe domains is seen in FIG.(6.14) in a field of 16 oe, (a), 31 oe, (b), 49 oe, (c), 65 oe, (d), 85 oe, (e), and 120 oe, (f). The field was applied in a direction from the top to the bottom in these photographs.

Unlike the case in the easy axis field none of the domains had its magnetisation oriented in the field direction, but the left-hand and right-hand structures both showed favourable orientations and expanded. The beginnings of this at 16 oe can be seen in FIG.(6.14a). On the left-hand side a triangular closure domain with type V stripes

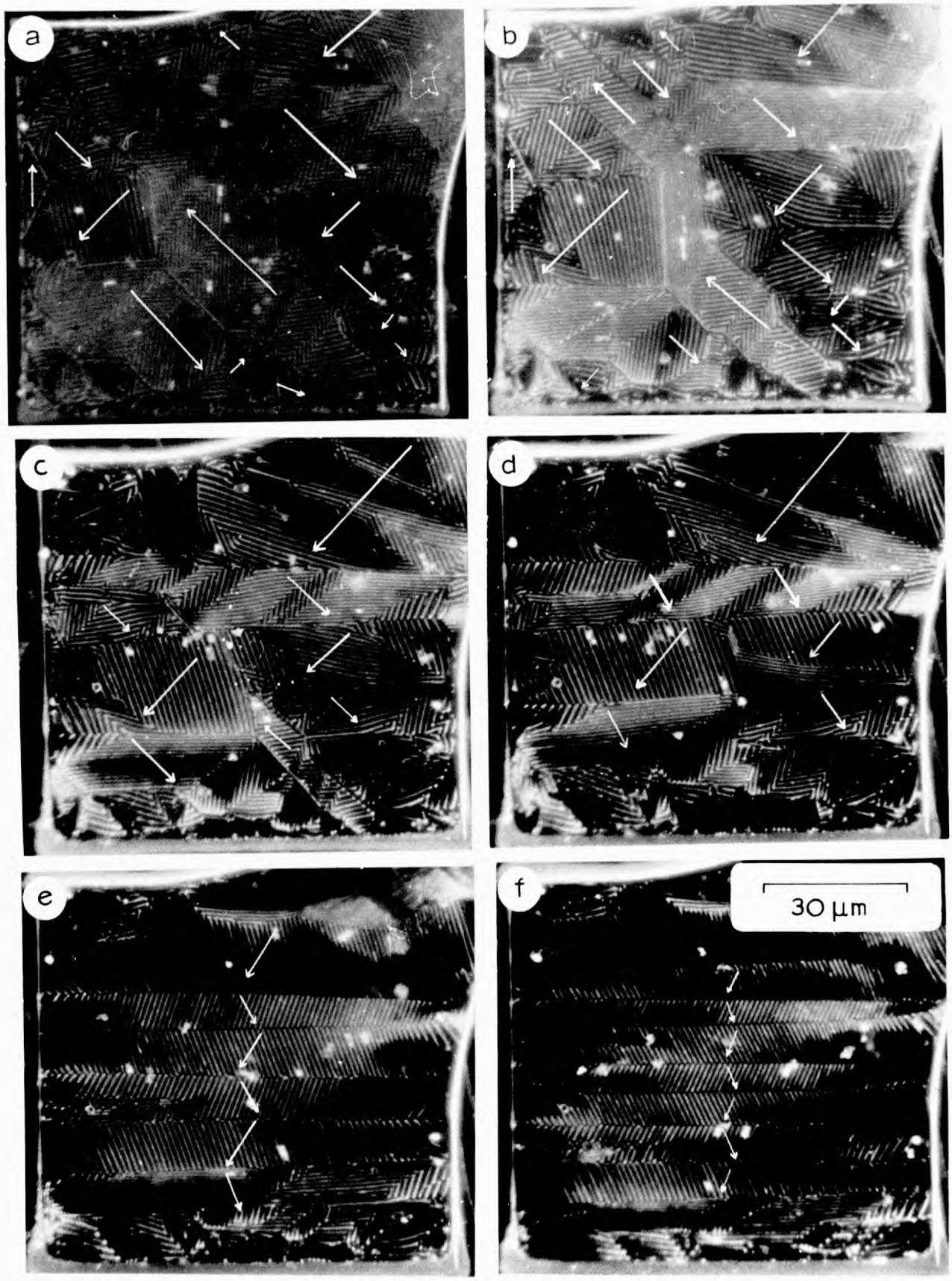

Fig. (6.14) Application of hard axis field

can be clearly seen, but with reversed magnetisation it shrank in higher fields.

The two main domains of the opposite echelons displaced the stripe domains existing in the centre of the platelet and met under an applied field of 49 oe, FIG.(6.14c). Smaller regions in (b) with stripes in the appropriate orientation also expanded at the expense of the horizontal stripes. This process continued and is seen at 65 oe, (d), and 85 oe, (e), where a very regular stripe structure covered the centre of the platelet. The behaviour of the bottom of the platelet is too complex to interpret, and with the minima in the anisotropy, the magnetic field and the magnetostatic energies all oriented in different directions, this is hardly surprising. Finally, (f) at 120 oe shows a further division of the stripes at higher fields.

The angle that these stripes made with the applied field direction as a function of that field is shown in FIG.(6.15). In the low fields this angle was taken from the stripes in the main domain of the left-hand echelon structure. The angle that the stripes made with the field would seem from these results to have increased linearly with field. An error of $\pm 2^{\circ}$ is shown in FIG.(6.15), being representative of the accuracy in setting the protractor used to measure the stripe angle. In addition to this it will be noticed that a slight angular variation also occurs along the length of the stripes in a given area, presumably in response to changing values of the local field.

Three photographs were taken in decreasing field immediately afterwards, and the stripe angles from these are also shown in FIG.(6.15). The fact that these lie on a lower curve can be tentatively explained by the sequence of measurement. The angles taken from FIG.(6.14) in increasing field were measured on a specimen that had just been demagnetised along a [110] direction, whereas those in decreasing field were from a specimen that had been saturated

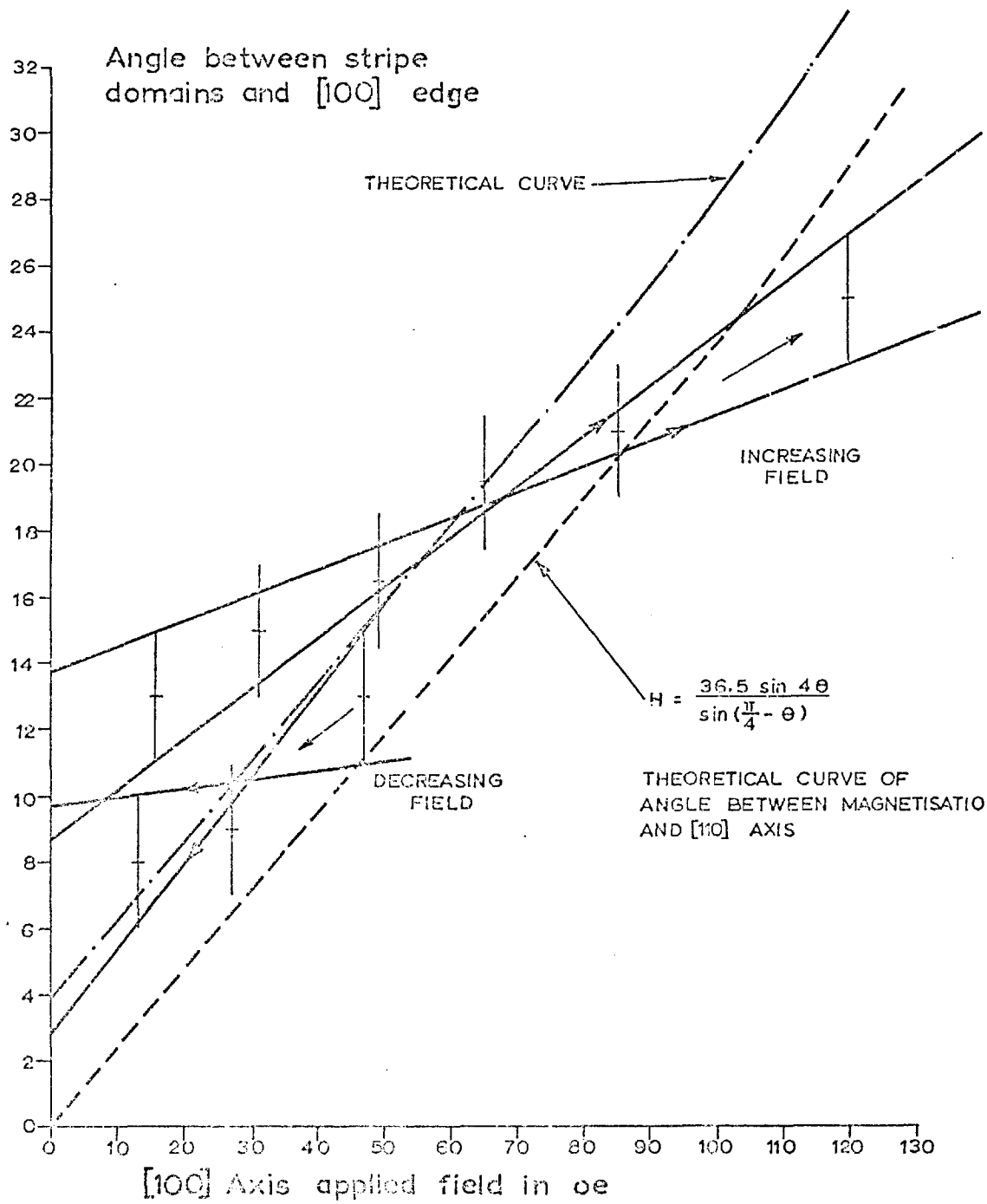

Fig (6.15) Stripe angle as function of hard axis field.

in a [100] direction. It is thus possible that the surrounding areas, having different magnetisation arrangements, had produced different local torques on the magnetisation in either case.

A basis for an explanation of the increase in the angle between the stripes and the [100] direction has been advanced by Leaver (1969). He considered the rotation of the magnetisation from the <111> directions by a field applied in the [100] direction, but at the same time constrained the magnetisation to maintain a constant angle ϕ with the [001] direction. He equated the field torque on the magnetisation with the rate of change of the anisotropy energy due to the angular rotation (see Appendix 'D') and found that the field excitation could be expressed by the equation

$$H = \frac{36.5 \sin 4\theta}{\sin (\frac{\pi}{4} - \theta)} \qquad (D.4)$$

where θ is the angle between the planar component of the magnetisation and the [110] direction.

This function is also plotted in FIG.(6.15) and is seen to be almost linear. The structures seen on this platelet have also been seen on much thicker platelets (see section 6.2.4) where the anisotropy is more important than the magnetostatic energy, which suggests that in zero field the magnetisation is already oscillating between <111> directions. Thus if the stripe structure itself tends to maintain the magnetisation angle ϕ with the [001] direction, the application of a field causes rotation of the stripe pattern as the magnetisation structure rotates towards the (100) plane in the field direction, pulling the stripes towards the [110] direction.

The theoretical values of H in FIG.(6.15) would be depressed slightly when the demagnetising field is considered, thus bringing the gradient into better agreement with the observed values. This field varies according to the position in the platelet of the region where the behaviour of the stripes is being studied.

A similar expression to equation D.4 can also be derived for the application of an easy axis field normal to the initial magnetisation direction. However, it is apparent from FIG.(6.11) that in this case the greater part of the magnetisation re-alignment is achieved by domain wall motion rather than by rotation.

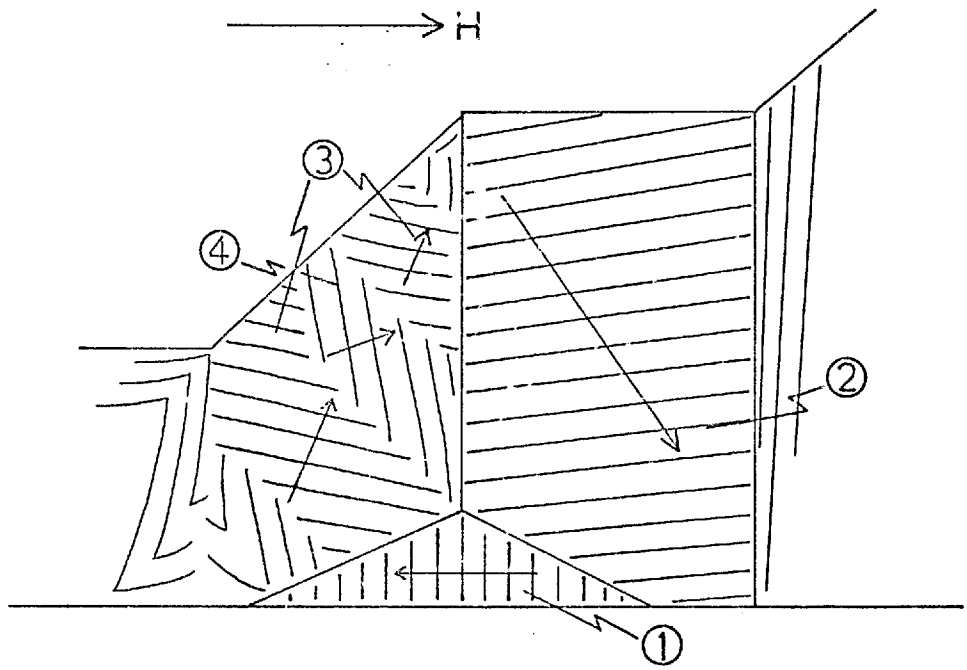

FIG.(6.16) ECHELON STRUCTURE IN STRIPE DOMAINS

Evidence from the application of an easy axis field, FIG.(6.11), has already suggested that the magnetisation in the various stripe regions within one domain is offset from the [110] direction. This was shown diagrammatically in FIG.(6.12). Further evidence for this is seen in FIG.(6.16) which is a representation of part of the left-hand side of FIG.(6.14a). In this diagram the triangular reverse closure domain (1) is thought, as in the thinner platelets, to have its net magnetisation lying parallel with the edge and must therefore have a type V stripe structure. The domain walls bounding this region will bisect the magnetisation directions on either side if no charges are formed along them and the planar components of magneti-

sation in each domain are equal. This therefore fixes the magnetisation directions in the type III stripe regions. Thus, a relationship between the magnetisation and stripes is established, and is seen in FIG.(6.16) to agree with the previous suggestion, shown in FIG.(6.12).

The magnetisation in region (2) of FIG.(6.16) makes an angle of 5° with the [110] direction and 60° with the stripes in that section. Thus, to get a true comparison between the theoretical and experimental curves in FIG.(6.15) for this particular region a -5° correction should be applied to the theoretical curve. Remembering that in this region the magnetisation makes a 60° angle with the stripes, the theoretical curve can be converted to represent the angle between the stripes and the field. This would then predict an angle of $+10^{\circ}$ for the zero field angle with the same slope as the curve representing equation D.4. Displacing the curve by $+4^{\circ}$, as shown in FIG.(6.15), brings it into better agreement with the range of experimental points, however the slope remains in error. This suggests that the magnetisation and the stripe pattern may not be as rigidly coupled as has been implied, and relative rotation may occur with the magnetisation turning away from the <111> directions and into the plane of the platelet.

Alternatively, it must be remembered that the rotational theory in Appendix 'D' has assumed that the entire magnetisation lies in the <111> direction, whereas in any real stripe structure other magnetisation directions are also present. If the effect of a complete distribution rotating were considered, the equilibrium between the torque and rate of change of anisotropy energy might not be the same. This would lead to a different dependence of the stripe angle on the applied field than given by equation (D.4) and might be in better agreement with the experimental results.

Region (3) in FIG.(6.16) is equivalent to region (2) and behaves in the same manner, but the magnetisation in region (4)

points 10° nearer to the field direction than in regions (2) or (3). With the increase in field the stripes in this region rotated until they lay normal to the field direction, see FIG.(6.14d). The stripe spacing had decreased and the magnetisation probably made an angle of 25° with the field direction. Further rotation of region (4) appeared blocked by the nature of the structure and the type (2) and (3) regions continued to grow at its expense, until only they existed. A change in the stripe spacing of the type (4) regions in FIG.(6.16) was also observed and may have occurred through a magnetisation rotation away from the <111> directions. The effect of the blocking of the stripe rotation and the change in spacing precludes the application of the above theory to these type (4) regions. Further details of this blocking are described in section 6.2.5.

6.2.4 Stripe Domains in Very Thick Platelets

Observations have also been made of stripe domains in platelets more than an order of magnitude thicker than those discussed in section 6.2.3. Two photographs of the virgin stripe structures in a triangular platelet, which was approximately 9 μm. thick but not of constant thickness, are seen in FIG.(6.17). The first (a) shows what is clearly an echelon structure on a [100] edge of the platelet, and the second (b) shows an enlarged view of a central domain area, with a similar structure to the area at the top right-hand corner of (a).

The central structure (b) shows what must have been two 180° walls extending vertically across the field of view, although there was effectively no colloid collection along them but a very precisely defined gap in the stripe pattern. Small triangular closure domains with an absence of stripe domains were visible on either side of these walls, although detailed examination of the original negative showed these to be smaller than the photograph suggests. Although shown clearly in FIG.(6.17b) the small triangular regions are not unique

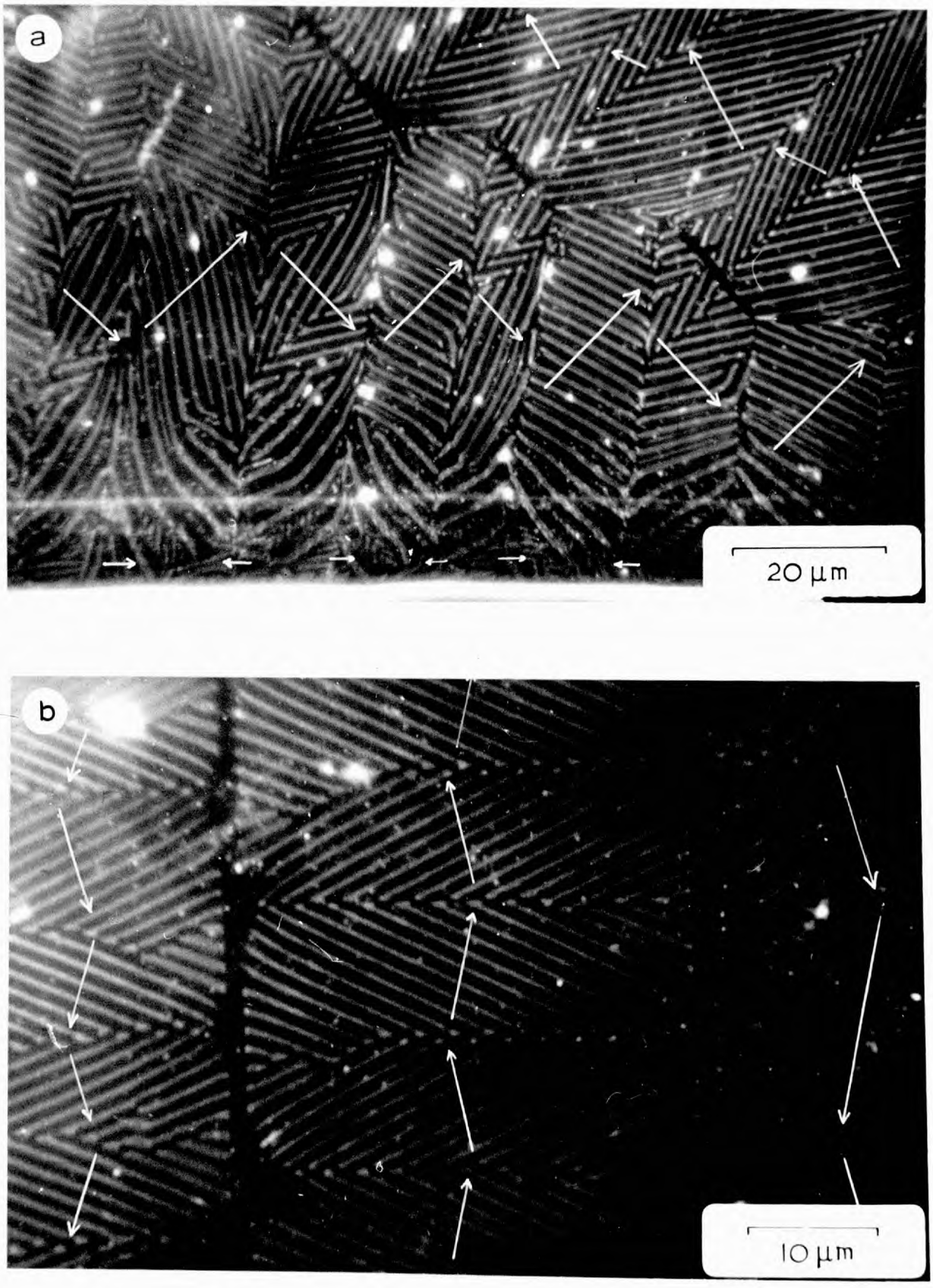

Fig. (6.17) Stripe domains in very thick platelets

to these very thick platelets and reference to the work on thinner platelets confirms their presence in platelets where the 180° walls are visible, see FIG.(6.10, 11 & 14). However, none of the observations that have been made have given any definite indications of the magnetisation directions in these very small regions. The acute angle between the stripe sections in any domain was 53° and the spacing 1.5 μm.

The stripe structure in the echelons was more complex than in the centre of the platelet, especially near the edge. Examination under an optical microscope showed that there was a thickening of the platelet along the [100] edge shown and the line across the bottom of FIG.(6.17a) was a real thickness contour on the crystal. At this edge the platelet was 9 μm. thick and decreased to 6-7 μm. in the centre. A significant increase in the stripe spacing could be seen with the appearance of a second weaker stripe between the strong stripes and near the very edge a complete set of fine stripes, showing the greatly increased width of the main stripes. Distinct closure domains were generally not visible and the complexity of the pattern was probably due in part to the increased magnetic freedom with the thicker edge, and in part to the amount of flux closure that was being achieved within the stripe patterns.

The top wall of the echelon structure in FIG.(6.17a) consisted of alternate 180° and 90° wall structures. It will be noticed that, in a similar manner to FIG.(6.17b), colloid failed to collect along the 180° boundary and the 90° wall was hardly visible except from the alternate intermeshing of the stripes. It would seem that this type of stripe pattern can accommodate a 90° magnetisation change within its structure but not the change required for a 180° wall.

The application of an easy axis field to another thick triangular platelet is seen in FIG.(6.18). The platelet measured 280 μm. along the hypotenuse and was 13 μm. thick. The four photographs were

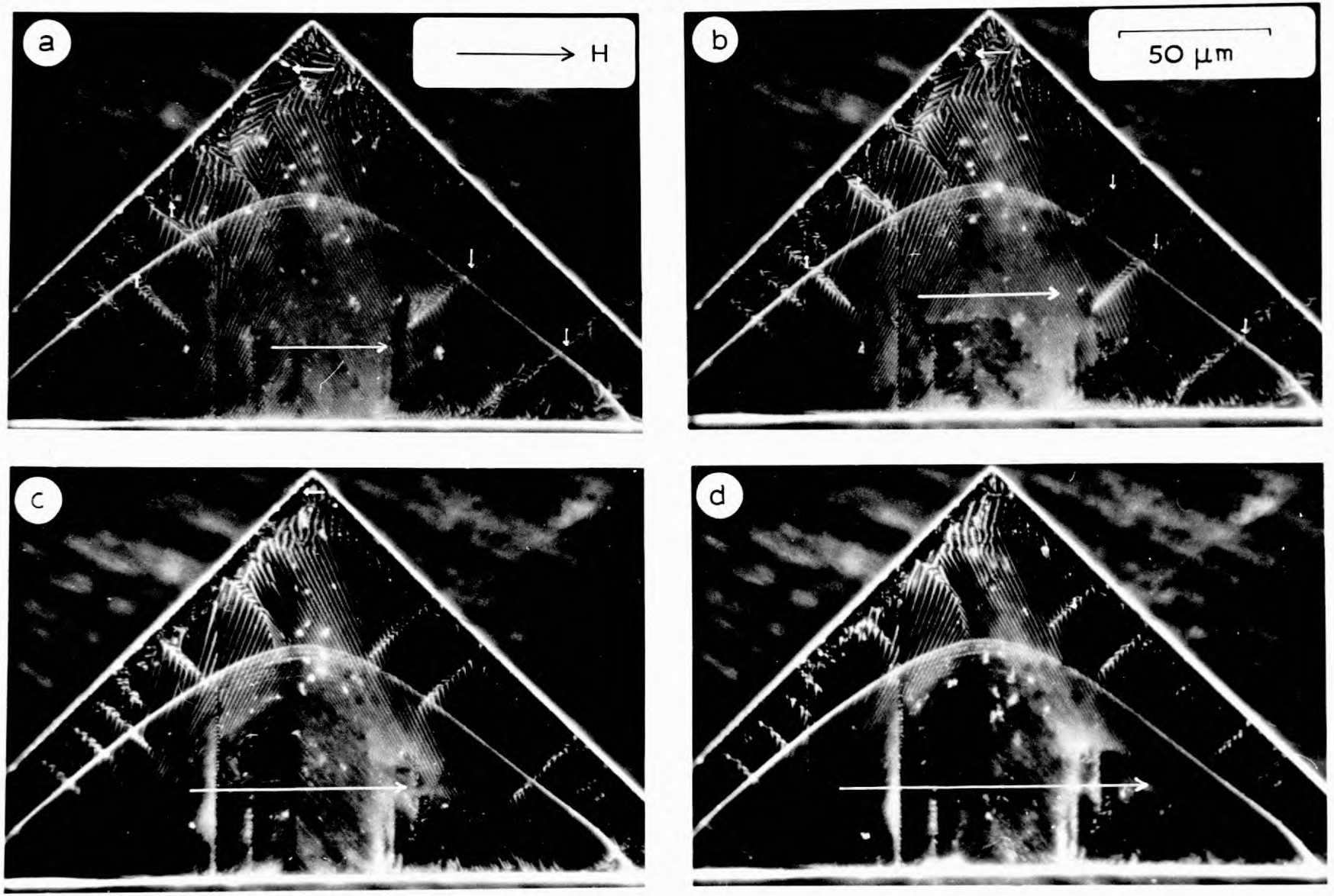

Fig. (6.18) Application of easy axis field in thick platelets

taken from a set and show the behaviour at intermediate fields 47 oe, (a), 58 oe, (b), 83 oe, (c), and 105 oe, (d).

Three features were immediately apparent. The major growth step and a series of minor ones inside it, which crossed the centre of the platelet in an arc, were at no time seen to have any effect on the behaviour of the stripes and could be ignored. Thus at these dimensions the thickness of the platelet was not critical in determining the behaviour of the stripes. Several vertical lines, parallel with the [110] direction appeared on all pictures. They appeared not to be structural, but exerted a large influence on the local stripe structure. Finally, the appearance and behaviour of spike domains forming on the [100] edges, then shrinking to disappear at higher fields, showed identical overall behaviour with that familiar from studies on thinner platelets, without stripe domains.

At 47 oe, FIG.(6.18a), two spikes had formed on the right-hand edge of the platelet and three on the left-hand side, with a fourth just emerging in the stripe pattern. The stripe angles both inside and out of these spikes fitted the now familiar type III description, but the pattern at the apex and along the top of the right-hand side showed great complexity and a wide spacing. Due to the proximity of the edge the effective field in these regions was lower but the kinks and terminations of the stripes were fascinating although unexplained. Another interesting region was the low angle stripe boundary near the centre of the hypotenuse of the platelet, formed by successive spikes terminating.

An increase in field to 58 oe, FIG.(6.18b), caused the spikes to decrease in size but increase in number, and the reverse closure complex to be pushed further towards the apex. This process was taken a stage further in a field of 83 oe, (c), with most of the platelet covered by large sweeping stripe domains. The effect of the vertical lines, mentioned earlier, showed very strongly, but the

stripes also underwent slight directional changes for no apparent reason. At occasional places across the platelet regions existed where the stripes completely disappeared, presumably because the magnetisation then lay entirely within the platelet plane. At 105 oe, FIG.(6.18d), the stripeless areas dominated the platelet but stripes still persisted at the apex. Eventually at higher fields these too should disappear. Again it will be noticed that these fields are much nigher than those required to remove domains from thin platelets.

Bearing in mind the greater thicknesses of these platelets it is perhaps rather surprising that a type III structure seems to fit their behaviour. This, however, cannot be certain because no sophisticated quantitative calculations have been performed. The possibility of structures similar or related to those discussed by Krinchik (1968), see FIG.(6.3), should not be overlooked.

6.2.5 Complexities in Stripe Structures

Detailed observations of flux reversal showed many features of stripe domains in platelets which are not understood. These are discussed in this section in conjunction with colloid pictures of stripe domains taken at higher magnification.

The domain photographs seen in FIG.(6.19) were taken from the centre of a long rectangular nickel platelet of dimensions 440 x 27.5 x 0.66 μm. The virgin pattern from a central region of this platelet can be seen in FIG.(6.19a). The magnetisation followed a zig-zag path along the [110] directions in the centre of the platelet. Reverse flux closure was achieved by triangular regions containing type V stripes, seen clearly on the left-hand edge.

Several features seen in FIG.(6.19a) are of interest. In section 6.2.4 the absence of colloid collections along the 180° domain boundaries was noted. In this photograph from a thinner platelet the termination of the stripes on either side of the wall is clearly visible, with a gap before the colloid collection along the

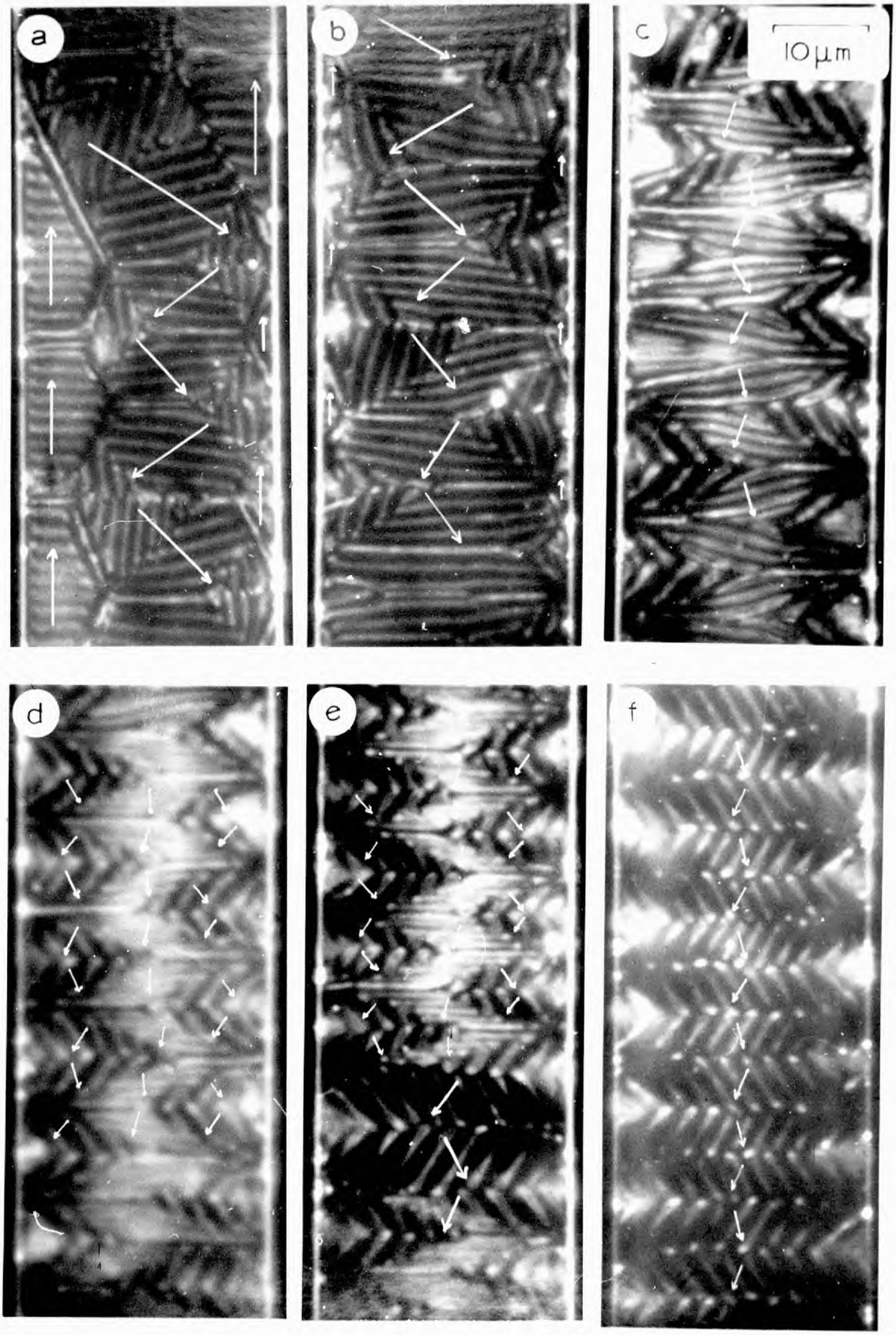

Fig. (6.19) Detailed behavior of stripes with hard axis field. H

wall itself. A slight increase in the colloid collection was sometimes visible at the end of the stripes. This is possibly where the magnetisation was locally rotating more rapidly to lie in the platelet plane. The 180° walls, although necessary from the overall flux pattern within the platelet do not therefore seem to fit well with the oscillations of the stripe domains. This can also be seen in FIG.(6.10).

The forward magnetisation in FIG.(6.19a) appeared to be divided by 90° walls across the width of the platelet. At one end the stripes lay parallel with these walls but at the other had diverged to leave a triangular closure region where the stripes lay almost in the [100] direction. This occurred at opposite ends on alternate walls and must have been important for flux closure. Again, regions like this can be found by referring to FIGS.(6.10 & 11) where stripe domains, although not of the type V lay in a [100] direction normal to the edge but rotated to connect with [100] stripes parallel with the edge. These particular regions played an important part during the application of hard axis fields.

In a field of 6.0 oe, FIG.(6.19b), the reverse triangles with type V domains had shrunk and the closure areas of the main domains expanded. The entire structure is now seen to resemble a Néel strip with a degree of rotation of the magnetisation occurring in the expanded closure areas. Another interesting feature, visible in the photograph, was the splitting of the colloid collection along some of the stripes. At this thickness it was not thought to arise from free poles on the under face of the platelet, as had been observed in thinner platelets, Gemperle and Kaczer (1969).

At higher fields 16 oe, FIG.(6.19c), 25 oe, (d), and 37 oe, (e), these closure areas continued to grow, with the volume of the central domains decreasing. At the same time the spacing of the stripes in this central region decreased, whilst they showed an increased tendency

to lie normal to the field direction and to split. This was unexpected as these regions already had a magnetisation component in the field direction. It would seem therefore that this structure was incapable of rotating fully into the field direction, being in some manner blocked, and therefore had to be displaced by the closure areas, which were apparently more free to expand.

This observation together with the behaviour seen in FIG.(6.14) suggests that the stripes which lie almost normal to the applied field direction show an increased resistance to rotation. This may be because stripe rotation is restrained by the overall magnetic structure of the neighbouring domains and only rotation of the magnetisation within the stripes is possible. Thus the closure domains with the intermeshing of the stripes in the two halves may provide a 'flexible joint' in the magnetisation structure and expand into the centre of the platelet, as seen in FIG.(6.19). The increased magnetic field also caused the spacing of the central stripes to decrease, where the magnetisation was probably locally rotating independently of stripes, and causing the stripes to split.

Finally, at 49 oe, FIG.(6.19f), the particular area shown contained only stripes originating from the closure domains. A light gathering of colloid showed areas where a small divergence of the magnetisation occurred at the edge of the platelet, but, in the main, the magnetisation must have been directed along the [100] axis. The angle that the stripes made with the field direction was, at 30°, much higher than angles previously measured for this field, i.e. about 16° at 49 oe. It could, however, be that the details of the stripe structure were different from that of FIG.(6.14e & f). The spacing of the stripes in the hard axis field in that platelet was 1 μm. whereas the ones seen in FIG.(6.19f) had a spacing of about 2 μm, i.e. twice as wide. A far larger displacement than would seem probable is required to make the theoretical curve in FIG.(6.15) fit this value, again indicating that perhaps these stripes are not exactly of the

same type as those discussed earlier.

Gaps in the colloid between successive orientations of the stripes could be clearly seen, as well as a non-uniformity in the colloid collection. This again indicates the complexity of the structures, even in higher fields.

As an interesting comparison FIG.(6.20a) shows the corner of a platelet 6,200 Å thick in a field of 27 oe applied along the easy axis. A close-up of part of it is seen in FIG.(6.20b). The overall magnetisation directions were certain from familiarity with thinner platelets, with spike domains formed from the edges, and triangular closure domains at the base of the spikes. Yet within this arrangement the stripe domains could be seen to execute very complex variations for no apparent reason.

Observations were also made on both sides of a platelet with stripe domains. Unfortunately, these observations could not be made simultaneously but were achieved by completely immersing a freely suspended platelet in colloid sandwiched between two microscope cover slips, spaced apart with grease. Successive observations were made on either face of the platelet, inverting the specimen under the microscope. These showed a similar overall structure on either face, as seen in FIG.(6.21a & b), but with slight variations in detail.

A 180° wall, if visible on one face, was also visible on the other. The absence of colloid in some of the triangular closure regions, which has already been commented on, occurred on both faces. A slight displacement of the stripes on one face compared with the other was possible but not completely proved. The nature of the stripe pattern in corresponding regions was similar although in detail there may have been differences. These differences are at the limit of resolution of the colloid and may even have arisen from slight obstructions to the free flow of colloid over both faces.

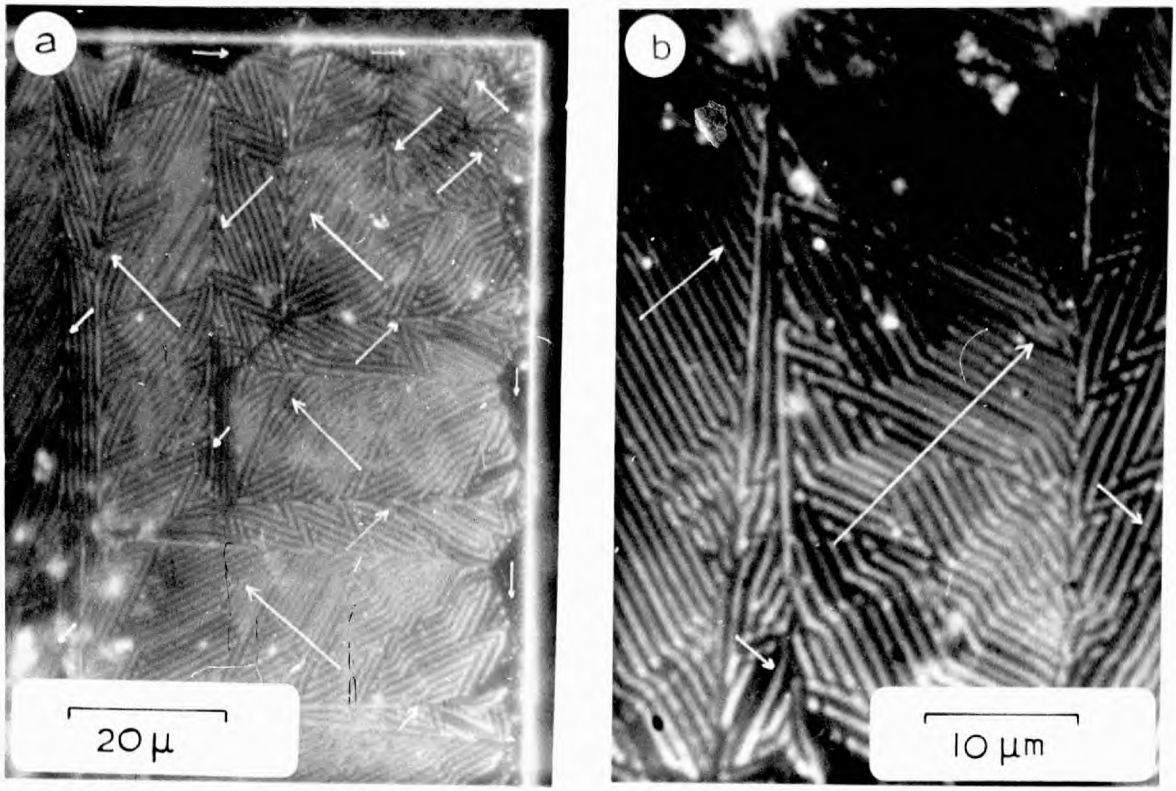

Fig. (6.20) Spike domains in stripe platelets

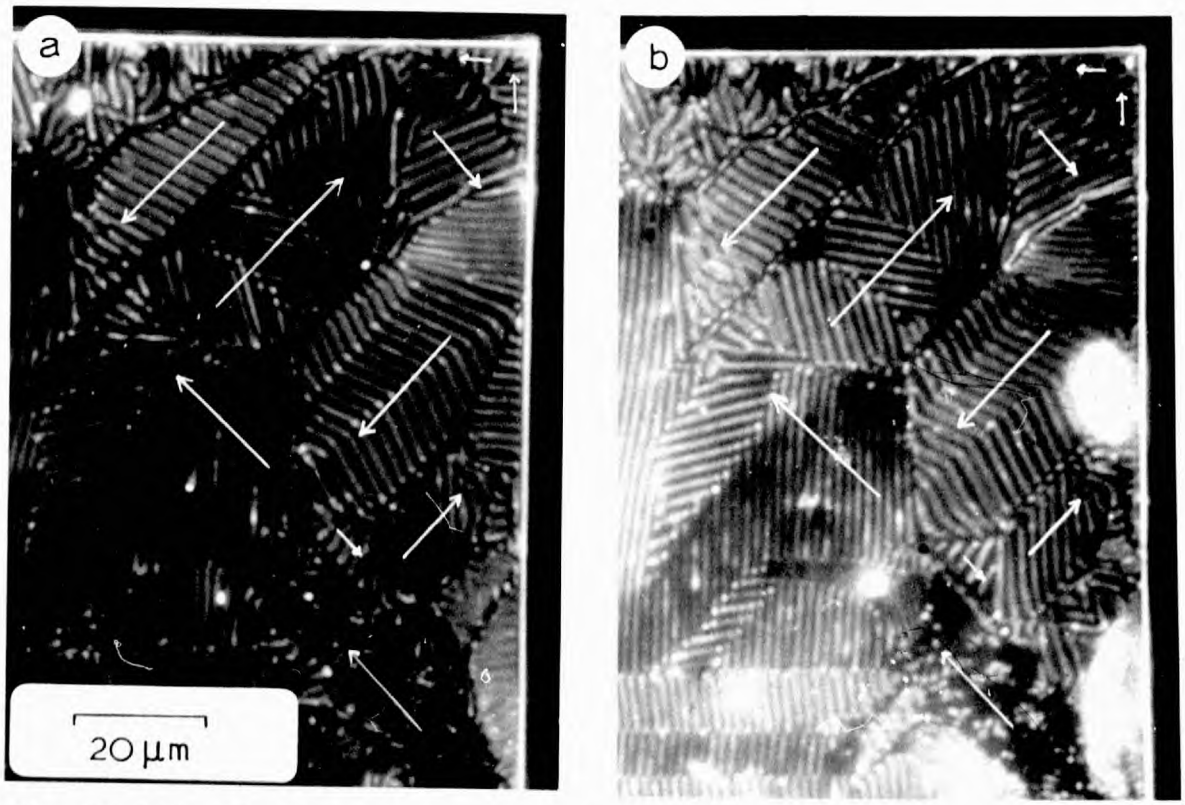

Fig. (6.21) Stripes on opposite faces of one platelet

6.2.6 Summary of Stripe Observations

Earlier sections have attempted to fit a crude model to explain the many varied stripe structures observed in platelets. De Blois (1968a) had observed the type IV structures in thicker platelets. No evidence of this structure has been found. The best approximation is the type III structure with magnetisation oscillating about the plane of the platelet angled at something near 45° to the colloid collections, however such a description is still obviously insufficiently sophisticated.

In zero field the flux closure patterns can be correlated with familiar structures in thin platelets. Yet the domains themselves are often subdivided into regions containing similar stripes, but in different orientations, and the stripes in the sub-domains can show angular variations of up to 20°. At the same time the stray field produced and the change in orientation between two sets of adjacent stripes in neighbouring domains separated by a 90° wall may be no greater than within the same domain. This, however, is not the case when the domains are separated by a 180° wall, and a distict break exists in the colloid pattern.

There is little change in structure through the thickness of the platelet in the thinner stripe bearing platelets. The fact that structures in platelets an order of magnitude thicker appear to be similar suggests that this may also be the case with these. At the bottom end of the thickness range the type III structures are found to be compatible with the type II Saito stripes, and at the top end of the range the circle Bloch lines, which probably exist through the centre of the platelet, expand to become Bloch walls.

The behaviour under both easy and hard axis fields is very complex. In the case of the former, long sweeping stripes form across the platelet with decreasing separation in increasing fields, until they finally disappear. The field necessary to saturate a

stripe bearing platelet in the easy axis is much higher than for a thin platelet and approaches the anisotropy field value. In the case of hard axis fields short sections of stripe domain form making an angle with the field direction which is a function of the applied field. These sections of stripes become shorter with increasing field.

No model has been found which adequately fits the many characteristics observed. The stripe patterns seen over quite large areas, in high fields or zero field, suggest that they may be formed by a reasonably simple magnetisation distribution. In this distribution the mean magnetisation is loosely coupled to the stray field pattern and its net direction lies somewhere in the region of 45° to the stripe direction. The first step to an understanding of these complex stripe structures requires a micromagnetic calculation but more limitations must first be put on possible models to enable this to be done. As these structures have been observed on nickel any calculation will probably have to include magnetostrictive terms.

CHAPTER 7

MAGNETOSTATICS IN PLATELETS

INTRODUCTION

In section 1.1 of this thesis the terms which contribute to the magnetic free energy of a body were examined and an expression obtained for the total energy. Various terms in the expression are dominant according to the size, shape and nature of the material body being considered. In the case of the ferromagnetic platelets studied in this thesis the magnetostatic energy played an important part in determining their behaviour, seen clearly in the observations reported in Chapters 5 and 6. Unfortunately, the magnetostatic energy of these platelets is difficult to evaluate and makes direct comparison between their observed behaviour and any theoretical models complex, an exception being the Néel strip treated in section 5.2.4.

The magnetostatic energy was shown in section 1.1.4 to consist of two terms, that arising from the applied field, $\underline{H}_o$, and that from the material itself, $\underline{H}'$, so that

$$\underline{H} = \underline{H}_o + \underline{H}' \qquad (7.1)$$

and

$$E_H = -\mu_o \int (\underline{H}_o + \tfrac{1}{2}\underline{H}') \cdot \underline{M}\, d\tau \qquad (1.7)$$

Unlike $\underline{H}_o$, $\underline{H}'$ usually lies in a direction such that $\underline{H}' \cdot \underline{M}$ is negative.

The Maxwell equations for the magnetostatic field are:

$$\text{curl } \underline{H} = 0 \tag{7.2}$$

$$\text{div } \underline{B} = 0 \tag{7.3}$$

$$\underline{B} = \mu_o (\underline{H} + \underline{M}) \tag{7.4}$$

in M.K.S. units

and from (7.3) and (7.4)

$$\text{div } \underline{H} = - \text{div } \underline{M} \tag{7.5}$$

Because the curl of the magnetic excitation is at all times zero it is possible to express $\underline{H}'$ as the gradient of the magnetic scalar potential

$$\underline{H}' = - \text{grad } \phi \tag{7.6}$$

and from equations (7.5) and (7.6)

$$\nabla^2 \phi = \text{div } \underline{M} \tag{7.7}$$

With the potential itself expressed as a combination of surface and volume pole densities, as seen earlier

$$\phi = \frac{1}{4\pi} \int_S \frac{\underline{M} \cdot \underline{ds}}{r} - \frac{1}{4\pi} \int_V \frac{\text{div } \underline{M}}{r} \, d\tau \tag{1.5}$$

With the volume integral taken over the entire volume of the specimen and the surface integral over the entire outside surface. In principle therefore the magnetostatic energy of any charge distribution may be calculated by first evaluating the magnetic scalar potential ϕ using equation (1.5), determining $\underline{H}'$ from ϕ using equation (7.6), and finally combining $\underline{H}'$ with $\underline{M}$ according to equation (1.7) to give the magnetostatic energy.

Alternatively we may write

$$E_H' = - \tfrac{1}{2} \mu_o \int_V \underline{H}' \cdot \underline{M} \, d\tau \tag{1.6}$$

which by using equation (7.6) becomes

$$E_H' = \tfrac{1}{2} \mu_o \int_V \text{grad } \phi \cdot \underline{M} \, d\tau$$

and can be rewritten as

$$E_H' = \tfrac{1}{2}\mu_o \int_V \text{div}\,(\phi\,\underline{M})\,d\tau \;-\; \tfrac{1}{2}\mu_o \int_V \phi\ \text{div}\,\underline{M}\,d\tau$$

which by using Gauss's theorem becomes

$$E_H' = \tfrac{1}{2}\mu_o \int_S \phi\,\underline{M}\cdot\underline{ds} - \tfrac{1}{2}\mu_o \int_V \phi\ \text{div}\,\underline{M}\,d\tau \qquad (7.8)$$

In magnetostatic calculations $\underline{M}$ is usually assumed to be uniform within the specimen so that the second term may be neglected.

Thus

$$E_H' = \tfrac{1}{2}\mu_o \int_S \phi\,\underline{M}\cdot\underline{ds} \qquad (7.9)$$

$$\text{or}\quad E_H' = \tfrac{1}{2}\mu_o \int_S \phi\,\sigma\,ds$$

where $\sigma = \underline{M}\cdot\underline{n}$

In this chapter a short review is given of the methods that have been used to evaluate magnetostatic energies. This is followed by a description of an incomplete attempt that has been made to evaluate the magnetostatic energy of a platelet, entirely numerically, and to incorporate this in a total energy expression. One of the simplest examples of the movement of domains is seen in FIG.(7.1). It should be possible to predict this observed behaviour from a minimisation of the fundamental expressions for the various energy terms involved. However, this has not yet provided definite answers.

7.1 EVALUATION OF MAGNETOSTATIC ENERGIES

Reference has already been made in section 1.1.4 to the evaluation of magnetostatic energies of specimens whose shape can be approximated by that of an ellipsoid. However, such calculations are of limited range and of little interest in explaining domain behaviour. Other approaches have therefore been made in attempts to enable domain

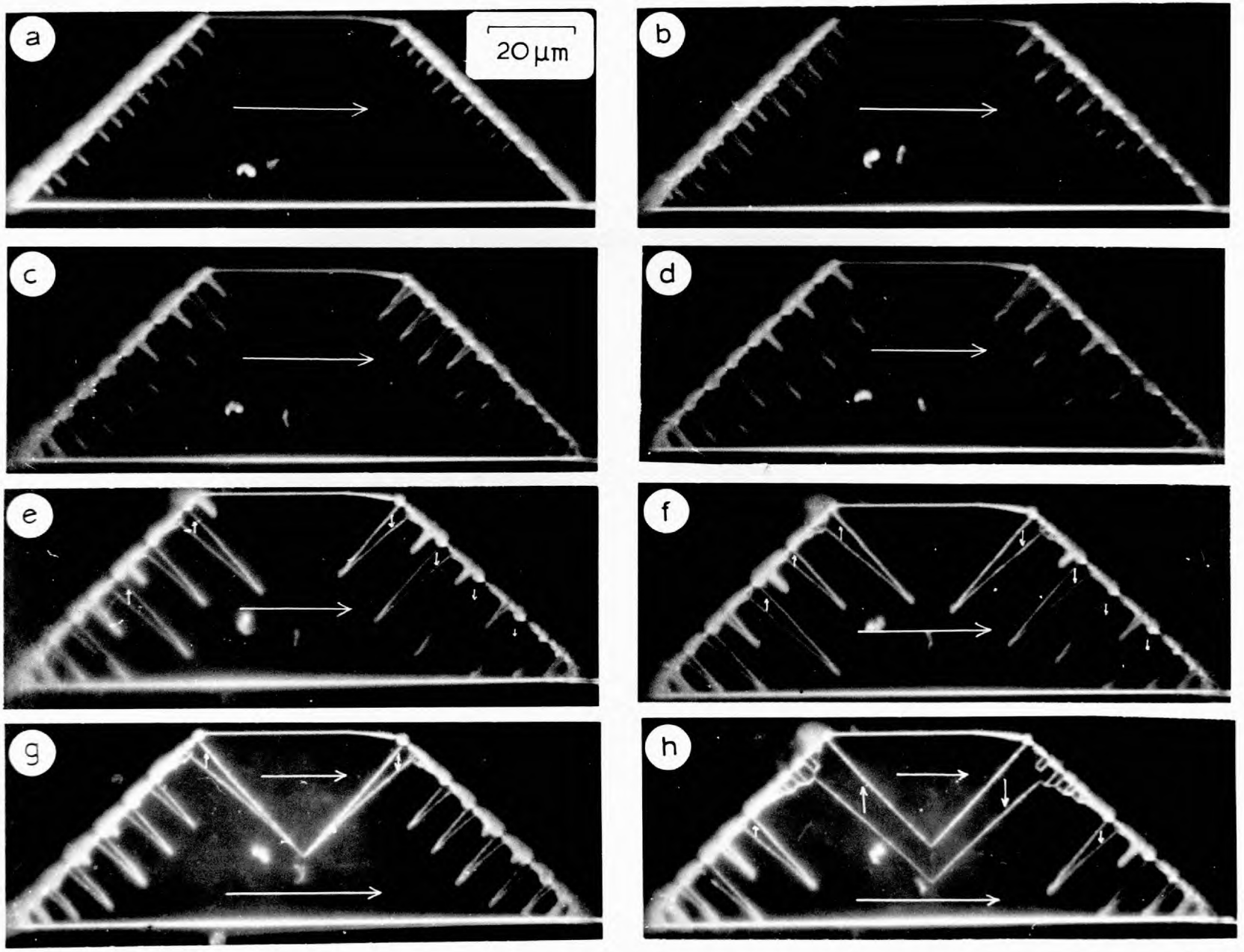

Fig. (7.1) Growth of Spike Domains

calculations to be put on a stronger theoretical foothold.

7.1.1 Fourier Methods

One important technique has been the application of Fourier methods in evaluating the energies of infinite periodic domain structures. This was first applied to the important problem of a thin plate with parallel strip domains, see FIG.(7.2), by Kittel (1946).

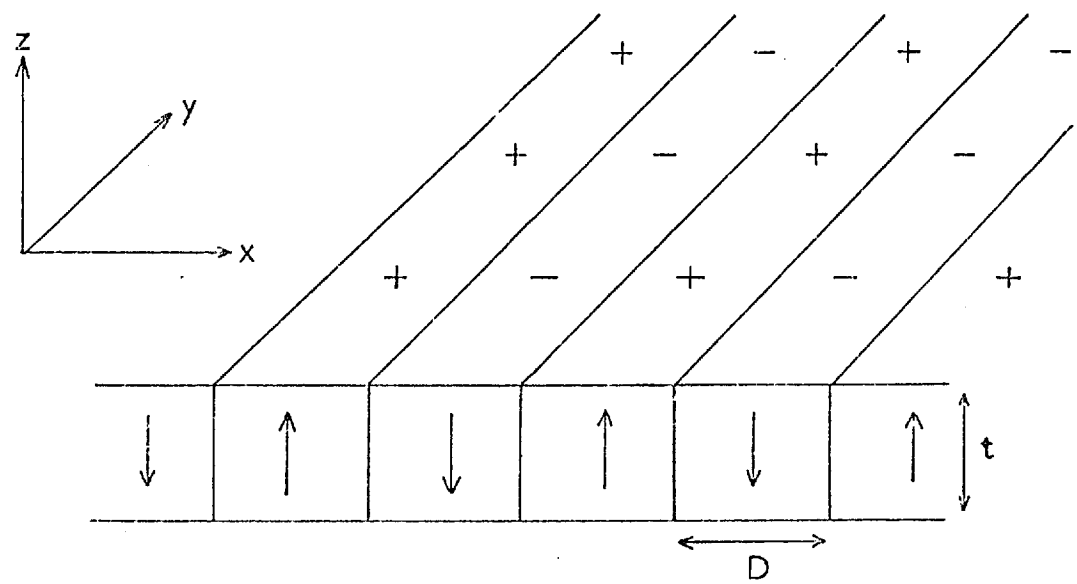

FIG.(7.2) THIN PLATE WITH STRIP DOMAINS

Kittel calculated the magnetostatic energy density per unit area of a single plane of alternating strips as

$$E_H' = 0.8525\ M_s^2\ D \qquad (7.10)$$

For a thin plate he took the value as being double that for one surface, i.e. $1.71\ M_s^2\ D$. This only strictly applicable when $t \gg D$ and interactions between the surfaces can be neglected. Malek and Kambersky (1958) included this interaction and determined the energy per unit area as:

$$E_H' = \frac{16 M_s^2 D}{\pi^2} \sum_{n}^{\infty} \frac{1}{n^3}\left(1 - 1^{-\frac{n\pi t}{D}}\right) \qquad (7.11)$$

where n is odd.

As $t \longrightarrow \infty$ equation (7.11) becomes equal to (7.10).

Silcox (1963) considered the case when both the magnetisation and easy axis were inclined to the plate normal but the expression required an experimentally measured parameter to generate the results. A completely theoretical expression was derived by Jakubovics (1966b) which was confirmed by Lorentz microscopy observations made on cobalt foils.

By expanding the potential in two Fourier series taking different forms inside and out of the plate, after Goodenough (1954), Kooy and Enz (1960) investigated the energy of reverse domains in a partially magnetised plate. They also considered the case of a single reversed cylindrical domain in an infinite plate.

The double Fourier series, suggested by Kittel (1949) was used by Spacek (1959) to calculate the magnetostatic energy of several different infinite strip, checkerboard and echelon structures on a single plane, all of which had zero overall charge. Simple and complex honeycomb structures were evaluated by Kozlowski and Zietek (1966) and concentric squares by Di Chen (1967).

7.1.2 Direct Integration

In crystals where the domain structure is large in relation to the size of specimen, which can no longer be regarded as infinite Fourier methods are no longer suitable. It therefore becomes necessary to use numerical methods to evaluate the integral of equation (7.9). Rhodes and Rowlands (1954) considered the problem of a bounded thin plate, i.e. similar to that shown in FIG.(7.2) but only containing a few domain walls in total. They expressed the mutual energies of two

parallel surface charge distributions as

$$E_{r_1} = \mu_o \iint \sigma_2 \, \phi_2 \, (x_2 y_2) \, dx_2 \, dy_2 \qquad (7.12)$$

$$\phi_2 = \iint \frac{\sigma_1}{r_{12}} \, dx_1 \, dy_1$$

i.e. ϕ_2 is the scalar potential at some point on surface (2) due to the integrated charge distribution of surface (1). The interaction energy between charge distributions is positive if they are of the same sign and negative if of opposite sign.

A calculation of this type was used by Craik and McIntyre (1967) to evaluate the critical size for the adoption of a single domain state by a rectangular block, as a function of its aspect ratio and of the ambient field.

In a review of the magnetic domain structures of small crystals by Craik (1970) this approach was extended to evaluate the equilibrium number of domains in a small uniaxial crystal as a function of its dimensions. This gave the interesting result that above certain ratios of crystal dimensions only odd numbers of domains are predicted. Craik also showed that in a very simple case the equilibrium position for a domain wall in a crystal need not leave the crystal in a demagnetised state.

7.1.3 The μ^* Correction

A decrease in magnetostatic energy can occur in crystals with out of plane easy axes by a rotation of the magnetisation away from these axes and into the plane of the crystal. The surface pole density is reduced at the expense of introducing anisotropy energy and a volume pole distribution, and thus is more likely to occur in materials with low anisotropy. Corrections of this type are generally known as μ^* corrections and were first used by Williams et al (1949). They derived an expression for the effective permeability normal to

the easy direction as

$$\mu^* = 1 + \left[\frac{2\pi M_s^2}{K}\right] \qquad (7.13)$$

(The permeability parallel with the easy direction is assumed unity since the magnetisation in that direction cannot be changed appreciably).

This allows the total energy of the system to be written as $\frac{1}{2}\int \sigma\phi \, ds$, where σ is the surface charge density on the assumption of infinite anisotropy, and ϕ is the potential at the surface evaluated from a charge density σ on a material with permeability μ^*.

By using this technique Fox and Tebble (1958) investigated energy reductions in high crystalline anisotropy materials as a function of the angle made with the basal plane. It has also been applied to the open Kittel type structure in uniaxial materials, and to the magnetostatic field in thin plates showing stripe domains, as was seen in section 6.1.

7.2 NUMERICAL APPROACH TO DOMAIN BEHAVIOUR IN PLATELETS

Although the methods described in section 7.1 have been useful in evaluating the magnetostatic energies of periodic magnetisation distributions they are unsuitable for the situations that exist in thin platelets with planar domain configurations. Often no symmetry or periodicity exists in the platelets and an attempt has therefore been made to evaluate the energy completely numerically.

Sommerfeld (1952) considered the case of a cylindrical bar magnet of length 2l and evaluated the magnetostatic potential produced by a uniform pole density on the circular faces at either end. He showed clearly the relationship between the magnetic excitation, H', the field, B, and the magnetisation M. This is shown in FIG.(7.3) where the field quantities are given as functions of position along the

axis of the magnet.

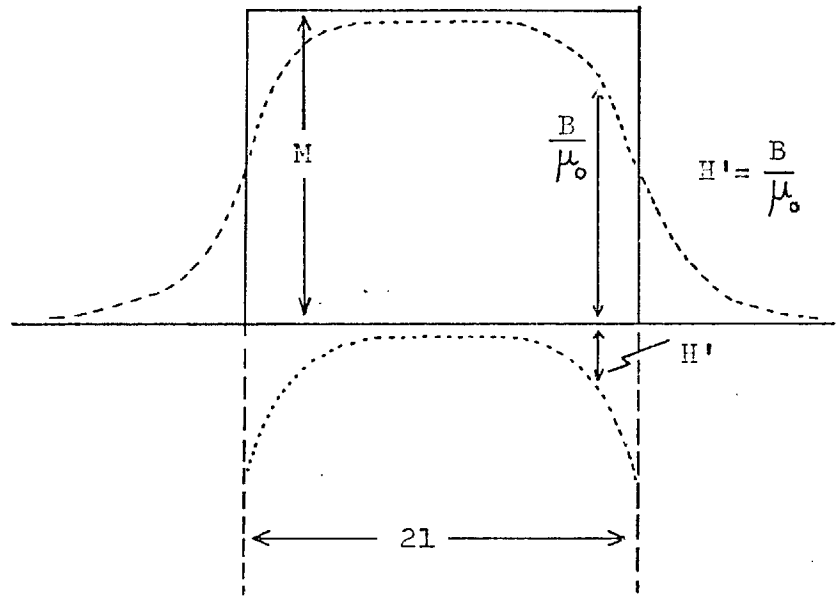

FIG.(7.3) DEMAGNETIZATION OF A UNIFORMLY MAGNETIZED BAR

The magnetisation is zero outside the body of the magnet and has a constant value M inside. The magnetic excitation H' is at all times negative inside the bar and thus has a demagnetising action with a very small value in the centre, but increasing to reach a value of $-M/2$ at either end. At the surface itself H' becomes $+M/2$, with a discontinuity M, and thereafter outside the body follows the magnetic field values, being related by $B = \mu_o H$. The magnetic field itself attains almost the full magnitude $\mu_o M$ at the centre of the bar, but is only half as large at the ends, and is of course continuous, in keeping with the boundary conditions at the surface.

This approach was extended by O'Dell (1960) who studied the magnetic excitation inside a cylindrical thin ferromagnetic film. The geometry of this situation was such as to give an expression for the magnetic potential ϕ and excitation H'. The expression for ϕ was valid at any point within the film, except within a distance t of the end, where t was the thickness of the film, because the integrand for

ϕ contained a singularity at this point. The excitation within the neighbourhood of either end was calculated from a separate expression which ignored the contribution from the opposite end and avoided the singularity, but was only valid near the one end. This limitation on the general expression for the potential is important in the platelet work considered below.

A set of photographs, FIG.(7.1), had been obtained recording one of the simplest domain movements observed in platelets, and the work below is an initial investigation of this behaviour.

The formation and behaviour of spike domains, near to saturation in increasing and decreasing fields applied along the easy axis of a platelet, has already been noted in Chapter 5. FIG.(7.1) shows in detail a decrease from saturation in a (100) plane trapezoidal platelet. Initially the large stray field which had existed along both of the [100] edges at saturation was lowered by the formation of numerous small spike domains, seen at 21 oe. in FIG.(7.1 a). These grew out, and at the same time decreased in number at 16 oe. (b) and further 11 oe. (c). At this stage, however, only some of the spikes continued to enlarge whilst others shrank, 8 oe. (d), continuing at 6 oe. (e). With a further decrease in field to 4.9 oe. (f) the spikes themselves became so wide that small closure structures formed at their own base. At 4.85 oe. the uppermost spikes on either side extended until they touched, and the remainder collapsed back FIG.(7.1g). Finally with a further slight decrease in field to 4.8 oe. the Bloch line which must have existed at this tip extended to form a vertical 180° Bloch wall, seen in (h).

Thus initially many spikes formed along the sides of the platelet, to lower the magnetostatic field on the <100> edges. With decreasing fields some spikes continued to grow and others to shrink, with the total number of spikes gradually decreasing, until eventually the configuration was changed by the formation of the 180° wall. As the process was performed quasi-statically over a period of several

minutes, this behaviour was assumed to represent successive equilibrium structures. Although initially a larger number of reverse domains were nucleated observations have shown that it is unfavourable for these all to grow. This type of behaviour has not previously been reported and is still unexplained. If it is assumed, and it would seem reasonable to do so for this type of behaviour has been seen on many occasions, that the platelet is always in its lowest free energy state, then energy minimisation calculations should give a prediction as to spike length and behaviour. This is investigated below.

7.2.1 Evaluation of Magnetostatic Field of Saturated Platelet

The magnetostatic potential at any point inside a saturated trapezoidal platelet seen in FIG.(7.4 a) is given by

$$\phi(z,x) = \frac{1}{4\pi}\int_{S_1}\frac{\underline{M}_s\cdot\underline{n}_1}{r_1}\,ds_1 + \frac{1}{4\pi}\int_{S_2}\frac{\underline{M}_s\cdot\underline{n}_2}{r_2}\,ds_2 \qquad (7.14)$$

If the magnetisation is assumed uniform throughout, the demagnetising field at the point (z,x) is given by

$$H'_x(z,x) = -\frac{\partial\phi}{\partial x} \quad \text{and} \quad H'_z(z,x) = -\frac{\partial\phi}{\partial z}$$

The total demagnetising energy of the platelet is then given by

$$E_{H'} = \tfrac{1}{2}\mu_o \int_{\text{volume of platelet}} H'_z M_s \, d\tau \qquad (7.15)$$

($\underline{H}'_x\cdot\underline{M}_s$ being zero at every point).

Alternatively, the platelet can be imagined as consisting of a series of n parallel bars all having the same uniform magnetisation and cross section, as seen in FIG.(7.4 b). The total surface area of the end has been reduced by $\sqrt{2}$, if faces normal to the x-direction are disregarded, therefore $\underline{M}_s$ is replaced by $\sqrt{2}\,\underline{M}_s$ to compensate for this change.

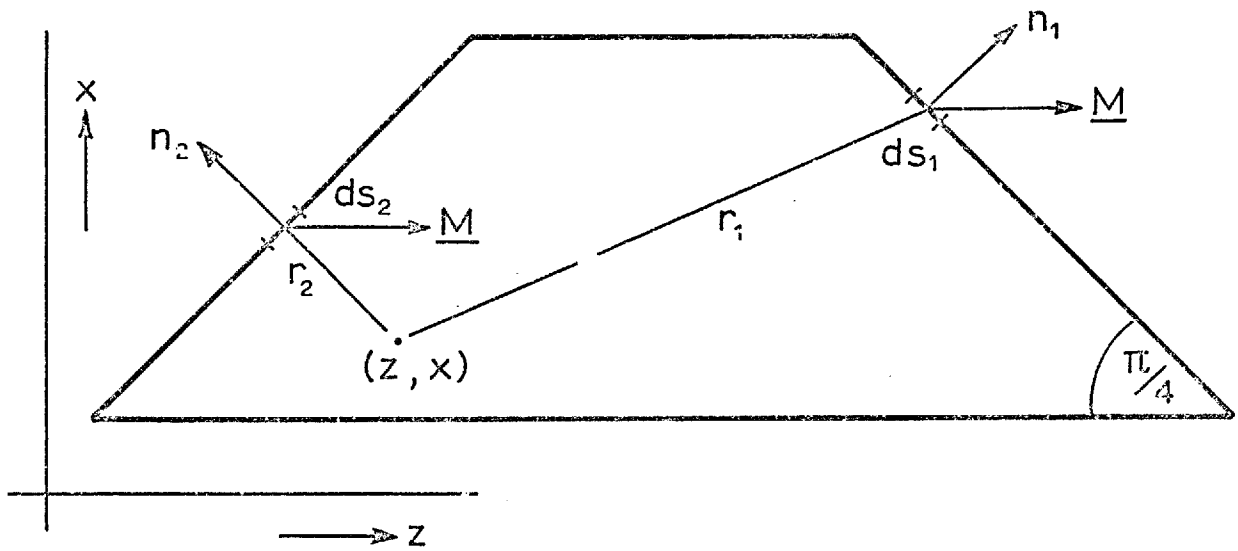

Fig. (7·4 a) Geometry used for saturated platelet

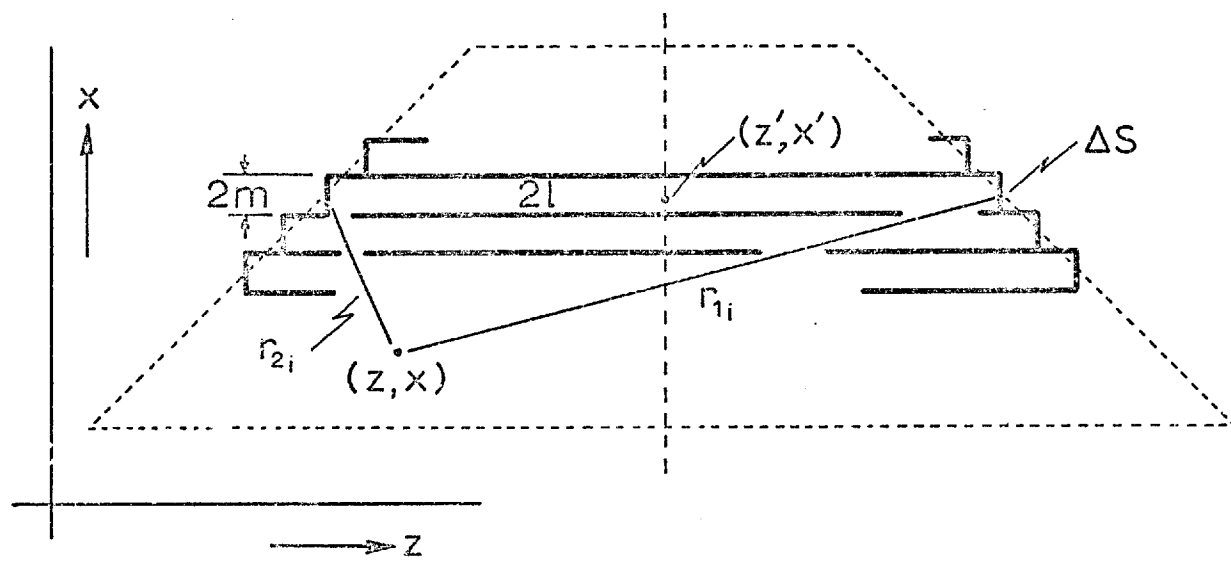

Fig. (7·4b) Synthesis of platelet by strips

The potential at any point can now be written as the summation of the potentials produced by each strip separately at that point

$$\phi\,(z,x) \;=\; \sum_{i\,=\,1}^{n} \left[\frac{1}{4\pi} \int \frac{M_s \Delta S}{r_{1i}} - \frac{1}{4\pi} \int \frac{M_s \Delta S}{r_{2i}} \right] \qquad (7.16)$$

where ΔS is the cross-sectional area of a strip.

The demagnetising energy at the point (z,x) remains as $\frac{1}{2}\,\mu_o\, H'_z(z,x)\, M_s$. If the platelet is thin any variation in r_{1i} and r_{2i} through the thickness of the platelet can be neglected when integrating over the end surfaces. Using the symbols defined in FIG.(7.4 b) the potential at (z,x) can be written as

$$\phi\,(z,x) \;=\; \sum_{i\,=\,1}^{n} \frac{M_s}{4\pi} \int_{x'-m}^{x'+m} \left\{ \frac{t\,dx''}{\left[(z'+l-z)^2+(x''-x)^2\right]^{\frac{1}{2}}} - \frac{t\,dx''}{\left[(z'-l-z)^2+(x''-x)^2\right]^{\frac{1}{2}}} \right\} \qquad (7.17)$$

It is more convenient to differentiate this expression with respect to z before evaluating the integral and this gives $H'_z(z,x)$.

Rearranging equation (7.15) using (7.17) the demagnetising energy can be rewritten in summation form as

$$E_{H'} \;=\; \tfrac{1}{2}\,\mu_o\, M_s \sum_{x} \sum_{z} H'_z(z,x)\, \delta z\, \delta x \qquad (7.18)$$

(the summation being carried out over all co-ordinates (z,x) inside the area of the platelet).

This expression is not valid within distances $\sim t$ from the edge of the platelet and such regions are omitted in evaluating equation (7.18).

The accuracy with which the bars substitute for the edge distribution increases with the number of bars, i.e. as the end steps

degenerate into a slope.

A simulation of a saturated trapezoidal platelet of base length 150 μm, height 50 μm and thickness 0.2 μm was made using strips of 1 μm width, i.e. putting n = 50. The value of $H_z(z,x)$ was determined over a mesh of co-ordinates, and at each co-ordinate was taken to be the value appropriate to the surrounding 25 sq. μms. A computer program was written which evaluated the ratios $H'_z(z,x)/M_s$ and $H'_x(z,x)/M_s$ over this mesh of co-ordinates using equation (7.17). The scalar product $\frac{1}{2}\mu_o \underline{M}_s.\underline{H}'_x(z,x)$ was at all times zero because $\underline{M}$ was assumed to lie uniformly along the z axis, and the product $\frac{1}{2}\mu_o \underline{M}_s.\underline{H}'_z(z,x)$ was at all times negative because the demagnetising field opposed the magnetisation. The value of $\underline{M}_s$ for Ni is 5.5×10^5 amps/m, and for a platelet of this volume (10^{-15} m^3) the total demagnetising energy given by equation (7.18) is found to be 3.9×10^{-13} joules. The applied field necessary to saturate the platelet was taken as 5×10^{-3} wb/m^2 making the applied field energy 2.75×10^{-12} joules.

With the magnetisation lying entirely along the [110] direction the cosines of the magnetisation vector are $\alpha_1 = \frac{1}{2}$, $\alpha_2 = \frac{1}{2}$ and $\alpha_3 = 0$. Taking the value K_1 from section 1.1.2 as -5.7×10^3 joules/m^3 this gives the total magnetocrystalline anisotropy energy of the platelet as 1.42×10^{-12} joules. If saturation is achieved entirely by wall motion, as happens when an easy axis field is applied, the anisotropy energy can be regarded as constant, and can therefore be neglected. If rotation occurs this is no longer true and allowance would have to be made for this energy change.

In addition to calculating the total energy of the platelet the computer program enabled the magnetic excitation to be plotted as a function of position at any point in the platelet. A typical result of the computations is seen in FIG.(7.5). The plots show the variation of H_z and H_x, normalised with respect to M_s, along a centre axis of the platelet, AB, parallel with the z axis. They are included to

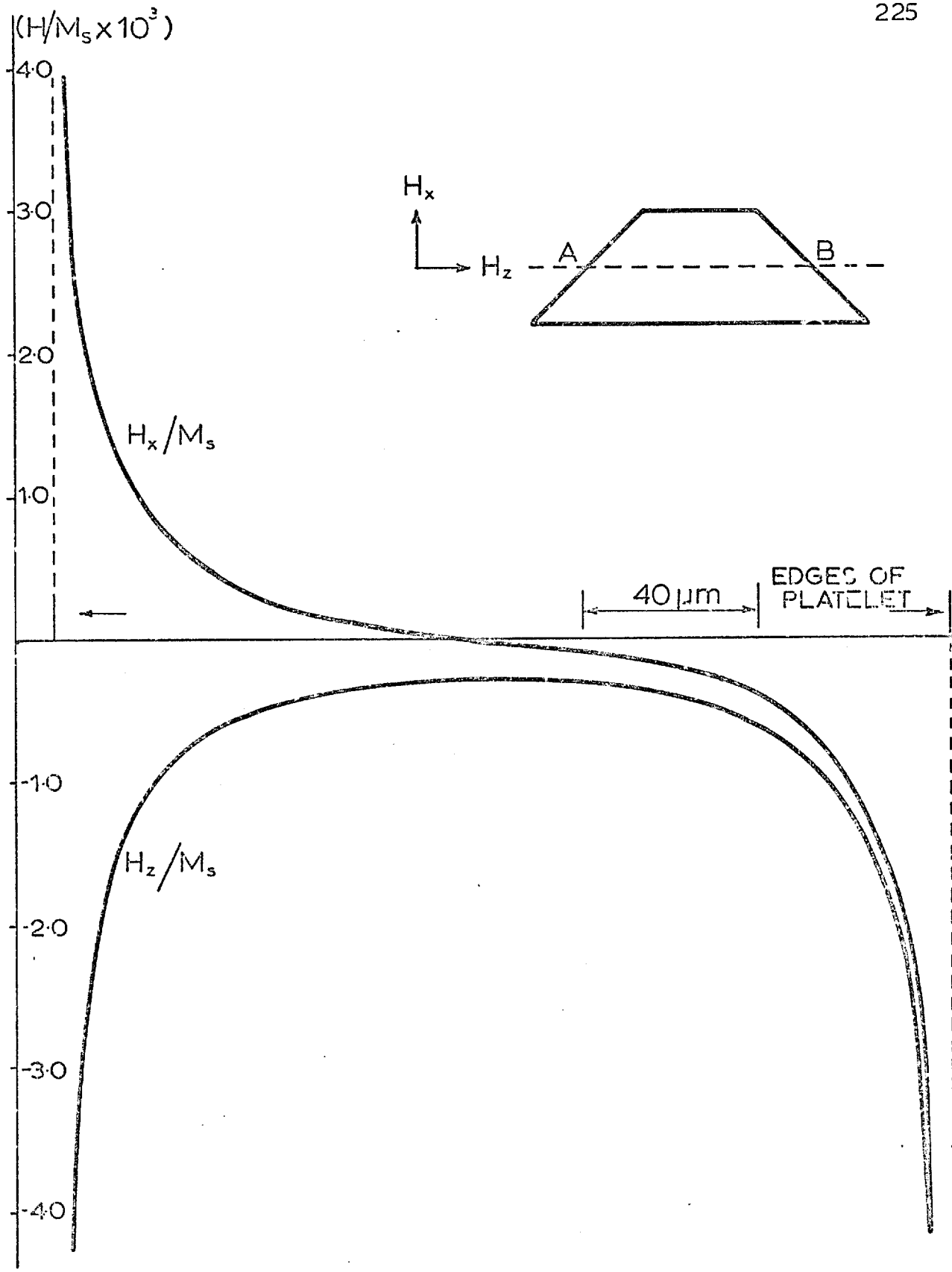

Fig. (7·5) Variation of H_z and H_x along centre of trapezoid platelet parallel with z-axis (A-B)

demonstrate the degree of variation within the platelet, with the largest contributions arising near the pole densities at either end. Little variation occurred in the excitation in a line close to and parallel with the pole densities at either end. It began to increase locally in the region of the corners, but these areas are in any case outside the limitations of the model.

7.2.2 Platelet With Mixed Edge Distribution

In the previous section the magnetostatic potential at any point in a saturated platelet was found by a summation process. This may have appeared cumbersome for the saturated platelet whose edge contributions could have been determined by direct integration, however, it has a wider flexibility.

When reverse domains form at the platelet edge the charge distribution is no longer of uniform sign. This can be easily reproduced in the summation process because any combination of positive and negative contributions can be included whereas direct integration would have been impossible. The effect of the formation of any distribution of reversed domains on the magnetostatic field from the edge is thus easy to study.

The effect of a non-uniform edge charge distribution resulting from spike formation is seen in FIG.(7.6). The variation of H_z across the width of the platelet is plotted for two cases. These are shown with a dotted line in the case of a saturated platelet and with an interrupted line for a non-uniform charge distribution. Two scans across the width are given for each case, the first, 'A', is made at a distance equivalent to 3 μm from the edge and the second, 'B', at 8 μm.

In the saturated platelet H_z does not vary substantially across the width of the platelet although it does increase towards the end marked X^1. At 8 μm from the edge it has a value $\frac{1}{4}$ of its value at 3 μm. Regions of reversed edge charge were included at locations

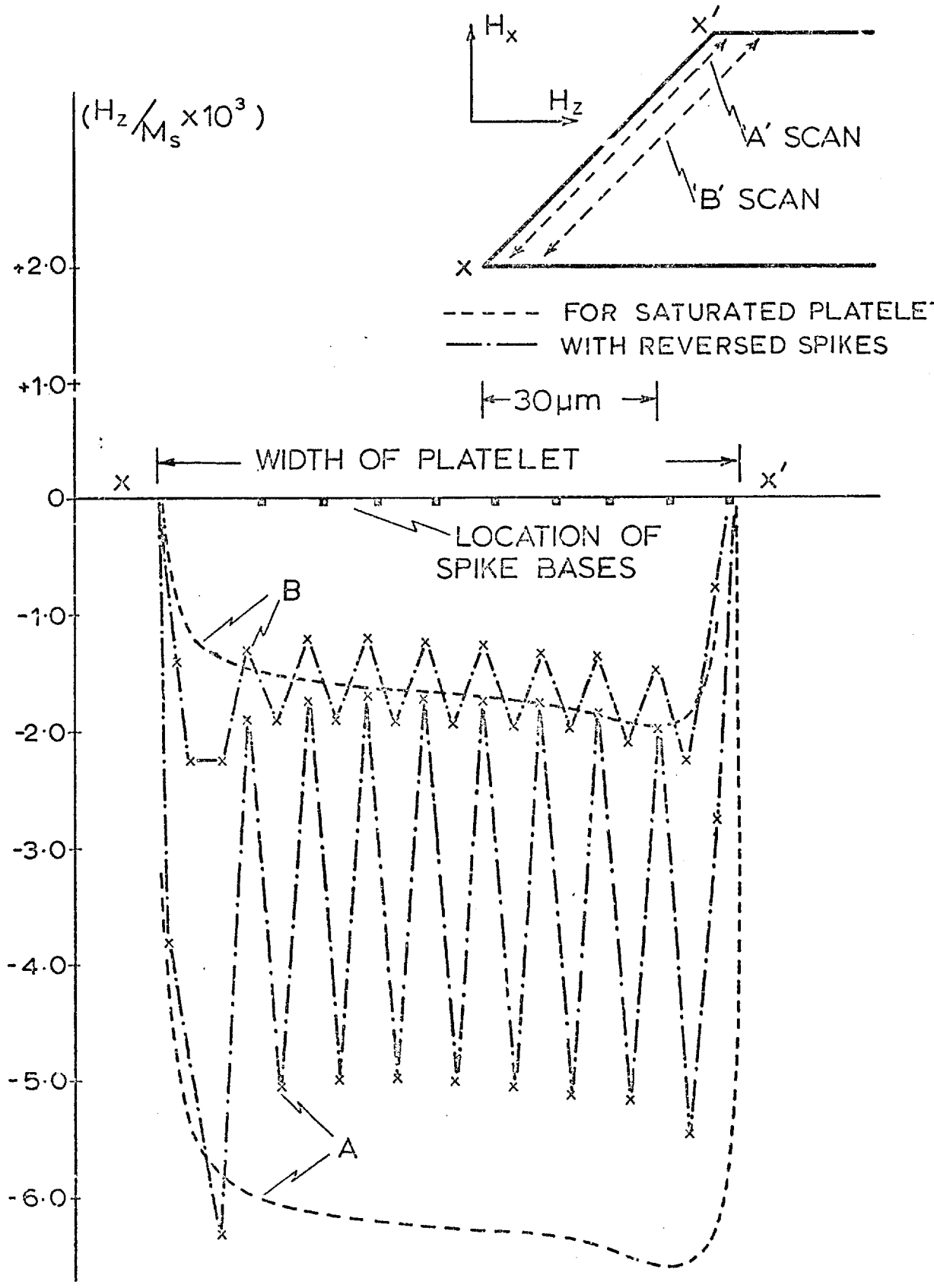

Fig. (7·6) Variation of H_z with and without reversed spikes.

indicated on the axis in FIG.(7.6) and their effect seen by the shape of the solid curve. Emphasis should not be placed on the detailed shape of this curve because it is to an extent dictated by the resolution of the evaluation points.

The 'A' scan at 3 μm shows an average H_z value with reversed charges half as large as that of the saturated platelet. The 'B' scan at 8 μm however, shows negligible change in its average value as the localised effect of the reversed regions begin to even out.

7.2.3 Energies in Platelet With Spike Domains

Both H_z/M_s and H_x/M_s were seen in FIG.(7.5) to fall to low values in the centre of the platelet away from the edge charges. Calculations can therefore be simplified by assuming that the field at any point in the platelet arises only from the nearest edge, the contribution from the far edge being neglected. Having made this change it is also more convenient to rotate the orientation of the platelet within the co-ordinate system. The geometry of this new position is shown in FIG.(7.7).

When a platelet with spike domains is considered the magnetostatic potential at any point (z,x) can be divided into two contributions, that from the edge charges, and that from the 90° walls which do not lie exactly along the <100> directions.

If the edge is subdivided into n equal segments, each of edge area ΔS whose charge can be positive or negative, the contribution to the potential at (z,x) from these edge charges can be expressed as

$$\phi_E(z,x) = \sum_{i=1}^{n} \frac{(\pm)_i}{4\pi} \int \frac{(M_s/\sqrt{2})\Delta S}{r_i} \qquad (7.19)$$

where r_i is the distance from the i'th segment to the point of evaluation (z,x).

Again, any variation in r_i through the thickness of the platelet

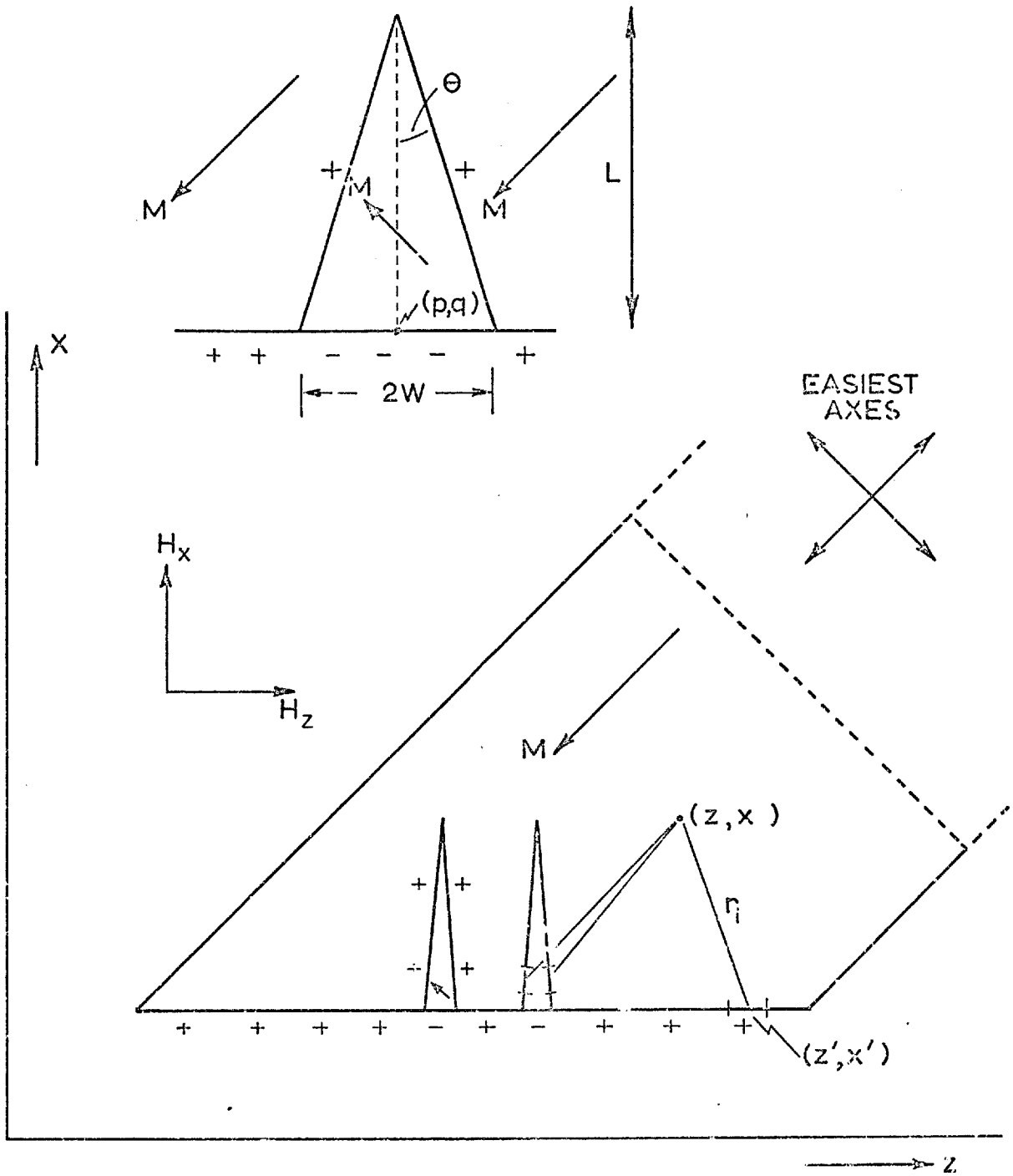

Fig. (7·7) Geometry used to evaluate energy of platelet with spike domains

is neglected and equation (7.19) becomes:-

$$\phi_E(z,x) = \sum_{i=1}^{n} \frac{(\pm)_i}{4\pi} \int_{z'-1}^{z'+1} \frac{t\, dz''}{\left[(z-z'')^2+(x-x')\right]^{\frac{1}{2}}} \qquad (7.20)$$

This expression is differentiated with respect to z and x to give $(H'_z)_E$ and $(H'_x)_E$ at every point and this field, resulting from the edge charges, is assumed applicable over the local area $\delta z\, \delta x$.

The potential at the same general point (z,x) from the charged spike domain walls may also be evaluated. The reason for their charge may be understood by reference to FIG.(7.8)

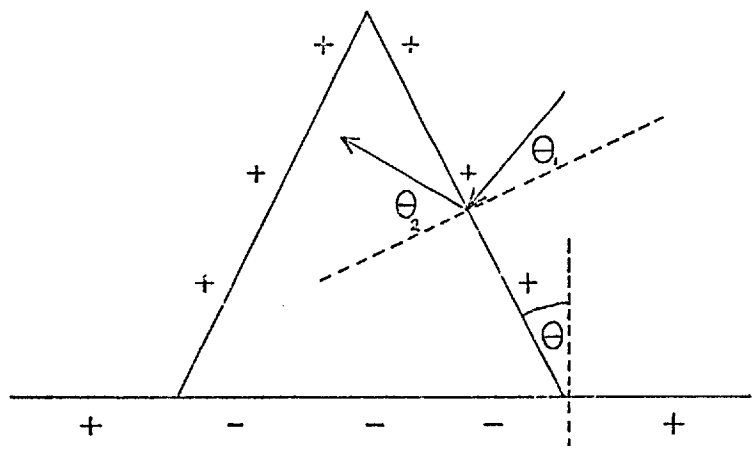

FIG.(7.8) CHARGE FORMATION ON SPIKES

The magnetic charge formed per unit length of the wall is given by:-

$$(M_s \cos\theta_1 - M_s \cos\theta_2)\, t$$

But $\theta_1 = (45 - \theta)$ and $\theta_2 = (45 + \theta)$ and the expression therefore simplifies to

$$\sqrt{2}\, M_s\, t \sin\theta$$

It is apparent that the sign of the charges on either spike wall

are identical, and opposite to the edge charges at the base of the spike.

The potential at the point (z,x) from a spike of base width 2ω and length L can be written as

$$\phi_s(z,x) = \frac{1}{4\pi} \frac{\sqrt{2}\, M_s\, t \sin\theta}{\cos\theta} \int_0^L \left[\frac{1}{r_{s1}} + \frac{1}{r_{s2}} \right] dx \qquad (7.21)$$

where r_{s1} and r_{s2} are the distances from the two area elements of length $\frac{dx}{\cos\theta}$ on either spike wall.

The quantities sin θ and cos θ in equation (7.21) can be expressed in terms of ω and L, and r_{s1} and r_{s2} as f (z,x,p,q,ω & L). This enables the magnetostatic potential at (z,x) from one spike of length L, semi-base width ω, and base co-ordinates (p,q) to be evaluated. The expression is differentiated with respect to z and x, before evaluating the integral, to give $(H'_z)_s$ and $(H'_x)_s$ at any point from this one spike. This field at (z,x) will in general arise from contributions from several spike domains and the appropriate values for r_{s1} and r_{s2} must be substituted in equation (7.21) to enable the contribution from each of the spikes to be included in the total value for $(H'_z)_s$ and $(H'_x)_s$.

If the case of a platelet with n spike domains is considered, with a certain fixed edge distribution the total demagnetising field at the point (z,x) is given by

$$\left.\begin{aligned} H'_z(z,x) &= (H'_z)_E + \sum_n (H'_z)_s \\ H'_x(z,x) &= (H'_x)_E + \sum_n (H'_x)_s \end{aligned}\right\} \qquad (7.22)$$

where n sums the contributions from all the spikes.

The total magnetostatic energy can no longer be found by an expression directly analogous to (7.18) because M_s does not bear the identical relationships to H'_z and H'_x over the entire platelet. This

is illustrated in FIG.(7.9).

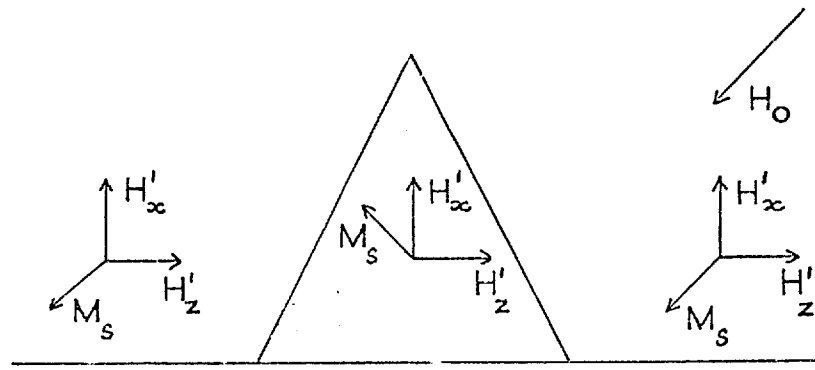

FIG.(7.9) RELATIONSHIP BETWEEN M_s AND FIELD

For locations outside the spikes the total magnetostatic energy is

$$E_{H'} = \tfrac{1}{2}\mu_o \sum_{\substack{x \\ \text{outside} \\ \text{spikes}}} \sum_{z} \left[M_s H'_z(z,x) \cos 135 + M_s H'_x(z,x) \cos 135 \right] \delta z \, \delta x \qquad (7.23)$$

and for locations inside the spikes

$$E_{H'} = \tfrac{1}{2}\mu_o \sum_{\substack{x \\ \text{inside} \\ \text{spikes}}} \sum_{z} \left[M_s H'_z(z,x) \cos 135 + M_s H'_x(z,x) \cos 45 \right] \delta z \, \delta x$$

By adding together these two expressions for the areas where each is appropriate the total magnetostatic energy of the platelet is obtained. This is the value appropriate for a platelet with a given edge distribution and spikes defined by parameters ω and L, where the values for ω correspond to the chosen edge distribution.

Other terms in this expression for the total energy of the platelet are more easily calculated. The applied field energy $\int \underline{M}_s . \underline{H}_o \, d\tau$ is constant over the entire volume of a saturated platelet. When spikes are formed the magnetisation within the spikes lies normal to the applied field, and thus $\underline{M}_s . \underline{H}_o = 0$ in these regions. This can

be seen in FIG.(7.9). The effective volume over which $\underline{M}_s \cdot \underline{H}_o = M_s H_o$ is taken as the volume of the platelet excluding the volume of the spike domains.

The wall energy can easily be calculated as the product of the total spike wall area and the assumed energy density of these walls. For convenience this energy density is taken as 1 erg/cm^2.

The anisotropy energy of the platelet does not effectively change with the presence of the spike domains because the magnetisation remains in the same relative orientation to the <111> directions.

A computer program was written which enabled the applied field, the magnetostatic and the domain energies to be calculated for a given spike distribution present in the platelet.

One investigation has considered a trapezoidal platelet with base 150 μm, width 50 μm, and thickness 0.2 μm, containing 10 spikes of base width 2 μm on the <100> faces. The computer program evaluated the energy contributions to the total energy of the platelet as the length of these spikes changed from 1 to 20 μm. The variation of the various terms with spike length are shown in FIG.(7.10) for an applied field of 15 oe.

The magnitude of the applied field energy decreased as the length of the spikes increased because a smaller volume of the platelet had magnetisation lying along the field direction. The wall energy showed an expected linear increase with spike length and the magnetostatic energy a decrease which was only linear above 8 μm length. The resulting value for the total energy showed a slow change with length and a shallow minimum at about 3 μm.

Comparison can be made here with FIG.(7.1 b) where, for an almost identical field, the spikes had an observed average length of about 7 μm. Two factors may account for this difference. The photograph shows a slightly greater number of spike domains and the

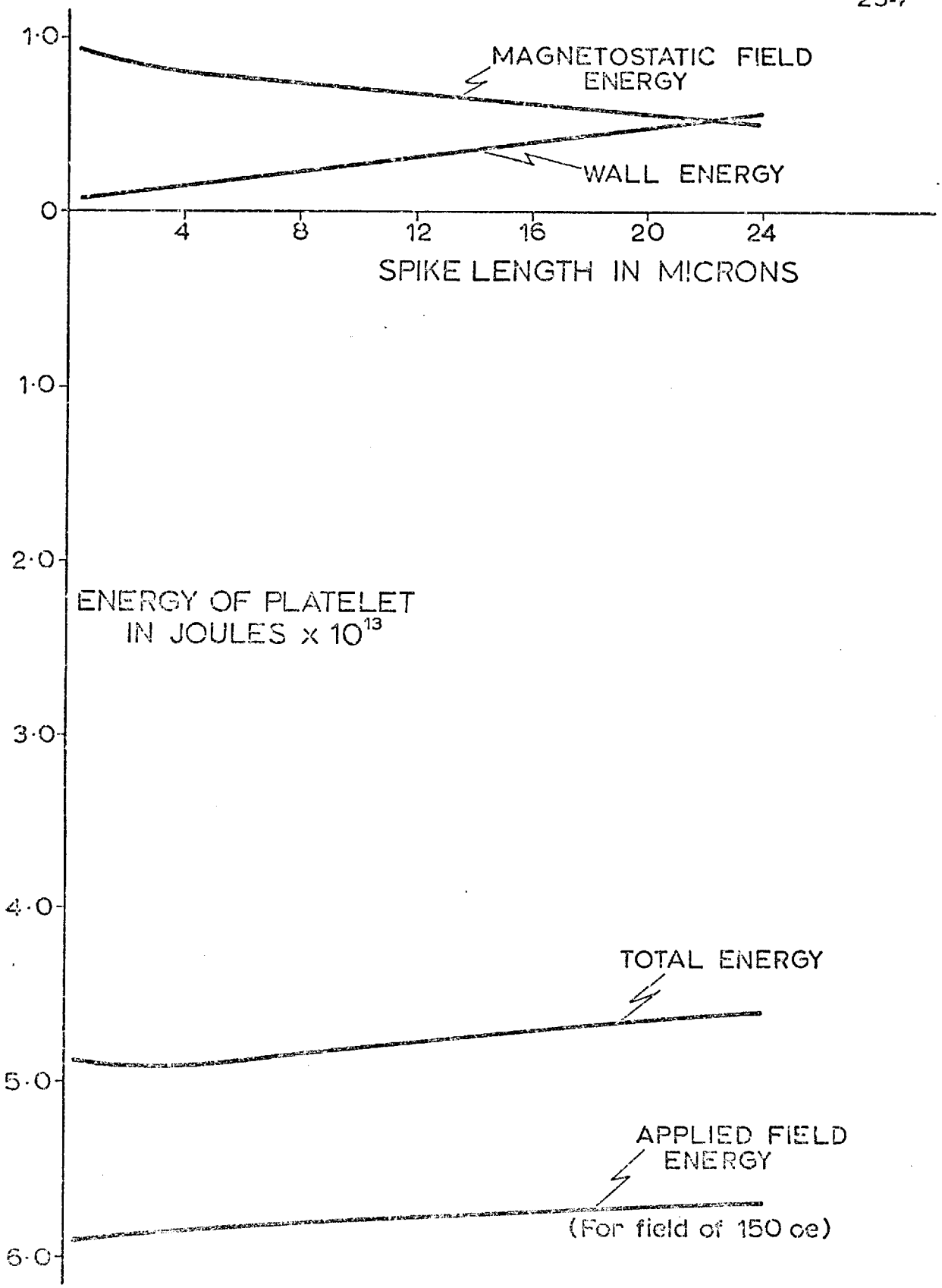

Fig. (7·10) Energy of platelet as function of spike length

presence of these might displace the position of the energy minimum. In addition the colloid particles between the spikes are seen to have collected over the edges of the platelet itself, suggesting a possible rotation of the magnetisation out of the platelet plane. To incorporate this effect local anisotropy energy changes would also have to be calculated. This would be difficult, but their omission may account for the difference between the two results.

Several precautions had to be taken during computation to ensure that no evaluations of the magnetostatic fields were made at locations on or very near to the spike walls. Due account was also taken in the summations of the difference in the magnetostatic field energies inside and out of the spikes, following equation 7.23 and FIG.(7.9).

The base widths of the spikes were chosen and then two parameters external to the computer program remained to be fixed, the wall energy of the spike walls and the value of the applied field. If these were kept within the limits of reasonable expectation the minimum in the total energy remained shallow, as shown in FIG.(7.10). This small change makes an investigation of the energy changes associated with the relative changes in spike lengths with field, as seen in FIG.(7.1), a dubious proposition.

The physical interpretation of FIG.(7.10) is of an interchange of magnetostatic energy with wall energy in the platelet as the spikes increase in length. This shift is recorded in the overall energy changes within the platelet. However, the change is localised and becomes masked by the larger volume of the platelet which remains virtually unaffected by these changes. It will be recalled from FIG.(7.6) that although at 3 μm from the edge the average internal field in a platelet with reversed domains was substantially lower than in a saturated platelet, at 8 μm. this difference was much less. This suggests that if an explanation of the spike domain behaviour in FIG.(7.1) is to be sought from an energy stand point attention should be paid to the local energy changes occurring near the platelet edge

rather than searching for a minimum in the overall free energy of the platelet.

Domains were introduced in Chapter I as being the result of two opposing requirements in a magnetic body. Their presence enables the total magnetic free energy to be reduced to a minimum value while maintaining low exchange, anisotropy and magnetostatic energy simultaneously. FIG.(7.1) shows some of the simplest domain configurations that have ever been observed, yet the mathematical analysis of the behaviour of these spikes by a consideration of the free energy is not straightforward.

It is stressed that this work is incomplete but the indications are that it might be more informative to consider the energy changes occurring in restricted regions or else to work in terms of the field forces acting between the spike domain walls in the platelet.

CHAPTER 8

CONCLUSIONS

8.1 SUMMARY

In Chapters 5 and 6 of this thesis observations on the domain properties of ferromagnetic crystals have been reported. In negative anisotropy platelets with (100) faces the domain structure is critically dependent on crystal thickness. At thicknesses less than 4000 Å planar domain configurations exist, but with increasing thickness the anisotropy, with easy axes in the <111> directions, becomes increasingly important. Structures in these thicker platelets thus arise from a balance, mostly between the anisotropy and magnetostatic energies, and form the stripe patterns discussed in Chapter 6.

The small size of these platelets causes their behaviour to be substantially influenced by the magnetostatic fields arising from the edges of the platelets. It is this same demagnetising field that accounts for the nature of the virgin domain structure, and the formation of echelon structures on <100> edges in negative anisotropy platelets or <110> edges on positive anisotropy platelets. In platelets with low anisotropy the magnetostatic energy becomes relatively more important and wall structures form in configurations which avoid the formation of any edge fields, and for this reason sometimes adopt unusual angles.

The degree of perfection of the platelets is high and, unless the platelets have been damaged in some way, structural considerations can be ignored when considering the movement of domain walls. Quasi-

static field observations show that saturation of a platelet by an in plane easy axis field is achieved almost exclusively by domain wall motion. The shape of the M against H plot shows that the behaviour of the platelet is largely controlled by the demagnetising field, making the final approach to saturation slow. Under a hard axis field wall motion first occurs by domains with a magnetisation component in the field direction growing at the expense of those with only a component in the reverse direction. However, above about 10 oe rotation begins to occur making the measurement of M against H plots from the domain areas impossible for the hard axis fields.

Very seldom has it been possible to give a quantitative interpretation of the observed behaviour because of the impossibility of obtaining an expression for the magnetostatic energy. An exception to this is the observations made on an induced Néel strip structure in a long rectangular platelet where the longitudinal demagnetising field could be easily calculated. The evaluation of magnetostatic energies and its possible application to explain some of the behaviour observed in platelets was outlined in Chapter 7. Situations of interest in this work often cannot be treated in analytic terms and the application of numerical methods has been suggested. The calculation of the magnetic excitation for a given situation by this method is comparatively simple, but rather inflexible in coping with changing domain structures, thus limiting its own application.

Magnetisation situations of interest which exist in observed platelet behaviour are usually too complex to enable a micromagnetic approach to be adopted. Alternatively the domain approach, and the numerical treatment of the magnetostatic field do not consider non-uniform magnetisation rotations and are thus often erroneous in their predictions. The magnetic energies in a platelet can often be very locally distributed as was seen in Chapter 7, making the quantitative interpretation of behaviour difficult, except in specialised cases.

In Chapter 5 the wall structures which exist in the platelets

and their variation with thickness and composition are seen to be more prolific and complex than the variation encountered in thin films. In the thickness range in which these variations are seen the differing wall structures must have very similar energies. Bloch lines play an important part, both in the initial formation of the domain structure and in the complexities that exist in the walls themselves where transitions between wall types occur. Of particular interest is the bright meta-stable wall structure which is frequently seen in the virgin domain structures, see for example FIG.(5.4). Its structure is still uncertain.

Many of the remarks made above on the behaviour of domains in thin platelets also apply to thicker platelets, where an additional complication is added by an oscillation of the magnetisation about the plane of the platelet. This decreases the anisotropy energy but at the same time establishes a vertical magnetostatic field. In the transition from planar to stripe configurations several types of oscillation exist, which are to a certain extent functions of platelet thickness. For example, the TYPE II stripe oscillations are only seen at the bottom of the thickness range. However, great similarities exist in the structures in platelets 6000 Å thick, and those an order of magnitude thicker at 6 μm. This suggests that the TYPE III structure thought to exist over this range is stable and is largely controlled by the anisotropy energy. Many details of behaviour were seen in Chapter 6 which are not adequately explained and a quantitative model is required for the TYPE III structure.

Finally, reference is made to Chapter 3 where the production of these platelets was considered. The bromide of the required metal alloy is placed in a wet dilute stream of hydrogen, where it is reduced to give tiny platelets of the metal itself. To obtain the platelet growth habit a low supersaturation is required to suppress two dimensional nucleation. This is obtained by using a low transport rate by careful choice of the reactions used. An analysis of the

thermodynamics of the possible transport reactions within this system corroborates the experimental findings. The growth mechanism of the platelet habit is difficult to explain but it would seem that, especially in the case of the triangular platelets, it is coupled with the growth of whiskers by a screw dislocation mechanism.

8.2 POSSIBLE DEVELOPMENTS

The small size of these platelets and the difficulty of their growth restricts any technological application and outweighs advantages otherwise gained from their perfection. An extension of the range of compositions investigated might be interesting, but is limited by difficulties of crystal growth. If this is confined to the current process, permalloy compositions can be produced but the number of independent parameters affecting growth is high, hence reproducibility is difficult to achieve. Alternative processes for producing platelets will be worth investigating in a search for a simpler system if the platelets are required in any number. The very nature of their non-epitaxial production which gives the platelets their high perfection is a severe disadvantage in any possible application.

As an extension of the present work further observations on the occurrence and behaviour of stripe domains are obviously required. In this direction, work was started towards adding the facility of applying magnetic fields normal to the platelet plane, during observations in the optical microscope. The effect of a vertical field should give further information on the magnetisation distribution within the stripe pattern. It might be useful to confirm by torque magnetometry whether the anisotropy values are as expected, but this may prove difficult with the small volume of material and the large shape anisotropy. In addition there is no underlying physical reason why any other anisotropy should exist.

The lack of a quantitative model to adequately explain the

behaviour of the stripe domains was evident in discussions in Chapter 6. A micromagnetic calculation based on the TYPE III stripes would be most interesting. However, reference to other similar calculations shows that this would not be easy and in any case a more detailed knowledge of the structure, in the form of a phenomenalogical model is needed before this can be attempted.

This additional information might come from the use of Lorentz microscopy together with low angle diffraction techniques. This, by necessity, will have to be done with high energy electron beams. Typical examples of the operation of the Cavendish 750 kV microscope in the Foucault and Fresnel mode are seen in FIG.(8.1).

The tip of a triangular nickel platelet is seen in FIG.(8.1a). The presence of a possible whisker thickening down one edge is clearly visible, as are other structural features which have not yet been explained. The whisker edge is a [110] edge and the other thought to be a [120] edge. The abrupt join to a [100] edge is seen in FIG.(8.1b), taken on the same platelet. The domain patterns of (a) and (b) do not correlate with those familiar from colloid work and are rather similar to the domains seen in uniaxial polycrystalline films. The change in pattern could result from strain present in the platelet, arising during mounting, or from the effect of vertical fields from the microscope objective lens. This latter case is thought to be more likely and the presence of this field could make Lorentz observations misleading.

A further illustration of this is seen in FIG.(8.1c) which shows the presence of reversed spikes of magnetisation at the edge of a platelet. The micrograph was taken with the microscope operated in the Fresnel mode and a field of 45 oe applied in the platelet plane. The magnetisation in the spikes is reversed by about 180° and thus shows a greater similarity with formations in uniaxial films than with the 90° spikes seen on platelets with the Bitter colloid technique, for example FIG.(7.1).

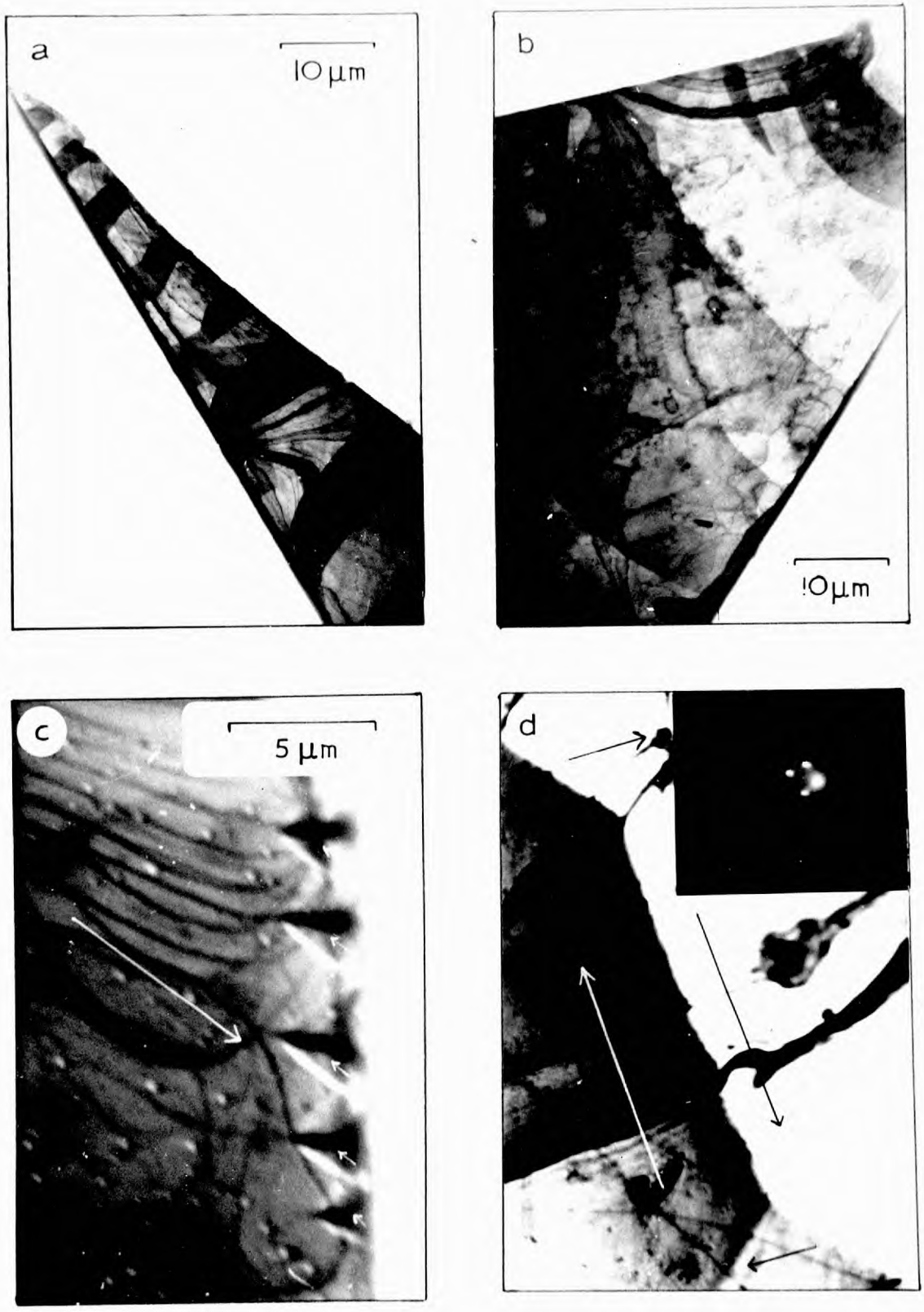

Fig. (8.1) High voltage Lorentz Micrographs from platelets

Finally, an area showing the flux closure circulation of the magnetisation is seen in FIG.(8.1d). This was taken in the Foucault mode and inset is seen the diffraction pattern produced by the magnetic splitting of the centre spot by the four domains in this area of the platelet.

Electron microscopy may also be useful in giving some guide to the structure of the meta-stable intermediate walls. It is possible to compare the electron beam intensity distribution measured at the photographic plate with that expected from the transmission of an electron beam through a given structure. The comparison of the observed distribution with one calculated from a theoretical model would provide a good check on the model itself, although this is not easy. A similar treatment could also be applied to walls in thinner platelets.

APPENDIX A

Calculation of the energy of a 180° wall in the (110) plane of a thin film with negative cubic magnetocrystalline anisotropy

(1) Bloch Wall

FIG (A.1) shows the co-ordinate system used for the calculation.

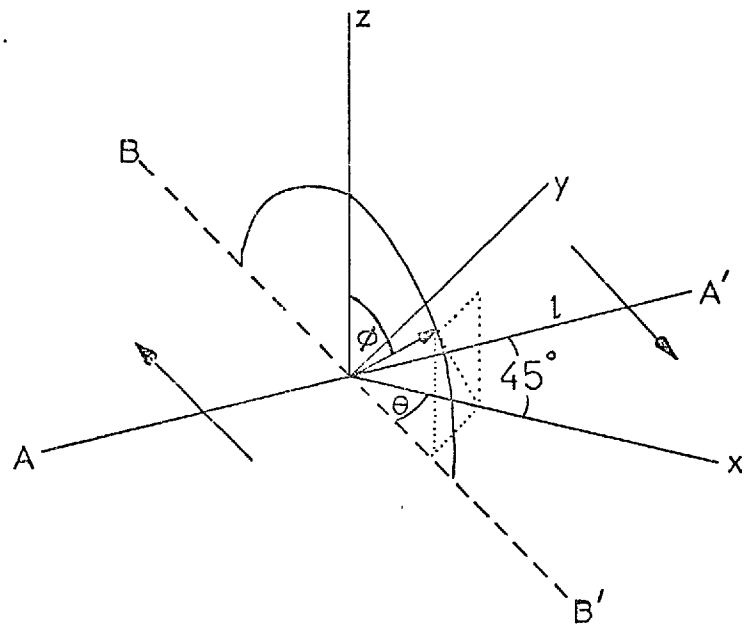

FIG (A.1)

The wall is considered to extend from $l = -\frac{a}{2}$ to $l = +\frac{a}{2}$ along the axis AA' shown.

From FIG (A.1) we can express the direction cosines of the M vector in terms of the angles θ and Ø:

$$\alpha_1 = \sin \phi \cos \theta$$

$$\alpha_2 = -\sin \phi \sin \theta$$

$$\alpha_3 = \cos \phi$$

M remains in the BB'Z plane, angled such that $\theta = \pi/4$ always.

Thus, ignoring K_2, the anisotropy energy can be written as:

$$E_K = \frac{K_1}{4} (\sin^4 \phi + \sin^2 2\phi)$$

This can be averaged over the wall width:

$$\frac{1}{a} \cdot \frac{K_1}{4} \int_{-a/2}^{a/2} (\sin^4 \phi + \sin^2 2\phi) \, dl = + \frac{7K_1}{32}$$

The expressions for exchange and magnetostatic energy will be identical with the expressions for a Bloch wall in a uniaxial thin film (Middelhoek 1961).

Thus we can write:

$$\gamma_{B\pi} = A(\frac{\pi}{a})^2 a + \frac{7}{32} K_1 a + \frac{\pi a^2}{(a + t)} M_s^2$$

which is equation (1.23).

(2) Néel Wall

FIG (A.2) shows the co-ordinate system used for the calculation.

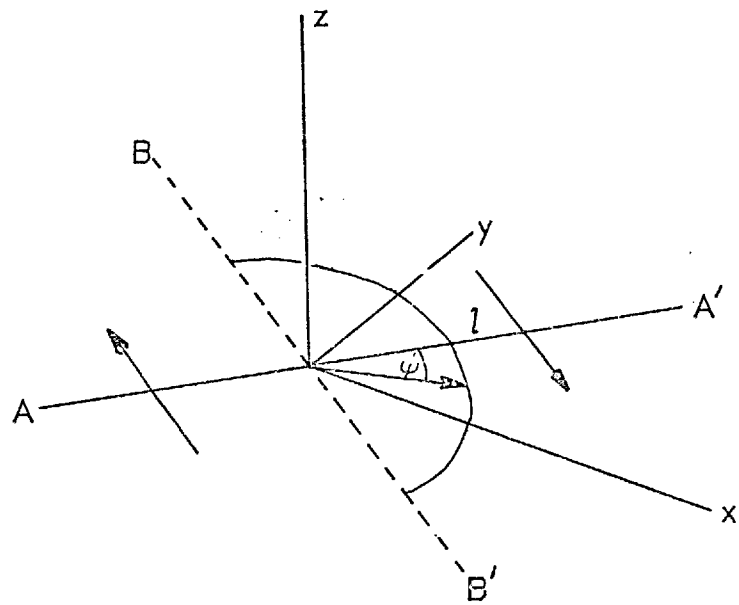

FIG (A.2)

Again the wall is considered to extend from $l = -\frac{a}{2}$ to $l = +\frac{a}{2}$ along the axis AA' shown.

$\emptyset$ is re-defined from the Bloch wall case as seen in FIG (A.2) and now the direction cosines of the $\underline{M}$ vector become:

$$\alpha_1 = \cos(45 - \emptyset)$$

$$\alpha_2 = \cos(45 + \emptyset)$$

$$\alpha_3 = 0$$

M remains in the BB'AA' plane.

Again, ignoring K_2 the anisotropy energy can be written as:

$$E_K = \frac{K_1}{4}(\cos^2 2\emptyset)$$

This is averaged over the wall width:

$$\frac{1}{a} \cdot \frac{K_1}{4} \int_{-a/2}^{a/2} \cos^2 2\phi \, dl = \frac{K_1}{8}$$

And, as before, the expressions for exchange and magnetostatic energy are identical with those of a Néel wall in a uniaxial thin film.

Hence:

$$\gamma_{N\pi} = A\left(\frac{\pi}{a}\right)^2 a + \frac{1}{8} K_1 a + \frac{\pi a t}{(a + t)} M_s^2$$

which is equation (1.24).

APPENDIX B

Preparation of colloidal magnetite (Bitter Colloid)

The method used in the production of colloid for the work reported in this thesis is given. The important points are underlined.

3 gms of hydrated $FeCl_3$ and 1.54 gms of hydrated $FeSO_4$ were dissolved in distilled water and the total volume of solution made up to 150 ml. 2.5 gms of NaOH were dissolved in 50 ml of distilled water and the solution brought to the boil.

The iron solution was stood between the poles of a 1.5 Kgauss permanent magnet and heated. The NaOH solution was allowed to drip in slowly while the solution was constantly stirred.

A dense brown-black precipitate formed

$$FeSC_4 + 2NaOH \longrightarrow Fe(OH)_2 + Na_2SO_4$$

$$FeCl_3 + 3NaOH \longrightarrow Fe(OH)_3 + 3NaCl$$

$$Fe(OH)_2 + 2Fe(OH)_3 \longrightarrow \downarrow Fe_3O_4 + 4H_2O$$

The solution was now boiled, whilst remaining in the magnetic field. This accelerates the ageing and polarises the chains as mentioned in the test. Boiling might continue for $\frac{1}{2}$, 1 or 2 hours.*

Boiling was stopped, the solution allowed to separate out and then decanted. Distilled water was added to the precipitate which

---

*The two colloids used in this work had had 1 and 2 hour boils.

was stirred so that all was thoroughly washed. It was again allowed to settle and then decanted and rewashed, the process being repeated three times. The pH of the last rinse was very carefully adjusted to pH5 by the addition of N/100 HCl.

The time required to settle the solution increased markedly with each rinse. In this respect it was found advantageous to stand the beaker above an inhomogeneous magnetic field so that magnetic as well as gravitational forces caused settling.

After the last rinse the slurry was added to 1 litre of $\frac{1}{2}\%$ Teepol solution with pH 5.0-5.2. This slurry was dispersed into a colloidal form by stirring with a 1" diameter paddle for several minutes at 4000 r.p.m. The solution was allowed to settle overnight in a weak magnetic field. If the process had behaved well a black colloid would remain above any settling which occurs. This colloid turns to a claret colour as oxidation occurs, and after a day or two can be used for domain observations.

APPENDIX C

Calculation of Equilibrium Domain Configuration in a Néel Block

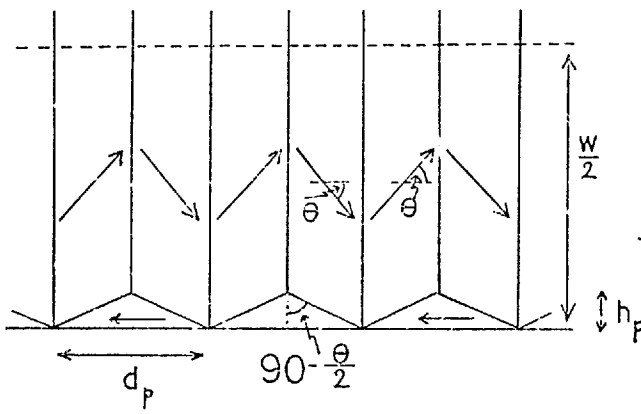

A Néel Block with only reversed 'p' closure domains
Length, L; Width, W; Thickness, t.

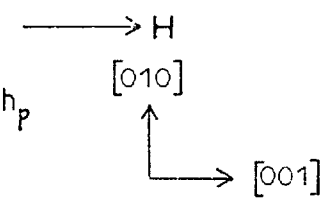

With the application of a magnetic field in the [001] direction the magnetisation turns away from the <110> directions rotating against the magnetocrystalline anisotropy to make an angle θ with the [001] axis. The rotation is assumed to be such that the normal component of magnetisation remains continuous across the boundary.

Magnetic energy in the main domains

$$E = K_1 \cos^2\theta \sin^2\theta - M_s H \cos\theta$$

$$= \frac{K_1}{4} \sin^2 2\theta - M_s H \cos\theta$$

$$\frac{\partial E}{\partial \theta} = K_1 \sin 2\theta \cos 2\theta + M_s H \sin\theta$$

$$= 0 \text{ when E reaches a minimum value, giving}$$

$$M_s H = -2K_1 \cos\theta \cos 2\theta \qquad (C.1)$$

The energy minimum is then

$$E_{min} = \frac{K_1}{4} \sin^2 2\theta + 2K_1 \cos^2\theta \cos 2\theta$$

$$= K_1 \cos^2\theta(2-3 \sin^2\theta)$$

Free-pole effects at the edges are reduced by the formation of 'p' closure domains, again with the normal component of magnetisation continuous across the boundary.

The energy/unit volume of the 'p' closure domain is

$$K_1 \cos^2 \frac{\pi}{2} \cos^2 0 + M_s H = M_s H = - 2K_1 \cos\theta \cos 2\theta$$

Hence the energy of formation of the 'p' domains/unit volume is

$$E_p = - 2K_1 \cos\theta \cos 2\theta - K_1 \cos^2\theta \, (2-3 \sin^2\theta)$$

which simplifies to

$$E_p = - K_1 \cos\theta \, (\cos\theta + 1)^2(3 \cos\theta - 2) \qquad (C.2)$$

The dimensions of the closure domains are d_p, t and

$$h_d = \tfrac{1}{2} d_p \cos(90 - \tfrac{\theta}{2}) = \tfrac{1}{2} d_p \tan\tfrac{\theta}{2} = \frac{\frac{1}{2} d_p \sin\theta}{(1 + \cos\theta)}$$

and hence the volume of these domains is

$$v_p = \tfrac{1}{2} d_p h_p t = \frac{\frac{1}{4} d_p^2 t \sin\theta}{(1 + \cos\theta)}$$

hence the energy of formation of a closure domain is

$$E_p v_p = \frac{- d_p^2 t \sin\theta K_1 \cos\theta \, (\cos\theta + 1)^2(3 \cos\theta - 2)}{4(\cos\theta + 1)}$$

$$= d_p^2 t K_p \quad \text{where } K_p = - \tfrac{1}{8} K_1 \sin 2\theta(\cos\theta + 1)(3 \cos\theta - 2)$$

The total energy of the Néel block/unit area of section t d_p is

$$E_N = \frac{1}{t d_p}\left[2\gamma_\omega t + 2 d_p^2 t K_p + \omega d_p t K_1 \cos^2\theta(2-3\sin^2\theta)\right]$$

where γ is the wall energy density, and assuming $\omega \gg d_p$ so that the closure domain walls are neglected.

$$\frac{\partial E_N}{\partial d_p} = -\frac{2\gamma_\omega}{d_p^2} + 2K_p$$

which reaches a minimum when $\frac{\partial E_N}{\partial d_p} = 0$

i.e. when $d_p^2 = \frac{\gamma_\omega}{K_p}$

resubstituting, the equilibrium value for d_p is given by

$$d_p^2 = \frac{-8\gamma_\omega}{K_1 \sin 2\theta\,(\cos\theta + 1)(3\cos\theta - 2)} \qquad (C.3)$$

APPENDIX D

Rotation of Type III Stripe Domains under Applied Fields

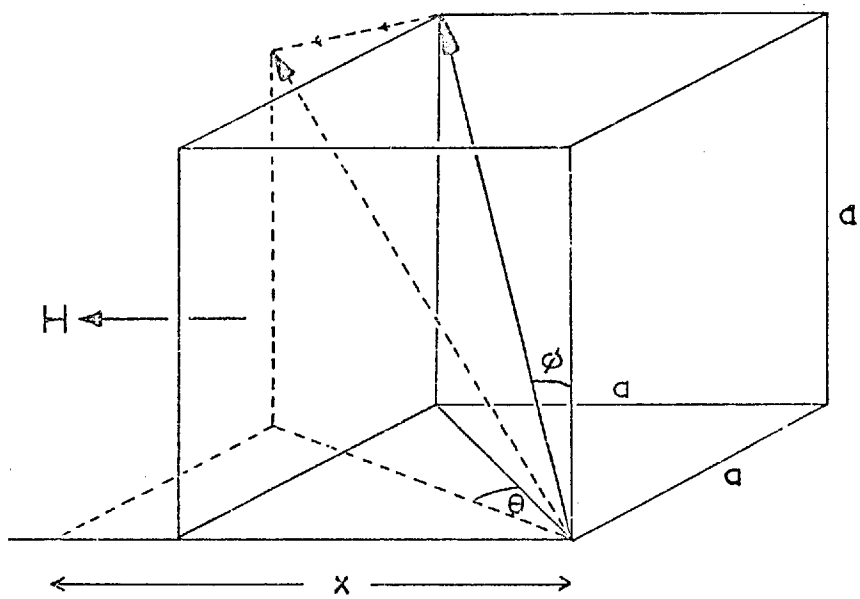

For the purpose of this calculation the presence of any non <111> direction magnetisation components from the oscillation of the magnetisation towards different <111> directions is ignored. Initially it is assumed to all lie in the [111] direction and the application of a [100] axis field causes the magnetisation to rotate towards the plane containing this direction, but with the angle ϕ remaining constant.

It will be noticed that $\cos \phi = \alpha_3 = \frac{1}{\sqrt{3}}$

where α_1, α_2 and α_3 are the direction cosines of the magnetisation.

The anisotropy energy/unit volume is expressed as

$$E_K = K_1(\alpha_1^2\alpha_2^2 + \alpha_2^2\alpha_3^2 + \alpha_3^2\alpha_1^2) + K_2(\alpha_1^2\alpha_2^2\alpha_3^2) + \ldots\ldots$$

which using $\alpha_3^2 = \frac{1}{3}$ simplifies to

$$E_K = K_1\left[\alpha_1^2\alpha_2^2 + \frac{1}{3}(\alpha_1^2 + \alpha_2^2)\right] + \frac{1}{3}K_2\alpha_1^2\alpha_2^2$$

But $\sum_{i=1}^{3} \alpha_i^2 = 1$ hence $\alpha_1^2 + \alpha_2^2 = \frac{2}{3}$

$$E_K = (K_1 + \frac{1}{3}K_2)\,\alpha_1^2\alpha_2^2 + \frac{2}{9}K_1$$

$$= -(K_1 + \frac{1}{3}K_2)(\alpha_1^4 - \frac{2}{3}\alpha_1^2) + \frac{2}{9}K_1 \qquad (D.1)$$

The projected angle of rotation is given by θ

where $\cos(\frac{\pi}{4} - \theta) = \frac{x}{a\sqrt{2}}$

thus $\alpha_1 = \frac{x}{a\sqrt{3}} = \sqrt{\frac{2}{3}}\cos(\frac{\pi}{4} - \theta)$

and $\alpha_2 = \sqrt{\frac{2}{3}}\sin(\frac{\pi}{4} - \theta)$

Hence E_K can be expressed in terms of this angle as

$$E_K = -(K_1 + \frac{1}{3}K_2)\left[\frac{4}{9}\cos^4(\frac{\pi}{4} - \theta) - \frac{4}{9}\cos^2(\frac{\pi}{4} - \theta)\right] + \frac{2}{9}K_1$$

Differentiating this expression with respect to θ we get

$$\frac{\partial E_K}{\partial \theta} = -\frac{4}{9}(K_1 + \frac{K_2}{3})\left[4\cos^3(\frac{\pi}{4} - \theta)\sin(\frac{\pi}{4} - \theta) - 2\cos(\frac{\pi}{4} - \theta)\sin(\frac{\pi}{4} - \theta)\right]$$

which simplifies to

$$\frac{\partial E_K}{\partial \theta} = -\frac{2}{9}\left(K_1 + \frac{K_2}{3}\right) \sin 4\theta \qquad (D.2)$$

With the field along the [100] axis in the plane of the platelet, the torque exerted on M due to the field is

$$\underline{M} \wedge \underline{H} = M H \alpha_1$$

$$= \sqrt{\frac{2}{3}}\, M H \sin\left(\frac{\pi}{4} - \theta\right) \qquad (D.3)$$

But $$\frac{\partial E_K}{\partial \theta} = \underline{M} \wedge \underline{H}$$

hence $$-\frac{2}{9}\left(K_1 + \frac{K_2}{3}\right) \sin 4\theta$$

$$= \sqrt{\frac{2}{3}}\, M H \sin\left(\frac{\pi}{4} - \theta\right)$$

using the values for K_1 and K_2 of Franse and De Vries (1968) quoted in Chapter 1. This equation reduces to

$$H = \frac{36.5 \sin 4\theta}{\sin\left(\frac{\pi}{4} - \theta\right)} \qquad (D.4)$$

REFERENCES

AHARONI, A. Rev. Mod. Phys. 34 227 (1962a).

AHARONI, A. J. Appl. Phys. 33 1324 (1962b).

AHARONI, A. J. Appl. Phys. 37 3271 (1966a).

AHARONI, A. J. Appl. Phys. 37 4615 (1966b).

AHARONI, A. J. Appl. Phys. 38 3196 (1967).

AHARONI, A. J. Appl. Phys. 39 861 (1968).

AHARONI, A. and NEEMAN, E. Phys. Lett. 6 241 (1963).

ALCOCK, C.B. and JEFFES, J.H.E. Trans. Instn. Min. Metall. 76 C246 (1967).

ALLAN, W.J. and WEBB, W.W. Acta. Met. 7 646 (1959).

ANDRÄ, W. Ann. Phys. Leipzig 17 233 (1956a).

ANDRÄ, W. Ann. Phys. Leipzig 17 78 (1956b).

ARGYRES, P.N. Phys. Rev. 97 334 (1955).

AUBERT, G. J. Appl. Phys. 39 504 (1968).

BACIGALUPI, J.J. J. Appl. Phys. 34 999 (1963).

BALTZ, A. J. Appl. Phys. 37 1485 (1966).

BANBURY, J.R. and NIXON, W.C. J. Sci. Inst. 44 889 (1967).

BARKHAUSEN, H. Phys. Zeits. 20 401 (1919).

BARNETT, M.E. and NIXON, W.C. J. Sci. Inst. 44 893 (1967).

BASSETFIELD, J. and PRESCOTT, M.J. J. Appl. Phys. 38 3190 (1967).

BATES, L.F. Proc. Phys. Soc. 84 625 (1964).

BATES, L.F. and SPIVEY, S. Brit. J. Appl. Phys. 15 705 (1964).

BERGMAN, W.H. Z. Ang. Phys. 8 559 (1956).

BEYERSDORF, K. Glas und Hochvakuum Technik 2 8 (1952).

BHIDE, V.G. and SHENOY, G.K. J. Appl. Phys. 34 1778 (1963).

BIRSS, R.R. Adv. in Phys. 8 252 (1959).

BITTER, F. Phys. Rev. 38 1903 (1931).

BLACKBURN, W.J.S. and FERRIER, R.P. J. Appl. Phys. 39 1163 (1968).

BLACKMAN, M. and GRUNBAUM, E. Proc. Roy. Soc. A241 508 (1957).

BLOCH, F. Z. Physik. 74 295 (1932).

BLOIS, M.S. J. Appl. Phys. 26 975 (1955).

BLOOR, D. and MARTIN, D.H. Proc. Phys. Soc. 73 695 (1959).

BOBECK, A.H., FISCHER, R.F. and PERNESKI, A.J. I.E.E.E. Trans. MAG 5 544 (1969).

BOERSCH, H., HAMISCH, H., WOHLLEBEN, D. and GROHMANN, K. Z. Physik 164 55 (1961).

BOERSCH, H., HAMISCH, H., GROHMANN, K. and WOHLLEBEN, D. Z. Physik 167 72 (1962).

BOERSCH, H. and LAMBECK, M. Z. Phys. 177 157 (1964).

BONGERS, P.F. I.E.E.E. Trans. MAG 5 472 (1969).

BONSE, U., HART, M. and NEWKIRK, J.B. Advances in X-Ray Analysis 10 1 (1967).

BOURRET, A. and DAUTREPPE, D. Phys. Stat. Sol. 13 559 (1966).

BOURRET, A. and KLEMAN, M. Phys. Stat. Sol. 23 207 (1967).

BOZORTH, R.M. Ferromagnetism, Van Nostrand (1951).

BRENNER, S.S. Acta. Met. 4 62 (1956).

BRENNER, S. and SEARS, G.W. Acta. Met. 4 268 (1956).

BROWN, W.F. Rev. Mod. Phys. 17 15 (1945).

BROWN, W.F. Magnetostatic Principles in Ferromagnetism, North Holland (1962a).

BROWN, W.F. J. Appl. Phys. 33 3022 (1962b).

BROWN, W.F. Micromagnetics, Interscience, J. Wiley (1963).

BROWN, W.F. and LA BONTE, A.E. J. Appl. Phys. 36 1380 (1965).

BUCKLEY, H.E. Crystal Growth, J. Wiley, N.Y. (1951).

BURTON, W.K., CABRERA, N. and FRANK, F.C. Phil. Trans. Roy. Soc. A243 299 (1951).

CALLEN, E. J. Appl. Phys. 39 519 (1968).

CAREY, D. and ISAAC, E.D. Magnetic Domains and Techniques for their Observation, E.U.P. (1966).

CASTAING, R. and DESCAMPS, J. J. Phys. Rad. 16 304 (1955).

CECH, R.E. Acta. Met. 7 787 (1959).

CECH, R.E. Acta. Met. 9 459 (1961).

CHANG, H. and FETH, G.C. I.E.E.E. Trans. Communications & Electronics 83 706 (1964).

CHANG, H. and LIN, Y.S. I.E.E.E. Trans. MAG 3 653 (1967).

CHIKAWA, J. and NAKAYAMA, T. J. Appl. Phys. 35 2493 (1964).

CHIKAZUMI, S. Physics of Magnetism, J. Wiley (1964).

COHEN, M.S. J. Appl. Phys. 33 2968 (1962).

COHEN, M.S. I.E.E.E. Trans. MAG 1 156 (1965).

COHEN, M.S. J. Appl. Phys. 38 4966 (1967).

COHEN, M.S. Chapter X, Thin Film Phenomena, ed. Chopra, K.L., McGraw Hill (1969).

COLEMAN, R.V. Met. Rev. 9 261 (1964).

COLEMAN, R.V. and CABRERA, N. J. Appl. Phys. 28 1360 (1957).

COLEMAN, R.V. and SCOTT, G.G. Phys. Rev. 107 1276 (1957).

COLEMAN, R.V. and SCOTT, G.G. J. Appl. Phys. 29 526 (1958).

COLEMAN, R.V. and SEARS, G.W. Acta. Met. 5 131 (1957).

COOPER, R.W., PEARSON, R.F., VAN HEEK, H. and PAGE, J.L. I.E.E.E. Trans. MAG 5 472 (1969).

COSSLETT, V.E. Contemp. Phys. 9 333 (1968).

CRAIK, D.J. Proc. Phys. Soc. B69 647 (1956).

CRAIK, D.J. Contemp. Phys. 11 65 (1970).

CRAIK, D.J. and GRIFFITHS, P.M. Proc. Phys. Soc. B70 1000 (1957).

CRAIK, D.J. and GRIFFITHS, P.M. Brit. J. Appl. Phys. 9 279 (1958).

CRAIK, D.J. and McINTYRE, D.A. Proc. Roy. Soc. A302 99 (1967).

CRAIK, D.J. and TEBBLE, R.S. Ferromagnetism & Ferromagnetic Domains, North-Holland (1965).

CROWTHER, T.S. and COHEN, M.S. J. Appl. Phys. 38 3 (1967).

DE BLOIS, R.W. J. Appl. Phys. 36 1647 (1965).

DE BLOIS, R.W. J. Vac. Sci. & Tech. 3 146 (1966).

DE BLOIS, R.W. General Electric Report AFCRL-67-0107 (1967).

DE BLOIS, R.W. General Electric Report AFCRL-68-0414 (1968a).

DE BLOIS, R.W. J. Appl. Phys. 39 442 (1968b).

DE BLOIS, R.W. and BEAN, C.P. J. Appl. Phys. 30 S 225 (1959).

DE BLOIS, R.W. and GRAHAM, C.D. J. Appl. Phys. 29 931 (1958).

DEY, S.K., BOWMAN, M.J. and BOOTH, A.D. J. Phys. E. (J. Sci. Inst.) 2 162 (1969).

DI CHEN J. Appl. Phys. 38 1309 (1967).

DIETZE, H.D. and THOMAS, H. Z. Phys. 163 523 (1961).

DILLON, J.F. J. Appl. Phys. 29 539 (1958a).

DILLON, J.F. J. Appl. Phys. 29 1286 (1958b).

DILLON, J.F. Annual Report of the Smithsonian Institution, p.385 (1960).

DILLON, J.F. J. Appl. Phys. 39 922 (1968).

DOVE, D.B. J. Appl. Phys. 34 2067 (1963).

DUPOUY, G. and PERRIER, F. J. de Microscopy 1 167 (1962).

ELLINGHAM, H.J.T. J. Soc. Chem. Ind. 63 125 (1944).

ELMORE, W.C. Phys. Rev. 51 982 (1937).

ELMORE, W.C. Phys. Rev. 54 309 (1938a).

ELMORE, W.C. Phys. Rev. 54 1092 (1938b).

ELMORE, W.C. Phys. Rev. 58 640 (1940).

ESHELBY, J.D. J. Appl. Phys. 24 176 (1953).

ESHELBY, J.D. Phil. Mag. 3 440 (1958).

FAUST, J.W. and JOHN, H.F. Trans. Met. Soc. A.I.M.E. 233 230 (1965).

FELDTKELLER, E. Symposium on the Electric and Magnetic Properties of Thin Metallic Layers (Louvain 1961) p.98.

FELDTKELLER, E. Z. Angew. Phys. 15 206 (1963).

FELDTKELLER, E. Z. Angew. Phys. 19 530 (1965).

FELDTKELLER, E. and FUCHS, E. Z. Angew. Phys. 18 1 (1964).

FELDTKELLER, E. and LIESK, W. Z. Angew. Phys. 14 195 (1962).

FELDTKELLER, E. and STEIN, K.U. Z. Angew. Phys. 23 100 (1967).

FELDTKELLER, E. and THOMAS, H. Phys. Kondens. Materie. 4 8 (1965).

FERRIER, R.P. Bull. Soc. fr. Min. Crystal. 90 464 (1967).

FERRIER, R.P. and MURRAY, R.T. J. Royal Microscopical Soc. 85 323 (1966).

FERRIER, R.P. and MUCHALSKA, I.B. Phys. Stat. Sol. 28 335 (1968).

FITZGERALD, A.G., MANNAMI, M., POGSON, E.H. and YOFFE, A.D. J. Appl. Phys. 38 3303 (1967).

FOWLER, C.A. and FRYER, E.M. Phys. Rev. 86 426 (1952).

FOWLER, C.A. and FRYER, E.M. J. Opt. Soc. America 44 256 (1954a).

FOWLER, C.A. and FRYER, E.M. Phys. Rev. 94 52 (1954b).

FOWLER, C.A. and FRYER, E.M. Phys. Rev. 104 552 (1956).

FOWLER, C.A., FRYER, E.M. and TREVES, D. J. Appl. Phys. 31 2267 (1960).

FOWLER, C.A., FRYER, E.M. and TREVES, D. J. Appl. Phys. 32 296S (1961).

FOX, M. and TEBBLE, R.S. Proc. Phys. Soc. 72 765 (1958).

FRAIT, Z., FRAITOVA, D., KOTRBOVA, M. and HAUPTMAN, Z. Czech. J. Phys. B16 837 (1966).

FRANK, F.C. Disc. Faraday Soc. 5 48 (1949).

FRANSE, J.J.M. Thesis, Univ. of Amsterdam (1969).

FRANSE, J.J.M. and DE VRIES, G. Physica 39 477 (1968).

FUCHS, E. Naturwissenschaften 12 450 (1961).

FUCHS, E. Z. Angew, Phys. 14 203 (1962).

FUJIWARA, H., SUGITA, Y. and SAITO, N. J. Phys. Soc. Japan 20 2088 (1965b).

FULLER, H.W. and HALE, M.E. J. Appl. Phys. 31 238 (1960a).

FULLER, H.W. and HALE, M.E. J. Appl. Phys. 31 1699 (1960b).

FULLER, H.W. and RUBINSTEIN, H. J. Appl. Phys. 30 84S (1959).

GARROOD, J.R. Proc. Phys. Soc. 79 1252 (1962).

GEMPERLE, R. Phys. Stat. Sol. 14 121 (1966).

GEMPERLE, R. and KACZER, J. Phys. Stat. Sol. 34 255 (1969).

GENOVESE, E.R. and CHANG, H. Rev. Sci. Inst. 39 733 (1968).

GILMAN, J.J. The Art & Science of Growing Crystals, J. Wiley, N.Y. (1963).

GOMI, Y. and ODANI, Y. J. Phys. Soc. Japan 15 535 (1960).

GONDO, Y. J. Phys. Soc. Japan 17 1129 (1962).

GONDO, Y. and FUNATOGAWA, Z. J. Phys. Soc. Japan 15 535 (1960).

GOODENOUGH, J.B. Phys. Rev. 95 917 (1954).

GORSUCH, P.D. A.I.M.E. Met. Soc. Conf. 8 771 (1959a).

GORSUCH, P.D. J. Appl. Phys. 30 837 (1959b).

GREEN, A. and PRUTTON, M. J. Sci. Inst. 39 244 (1962).

GREEN, A., PRUTTON, M. and CARTER, W.S. J. Sci. Inst. 40 490 (1963).

GREEN, A. and THOMAS, B.W.J. J. Sci. Inst. 43 399 (1966).

GRUNDY, P.J. Brit. J. Appl. Phys. 16 409 (1965).

GRUNDY, P.J. and TEBBLE, R.S. Advances in Physics 17 153 (1968).

HALE, M.E., FULLER, H.W. and RUBINSTEIN, H. J. Appl. Phys. 30 789 (1959).

von HAMOS, L. and THIESSEN, P.A. Zeit. für Phys. 71 442 (1931).

HARRINGTON, J.V. M.I.T. Tech. Rep., Lincoln Lab. No.166 (1958).

HAUPTMANN, Z. and SVOBODA, E. Czech. Chem. Commun. 30 1373 (1965).

HIRTH, J. and FRANK, F.C. Phil. Mag. 3 1110 (1958).

HOFFMANN, H. I.E.E.E. Trans. MAG 4 32 (1968).

HOLZ, A. and KRONMULLER, A. Phys. Stat. Sol. 31 787 (1969).

HORNREICH, R.M. J. Appl. Phys. 34 1071 (1963).

HUBERT, A. Phys. Stat. Sol. 32 519 (1969).

HUBER, E.E. and SMITH, D.O. J. Appl. Phys. 30 267 (1959).

HUBER, E.E., SMITH, D.O. and COODENOUGH, J.B. J. Appl. Phys. 29 294 (1958).

HUTCHINS, G.A. The Electron Microprobe, ed. T.D. McKinley et al, J. Wiley, N.Y. p.390 (1966).

IWATA, T., PROSEN, R.J. and GRAN, B.E. J. Appl. Phys. 37 1285 (1966).

JAKUBOVICS, J. Phil. Mag. 13 85 (1966a).

JAKUBOVICS, J.P. Phil. Mag. 14 881 (1966b).

JANAK, J.F. Appl. Phys. Letts. 9 225 (1966).

JEFFES, J.H.E. J. Cryst. Growth 3 13 (1968).

JOY, D.C. and JAKUBOVICS, J.P. Phil. Mag. 17 61 (1968).

JOY, D.C. and JAKUBOVICS, J.P. Brit. J. Appl. Phys. Ser.2 2 1367 (1969).

KACZER, J. Czech. J. Phys. 7 557 (1957).

KACZER, J. J. Appl. Phys. 29 569 (1958).

KACZER, J. and GEMPERLE, R. Czech. J. Phys. 9 306 (1959a).

KACZER, J., GEMPERLE, R. and HAUPTMAN, Z. Czech. J. Phys. 9 606 (1959b).

KACZER, J., ZELENY, M. and SUDA, P. Czech. J. Phys. B13 579 (1963).

KANAMORI, J. Magnetism 1 127 (1963) Academic Press (Ed. Rado, G.T. and Suhl, H.)

KAYSER, W. I.E.E.E. Trans. MAG 3 141 (1967).

KERR, J. Rept. Brit. Assoc. Adv. Sci. p.40 (1876).

KITTEL, C. Phys. Rev. 70 965 (1946).

KITTEL, C. Rev. Mod. Phys. 21 541 (1949a).

KITTEL, C. Phys. Rev. 76 1527 (1949b).

KITTEL, C. and GALT, J.K. Solid State Physics 3 (1956), p.437 Ferromagnetic Domain Theory.

KOIKEDA, T., SUZUKI, K. and CHIKAZUMI, S. Appl. Phys. Letts. 4 160 (1964).

KOOY, C. and ENZ, U. Philips Res. Repts. 15 7 (1960).

KOTRBOVA, M. and HAUPTMAN, Z. Czech. J. Phys. B15 64 (1965).

KOZLOWSKI, G. and ZIETEK, W. Acta Physica Polonica 29 261 (1966).

KRANZ, J. Naturwissenschaften 43 370 (1956).

KRANZ, J., HUBERT, A. and MULLER, R. Z. Phys. 180 80 (1964).

KRINCHIK, G.S. J. Appl. Phys. 39 859 (1968).

KRYDER, M.H. and HUMPHREY, F.B. J. Appl. Phys. 40 2469 (1969).

KUBASCHEWSKI, O., EVANS, E.Ll. and ALCOCK, C.B. Metallurgical Thermochemistry, Pergamon (1967).

LA BONTE, A.E. J. Appl. Phys. 40 2450 (1969).

LA BONTE, A.E. and BROWN, W.F. J. Appl. Phys. 37 1299 (1966).

LAMBECK, M. Z. Physik 179 161 (1964).

LAMBECK, M. Z. Angew. Phys. 18 506 (1965).

LAMBECK, M. I.E.E.E. Trans. MAG 4 51 (1968).

LANDAU, L. and LIFSHITZ, E. Physik. Z. Sowjetunion 8 153 (1935).

LANG, A.R. Acta. Cryst. 12 249 (1959).

LANG, A.R. and POLCAROVA, M. Proc. Roy. Soc. London A285 297 (1965).

LEAVER, K.D. Thin Solid Films 2 149 (1968).

LEAVER, K.D. Private Communication (1969).

LEE, E.W. Proc. Phys. Soc. A66 623 (1953).

LEE, E.W. Rep. Progr. Phys. 18 184 (1955).

LEHRER, S.S. J. Appl. Phys. 34 1207 (1963).

LIFSHITZ, E. J. Phys. U.S.S.R. 8 337 (1944).

LILLEY, B.A. Phil. Mag. 41 792 (1950).

LISSBERGER, P.H. J. Opt. Soc. Amer. 51 948 (1961) (2 papers).

LISSBERGER, P.H. J. Opt. Soc. Amer. 54 804 (1964).

LO, D.S. and HANSON, M.M. J. Appl. Phys. 38 1342 (1967).

LUBORSKY, F.E. J. Appl. Phys. 32 171S (1961).

McKEEHAM, L.W. and ELMORE, W.C. Phys. Rev. 46 226 (1934).

MALEK, Z. and KAMBERSKY, V. Czech. J. Phys. 8 416 (1958).

MARTIN, D.H. Proc. Phys. Soc. B70 77 (1957).

MAYER, L. J. Appl. Phys. 26 1228 (1955).

MAYER, L. J. Appl. Phys. 28 975 (1957).

MAYER, L. J. Appl. Phys. 30 252S (1959).

MAYER, L. J. Appl. Phys. 31 346 (1960).

METHFESSEL, S., MIDDELHOEK, S. and THOMAS, H. I.B.M. J. Res. Develop. 4 96 (1960).

METZDORF, M. and WIEHL, H.E. Phys. Stat. Sol. 17 285 (1966).

MICHALAK, J.T. and GLENN, R.C. J. Appl. Phys. 32 1261 (1961).

MIDDELHOEK, S. Van Soest, Amsterdam (1961), Ph.D. Thesis.

MIDDELHOEK, S. J. Appl. Phys. 33 1111S (1962).

MIDDELHOEK, S. J. Appl. Phys. 34 1054 (1963).

MOHIUDDIN, M. Brit. J. Appl. Phys. 17 789 (1966).

MOON, R.M. J. Appl. Phys. 30 82S (1959).

MORELOCK, C.R. and SEARS, G.W. J. Chem. Phys. 31 926 (1959).

MORELOCK, C.R. and SEARS, G.W. J. Chem. Phys. 34 1008 (1961).

MURAYAMA, Y. J. Phys. Soc. Japan 21 2253 (1966).

MURAYAMA, Y. J. Phys. Soc. Japan 23 511 (1967).

NABARRO, F.R.N. and JACKSON, P.J. Growth and Perfection of Crystals p.13, J. Wiley, N.Y. (1958).

NEEL, L. J. Phys. Radium 5 241 (1944).

NEEL, L. Cahiers de Phys. 25 1 (1944).

NEEL, L. Compt. Rend. 241 533 (1955).

O'DELL, T.H. I.E.E. Monograph No. 396 M (1960).

OATLEY, C.W., NIXON, W.C. and PEASE, R.F.W. Adv. Electronics & Electron Physics 21 181 (1965).

OLSON, A.L. J. Appl. Phys. 38 1869 (1967).

OLSON, A.L., OREDSON, H.N., TOROK, E.J. and SPURRIER, R.A. J. Appl. Phys. 38 1349 (1967).

OSBORN, J.A. Phys. Rev. 67 351 (1945).

PALIK, E.D. Applied Optics 6 597 (1967).

PERNESKI, A.J. I.E.E.E. Trans. MAG 5 554 (1969).

POLCAROVA, M. I.E.E.E. Trans. MAG 5 536 (1969).

POLCAROVA, M. and KACZER, J. Phys. Stat. Sol. 21 635 (1967).

POLCAROVA, M. and LANG, A.R. Appl. Phys. Letts. 1 13 (1962).

POLCAROVA, M. and LANG, A.R. Bull. Soc. fr. Min. Crystal 91 645 (1968).

PRICE, P.B. Phil. Mag. 5 473 (1960).

PRICE, F.P., VERMILYEA, D.A. and WEBB, M.B. Acta. Met. 6 524 (1958).

PRUTTON, M. Phil. Mag. 4 1063 (1959).

PRUTTON, M. Phil. Mag. 5 625 (1960).

PRUTTON, M. Thin Ferromagnetic Films, Butterworths (1964).

PUCHALSKA, I.B. and FERRIER, R.P. Thin Solid Films 1 437 (1967/8).

REGIS, M. and CALVIAC, J.C. J. Cryst. Growth 6 43 (1969).

RHODES, P. and ROWLANDS, G. Proc. Leeds. Phil. Soc. 6 191 (1954).

RICKER, Th. Phys. Stat. Sol. 30 K93 (1968).

RICKER, Th. I.E.E.E. Trans. MAG 5 179 (1969).

ROBINSON, C.C. J. Opt. Soc. Amer. 54 1220 (1964).

RODBELL, D.S. Phys. Rev. Letters 13 471 (1964).

RODBELL, D.S. Physics 1 279 (1965).

RODGERS, J.M. Proc. Int. Conf. Magnetism, Nottingham (1964) p.866.

ROESSLER, B., KRAMER, J.J. and KURIYAMA, M. Phys. Stat. Sol. 11 117 (1965).

RUBINSTEIN, H. and SPAIN, R.J. J. Appl. Phys. 31 306S (1960).

SAITO, N., FUJIWARA, H. and SUGITA, Y. J. Phys. Soc. Japan 19 421 (1964a).

SAITO, N., FUJIWARA, H. and SUGITA, Y. J. Phys. Soc. Japan 19 1116 (1964b).

SAITO, N. Ph.D. Thesis, Tokyo Univ. (1966).

SATO, H. and ASTRUE, R.W. J. Appl. Phys. 33 2956 (1962).

SATO, H., TOTH, R.S. and ASTRUE, R.W. J. Appl. Phys. 33 1113 (1962).

SATO, H., TOTH, R.S. and ASTRUE, R.W. J. Appl. Phys. 34 1062 (1963).

SATO, H., TOTH, R.S. and ASTRUE, R.W. Single Crystal Films, Pergamon Press Inc. New York (1964) p.395.

SATO, H., ASTRUE, R.W. and SHINOZAKI, S.S. J. Appl. Phys. 35 822 (1964).

SCHAFER, H. Chemical Transport Reactions, Academic Press (1964).

SCHLENKER, M., BRISSONNEAU, P. and PERRIER, J.P. Bull. Soc. fr. Min. Cristal 91 653 (1968).

SEARS, G.W. Acta. Met. 1 457 (1953).

SEARS, G.W. Acta. Met. 3 361 (1955a).

SEARS, G.W. Acta. Met. 3 367 (1955b).

SEARS, G.W. J. Chem. Phys. 25 637 (1956).

SEARS, G.W. J. Chem. Phys. 29 1045 (1958).

SEARS, G.W. and COLEMAN, R.V. J. Chem. Phys. 25 635 (1956).

SHERWOOD, R.C., REMEIKA, J.P. and WILLIAMS, H.J. J. Appl. Phys. 30 217 (1959).

SHTRIKMAN, S. and TREVES, D. J. Appl. Phys. 31 147S (1960a).

SHTRIKMAN, S. and TREVES, D. J. Appl. Phys. 31 1304 (1960b).

SHTRIKMAN, S. and TREVES, D. J. Appl. Phys. 31 72S (1960c).

SHTRIKMAN, S. and TREVES, D. Magnetism 3 395 (1963).

SHUR, I.S., SHTOL'TS. E.W. and MARGOLINA, W.I. Sov. Phys. J.E.T.P. 11 33 (1960).

SILCOX, J. Phil. Mag. 8 1395 (1963).

SOMMERFELD, A. Electrodynamics. Academic Press (1964).

SPACEK, L. Czech. J. Phys. 9 186 (1959) (2 papers).

SPAIN, R.J. Appl. Phys. Letters 3 208 (1963).

SPAIN, R.J. and FULLER, H.W. J. Appl. Phys. 37 953 (1966).

STONER, E.C. Phil. Mag. 36 803 (1945).

STONER, E.C. Rep. Prog. Phys. 13 83 (1950).

STRANSKI, I.N. Z. Physik Chem. 136 259 (1928).

SUGITA, Y., FUJIWARA, H. and SAITO, N. J. Phys. Soc. Japan 19 782 (1964).

SUGITA, Y., FUJIWARA, H. and SAITO, N. J. Phys. Soc. Japan 20 469 (1965a).

SUGITA, Y. and FUJIWARA, H. J. Phys. Soc. Japan 20 98 (1965b).

SUGITA, Y., FUJIWARA, H. and SATO, T. Appl. Phys. Letters 10 229 (1967).

SUKIENNICKI, A. Phys. Stat. Sol. 29 417 (1968).

SUZUKI, T., WILTS, C.H. and PATTON, C.E. J. Appl. Phys. 39 1983 (1968).

SWALIN, R.A. Thermodynamics of Solids, J. Wiley, N.Y. (1962).

TATSUMOTO, E., HARA, K. and HASHIMOTO, T. Japan J. Appl. Phys. 7 176 (1968).

TOROK, E.J., LO, D.S., OREDSON, H.N. and SIMON, W.J. J. Appl. Phys. 40 1222 (1969).

TOROK, E.J., OLSON, A.L. and OREDSON, H.N. J. Appl. Phys. 36 1394 (1965).

TREVES, D. J. Appl. Phys. 32 358 (1961).

VOIGT, W. Magneto and Electro Optics, B.G. Teubner, Leipzig (1908).

VOLMER, M. and ESTERMANN, I. Zeit. für Phys. 7 13 (1921).

WADE, R.H. Proc. Phys. Soc. 79 1237 (1962).

WADE, R.H. and SILCOX, J. Appl. Phys. Letters 8 7 (1966).

WAGNER, R.S. and ELLIS, W.C. Appl. Phys. Letters 4 89 (1964).

WANG, F.F.Y. J. Appl. Phys. 39 865 (1968).

WARRINGTON, D.H. Phil. Mag. 9 261 (1964).

WARRINGTON, D.H., ROGERS, J.M. and TEBBLE, R.S. Phil. Mag. 7 1783 (1962).

WEBB, W.W., DRAGSDORF, R.D. and FORGENG, W.D. Phys. Rev. 108 498 (1957).

WEBER, R. I.E.E.E. Trans. MAG.4 28 (1968).

WEISS, P. J. Phys. 6 661 (1907).

WHITE, E.A.D. Acta. Cryst. 8 845 (1955).

WILLIAMS, H.J., BOZORTH, R.M. and SHOCKLEY, W. Phys. Rev. 75 155 (1949).

WILLIAMS, H.J. and GOERTZ, M. J. Appl. Phys. 23 316 (1952).

WILLIAMS, H.J. and SHERWOOD, R.C. J. Appl. Phys. 28 548 (1957).

WILLIAMS, H.J., FOSTER, F.G. and WOOD, E.A. Phys. Rev. 82 119 (1951).

WOHLLEBEN, D. Phys. Letters 22 546 (1966).

WOHLLEBEN, D. J. Appl. Phys. 38 3341 (1967).